TO MY PARENTS

VOLTAMMETRIC STUDIES IN MOLTEN SALTS

A thesis submitted for the degree of

Doctor of Philosophy

University of Southampton

by

Vinij Jiamsakul

July 1978

ACKNOWLDEGEMENTS

I would like to thank Professor Graham Hills for his advice, encouragement and hospitality throughout this research.

I should like to record my own indebtness to Drs. A.F. Gaines, M.H. Miles and M.C. Flowers who recommended me to 'Southampton'. Dr. Gaines was a former senior lecturer in physical chemistry at Chiengmai University, Thailand. He played an active part in developing chemistry of our country and has done so much to my future. The debt I owe him is immeasurable.

I would like to thank Dr. Canoe, a visiting professor from Belgium; my friends, Gamini and Irene for some experimental assistance.

I would also like to thank my wife, Prapar, for having transformed my handwritten text into a presentable thesis, for her continual understanding, sacrifice and forbearance throughout my career. My brother-in-law, Prasarn, for drawing the cell diagrams.

Finally, the award of research assistantship from University of Southampton is gratefully acknowledged.

ABSTRACT

FACULTY OF SCIENCE

CHEMISTRY

Doctor of Philosophy

VOLTAMMETRIC STUDIES IN MOLTEN SALTS

by Vinij Jiamsakul

A study has been made of the electrodeposition of silver onto platinum from aqueous solutions and from molten alkali nitrates using the linear sweep technique and measurement of step-function transients. The nature and role of the platinum oxide film and its effect upon the rate of new phase formation on it have been studied. The investigations included copper deposition on platinum and silver deposition on vitreous carbon from aqueous media, both of which are invariably preceded by three dimensional nucleation and growth controlled by hemispherical diffusion of the depositing ions.

Electron micrographs show a radial growth of silver nuclei on platinum in support of the assumption that nucleation is an essential precursor of the appearance of macrosteps.

A detailed study of the early stages of the silver deposition on vitreous carbon in $NaNO_3$-KNO_3 eutectic at 250°C has been made using galvanostatic, potentiostatic and potentiostatic-galvanostatic-potentiostatic pulse trains. The second potentiostatic pulse was used to estimate the nuclear number density at the galvanostatic potential maximum. The maximum in the galvanostatic potential-time response was used as a basis for the determination of the charge transfer rate constant for the bulk

silver $\rightleftharpoons$ silver ion reaction in nitrate melt and found to be in satisfactory agreement with previously published values.

A further study encompasses the deposition of other metals such as Pb(II), Cd(II), Co(II), Ni(II) and Cu(II) onto platinum from molten nitrates which in these cases behaves as a reactive solvent. The results are found to be complicated by a rapid reduction of the nitrate melt by the depositing metals. Thus no evidence of the birth of a new phase could be obtained. The corresponding ionic diffusion coefficient was evaluated by each voltammetric technique and the values obtained compared to those reported in the literature.

A novel feature of the electrochemical investigations in LiCl-KCl eutectic at $\sim 450^{o}C$ was the successful use of vitreous carbon substrate for the study of nucleation and crystal growth processes of Cu(I) and Co(II). The relation between the potentiostatic current-time transients and the nuclear density for these systems has been established. Attempts to use other electrode materials to study the deposition of silver from alkali molten chlorides were made using electrodes of platinum, tungsten, copper and nickel but no reproducible results for the last three electrodes were obtained.

CONTENTS

1. INTRODUCTION

Molten salts are useful non-aqueous solvents for electrochemical studies. They have many remarkable and attractive characteristics, such as their ionic character, their high electrical and thermal conductivity and their ability to dissolve a wide range of other ionic compounds. Molten-salt systems are also of increasing technological importance in metallurgy, glasses, fuel cells and, more recently, in the development of nuclear and conventional power and space engineering. For theoretical purpose, they can be regarded as a novel class of simple ionic liquids providing a focal point for currently developing theories of the liquid state.

From the practical point of view, molten salts may be classified in terms of their melting points which may restrict the application of conventional techniques. Nitrates, for instance, have low melting points and it is possible to apply most of the established electrochemical procedures to their eutectic systems. It is thus possible to use a range of solid electrodes commonly used in aqueous or non-aqueous systems at room temperature or even liquid metal electrodes such as mercury. The simplest, although not the lowest melting ionic solvents are the alkali metal halides and their eutectic mixtures have been frequently employed and studied. The other less simple ionic liquids include the other oxy-anion liquids apart from alkali metal nitrates, i.e. alkali molten nitrites, acetates, thiocyanates, sulphates and carbonates. Even more complex melts are the molten phosphates, borates and silicates which contain highly polymerized anionic species. All of these fused salt systems can be studied at temperatures less than 1000^{o}C, whilst other molten electrolytes such as molten oxides require temperatures $\geqslant$ 2000^{o}C.

The essential aspects of high temperature work are initially concerned with the design of furnaces and apparatus for the control and measurement of temperature; the choice of a suitable container which may be glass, metal, graphite or porcelain; the purification of melts by prolonged vacuum drying followed by fusion in an inert or other gaseous atmosphere to minimise hydrolytic decomposition; filtration and pre-electrolysis using inert electrodes may also be carried out and finally, probably the most important, the design of electrodes. It is evident that progress of work involving molten salts has been retarded by these difficulties. A prime problem, for example, is that of finding a suitable

container which is not attacked and corroded by the particular molten salt. Pyrex glass can be used at $\sim$ 550°C but beyond this temperature it begins to soften. Glasses are also subject to chemical attack by alkaline oxides and hydroxides as well as by molten fluoride. At higher temperatures, silica can be used although it is also easily attacked by alkalis. Graphite or molybdenum crucibles are suitable up to $\sim$ 2000°C, though the former may introduce a range of impurities and they frequently crack upon cooling.

The preparation of reference electrodes is another major problem. Different workers use different reference electrodes depending upon the nature of the system and the temperature. No universal all-purpose reference electrode for molten-salt systems is available. Nevertheless, a metal whose ions dissolve readily in most melts (such as Ag/Ag(I), Pt/Pt(II)) is frequently used, while gas electrodes such as chlorine or oxygen are much less frequently used, if only because their handling is inconvenient. A typical reference electrode needs to be reproducible, constant in emf over long periods, robust and compatible with the melt at the working temperature. Of particular importance is the junction of the electrode compartment with the bulk melt, which must be such that the extent of contamination is reduced to a minimum.

The working electrode may be of liquid metal which is ideal for high temperature systems as the surfaces would be homogeneous and smooth. There are, however, limitations on the range of such electrodes because of the temperature ranges, because of undesired reactions with the melt and because of technical problems of maintaining free flowing capillaries. For most investigations in molten salts, therefore, solid electrodes are more extensively used. Platinum wire may be sealed in a suitable glass bead then into a glass tubing protruding from the seal, be welded to a hemispherical sphere or be ground flat as a planar surface. Tungsten which has the same thermal expansion coefficient as Pyrex glass or other borosilicate glasses is a potentially attractive alternative but this material frequently splinters during fabrication due to defects in its structure. Vitreous carbon rods can be sealed into glass tubing and after being well polished and cleaned can be used in molten nitrates and chlorides. The choice of suitable insulating material is thus seen to be a vital part of the construction of electrodes. Apart from these problems, there still remain some others, such as the seepage of melt

between electrode and insulator and the solubilities of metals in melts. Nevertheless, once the problems of melt purification, electrode fabrication and reference electrode preparation have been overcome, then, following the substantial recent improvements in instrumentation, the application of voltammetric techniques to melts becomes a convenient and rapid basis of electrochemical studies.

Electrochemical investigations in molten-salt systems have been recently concerned with nucleation and growth phenomena[1]. These processes have been extensively studied in aqueous systems[2-10] and some nucleation processes in molten salts are similar in character to those observed with aqueous solutions. However, many processes are found to be complicated by the influence of several factors associated with the high temperature conditions.

For example, at high temperatures, intermetallic solubilities, say between the metallic electrode and the depositing metal, enhance the likelihood of alloy formation. Furthermore, some depositing materials may react further with the oxidising solvent to form metal oxides. To avoid this latter complication, it would be useful to turn to liquid electrodes such as mercury which are widely used in aqueous solutions, but this is seldom possible in molten salts because of the increase in vapour pressure of mercury at higher temperatures. In any case, the ease of oxidation of other liquid metals may give rise to similar problems.

In molten salt systems, it is found that the early stages of metal deposition depend crucially on the surface state of a platinum substrate, i.e. its degree of oxidation. An oxide-covered electrode which may be free from intermetallic penetration is found to require a considerable nucleation overpotential. On the other hand, a pre-treated, oxide-free electrode behaves in a simpler way and free from surface effects.

It should be noted that these interferences are actually concerned with the interaction between electrode/melt (e.g. to form platinum oxide), newly-deposited materials/melt and electrode/newly-deposited materials. Some are evident experimentally, some are speculations, but all are likely to have influence on the formation of nuclei. It is not yet clear at which stages of nucleation these complications take place and it will probably require more than just electrochemical studies for them to be properly delineated.

In some metal deposition processes, there is no evidence of nucleation. It is likely that such metal deposition reactions proceed by a different mechanism, for example, by monolayer formation or underpotential deposition.

As mentioned above, the study of nucleation on platinum is often influenced by its surface oxides. Because of these uncertainties, it seemed appropriate to seek alternative electrode materials such as vitreous carbon. The characteristics of vitreous carbon depend on its preparation. Normally, it is produced by the slow pyrolysis of organic polymers containing some degree of cross-linking. It resembles a black glass with typical fracture characteristics. Glassy carbon has a low density and closed microporosity. It is inert to chemical attack and withstands high temperatures. This electrode can therefore be usefully employed widely for molten-salt investigations.

No studies of nucleation of metals on vitreous carbon in fused salts have been made hitherto, although some electrodeposition reactions on it have been studied. In the present work it was used as a substrate for nucleation of various metals from both aqueous solutions and molten salts. In several cases nucleation is found to take place on vitreous carbon but not on the other common electrode materials. Because of this, it seems probable that glassy carbon will be more widely used in the study of nucleation from molten salts.

On the other hand, there are disadvantages to its use particularly at higher temperatures. After such experiments the electrode frequently cracks on being cooled and even at lower temperatures its surface porosity may introduce uncertainties. Nevertheless, its present use here in the galvanostatic and potentiostatic studies of nucleation was found to be highly satisfactory.

In the study of the initial stages of metal deposition onto foreign substrates it is desirable that, as far as possible, the surface state remains unchanged. However, metal surfaces may form the oxide layers which impose a barrier to the nucleation process. Furthermore, they may readily adsorb impurities, possibly at the active centres important for the crystal growth process. Although because the measurements can be made in highly purified solutions they are ever sensitive to surface effects. To minimise some of these difficulties it is possible to investigate on a substrate of microscopic area whereby the degree of

surface oxidation and the extent of surface adsorption are probably less. This arrangement also confers the advantage that the diffusive flux of the electroactive species to the microsurface is very high.

In addition to using electrodes of small area, it is generally convenient to make observations of the kinetics of nucleation at a particular overpotential over a short time interval, i.e. before other factors intervene. The so-called transient techniques involve the perturbation of the equilibrium state of the electrode by means of an abrupt change of the applied overpotential (potentiostatic method) or of the applied current (galvanostatic method). The relaxation of the non-equilibrium state back to that of equilibrium can be followed through the resulting current-time transients and the overpotential-time transients respectively. The potentiostatic method has an advantage that the effect of double layer capacity can be minimised because it is charged much more rapidly and to a known potential. The galvanostatic method is not convenient in this respect, especially when used to investigate a fast electrode reaction. It becomes difficult to define the 'zero time' of the faradaic process or, in other words, to separate the electrochemical process from the charging of the interfacial capacitance. Nevertheless, in the present study of nucleation kinetics, the analysis of the galvanostatic potential-time relation has proved to be one of the most fruitful methods. This remark is not intended to belittle the importance of the linear sweep method which is invariably used in the preliminary examination of electrode processes including those involving phase formation. In fact, the technique most usefully displays the immediate aspects of complex electrode processes, though, in general, little quantitative kinetic information can be deduced because of the present difficulties in establishing a firm theoretical foundation of the method. The linear sweep method as used here also reveals qualitatively some of the associated reactions coupled with the main electrode process. Often, it is helpful to apply both electrochemical and optical techniques, especially electron microscopy.

Another promising mathematical tool for analysing nucleation phenomena, as well as the behaviour of more conventional electrochemical systems are the simulation methods based on finite difference algebra and the consequent numerical procedures. These are invariably concerned with the implicit or explicit methods of computer simulation. These

techniques based on high speed digital computers have recently been rapidly expanded and applied to several electroanalytical relaxation techniques for which previously only approximate analytical theories had been obtained. It may be anticipated that the future studies of nucleation will rely increasingly on these methods.

The initial purpose of this research was to study the effect on metal deposition reactions of the surface oxides on platinum and especially in relation to the deposition of silver and copper and dissolution from aqueous alkali nitrates. These results are then compared to those observed at a vitreous carbon electrode. The effects of platinum oxide were further investigated in a study of the deposition of silver from molten alkali nitrates. A further purpose was to study the kinetics of nucleation of silver on vitreous carbon in nitrate melts. That study was extended to include the electro-reduction of lead, cadmium, cobalt, nickel and copper on platinum. Vitreous carbon was also used to study the nucleation of copper and cobalt from molten alkali chlorides. Attempts were made to employ other electrode materials to study metal deposition from chloride melts, such as tungsten, copper, nickel and platinum. Only in the case of the last named metal were useful results obtained.

2. A BRIEF SUMMARY OF PREVIOUS WORK IN MOLTEN SALTS

2.1 Molten nitrates as solvents for electrochemical studies

2.2 Previous studies of electrode processes in molten nitrates

2.3 Previous studies of electrode processes in molten chlorides

2.1 Molten nitrates as solvents for electrochemical studies

Several comprehensive reviews[11-21] of the electrochemistry of molten salts have recently been published and it seemed sensible here to concentrate attention on previously published studies of electrode processes in alkali molten nitrates and chlorides which are directly or closely related to the present work.

Molten alkali nitrates are non-aqueous ionic solvents having many desirable physical characteristics, i.e. they are colourless, they have low vapour pressures, low viscosities and high electrical conductivities. In addition, they have low melting points which make it possible to apply conventional electrochemical techniques similar to those used with aqueous systems.

Molten equimolar $NaNO_3$-KNO_3 eutectic has a melting point of 228°C and cathodic and anodic decomposition potential limits of -1.3 and +1.2 V *vs* Ag/Ag(I)(0.07 M)[22]. It is therefore very useful for basic investigations of the electrodeposition-dissolution reactions of a range of metals. There remains some controversy as to its exact chemical nature and, in particular, as to the nature of the oxidizing species. In an early study Kust and Duke[23] postulated that it is the nitronium ion which is the oxidizing agent and which is formed from the self-dissociation of NO_3^- by the reaction

$$NO_3^- \rightleftharpoons NO_2^+ + O^{2-} \qquad (2.1)$$

followed by

$$NO_2^+ + NO_3^- \rightleftharpoons N_2O_5 \xrightarrow{\text{slow}} 2NO_2 + \tfrac{1}{2}O_2 \qquad (2.2)$$

This mechanism can account for the thermal decomposition of nitrates at high temperature as shown in equation (2.2). Besides this, the nitronium ion has been assumed as act as an intermediate in the kinetics of related non-electrochemical reactions[17]. However, using the galvanostatic method Topol *et al*[26] found no evidence of nitronium ion in this melt at 280-350°C. They proposed instead that the acidic species is nitrogen dioxide itself, i.e.

$$2NO_3^- \longrightarrow 2NO_2 + \tfrac{1}{2}O_2 + O^{2-} \qquad (2.3)$$

They also attributed the cathodic limiting potential at -1.6 V *vs* Ag/Ag(I) to the reduction reactions

$$NO_3^- + 2e^- \longrightarrow NO_2^- + O^{2-} \qquad (2.4)$$

or

$$NO_3^- + e^- \longrightarrow NO_2 + O^{2-} \qquad (2.5)$$

and the anodic limiting potential at 1.2 V to the oxidation reaction

$$NO_3^- \longrightarrow NO_2 + \tfrac{1}{2}O_2 + e^- . \qquad (2.6)$$

These observations by Topol *et al* as well as of others[27] are in agreement with those of Swofford and Laitinen[22] who followed an earlier electrochemical investigation of the $NaNO_3$-KNO_3 eutectic by Hills and Johnson[28].

There is also disagreement on the nature of basic oxygen species apart from NO_3^-. Recently, Zambonin and his co-workers[29-34] have suggested that the stable basic species found in nitrate melts are the superoxide ion O_2^- and the peroxide ions O_2^{2-} arising from the reactions

$$NO_3^- + O^{2-} \longrightarrow NO_2^- + O_2^{2-} \qquad (2.7)$$

$$2NO_3^- + O_2^{2-} \longrightarrow 2NO_2^- + 2O_2^- \qquad (2.8)$$

and

$$O_2^{2-} + O_2 \longrightarrow 2O_2^- \quad . \qquad (2.9)$$

Zambonin has pointed out that the failure of previous workers to detect these oxide ions is the result of contamination by impurities by water and by reactions with the glass container. To eliminate this problem, he prepared his nitrate melts in a specially designed vacuum tight cell of platinum. He has also used a platinum tube to protect the glass tubing of his rotating disc and reference electrode, although, whether and to what extent the melt may have penetrated between the platinum and the glass tubes is perhaps not certain.

One final view is that of Kerridge[35-37] who is inclined to accept the existence of a short lived acidic nitronium ion in the nitrate melt. He is also largely in agreement with the conclusions of Zambonin regarding the range of oxide species.

2.2 Previous studies of electrode processes in molten nitrates

Steinberg and Nachtrieb[38] were the first to use a dropping mercury electrode in molten nitrates. They investigated the reduction of Ni(II), Pb(II), Cd(II) and Zn(II) in the ternary eutectic melt $LiNO_3$-$NaNO_3$-KNO_3 at 150°C. The Ilkovic equation was verified and used to calculate the diffusion coefficients of the dissolved ions. These were stated to depend markedly upon the extent of residual water in the melt, which is difficult to remove from system containing lithium ions. Similar polarographic studies in molten ternary nitrates were carried out by Inman *et al*[39] in which greater care was taken to dry the eutectic as well as the added salts.

Inman and Bockris[40] applied the galvanostatic technique to determine the diffusion coefficients of various dissolved ions in molten nitrates and chlorides, e.g. Ag(I), Pb(II), Cd(II) in molten $NaNO_3$-KNO_3 at 264°C and Pb(II) in LiCl-KCl at 400°C and for Ag(I) over a range of temperatures. In each case the Sand equation was obeyed. They suggested that for metals, such as Pb and Cd, which were liable to oxidation by the nitrate solvent a solid working electrode was inappropriate. Instead, they used the hanging drop mercury electrode and were the first to do so at temperatures > 200°C.

The voltammetric characteristics of metal deposition at a mercury electrode were normal but not so when a solid electrode was employed. Mamantov *et al*[41] observed a pre-peak and occasionally a post-peak in the deposition of Pb(II) onto Pt using the linear sweep method, the post-peak being attributed to the reduction of metal oxide. Two peaks were observed for the reduction of $Cu(NO_3)_2$ and three peaks for $CuCl_2$. No firm conclusions concerning these multiple charge transfer steps could be drawn. The voltammograms for the reduction of Cd(II) were more 'drawn-out' and the 'n' value was usually less than 1. The silver deposition reaction, however, showed the characteristics of a simple reversible reaction with no evidence of a complicating reaction between the depositing metal and the nitrate solvent.

Linear sweep voltammetry was used by Behl and Gaur[42] to study the reduction of Ag(I) and Pb(II) on Pt in molten $NaNO_3$-$Ba(NO_3)_2$ eutectic at 350°C. The peak current was linearly dependent on the concentration of Ag(I) and on the square root of the sweep rate up to 6 V sec^{-1}. The reduction of Pb(II) showed, again, a post-peak at the sweep rate $\sim$ 9 V sec^{-1},

whilst at higher sweep rates (20-130 V sec^{-1}), a single peak appeared. Behl and Gaur accounted for this in terms of reduction of lead oxide which was thought to be a negligible factor at high scan rates.

Narayan and Inman[43] used chronopotentiometry to study the deposition of Ni(II) and Co(II) on platinum microelectrodes in molten $NaNO_3$-KNO_3 eutectic at 300°C. The oxidation of cobalt by nitrate was more rapid than for Ni(II), resulting a black layer of oxide on platinum surface. Current-reversal chronopotentiometry was used to remove the metal oxide and thereby to maintain a clean electrode surface which could be used repeatedly.

Casadio et al[44] examined the reduction of Cd(II) on Pt in molten $NaNO_3$-KNO_3 at 325°C by current-reversal chronopotentiometry. The results showed that the cathodic discharge of Cd(II) involved a charge transfer reaction followed by the irreversible oxidation of $Cd + NO_3^- \longrightarrow CdO + NO_2^-$. The latter reaction was evident from the splitting of the anodic transition time into two sections.

Hills et al[1] investigated the electrodeposition of Ag(I) on platinum in molten $NaNO_3$-KNO_3 eutectic at 275°C using linear sweep voltammetry, potential step and galvanostatic methods. In each case, the diffusion coefficient was calculated and discrepancies between the values were noted, arising it was suggested from neglect of a precursor step involving three dimensional nucleation and growth. The occurrence of nucleation was confirmed from electron micrographs. Attempts were also made to study the kinetics of nucleation of silver from this melt using the double potential step technique. Non-linear logarithmic plots of relaxation time (i.e. the time required for the growth of stable nuclei) against the overpotential were observed. The existing theory of nucleation was further developed by taking into consideration the effect of nuclear size and interfacial tension.

Baraboshkin et al[45] investigated the deposition of Ag(I) on platinum in molten $NaNO_3$-KNO_3 eutectic at 250°C using the galvanostatic technique. All the investigations showed maxima on the resulting potential-time curves which increased with increasing applied current density and a corresponding decreased of time from the beginning of the constant current pulse to the point of maximum potential. This was also the case for the deposition of silver from pure molten $AgNO_3$ although the shape of peak potential maximum was sharper, i.e. the decrease of overpotential after

the maximum occurred more rapidly. The authors explained these observations as follows. In both cases, the maximum potential could be regarded as a crystallization overpotential. Silver nuclei grew on the platinum surface more easily and rapidly in the pure $AgNO_3$ melt, resulting in a sharp maximum peak potential followed by a sharp fall, reaching a state whereby the growth of further nuclei seemed unlikely. The surface state of the platinum substrate, i.e. its degree of oxidation, was found to affect the magnitude of the maximum potential. The platinum electrode was anodically pretreated at the potential +1 to +4.4 V *vs* Ag/Ag(I) before the galvanostatic transients were recorded and showed an increase of magnitude of the maximum potential. This effect was almost certainly the result of the formation of a thick layer of platinum oxide. In their paper, Baraboshkin and his co-workers also referred to their previous work concerning the galvanostatic studies of the deposition of copper and silver in chloride melts. In such investigations, no maximum on the potential-time response was observed. They attributed this to alloy formation of these metals with platinum, especially at the higher temperatures of 380-700°C.

Toschev *et al*[46] studied the kinetics of nucleation of Ag(I) on platinum in molten $NaNO_3$-KNO_3 eutectic using the double potential step technique. The logarithmic rate of nucleation was found to vary linearly with the reciprocal of the square of overpotential in accord with the classical theory of nucleation. The slope of the line at temperature 281°C was greater than that at 316°C in accordance with the understanding that lower overpotentials are required for nucleation in molten salts in comparison with lower temperature aqueous system. However, the main features of the process of heterogeneous nucleation in both systems were similar.

Bansal and Plambeck[47] have studied the deposition of Tl(I) on a mercury drop electrode in calcium nitrate tetrahydrate at 50°C using galvanostatic, potentiostatic and cyclic voltammetric methods. Here also the early stages of metal deposition were controlled by a nucleation process. The maximum in the galvanostatic potential-time transients, the shape of the potentiostatic growth transients and the anodic migration of the reduction peak potential in subsequent cyclic voltammetric scan were all in accord with a process of nucleation.

Inman et al[48] measured the exchange current density for the molten salt system $Ag/AgNO_3$, $NaNO_3$-KNO_3 by means of the single pulse galvanostatic method. A fast response instrument was developed so that the interfacial capacitance, the ohmic overpotential and the exchange current could be deconvoluted and determined from one experiment. The method was sophisticated but limited in its application.

2.3 Previous studies of electrode processes in molten chlorides

Molten alkali chlorides have also been used extensively as solvents for electrochemical investigations. Molten LiCl-KCl eutectic at $\sim 450^{\circ}C$ has a wide potential range (~ 3 V) between its cathodic and anodic decomposition limits. The cathodic limit is set by the deposition of lithium and the anodic limit by the chlorine evolution reaction. At higher temperatures, the deposition of potassium predominates. Special precaution needs to be taken to purify this eutectic, since lithium salts tenaciously retain traces of moisture. Even prolonged drying of the eutectic mixture in vacuo followed by melting in an inert gaseous atmosphere is insufficient to avoid hydrolytic decomposition. Laitinen et al[49] therefore suggested drying by treatment with excess hydrogen chloride to displace the hydrolytic equilibrium.

$$H_2O + Cl^- \rightleftharpoons OH^- + HCl\uparrow$$

to the left. Since then this method has become widely used in the routine purification of chloride melts.

Early studies in molten chlorides were mainly concerned with the determination of diffusion coefficients. For example, diffusion coefficients for Ag(I), Cu(I), Cd(II) and Bi(III) in molten LiCl-KCl at $450^{\circ}C$ were evaluated by Laitinen and Ferguson[50] using the chronopotentiometric technique. Laitinen and Gaur[51] obtained diffusion coefficients for Cd(II), Co(II), Pb(II) and Tl(I) in the same system using the same method. Thalmayer et al[52] measured the diffusion coefficients of various solute ions in the LiCl-KCl eutectic at various temperatures. Large deviations of these values were noted and ascribed to uncertainties in the solute concentration. Chronopotentiograms for the reduction of Zn(II) and Cd(II) on a liquid bismuth pool electrode in LiCl-KCl eutectic were obtained by Van Norman[53] and diffusion coefficients for these ions were evaluated.

Hills et al[54] studied the deposition of nickel and silver on platinum from molten LiCl-KCl eutectic at 400°C using chronopotentiometric, cyclic voltammetric and potentiostatic methods. The deposition of nickel was observed to take place via monolayer formation, this underpotential predeposition occurring at 0.4 V anodic to the main reduction peak. A potentiostat and phase-sensitive detection system were used to examine the monolayer formation. A similar, but less well-defined underpotential deposition peak was obtained for silver at 0.1 V anodic to the main reduction peak. Diffusion coefficients of both ionic species were calculated from each technique and were in satisfactory agreement with published values.

Inman and Lovering[55] have, however, proposed an alternative explanation for this observation in terms of the discharge of adsorbed nickel ions taking place before the main discharge reaction. Nevertheless, no clear-cut separation of these two mechanisms has been confirmed. Specular reflectance studies strongly support the existence of metal monolayers.

Linear sweep voltammograms for the deposition of Ag(I) on platinum in LiCl-KCl at 450°C were recorded by Behl[56]. He also observed a pre-deposition peak at potentials 0.5 V positive to the main reduction peak and at sweep rate > 2 V sec^{-1}. The voltammogram also showed two peaks on the anodic dissolution region. At lower sweep rate, however, a single peak was obtained. Behl has accounted for the pre-deposition peak to monolayer formation of silver and the small anodic peak to the dissolution of the monolayer and thus supports the view of Hills et al[54].

Behl[57] has also investigated the reduction of Ni(II), Co(II), Cd(II) and Pb(II) at vitreous carbon in molten LiCl-KCl eutectic at 450°C by the linear potential sweep technique. Current peak heights were as expected dependent upon concentration and the square root of the sweep rate in the range of 0.01 to 1.0 V sec^{-1}. Diffusion coefficients for these dissolved ions were calculated and discrepancies from previously reported values were noted.

Lantelme et al[58] determined the diffusion coefficient of Cu(I) to vitreous carbon in molten LiCl-KCl eutectic at 400°-480°C. Both the capillary method and chronopotentiometry were used and both gave results in good agreement with each other. The galvanostatic transient of Cu(I) on vitreous carbon also showed a potential maximum indicative of nucleation and crystal growth.

Reddy[59] studied the deposition of Ag(I) on platinum in fused LiCl-KCl at 450°C using galvanostatic and potentiostatic methods. After the silver had been deposited on the platinum, the electrode was allowed to remain in the melt for a certain period of time before being subjected to anodic stripping. The substrate surface was then examined by emission spectroscopy which indicated the persistence of silver on or in the platinum. This was further evident by X-ray milliprobe studies. The possibility of alloy compound formation between silver and lithium from the melt, as indicated from electron diffraction, has also been discussed.

In a series of papers, Naryshkin and his co-authors[60-62] reported linear sweep diffusion coefficients for Ag(I), Pb(II), Bi(III), Co(II), Ni(II), Mn(II), Cr(II), Tl(I), Cd(II), Cr(III) and Cu(I) on platinum in molten LiCl-KCl eutectic in the temperature range 360-560°C. Peak currents were dependent upon the square root of the sweep rate. Linear plots of log D *vs* 1/T were obtained, the slope of which giving the activation energies of each diffusing metal ions and found to be in good agreement with previously published data. Oscillographic polarograms for the reduction of trivalent chromium ions exhibited two peaks which were ascribed to the two step reduction mechanism, i.e. $Cr^{3+} + e^- \longrightarrow Cr^{2+}$ and $Cr^{2+} + 2e^- \longrightarrow Cr$.

Laitinen *et al*[63] measured the exchange currents corresponding to a wide concentration range of Cd(II) and Zn(II) in molten LiCl-KCl eutectic using the double pulse method of Gerischer and Krause[64] and the voltage step method of Vielstich and Delahay[65]. A tungsten microelectrode was chosen to avoid the intermetallic compound formation which can occur with platinum. The exchange currents and transfer coefficients were determined and found to be in agreement with those of Laitinen and Gaur[66].

Hill *et al*[67] measured the exchange currents and the rate constant for the reaction $Ag \rightleftharpoons Ag^+ + e^-$ in molten $LiNO_3$-$NaNO_3$-KNO_3 and molten LiCl-KCl, and of the reaction $Ti^{2+} \rightleftharpoons Ti^{3+} + e^-$ in molten LiCl-KCl using the a.c. impedence technique. Results were in good agreement with previously determined values.

Inman and Weaver[68] studied the properties of an anodic oxide film formed on platinum in molten LiCl-KCl eutectic containing oxide ion (added as Li_2O) at 430°C using galvanostatic, potentiostatic and e.m.f. decay transients. The formation of oxide film could be explained by the same 'place exchange' mechanism as in aqueous systems[69,70]. It was evident

that the exchange between metal-oxide ions, i.e. Pt^{+2} and O^{2-}, was probably a slow process and hence the rate-determining step. The reduction of the film took place over a wide potential range and was ascribed to an inhomogeneity of site energies within the oxide layer. Recent work concerning the platinum oxide film was reviewed by Weaver[71].

Although this literature survey has been restricted to a certain area of research in molten salts, it seems inappropriate to overlook work from the Russian school of Delimarskii. In fact, this author and his co-workers have published an impressive number of papers based on their work in fused salt systems. Much of the work may be found in the book of Delimarskii and Markov.[21] The most recent sources of references, information, data and reviews for molten salts were collected, examined and summarized by Janz, Allen and Tomkins[72].

3. THE THEORY OF VOLTAMMETRY AT STATIONARY SOLID ELECTRODES

3.1 Introduction

Electrode processes are concerned with a sequence of reactions: (i) the charge transfer reaction, (ii) the transfer of electroactive species to the electrode surface and (iii) the associated reactions at the electrode surface. The overall rate of electrode processes is principally determined by the slowest of these three steps. The magnitude and type of 'overpotential', which is the potential difference between the applied potential and the reversible potential measured against a suitable non-polarized reference electrode, will therefore be specified by the slowest step.

The charge-transfer step of metal deposition reactions in molten salt systems is invariably fast, and thus the overall rate of the reaction is controlled by the rate of mass transfer of electroactive species to the electrode surface. Such electrode reactions are called mass-transfer controlled or, more loosely, reversible processes. This is the case when the ohmic overpotential is minimised and the overpotential relating to charge-transfer is negligibly small, i.e. the electrode exhibits no activation overpotential. Hence, only the concentration overpotential becomes important for it is associated with the rate-determining mass transport of electroactive particles from the bulk solution to the interphase.

The overall rate of mass transfer is normally dependent on three processes: diffusion, convection and migration. Diffusion takes place as the result of concentration gradients whereas convection is observed when the solution is stirred mechanically or thermally. Migration arises from the movement of charged particles under the influence of an electric field. Among these three different modes of mass transfer, diffusion is the most widely involved in voltammetry; invariably migration is suppressed by a large excess of inert, supporting electrolyte, (which makes the transport number of the electroactive species effectively zero) and convection is eliminated by working in unstirred solutions and using polarisation times which are not too long. Thus diffusion is the only means whereby the electroactive species arrives at the electrode surface. The current will then be controlled by the diffusive flux of electroactive materials to the electrode interface. It should be stated here that throughout this study the treatment of electrode processes involves only diffusional mass transfer. Adsorption effects at the electrode surface are not considered.

The rate of diffusion to an electrode depends on the electrode geometry which can be chosen as desired. In other words, the transport of the electroactive species may occur by semi-infinite, linear, spherical or cylindrical diffusion. The theoretical expression for current-voltage-time relationship in each case is also dependent upon the experimental conditions. For example, the equilibrium rest potential of the working electrode (at zero current) can be changed by applying a sudden voltage difference, a sudden current difference or a continuously varying voltage difference. The first method gives rise to a current, the second method to a clearly defined transition time and the third method to a well-defined peak current, each of which is of primary analytical importance. These methods are briefly discussed as follows.

3.2 The potential step method

This technique is concerned with a sudden change of the potential of the working electrode to a specified value which is kept constant thereafter. The electro-reduction or oxidization of one of the species in solution will cause depletion of the surface concentration of the reactants and give rise to changes of the concentrations of reactants and products as a function of the distance from the electrode surface and of time, the so-called 'concentration profile'. By means of Fick's laws of diffusion and taking boundary and initial conditions into account, Delahay[73] solved the differential equation analytically and obtained an expression for the resultant current for the case of linear diffusion to a planar surface, which is directly proportional to the flux of electroactive species at the electrode surface, x = o, as given by

$$I = zFAJ(o,t) \quad , \tag{3.1}$$

where z is the number of electrons involved in the reduction of each molecule of substance O, F is the faraday and A is the geometric electrode area.

By substituting the correct value of the flux of O, J(o,t) in equation (3.1), the current-time relation will then be

$$I = zFAD_O^{\frac{1}{2}}c \; \frac{1}{\pi^{\frac{1}{2}}t^{\frac{1}{2}}} \quad , \tag{3.2}$$

where I is in amp, F in coulombs, A in cm^2, D_O in $cm^2\ sec^{-1}$, c in mol cm^{-3} and t in sec.

It is seen that the observed current is directly dependent on the bulk concentration and decays with time, approaching zero at long polarisation times. A plot of I vs $t^{-\frac{1}{2}}$ gives a straight line passing through the origin and the diffusion coefficient can be calculated from the slope.

For different shapes of working electrode, e.g. for spherical electrode and hence spherical diffusion, the current-time relationship is given by

$$I = \frac{zFAD^{\frac{1}{2}}c}{\pi^{\frac{1}{2}}t^{\frac{1}{2}}} + \frac{zFADc}{r_o} \quad , \tag{3.3}$$

where r_o is the radius of a shpere and A is the electrode area, i.e. $4\pi r_o^2$. The current is seen to be composed of two terms, i.e. the time-dependent and the time-independent terms. At long electrolysis times, the current is virtually equal to the time-independent term, i.e.

$$I = \frac{zFADc}{r_o} \quad . \tag{3.4}$$

It is to be noted that for very small electrode radii, this term becomes predominant.

For cylindrical diffusion, the current-time relation is

$$I = \frac{zFADc}{r_o}\left[\frac{1}{\pi^{\frac{1}{2}}\phi^{\frac{1}{2}}} + \frac{1}{2} - \frac{1}{4}\left(\frac{\phi}{\pi}\right)^{\frac{1}{2}} + \frac{\phi}{8} \quad \ldots\right] \quad , \tag{3.5}$$

where r_o is the radius and A the area of the cylindrical wire electrode and $\phi = Dt/r_o^2$. At short times of electrolysis, all but the first two terms can be neglected and the current is then still a linear function of $t^{\frac{1}{2}}$ as in the case of linear diffusion.

3.3 The current step method

This technique is also called the galvanostatic method. It is the converse of the potential step procedure. Instead of changing the potential and measuring the observed current, the current is changed instantaneously to a new value and the resulting variation of potential of working electrode with time is recorded.

As a result of the constant current the electrolysis proceeds and there is a progressive depletion of the electroactive species at the

electrode surface. As a consequence, the electroactive species will diffuse from the bulk solution to the electrode surface resulting a concentration gradient growing out from the electrode surface into the solution. When the surface concentration of reactants become zero, the potential of the working electrode varies abruptly until some new cathodic process occurs, e.g., the reduction of the cation of the supporting electrolyte. The interval of time between the beginning of electrolysis and the immediate change of potential is termed the 'transition time', designated by τ and which can be calculated by a clearly defined 'Sand' equation,

$$\tau^{\frac{1}{2}} = \frac{\pi^{\frac{1}{2}} zFcD^{\frac{1}{2}}}{2I} \quad , \tag{3.6}$$

where τ is transition time, sec, I is current density in amp cm^{-2}, c is the concentration in mol cm^{-3} and the other symbols have their usual meaning.

The verification of these relationships is possible by assuming that D does not vary significantly with concentration. Then $\tau^{\frac{1}{2}}$ may vary either directly with concentration or with reciprocal of the current density. At constant current density, $\tau^{\frac{1}{2}}$ is thus directly dependent on the concentration.

Karaoglanoff[74] has solved Fick's law of diffusion and derived an expression for the potential-time relation of a reversible process.

$$E = E_{\tau/4} + \frac{RT}{zF} \ln \left[\frac{\tau^{\frac{1}{2}} - t^{\frac{1}{2}}}{t^{\frac{1}{2}}} \right] \quad , \tag{3.7}$$

where $o < t < \tau$, $E_{\tau/4}$ is the quarter-time potential, i.e. the potential when $t = \tau/4$. This potential corresponds to the half-wave potential in polarography. A plot of E vs $\log \left[\frac{\tau^{\frac{1}{2}} - t^{\frac{1}{2}}}{t^{\frac{1}{2}}} \right]$ should give a straight line with a slope $\frac{2.303RT}{zF}$.

3.4 The cyclic voltammetry method

This technique is one of the most powerful, particularly for investigations of intermediates in electrochemical reactions. In this work, it served as an excellent method for the study of the silver deposition and dissolution reactions and especially for the detection of a possible second anodic reaction.

The principle of cyclic voltammetry is that the potential of the electrode changes with time in a triangular wave form. It is increased at a constant rate up to a preset limit, e.g., ± 1 V from the equilibrium potential and then the direction of the sweep is reversed. There will be an electrode potential at which the electro-reduction or oxidation takes place and the measured current through the cycle will depend on the concentration of species present.

The applied potential, E, can be expressed as a linear function of time, i.e. as

$$E = E_i - vt \quad , \tag{3.8}$$

where E_i is the initial potential, v is the rate of potential change and t is the time of electrolysis.

By combining equation (3.8) with the Nernst equation and Fick's law of diffusion and again assuming initial and boundary conditions, an equation can be derived which relates the flux of reductant to the potential at the electrode surface. This differential equation was solved and transformed to a current-potential relationship by Randles and Sevcik. Details and original literatures are given by Delahay[73].

The qualitative explanation of the current-potential curve is as follows. When the applied potential approaches the reversible potential, a small current flows. As the potential of the working electrode becomes sufficiently cathodic, the reduction occurs and the current increases. This results in progressive depletion of reactants at the electrode surface. The two counteracting effects, depletion of reactants and increase in current as caused by changing of applied potential toward more cathodic values, give rise to a maximum. For linear diffusion to a planar stationary electrode, the rate of diffusive transport beyond the maximum falls and the observed current drops correspondingly. For reversible processes involving soluble reaction products, the well-defined maximum (peak) current is given by

$$I_p = 0.466 \frac{z^{3/2} F^{3/2}}{R^{\frac{1}{2}} T^{\frac{1}{2}}} A D^{\frac{1}{2}} c v^{\frac{1}{2}} \quad , \tag{3.9}$$

where I_p is in amp, A in cm^2, c in mol cm^{-3}, D in cm^2 sec^{-1} and v in volt sec^{-1}. The numerical constant of equation (3.9) was derived by Nicholson and Shain[75]. This equation can be easily experimentally

verified for the peak height varies linearly with the square root of the sweep rate.

When the direction of potential change is reversed, the applied potential is progressively reduced first to zero and then to an anodic value of the same magnitude. The resultant voltammogram exhibits a peak height given as before by equation (3.9). For reversible processes, the reduction peak and re-oxidation peak are separated by

$$\Delta E = 2.2 \frac{RT}{zF} \quad \text{volts} \quad , \tag{3.10}$$

but with increasing irreversibility, the peak separation becomes progressively greater.

Delahay solved the boundary value problem for irreversible electrochemical reaction and obtained for the resulting peak current

$$I_p = \frac{0.282\,\pi^{\frac{1}{2}}F^{\frac{1}{2}}}{R^{\frac{1}{2}}T^{\frac{1}{2}}} z(\alpha n_a)^{\frac{1}{2}} A D_0 c v^{\frac{1}{2}} \quad , \tag{3.11}$$

where α is the transfer coefficient, n_a is the number of electron involved in the rate-determining step. The peak current is again proportional to $D_0^{\frac{1}{2}}$, c and $v^{\frac{1}{2}}$ as in a reversible process. Since α is less than unity and n_a is generally less than z, the peak current for irreversible process will be less than in case of the corresponding reversible reaction.

The equation for the peak potential also derived by Delahay is

$$E_p = E^o - \frac{RT}{\alpha n_a F} (0.780 - \ln k_o + 0.5 \ln D_0 b) \quad , \tag{3.12}$$

where k_o is the rate constant for the electrode process and

$$b = \frac{\alpha n_a F}{RT} v \quad . \tag{3.13}$$

From equations (3.12) and (3.13), it can be seen that the peak potential varies linearly as ln v. Consequently, a plot of E_p vs ln v will give a straight line enabling the values of αn_a and k_o to be calculated.

The case of a reversible electrode process involving the deposition of an insoluble substance has also been studied, i.e. by Berzins, Delahay[73] and Nicholson[76] and the equation of peak current obtained is

$$I_p = \frac{0.610 z^{3/2} F^{3/2}}{R^{\frac{1}{2}}T^{\frac{1}{2}}} A c D_0^{\frac{1}{2}} v^{\frac{1}{2}} \quad , \tag{3.14}$$

which is the same form as that for soluble product, the only difference being in the numerical constant. The corresponding peak potential is then

$$E_p = E^o + \frac{RT}{zF} \ln f_0 c - \frac{0.8539RT}{zF} \quad . \qquad (3.15)$$

3.5 The electrical double layer

The structure of the electrical double layer is of fundamental importance in the study of electrode kinetics. An electrical double layer exists when two phases are in contact. Across almost any boundary between two phases, i.e. between two materials, a potential difference will develop. An example of such a system is the interface between a metallic electrode and the electrolyte solution. This interface behaves like an electric capacitor being capable of storing electric charge.

The theories of the structure of the electrical double layer are several. The presently accepted theory is that of Devanathan, Bockris and Müller.[77] According to this theory, the electrode is covered with strongly oriented adsorbed water molecules. These water molecules are bound to the electrode at least partly by electrostatic forces which are directly proportional to the charge on the metal. When this charge approaches zero, the water molecules are bound relatively poorly to the metal surface, hence specific adsorption of ions can take place by a replacement of some of these water molecules by some of partially desolvated ions. The locus of the centroids of these adsorbed ions is called the inner Helmholtz plane (IHP). Adjacent to this layer is a layer of water molecule which is not so oriented because these water molecules are under the influence of both the electric field and thermal fluctuation. They behave like a secondary hydration sheath of an ion. Some of these water molecules belong to the primary hydration sheath of the metal ions. The plane passing through the electrical centres of these metal ions is known as the outer Helmholtz plane (OHP). An important quantity which affects the calculation of the capacity of the double layer is the dielectric constant of the medium, which, between the metal and the IHP is about 6 to 7, whilst between the IHP and the OHP is about 30 to 40.

The investigation of the structure of the double layer can be made directly by measuring the interfacial tension or the differential capacity, or indirectly by its effect on electrode processes. For example, in galvanostatic experiment, when a constant current is applied, the double

layer is charged before the onset of the charge-transfer reaction. This is reflected in the initial sharp rise of the resulting potential-time response. The charging process is relatively fast, i.e. < 10 μsec and usually does not interfere with the main process unless a very fast reaction is being studied. The determination of the capacity of the double layer can simply be made from the slope of the initial jump of the potential-time transients. For potentiostatic experiment, the resulting current-time curve shows an initial sharp rise due to double layer charging. The capacity of the double layer is calculated from the area under the curve.

The theories of electrical double layer for the metal-melt interface were discussed by Graves and Inman.[78] The interfacial capacitance can be measured by an impedance technique. Alternatively, the double layer charging could be separated instrumentally from the charge transfer process, provided the measurement was carried out in a sufficient short time.

In the sense that, in the limit, a molten salt is a very concentrated electrolyte solution it is to be expected that the interfacial capacitance between an inert electrode and a simple molten salt will resemble that for mercury in contact with, say, 5M aqueous $NaNO_3$. The capacitance will therefore be a shallow parabola contained in steeply rising 'walls' at those anodic and cathodic potentials where electrode reactions take place and faradaic factors intervene. There is direct experimental evidence for mercury in molten nitrates that this is so. At higher temperatures in more reactive melts and with presence of more reactive metals there is likely to be a larger contribution from pseudo-capacitances and even for platinum in LiCl-KCl it may be that there is no potential range over which the electrode is completely polarisable. The present evidence is that the interfacial double layer capacity at solid metals in molten salts is $\gtrsim 100$ μF cm^{-2} which may reflect both roughness and reactivity. In the presence of depositing metallic ions it is likely that ad-ion or ad-atom adsorption will occur and add greatly to any pseudo-capacitance. It is as well therefore to assume that the double layer capacity may be both large and potential dependent and that it should be determined directly in those experiments where its effects are finite.

4. GENERAL THEORIES OF NUCLEATION

4.1 Introduction

Nucleation describes the first act in the formation of a small new condensed phase. It is the precursor of crystal growth and of the overall crystallization process. In 1876 Gibbs[79] was the first to propose the concept of nucleation and to explain the necessity of 'critical' supersaturation or supercooling for nucleation.

The first report on 'critical supersaturation' phenomena was that of Fahrenheit[80] who described the sudden solidification of supercooled water upon mechanical agitation. In the following years much of the work on the supercooling of inorganic salts from aqueous solutions were carried out. However, results were less reliable because of poor reproducibility and although this phenomenon was repeatedly investigated, no satisfactory interpretation was forthcoming. It is interesting that, following the discovery of bacteria by Pasteur in 19th century, the reason for the lack of reproducibility of the critical supersaturation data was understood. Just as bacteria can fall from the air and start a culture in a suitable liquid, so microparticles such as dust can enter from the air into a saturated solution and induce what might be regarded as heterogeneous nucleation. When ions or impurities are removed from the system, a greater supersaturation is needed for the nucleation which is then called homogeneous or self-nucleation. The theories of homogeneous and heterogeneous nucleation from the vapour phase will therefore be described and extended to electrochemical systems directly related to the present work.

4.2 Theory of homogeneous nucleation[81]

4.2.1 Steady-state theories

The formation of a new condensed phase, as for example, the condensation of a vapour is initiated by statistical density fluctuation arising from random absorption and evaporation of single molecules. This will give rise to molecular clusters which decay unless they exceed a critical size. However, clusters exceeding the critical size will grow by accretion of molecules from the vapour to yield macrosopic of the new phase. The dynamic picture of nucleation in a supersaturated vapour is such that the 'critical' supersaturation pressure drives a large traffic of nuclei past the critical size with the result that a fog of liquid droplets is produced.

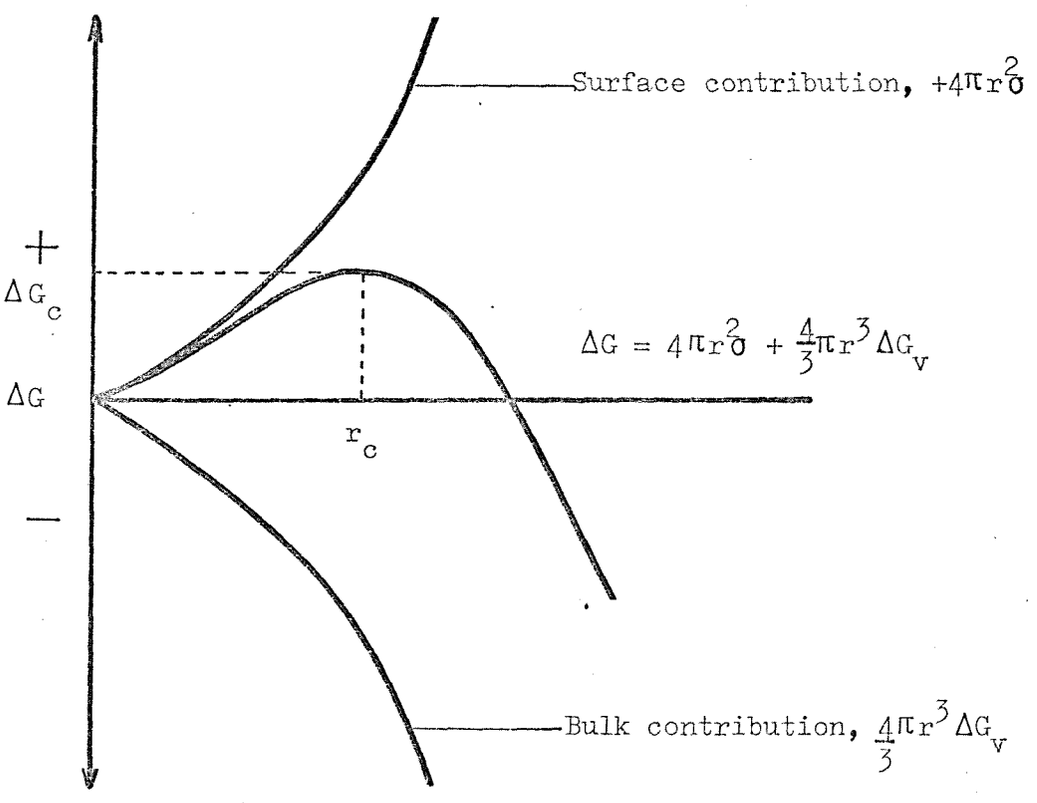

Figure 4.1 Free energy change ΔG of nuclei as a function of their radii. The surface and bulk contributions are separately shown. ΔG_c is the free energy of formation of critical nucleus.

According to steady state theories of homogeneous nucleation, each cluster develops initially with an increase in free energy until a critical size is reached, above which growth continues spontaneously with a decrease in free energy. The free energy of formation of clusters from supersaturated vapour is normally composed of two parts, namely the volume and surface free energies. The negative volume term arises from the decrease of free energy on condensing the vapour to bulk liquid and the positive surface tension from the creation of a new surface. Therefore, the condensed phase tends to minimise its surface area by forming a spherical shape in order to have lowest free energy and greatest stability. Hence the clusters are assumed to differ from bulk liquid in terms of a large surface to volume ratio. It follows that the Gibbs free energy of formation of nuclei is given by

$$\Delta G = \frac{4}{3}\pi r^3 \Delta G_v + 4\pi r^2 \sigma \ , \qquad (4.1)$$

where r is nuclear radius, σ is the surface tension and

$$\Delta G_v = -\frac{RT}{V_m} \ln \frac{p}{p_{eq}} \ , \qquad (4.2)$$

is the Gibbs free energy difference per unit volume of liquid between the supersaturated vapour of pressure p and bulk liquid of equilibrium vapour pressure p_{eq} and molar volume V_m. A plot of equation (4.1) as shown in Figure 4.1 shows the variation of the total free energy with the radius of the condensed phase which can be explained as follows.

Initially when the condensed phase is very small ($r < r_c$), the surface free energy term must be larger of the two terms on the right hand side of equation (4.1) and the free energy of formation ΔG increases with nuclear radius and becomes positive. Therefore, nuclei in this range of sizes are unstable. Above a critical size ($r > r_c$) however, the bulk contribution becomes larger and dominates since it increases as $\sim r^3$, but the surface contribution increases only as $\sim r^2$. The free energy of formation of supercritical nuclei is now negative and hence energetically favoured. Thus nuclei of that size or larger grow spontaneously. When ΔG approaches a maximum, i.e. $\frac{\partial \Delta G}{\partial r} = 0$, nuclei reach the critic size r_c which is represented by

$$r_c = -\frac{2\sigma}{\Delta G_v} = \frac{2\sigma V_m}{RT \ln \frac{p}{p_{eq}}} \ . \qquad (4.3)$$

By substituting equation (4.3) in equation (4.1), the maximum free energy of a critical nucleus will then be

$$\Delta G_c = \frac{16\pi\sigma^3}{3\Delta G_v^2} = \frac{4}{3}\pi r_c^2\sigma \quad . \tag{4.4}$$

Thus the total free energy of a spherical nucleus of critical size is one-third of its surface free energy.

Volmer[82] has defined the critical nucleus in two ways. The first is based on the dependence of the free energy on the radius and is the condition for maximisation of ΔG, i.e.

$$\frac{\partial \Delta G}{\partial r} = 0 \quad , \tag{4.5}$$

as clearly shown in Figure 4.1. The critical radius is then given by equation (4.3). The second definition is based on the dependence of the free energy on the number of atoms or molecules, i, belonging to the nucleus

$$\frac{\partial \Delta G}{\partial i} = \mu - \mu_{eq} = 0 \quad , \tag{4.6}$$

where μ and μ_{eq} are the chemical potentials of the critical nucleus and the supersaturated vapour respectively. This definition indicates that these two potentials are equal. This concept still allows the existence of an activation energy for nucleation, i.e. a local increase in free energy which is shown in Figure 4.1 and which is possible only by a small number of molecules undergoing a statistical fluctuation.

The rate of nucleation can be derived by two methods. The first was that of Volmer[82] in terms of metastable equilibrium, the so called pseudo-equilibrium model. The second was that of Becker, Doering and Zeldovich[83-85] which is essentially a kinetic model.

In order to calculate the rate of nucleation it is necessary to know first the concentration of critical nuclei. The concentration of critical nuclei cannot be calculated by Boltzmann statistics because during the nucleation process, no equilibrium state is attained and the supercritical nuclei grow spontaneously to macroscopic crystals. However, Volmer overcame this difficulty by assuming conditions of metastable equilibrium, i.e. critical nuclei which cannot grow further will redissolve. Under these conditions Boltzmann statistics can now be applied to give

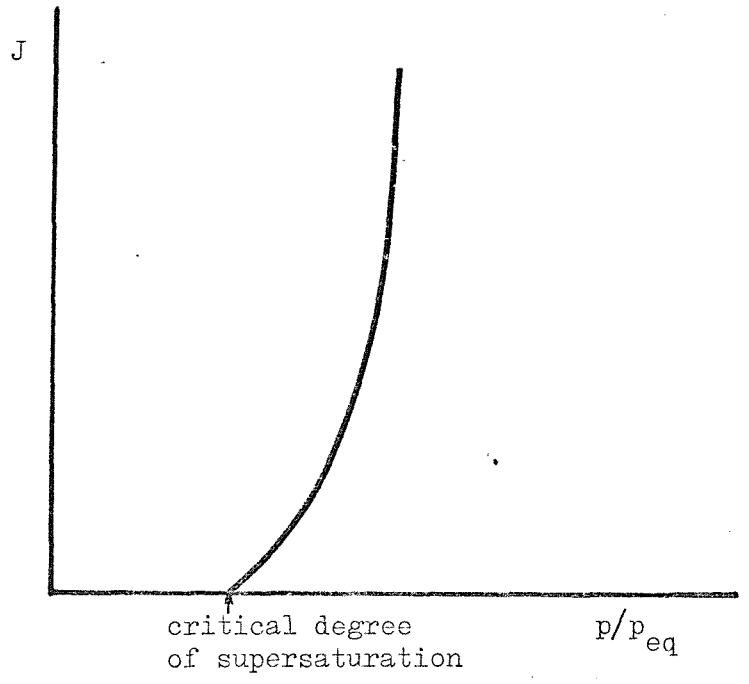

Figure 4.2 Dependence of the nucleation rate on the degree of supersaturation.

the probability the formation of critical nuclei. The nucleation rate equation according to Volmer is as follows:

$$J = \alpha_c 4\pi r_c^2 \frac{p}{(2\pi mKT)^{\frac{1}{2}}} n_1 \exp\left(-\frac{\Delta G_c}{kT}\right) , \qquad (4.7)$$

where J is the rate of nucleation, α_c is the condensation coefficient, n_1 is the monomer concentration, p is an equivalent supersaturation pressure and the other terms have their usual meaning.

Becker, Döering and Zeldovich[83,84] considered the growth of clusters as a sequence of bimolecular reactions, i.e. clusters grow only by successive additions of monomeric molecules per reaction. Thus other processes such as collision or combination between clusters or decomposition of a large cluster into smaller ones or simultaneous aggregation of single molecules are negligibly insignificant. They derived a nucleation rate expression from a solution of more than 100 bimolecular reactions of the type,

$$A_{i-1} + A = A_i , \qquad (4.8)$$

where A is a monomeric species and A_i is cluster made out of i monomers. Their rate equation based on this kinetic model is

$$J = \alpha_c Z\, 4\pi r_c^2 \frac{p}{(2\pi mkT)^{\frac{1}{2}}} n_1 \exp\left(-\frac{\Delta G_c}{kT}\right) , \qquad (4.9)$$

where Z is a non-equilibrium factor.

Experimentally, it would seem that the most important feature of the nucleation rate equation is its strict dependence on the degree of supersaturation (compare equations 4.9, 4.4 and 4.2). In addition, it is evident that changes in interfacial tension will also have a large effect. Figure 4.2 illustrates schematically the predicted nucleation rate on the degree of supersaturation.

It is seen that the free energy of formation of microscopic critical ΔG_c in equation (4.7) as defined by equation (4.4) contains macroscopic thermodynamic quantities such as the surface tension, i.e. the theory assumes that the surface tension of the new phase is identical with that of the bulk phase. This gives rise a fundamental difficulty which inevitably causes a discrepancy between theory and experiment as, for example, in the calculation of critical nuclear radius. Efforts have

been made by a number of authors[86-95] to modify the theory by using statistical mechanical treatments of the thermodynamics of small clusters. They came to the conclusion that the surface tension actually decreases with decrease in droplet size. However, the main problems of applying standard capillarity theory to free surfaces of small nuclei and of locating their surfaces remain unresolved. It would thus appear that one would not expect the surface tension of the bulk liquid to obtain at high curvatures. Further, thermodynamic methods of extrapolation are not applicable to such small clusters. Indeed it will ultimately seem more promising to use the concept of forces exerted by individual molecules and the more detailed methods of molecular mechanics.

Another useful approach to the refinement of these theories is concerned with the application of interfacial tensions between two coexisting phases which was unfortunately calculated from an incompressible fluid system. This is not the case for homogeneous nucleation involving a compressible fluid[93].

In addition the rate equation, equation (4.7) has been further developed by taking into account the free energy of translation and rotation. This arises because the liquid droplets behave as large vapour molecules which rotate as a whole and are free to translate throughout the volume of the vapour. Therefore the free energy terms associated with this motion must be considered. Furthermore, the free energy of separating a group of molecules from a larger ensemble is also important though its contribution is small. These factors were included in the corrected pre-exponential term, i.e. Z' of equation (4.10) below

$$J = \alpha_c Z' \Gamma 4\pi r_c^2 \frac{p}{(2\pi mkT)^{\frac{1}{2}}} n_1 \exp\left(\frac{-\Delta G_c}{kT}\right) , \qquad (4.10)$$

where Γ is the Lothe-Pound correction factor and Z' is the corrected non-equilibrium factor.

Feder *et al*[94] have proposed that when a molecule adds onto a cluster a corresponding energy equivalent to a latent heat is released. This raises the temperature and evaporation rate of the cluster thereby retarding nucleation. Besides this, the consumption of monomers by growing clusters could reduce the supersaturation and thus terminate the nucleation process. They have included these two factors in further developing the rate expression.

However, not all nucleation data are described either by the classical theory or by the revised theory. It would appear that not only the theory needs further development, but also the experiments which must be performed under conditions of strictly homogeneous nucleation.

4.2.2 Non-steady-state theories

When a vapour is suddenly cooled and made supersaturated it will still initially exist presumably as monomers. Few clusters of larger than monomer size will be inherited from the saturated vapour. The time required for this system to establish a new equilibrium or steady state distribution of clusters and therewith the steady state flux is called the relaxation time (also called time lag, delay time or induction time). In other words, before the onset of nucleation there is a relaxation time for the establishment of a new unstable distribution. This concept has been proposed by a number of authors[96-98] who considered the nucleation process as a non-steady state rather than a steady-state reaction. The rate equation for time-dependent nucleation is invariably concerned with the kinetics of growth of a nucleus by aggregation of molecule from the parent phase. This expression is rather complex and the approximate result is as follows:

$$J(t) = J_o\left[1 + 2\sum_{n=1}^{\infty}(-1)^n \exp\left(-n^2\frac{t}{\tau}\right)\right] \quad , \qquad (4.11)$$

where $J(t)$ is the time-dependent nucleation rate, J_o is the steady state rate of nucleation and τ is the time lag. When $t \longrightarrow \infty$, $J(t) \longrightarrow J_o$ but practically the non-steady state nucleation rate, $J(t)$, will approach the steady state rate of nucleation J_o when $t \gg 5\tau$. The induction time can be represented by

$$\tau = \frac{akT\sigma^3 V_m^2}{\Delta\mu^4 D_k} \quad , \qquad (4.12)$$

where a is a constant of the order of unity, σ is the specific surface energy of the new phase, V_m the volume of one molecule of the new phase, $\Delta\mu$ the difference in chemical potential per molecule between the two bulk phase and D_k the flow of molecules towards the critical nucleus.

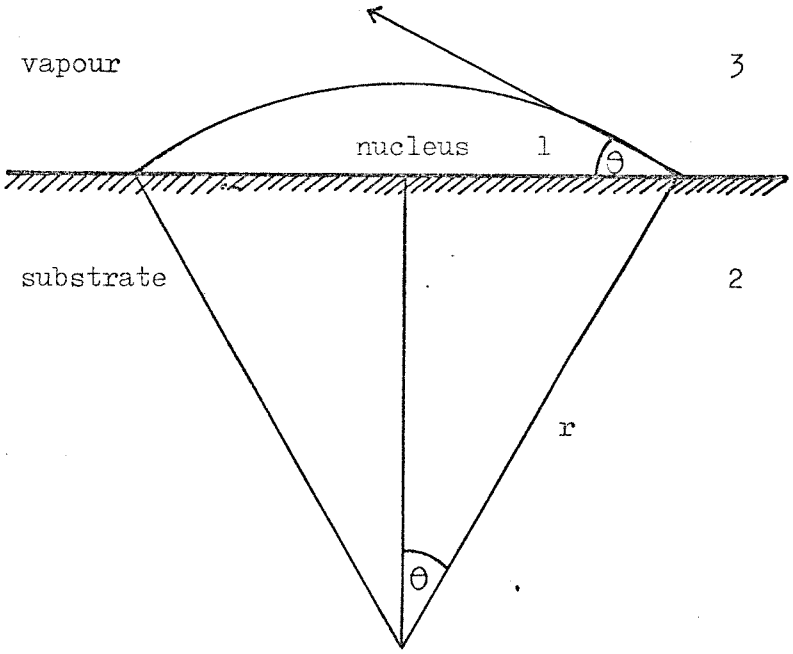

Figure 4.3 Model of heterogeneous nucleation

4.3 Theory of heterogeneous nucleation[95,99]

Nucleation which takes place on a foreign surface is called heterogeneous nucleation. The existence of a substrate is likely to reduce appreciably the energy of nucleation and thus the rate of nucleation will be enhanced. The basic principles in the formulation of the rate are the same as homogeneous nucleation. The only difference is that of the contact angle, θ, which reveals the relationship between the surface forces of the condensed phase and the substrate, i.e. whether wetting does or does not take place.

The model of heterogeneous nucleation which will be described here (Figure 4.3) is that of a spherical, cap-shaped segment of phase 1 deposited on the plane of non-deformable substrate phase 2 from a vapour of phase 3. The spherical cap has the radius of curvature r and the equilibrium contact angle between cap and substrate is θ.

The free energy of a spherical cap is the sum of the bulk term and surface term as given by

$$\Delta G = \frac{4}{3}\pi r^3 f(\theta) + 4\pi r^2 \sigma f(\theta) \quad , \tag{4.13}$$

where $f(\theta)$ is a geometric quantity expressing the fraction of the total sphere intersected by the substrate as is defined by

$$f(\theta) = \frac{(2+\cos\theta)(1-\cos\theta)^2}{4} \quad . \tag{4.14}$$

The contact angle is given by the Young equation

$$\sigma_{23} = \sigma_{12} + \sigma_{13}\cos\theta \quad , \tag{4.15}$$

where σ_{12} is the surface free energy between condensate-substrate; σ_{23} substrate-vapour and σ_{13} condensate-vapour.

Maximisation the free energy of formation with respect to nuclear radius and obtain r_c which is given, as before, by the Gibb-Thomson relation namely

$$r_c = -\frac{2\sigma}{\Delta G_v} \quad . \tag{4.16}$$

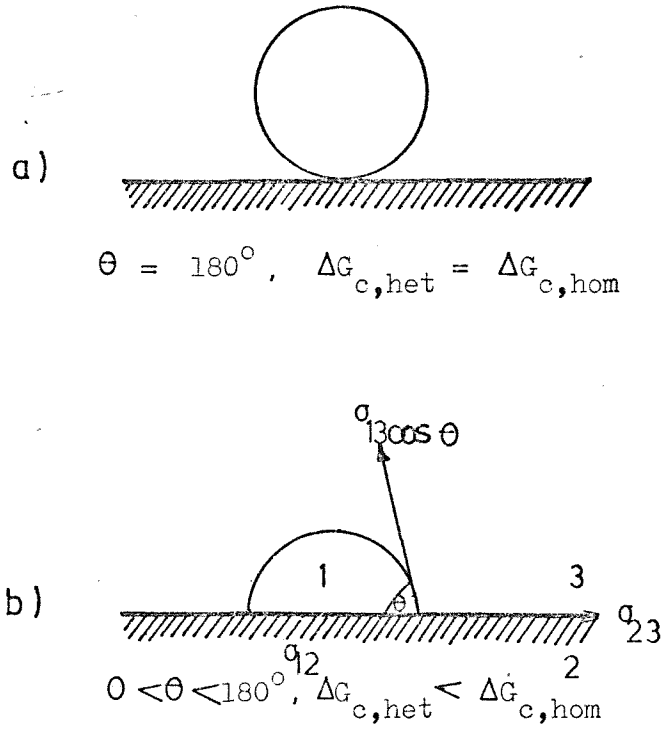

Figure 4.4 Dependence of the shape of a spherical nucleus and of the free energy change for heterogeneous nucleation ΔG_{het}, on the specific surface energies σ, or the contact angle θ.

Substituting equation (4.16) into equation (4.13), the free energy of formation of the critical nucleus will be

$$\Delta G_c = \frac{16 \pi \sigma^3 f(\theta)}{3 \Delta G_v^2} \quad . \tag{4.17}$$

Comparing this with equation (4.4) one obtains

$$\Delta G_{c,\ het} = \Delta G_{c,\ hom} f(\theta) \quad . \tag{4.18}$$

It should be noted here that equation (4.3) neglects the line tension at the periphery of the cap as compared with the free energy of formation of critical nucleus. If this contribution is significant and taken into account, the shape of nucleus will not be a sphere and equation (4.15) is no longer valid. However, to simplify the problem, this contribution is ignored.

Figure 4.4 shows the dependence of the shape of a spherical nucleus on the contact angle. It is seen that for $\theta = 180^\circ$ (Figure 4.4a), $f(\theta) = 1$ no wetting occurs and the free energy change for heterogeneous nucleation is equal to that for homogeneous nucleation. For $\theta = 0$ (Figure 4.4c), $f(\theta) = 0$ and $\Delta G_{c,het} = 0$, or complete spreading or wetting takes place or in other words nucleation becomes a non-activated process. For values of θ between 0 and 180° (Figure 4.4b) $0 < f(\theta) < 1$, therefore the substrate reduces the activation energy of nucleation, i.e. $\Delta G_{c,het} < \Delta G_{c,hom}$.

The kinetics of nucleation on the substrate may be analysed on the basis of following assumptions: (1) All atoms from vapour strike on the substrate surface without reflection from the surface by semi-elastic collision. All incident atoms once striking are adsorbed at least temporarily and come to thermal equilibrium with the substrate surface. (2) These adsorbed atoms may diffuse randomly over the surface until they join a growing subcritical cluster or leave the surface by evaporation. The critical nucleus grows by surface diffusion rather than by direct addition from the vapour. The surface diffusion will be preferable if the desorption energy of the adsorbed atoms exceeds the activation energy for surface diffusion. This approximate model was proved generally valid from the available experimental data.

The heterogeneous nucleation rate equation based upon the model just described can be expressed as

$$J = C_1 p \exp \frac{(\Delta G_{des} - \Delta G_{sd} - \Delta G_c)}{kT} , \qquad (4.19)$$

where C_1 is a constant which is relatively insensitive to the pressure p and temperature, ΔG_{des} is the free energy for desorption of an adatom and ΔG_{sd} is the activation energy for surface diffusion.

However, at high temperature, i.e. $\Delta G_{sd} < kT$, the model described above breaks down. The adatoms are no longer associated with the substrate surface. It is more reasonable to assume that critical nuclei move relatively freely as a two dimensional gas. Therefore, the free energy of rotation and translation must be considered. These factors were included in the nucleation rate equation which now becomes

$$J = C_2 p \exp \frac{(\Delta G_{des} - \Delta G_c)}{kT} , \qquad (4.20)$$

where C_2 is a constant which related to temperature and free energy of rotation and vibration. Note that the activation energy for surface diffusion disappeared from the nucleation rate equation.

In case of low temperature, the adatoms are strongly associated to the substrate surface and the rate equation is as follows

$$J = C_3 n' \exp - \frac{(\Delta G_{sd} + \Delta G_c)}{kT} , \qquad (4.21)$$

where C_3 is a constant and n' is the adatom population.

Up to this point we have been concerned with the formation of a cap-shape nucleus on an idealized flat surface. In fact, surface defects will affect the nucleation process. Generally speaking all surface imperfections will tend to be preferential nucleation sites. For example, the forming nucleus prefers the step (produced by imperfections of the substrate) to the flat surface since the step has higher energy of formation. In addition to surface inhomogeneities, the adsorption of impurities on the substrate surface can also affect nucleation through change of surface free energies. In view of the scarcity of significant quantitative data in the study of nucleation it would appear that if the degree of imperfection and extent of contamination of the substrate are known and controlled, one would have at a least a satisfactory basis of developing the theory further.

4.4 Current theories of electrochemical nucleation

4.4.1 Introduction

The overall process of electrodeposition, i.e. the process commencing with the deposition of metal ions in solution to a stable lattice built up of metal atoms is complex and involves several steps. Eventually, however, once a small new phase has been nucleated, its subsequent growth can proceed. The morphology of crystal growth may be one-dimensional, two-dimensional or three-dimensional. The degree of supersaturation required for nucleation and crystal growth to take place now corresponds to an additional applied overpotential.

The theoretical expression for electrochemical nucleation is based principally on two models, namely the thermodynamic and atomistic models. The thermodynamic model uses the macroscopic surface energy to calculate the free energy for defining the critical nucleus. This is a major shortcoming because the exact value of this quantity is usually not known. The application of this theory is thus restricted to the system of low supersaturation, i.e. when the surface tension concept does not lack physical sense which is the case when large clusters are formed. On the other hand, the atomistic model involves no macroscopic physical quantity. Instead, the interaction among the atoms of the clusters is considered, i.e. the computed potential energies of the clusters are used to characterize the critical nucleus. Although, these quantities have clear physical meaning their values are usually unknown. The atomistic theory is valid for the system of high supersaturation, i.e. when small critical nuclei are formed. At the present time, neither theory has been proved to be more adequate. Nevertheless, the thermodynamic theory is usually formally applied to the interpretation of results.

4.4.2 The thermodynamic theory of nucleation

The electrodeposition of metal ions onto a foreign substrate often requires a significant nucleation overpotential. This is associated with the extra energy required to overcome the surface forces when a small new condensed phase is formed. Provided the applied overpotential is high enough, i.e. greater than the nucleation overpotential a new phase will be initiated and the subsequent phase growth can propagate.

The excess free energy of formation of a single nucleus, ΔG is a function of its radius and is expressed by the Gibbs-Kelvin relation as

$$\Delta G = \frac{4}{3}\pi r^3 \frac{\rho}{M} - zF\eta + 4\pi r^2 \sigma \quad , \tag{4.22}$$

where r is nuclear radius, ρ is the density of the condensed phase, η is the overpotential (note that $z\eta$ is always negative) σ is the surface tension of the new phase and the other terms have their normal significance. The maximum free energy and the corresponding critical nuclear radius, r_c, are obtained by differentiating ΔG with respect to r and equating to zero, i.e.

$$r_c = \frac{2\sigma M}{\rho z F |\eta|} \tag{4.23}$$

$$\Delta G_{max} = \frac{4\pi r_c^2 \sigma}{3} \quad , \tag{4.24}$$

or substituting for r_c

$$\Delta G_{max} = \frac{16\pi\sigma^3 M^2}{3\rho^2 z^2 F^2 \eta^2} \quad . \tag{4.25}$$

This maximum free energy can be regarded as the activation energy for nucleus formation and may be regarded as determining the rate of nucleation.

Hence the rate of nucleation formation which was in the form

$$J = A \exp\left(\frac{-\Delta G_{max}}{RT}\right) \quad , \tag{4.26}$$

can now be re-expressed by substituting ΔG_{max} from equation (4.25) and becomes

$$J = A \exp\left(-\frac{k}{\eta^2}\right) \quad , \tag{4.27}$$

where A is a constant and $k = \frac{16\pi\sigma^3 M^2}{3\rho^2 z^2 F^2}$.

We note that the rate of formation of nuclei is strictly dependent upon

the applied overpotential or degree of supersaturation as in vapour phase condition schematically shown in Figure 4.2.

The process of nucleation just described is a time-independent or steady state process. However, as mentioned earlier in the discussion of nucleation in vapour phase, the birth of stable nuclei often requires a certain period of time, so called induction time, to reach a steady state nucleation. This is due to the necessity of creating a distribution of clusters of the new phase by molecular transport in the parent phase and also to lattice incorporation into clusters. The non-steady state rate equation was represented by equation (4.11), i.e.

$$J(t) = J_o\left[1+2\sum_{n=1}^{\infty}(-1)^n\exp(-n^2\frac{t}{\tau})\right] ,$$

and the 'induction time', τ , is defined by equation (4.12), i.e.

$$\tau = \frac{akT\,\sigma^3 V_m^2}{4\mu^4 D_k} .$$

In the case of electrochemical nucleation the difference in chemical potential per molecule between the two bulk phases is proportional to the overpotential η , and D_k, the flow of molecules towards the critical nucleus to ΔG and also to $\frac{1}{\eta^2}$. Hence

$$\tau \propto \frac{1}{\eta^2} . \qquad (4.28)$$

The experimental verification of the time-dependent nucleation rate according to equation (4.11) is not convenient since it is the number of nuclei, $N(t)$, and not their rate of accumulation which can be measured directly, i.e.

$$N(t) = \int_o^t J(t)dt . \qquad (4.29)$$

Therefore, upon integration of equation (4.29) gives

$$N(t) = J_o\left[t - \frac{\pi^2\tau}{6} - 2\tau\sum_{n=1}^{\infty}\frac{(-1)^n}{n^2}\exp\left(-n^2\frac{t}{\tau}\right)\right] . \qquad (4.30)$$

When $t > 5\tau$ equation (4.30) can be approximated to

$$N(t) = J_o(t - \frac{\pi^2 \tau}{6}) \quad . \tag{4.31}$$

Using the double potential step technique whereby nuclei once formed at a high pre-pulse overpotential are allowed to grow at a lower overpotential, then assuming no further nucleation takes place, we can count the number of nuclei formed at various pre-pulse potentials. The ~~the~~ steady state nucleation rate, J_o, can be calculated from the linear plot of N vs t according to equation (4.30). The relaxation time, τ, can be easily determined by extrapolation to N = 0, i.e.

$$\tau = \frac{6}{\pi 2} t_o \quad , \tag{4.32}$$

where t_o is the intercept on the t axis.

There are basically two methods for the investigation of electrochemical phase formation, i.e. those based on transients and that based on optical techniques. The transient techniques, e.g. potentiostatic and galvanostatic experiment, are used to study the kinetics of nucleation whilst the optical techniques, e.g., electron microscopy, are suitable for surface observation. The potentiostatic technique involves the control of the overpotential (or degree of supersaturation) which is strictly required for nucleation to take place. While the galvanostatic technique involves the analysis of the resulting overpotential-time relationship. These two methods are powerful, convenient and successful for studying the kinetics of nucleation. Their theoretical basis will be described as follows.

4.4.3 Potentiostatic studies of nucleation

Astley et al[100] derived the expression for 3D growth of a hemispherical nucleus under diffusion control by assuming linear (planar) diffusion to each nucleus and applied equation (3.2) in the form

$$I_t = 2\pi r_t^2 zFc \left[\frac{D}{\pi t} \right]^{\frac{1}{2}} \quad , \tag{4.33}$$

where I_t is the total current flowing to a hemispherical nucleus of radius r_t, at time t since its initiation, ρ is the density of the deposit.

The quantity of charge required to grow a hemispherical nucleus in a time t from its birth is from Faraday's law simply given by

$$Q_t = \frac{2\pi r_t^3 \rho z F}{3M} \quad , \tag{4.34}$$

where M is the molecular weight of the depositing metal. The corresponding current is

$$I_t = \frac{dQ_t}{dt} = \frac{2\pi\rho z F r_t^2}{M}\frac{dr}{dt} \quad . \tag{4.35}$$

Equating equations (4.35) and (4.33) gives

$$\frac{dr}{dt} = \frac{Mc}{\rho}\left[\frac{D}{\pi t}\right]^{\frac{1}{2}} \quad . \tag{4.36}$$

Upon integration

$$r_t = \frac{2McD^{\frac{1}{2}}t^{\frac{1}{2}}}{\pi^{\frac{1}{2}}\rho} \quad . \tag{4.37}$$

Substituting r_t in equation (4.33) gives

$$I_t = \frac{8zFMc^2D^{3/2}t^{\frac{1}{2}}}{\rho^2\pi^{\frac{1}{2}}} \quad , \tag{4.38}$$

which is the current flowing to one nucleus for instantaneous nucleation.

However, Hills *et al*[1] have pointed out that the more probable model should be that of hemispherical diffusion. In other words, they applied equation (3.3) instead of equation (3.2) to describe the diffusion of metal ions. From equation (3.3)

$$I_t = \frac{zFD^{\frac{1}{2}}cA}{\pi^{\frac{1}{2}}t^{\frac{1}{2}}} + \frac{zFDcA}{r_t} \quad ,$$

for which it is apparent that for small nuclei, the second term is much larger than the first, i.e.

$$I_t \simeq \frac{zFDcA}{r_t} = 2\pi zFDcr_t \quad . \tag{4.39}$$

Equating equation (4.39) with equation (4.35) and on integration gives

$$r_t = \left[\frac{2DcMt}{\rho}\right]^{\frac{1}{2}} \quad . \tag{4.40}$$

Substituting back into equation (4.39), one obtains

$$I_t = \frac{zF\pi(2Dc)^{3/2}M^{\frac{1}{2}}t^{\frac{1}{2}}}{\rho^{\frac{1}{2}}} \quad , \tag{4.41}$$

which is the current flowing to one nucleus for instantaneous nucleation under hemispherical diffusion control.

Fleischman and Thirsk[2] have derived a complete equation for charge-transfer controlled nucleation under potentiostatic current-time transients for processes in which the growth of the new phase, i.e. lattice incorporation, is slow. They assumed that the nuclei usually form randomly on preferred sites which may be imperfections on the surface of the substrate. Assuming a uniform probability of conversion of growth centres into nuclei with time, the first order nucleation rate law is expressed by

$$N_t = N_o\,(1-\exp(-At)) \quad , \tag{4.42}$$

where N_t is the total number of nuclei growing at a time t, N_o is the total number of available nucleation sites and A is the rate constant for the nucleation process.

Two limiting forms are encountered in the initial time range.

(i) When A is large, $At \gg 1$ for much of the period of growth and thus

$$N_t \simeq N_o \quad , \tag{4.43}$$

so that the number of nuclei immediately nucleated onto almost all the initial available sites, i.e. to instantaneous nucleation.

(ii) If A is small, then

$$N_t = AN_o t \quad . \tag{4.44}$$

This is the case when the number of nuclei will steadily increase with time, i.e. to progressive nucleation.

Under these conditions, the current flowing to a single hemispherical nucleus is given in terms of the dimensions of the particle

$$I = zFk2\pi r^2 \quad , \tag{4.45}$$

where k is the rate constant.

By equating equation (4.45) with equation (4.35) one obtains

$$\frac{dr}{dt} = \frac{kM}{\rho} \quad . \tag{4.46}$$

Upon integration

$$r_t = \frac{kMt}{\rho} \quad . \tag{4.47}$$

Substituting back into equation (4.45) the current at one nucleus will be

$$I_t = \frac{2zF\pi k^3 M^2 t^2}{\rho^2} \tag{4.48}$$

and combining equation (4.42) with equation (4.48) the total current for instantaneous nucleation will therefore be

$$\Sigma I_t = \frac{2zF\pi k^3 M^2 t^2 N_o}{\rho^2} \tag{4.49}$$

and for progressive nucleation

$$\Sigma I_t = \frac{2zF\pi k^3 M^2 A N_o t^3}{3\rho^2} \quad . \tag{4.50}$$

It should be noted that the above relations (equation 4.49 and equation 4.50) are valid when the growth process of the new phase is slow. However, when the growth process is fast and controlled by the rate of diffusion of metal ions from the bulk of the solution to the sites, the total current flowing to all nuclei for instantaneous nucleation when combine equation (4.43) to equation (4.38) will then be

$$\Sigma I_t = \frac{8zFMc^{\frac{2}{3}} D^{3/2} t^{\frac{1}{2}} N_o}{\rho^2 \pi^{\frac{1}{2}}} \tag{4.51}$$

for linear (planar) growth and a combination of equation (4.43) with equation (4.41) gives

$$\Sigma I_t = \frac{zF\pi (2Dc)^{3/2} M^{\frac{1}{2}} t^{\frac{1}{2}} N_o}{\rho^{\frac{1}{2}}} \tag{4.52}$$

for instantaneous nucleation and spherical growth.

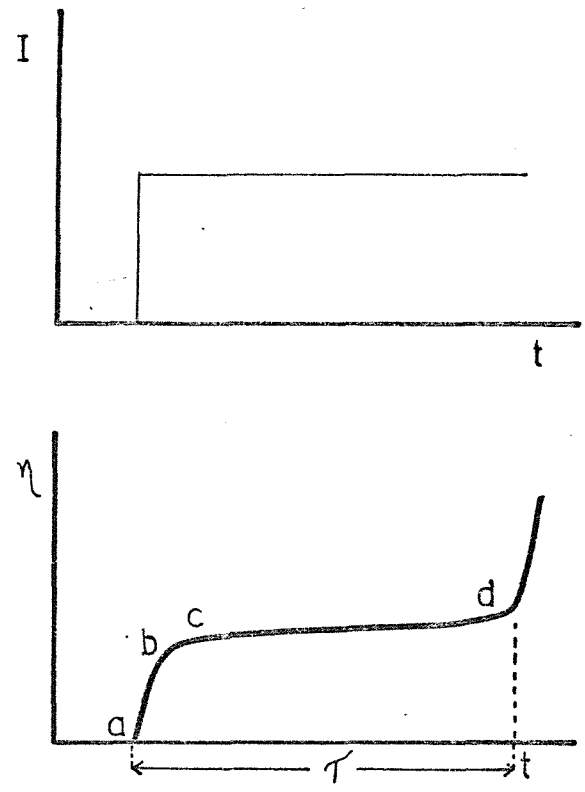

Figure 4.5 Galvanostatic transient for non-nucleation reaction.

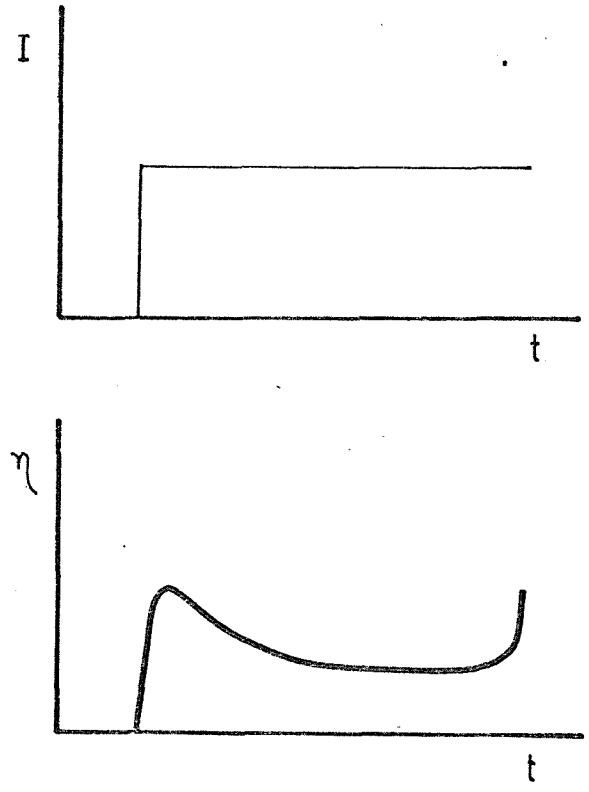

Figure 4.6 Galvanostatic transient for nucleation reaction.

The corresponding total current for progressive nucleation becomes respectively

$$\Sigma I_t = \frac{16AFzM^2c^3D^{3/2}t^{3/2}N_o}{3\rho^2\pi^{\frac{1}{2}}} \qquad (4.53)$$

and

$$\Sigma I_t = \frac{4zFA\pi(Dc)^{3/2}M^{\frac{1}{2}}t^{3/2}N_o}{3\rho^{\frac{1}{2}}} \quad . \qquad (4.54)$$

It should be noted that in each case the total current increases with time.

4.4.4 Galvanostatic studies of nucleation

If a constant current, I_g, is switched onto an electrode this current is divided into two components. The first one, I_c, is used for charging the interfacial capacitance at the electrode-solution interface. The second one, I_f, is associated with the transfer of ions across the double layer from the solution to the electrode surface. Therefore

$$I_g = I_c + I_f \quad . \qquad (4.55)$$

from which it is evident that since the applied current, I_g, is constant and the current, I_c, rapidly decreases with time during the galvanostatic charging process, then the faradaic current, I_f, will increase with time.

The current for charging the double layer is determined by the capacity of the interface C_{dl}, i.e.

$$I_c = C_{dl}\frac{d\eta}{dt} \quad . \qquad (4.56)$$

Initially a sharp change of η is to be expected whence $\frac{d\eta}{dt}$ is large and the charging current is large. After that, the overpotential increases much more slowly and the faradaic current predominates.

Figure 4.5 illustrates the galvanostatic stimulus and response for the process without nucleation[101,102]. It is seen that the resulting η-t transient is composed of four significant regions alphabatically labelled in order by a to d, this may be described as (a) the ohmic drop

of the system; (b) the charging of the electrical double layer; (c) the onset of the faradaic process and (d) the beginning of the new cathodic process, e.g., the reduction of the cation of the supporting electrolyte. The transition time, τ , is determined, as before, by Sand equation

$$\tau = \frac{z^2F^2c^2\pi D}{4I^2} \quad .$$

However, when the electrode process is preceded by the nucleation reaction, the η-t response particularly at the beginning of the transition time, is different as schematically shown in Figure 4.6.

The potential peak maximum can be regarded as a nucleation overpotential. This is due to the enforced growth of nuclei as the surface energy term increases reaching a maximum whereby a considerable number of stable nuclei are formed. Then the activation overpotential decreases with time. The overall process is likely to be controlled by charge transfer because of the rapid mass transfer to a small nucleus.

Since the total current is the sum of the two components, the charging current and the faradaic current as defined by equation (4.55), then, assuming that the initial slope of the transient is solely charging current, the double layer capacity C_{dl} can be determined from equation (4.56). If C_{dl} is assumed to be constant, the charging current I_c and the faradaic current I_f could then be deconvoluted from the whole transient, i.e.

$$I_f = I_g - I_c \quad . \tag{4.57}$$

Again, it will be assumed that the geometry of the growing nuclei is a perfect hemisphere of volume for one nucleus, V_t, at a time t given by

$$V_t = \frac{2}{3}\pi r_t^3 \tag{4.58}$$

and the charge flowing to a single nucleus is

$$Q_t = \frac{2\pi r_t^3 \rho zF}{3M} \quad .$$

Under galvanostatic conditions, the maximum charge required to grow a number of nuclei starting at the time from the beginning of the transient to a point corresponding to maximum overpotential, t_{max},

is simply given by

$$Q_{max} = \int_{o}^{t_{max}} I_f \, dt \qquad (4.59)$$

i.e.

$$\int_{o}^{t_{max}} I_f \, dt = It_{max} - C_{dl}\eta_{max} = \frac{2\pi r_{max}^3 \rho z F N_o}{3M} \quad , \qquad (4.60)$$

where N_o is the total number of nuclei obtained experimentally from a separate potentiostatic experiment at the corresponding maximum overpotential.

Substituting I_f from equation (4.57) in equation (4.60), the nuclear radius, r_{max}, can be calculated and hence the total electroactive area, i.e. its nuclear surface area, A, from

$$A = 2\pi r_{max}^2 N_o \quad . \qquad (4.61)$$

Since the rate of the electrochemical nucleation process is sufficiently small, i.e. the whole process is charge transfer controlled, therefore, the Tafel equation is obeyed,

$$I = I_o \exp\left(-\frac{\alpha n F}{RT}\right) \quad , \qquad (4.62)$$

where I_o is the exchange current density, I is the current density ($I = I_{f/A}$).

From the galvanostatic experiment, a series of transient at various applied currents is recorded from which a plot of log I vs η should therefore be a straight line. This is so, even though the electroactive surface area at each potential maxima may be varied. The slope of a linear log I vs η plot gives the value of the transfer coefficient α, whilst the intercept of the same plot gives the value of the exchange current density, I_o. It follows that

$$I_o = nFk^o c_o^{1-\alpha} \quad , \qquad (4.63)$$

where k^o is the standard rate constant in cm sec^{-1}, c_o is the concentration

of the reactant. It is evident from equation (4.63) that the exchange current density, I_o, does not, in fact, uniquely describe the rate of the electrochemical reaction because it depends on the concentration of the reactant. Instead the rate constant, k^o, as may be calculated from various method, will be used to evaluate the various electrochemical reactions.

4.4.5 The atomistic theory of nucleation[103-105]

This theory originates from the work of Walton[103] who utilized statistical mechanics and kinetic theory to derive the expression for the rate of nucleation. The theory was further developed recently by Milchev et al[104]. They applied the atomistic approach to the process of metal electrodeposition occuring at a very high supersaturation, which the critical nuclei are very small. The theory defines the free energy of formation of nuclei in terms of potential energies of the clusters, i.e.

$$\Delta G_i = U_i - iu_o - kT(\ln Q_i^{vib} - i\ln q_i^{vib}) - i\Delta\mu \quad , \qquad (4.64)$$

where U_i, u_o, Q_i^{vib} and q_i^{vib} are the potential energies and the vibration partition function of the cluster of size i and of an atom in the bulk crystal, $\Delta\mu$ is the supersaturation. Since the vibration partition function terms are negligibly small comparing to the total free energy, therefore

$$\Delta G_i = U_i - iu_o - i\Delta\mu \quad . \qquad (4.65)$$

The supersaturation, $\Delta\mu$, is related to the overpotential η, by the relation

$$\Delta\mu = ze\eta \quad . \qquad (4.66)$$

where z is the valence of the depositing ion and e is the electric charge.

The mechanism of phase transformation can be described into two ways. One is the direct addition mechanism and the other is surface diffusion mechanism. The direct addition mechanism is concerned with the addition of one atom directly to the clusters only or to the substrate surface only or to both the clusters and to substrate surface. The surface diffusion mechanism is concerned with the surface transfer of one atom to the adjacent site. However, experimental evidence shows that

the kinetics of the heterogeneous electrochemical nucleation is more likely to be a direct addition mechanism. For simplicity, we shall assume the direct addition of an atom to the clusters only.

The atomistic model for determining the steady state nucleation rate is based upon the relation

$$J = \frac{\omega_{+0} Z_0}{\lambda \frac{\omega_{-1}\omega_{-2}}{\omega_{+1}\omega_{+2}} \cdots \frac{\omega_{-1}\omega_{-n_k}}{\omega_{+1}\omega_{+n_k}}} , \qquad (4.67)$$

where ω_{+i} and ω_{-i} are the frequencies of addition and separation of one atom to and from clusters consisting of i atoms, Z is the Zeldovich factor from the classical nucleation theory. Assuming a direct addition mechanism, ω_{+1} and ω_{-1} can be defined, then the rate equation now becomes

$$J = K' \exp\left[-\frac{\phi(n_k)}{kT}\right] \exp\left[\frac{(n_k + \alpha)ze\eta}{kT}\right] , \qquad (4.68)$$

where $\phi(n_k)$ is related to the energetic state of critical nucleus or can be regarded as 'surface energies' of the clusters.

In the case of surface diffusion mechanism, ω_{+1} and ω_{-1} must be properly redefined, hence the rate equation becomes

$$J = K'' \exp\left[-\frac{\phi(n_k)}{kT}\right] \exp\left[\frac{(n_k+1)ze\eta}{kT}\right] . \qquad (4.69)$$

It should be noted that these two rate equations are similar since the rate of nucleation depends exponentially upon the supersaturation ($\Delta\mu = ze\eta$). Their difference lies in the pre-expotential terms K' and K'' which are related to the different mechanisms of nucleation, i.e. whether it is the direct addition or surface diffusion mechanism. Unfortunately these quantities cannot, at the present stage, be determined experimentally. For this reason, the actual mechanism of formation of critical nuclei remains unclear.

From equation (4.68) and equation (4.69), a plot of $\ln J$ *vs* $\Delta\mu$ should be linear, the slope of which can be used to calculate the number of atoms in clusters, n_k. However, it would appear that the atomistic model of nucleation is obeyed only when the dependence of $\ln J / \Delta\mu$ exists, i.e. at a certain range of high supersaturation. It is apparent that when the supersaturation is increased still further, the dependence of

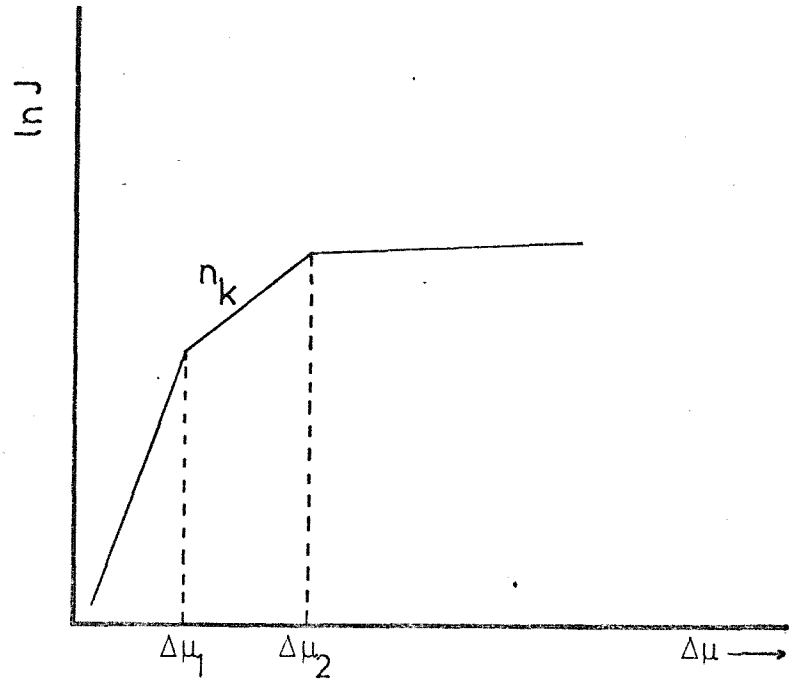

Figure 4.7 Relationship between logarithmic rate of nucleation and degree of supersaturation.

$\ln J / \Delta\mu$ cannot be derived as schematically shown in Figure 4.7. Therefore, the number of atoms in critical nuclei is not known. Although the atomistic theory defines the critical nucleus in terms of the probability of decay being greater than the probability of further growth, the addition of one atom to critical nucleus will make it stable and then grow spontaneously. In fact, the greater the difference in the size of the neighbouring critical nuclei, the more will be the dependence of lnJ on η , i.e. the atomistic approach is valid.

Comparing this concepts to the classical thermodynamic theory, it is seen that the atomistic theory required a linear dependence of lnJ upon η as in equations (4.68, 4.69) not on $\frac{1}{\eta^2}$ as in equation (4.27). In addition, the number of atoms in the critical nuclei can be estimated, though within a restricted range of high supersaturation. As mentioned earlier, the classical theory has inherently introduced an error through the application of macroscopic surface energies to a microscopic situation. The atomistic theory is an attempt to overcome this difficulty but has not been entirely successful. To date, both of the existing theories merit further development. Whether or to what extent this can be achieved is not clear; but one point stands out namely that the relationship between the supersaturation and the nucleation rate is always most striking. As a consequence the interpretation of the experimental data is still possible.

5. EXPERIMENTAL

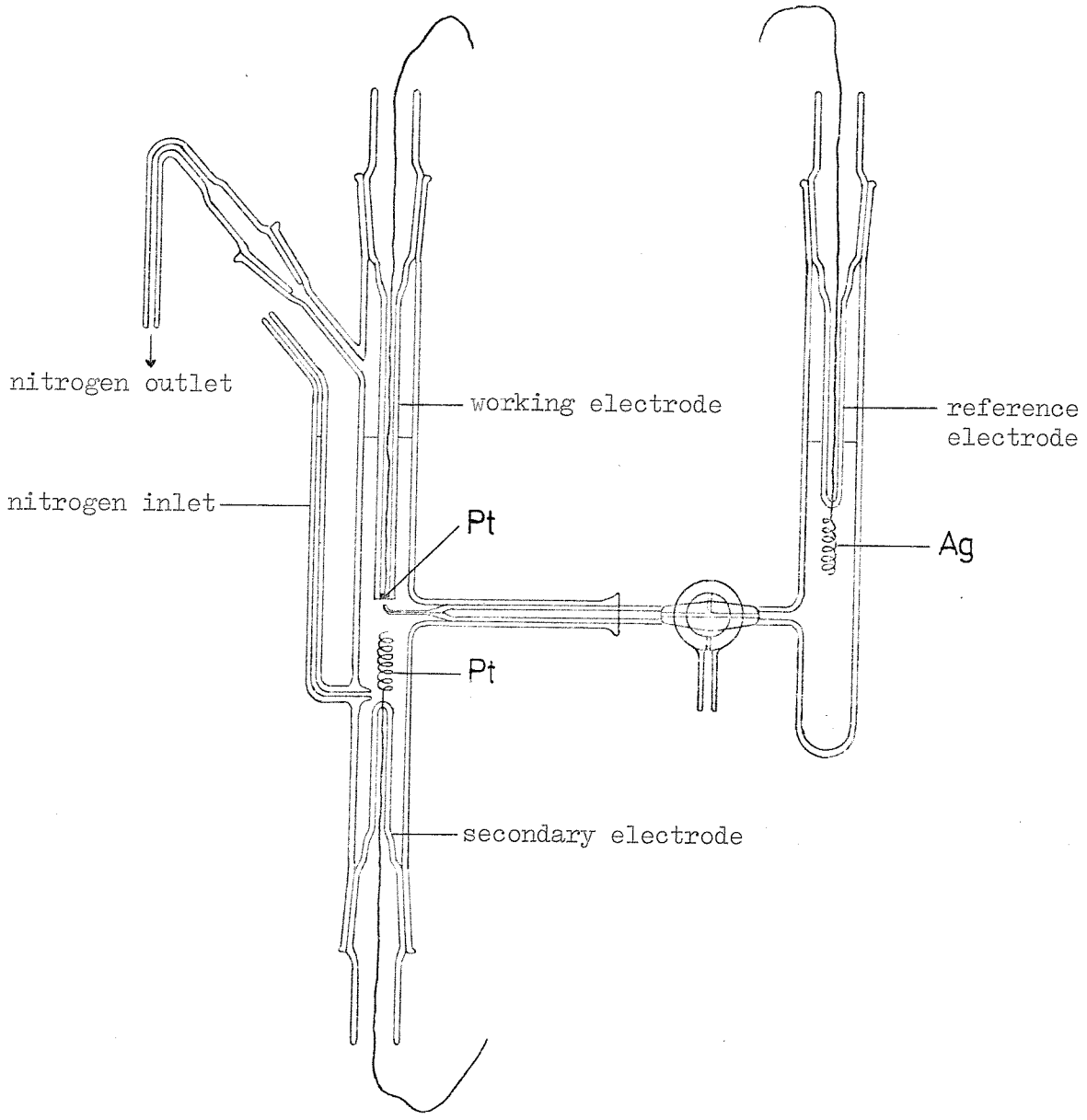

Figure 5.1 Three-electrode cell for use with aqueous solutions.

5.1 Aqueous Systems

5.1.1 Cell assembly: A conventional cell was used with a Luggin capillary joined to a Ag/Ag(I)(0.01 M) reference electrode. A separate compartment contained a platinum wire secondary electrode of large area. The Luggin tip of the reference electrode was positioned adjacent to the working electrode surface to minimise the uncompensated cell resistance. The cell assembly is shown schematically in Figure 5.1.

The cell and all glassware used were cleaned with hot concentrated nitric acid and rinsed repetitively with triply distilled water, left in water overnight and dried in an electric oven before use.

5.1.2 Electrodes: A platinum working electrode was constructed by sealing one end into Pyrex glass tubing using an epoxy mixture (Buechler, 20-8130 AB plastic epoxide). The electrode was further prepared by grinding the end flat with various grades of alumina powder on a rotating buffing wheel and finally polished to a mirror-like surface with 0.05μ alumina on Buechler microcloth. The geometrical area of the electrode was 0.189 cm^2 and the purity of the metal was $\leq$ 99.99%.

Vitreous carbon rod was thermally sealed into a glass tube and the end was ground flush with the seal exposing the cross section of the rod. The electrode was polished to a mirror finish. Contact to the electrode was made by a sharply pointed stainless steel rod pressed onto the back face of the graphite.

5.1.3 Electrode pretreatment: Electrochemical pretreatment of platinum working electrode was carried out in 'air free' 0.1 M nitric acid solution for several minutes at alternate potentials of $\pm$3.0 V, using a power supply (Farnell), so that oxygen and hydrogen gases were evolved. The electrode was then cleaned with 'air free' distilled water and inserted into the cell.

5.1.4 Chemicals: Chemicals used were of British Drug Houses 'Analar' grade. Solutions were prepared using triply distilled water. They were de-aerated with dry oxygen free nitrogen for twenty minutes before use.

5.1.5 Instrumentation: A transistorized potentiostat (Chemical Electronics, Type 70/2A) coupled with a waveform generator (Chemical Electronics, Type R.B.1) was used to apply a potential difference across a working electrode/electrolyte interface. These instruments have a

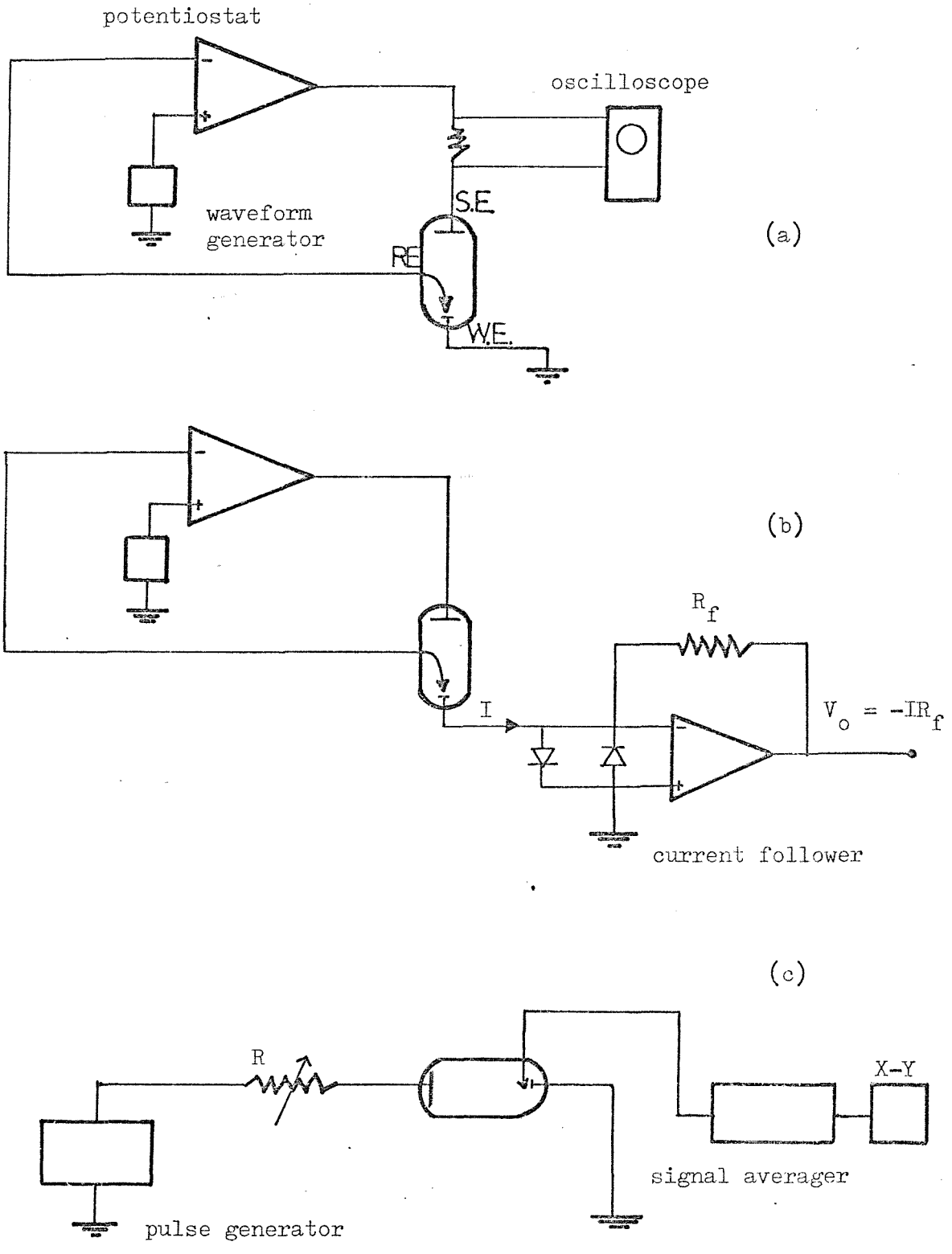

Figure 5.2 General circuit diagrams of the apparatus used for the potential step experiments (a & b) and for the galvanostatic experiment (c).

fast rise time, of the order 1 μsec, and response time of the order 10 μsec, i.e. sufficient for the electrochemical measurements here. The potentiostat had a maximum output of ±2 amp at ±70 V. It was constructed from an operational amplifier, basically for the circuit control of the feedback network. This polarized the working electrode with respect to unpolarized reference electrode and caused current to flow between secondary electrode and working electrode. A typical circuit diagram for potential step experiment is shown in Figure 5.2a and 5.2b.

The cell current generated from the potential step experiment is normally measured by connecting a recorder or oscilloscope with differential inputs across a resistor in series with the secondary electrode as shown in Figure 5.2a. In this work, however, a current follower was employed (see Figure 5.2b). The working electrode was connected to the input of a current follower which then remained at virtual ground and the observed current from a working electrode did not pass into the ground, but was diverted through a resistor R_f to generate the output voltage $V_o = -I_{cell} \times R_f$. Thus V_o 'follows' the cell current I. The output signal was then recorded and stored in a signal averager.

A signal averager (Hi-Tek, type AA1) was used to store single transients or average repetitive signals in digital form of 256 successive samples at intervals selected by timing control. The stored data could be read out word by word simultaneously in digital form and fed into a tape punch using Facit 4070 paper punch and read out by ICI 1907 computer, or displayed in analogue form at a desired rate on X-Y recorder (Bryans, type 26000 A4) or storage oscilloscope (Tektronic, type 564). The resulting data were accurate because hum and noise had been removed.

Linear sweep voltammograms were recorded on the X-Y recorder at sweep rate lower than 0.3 V sec^{-1}. Beyond this speed, a signal averager was employed.

Coulometric measurements, e.g., in cyclic voltammetry, experiments were made by using digital electronic integrators (Hi-Tek) connected directly to the output of a current follower.

Galvanostatic measurements were made by passing a constant current to the cell simply using a pulse generator (Farnell) connected in series with a known resistance as a current source through the secondary electrode. The measuring circuit is shown schematically in Figure 5.2c. The polarization current passing through the secondary electrode was controlled

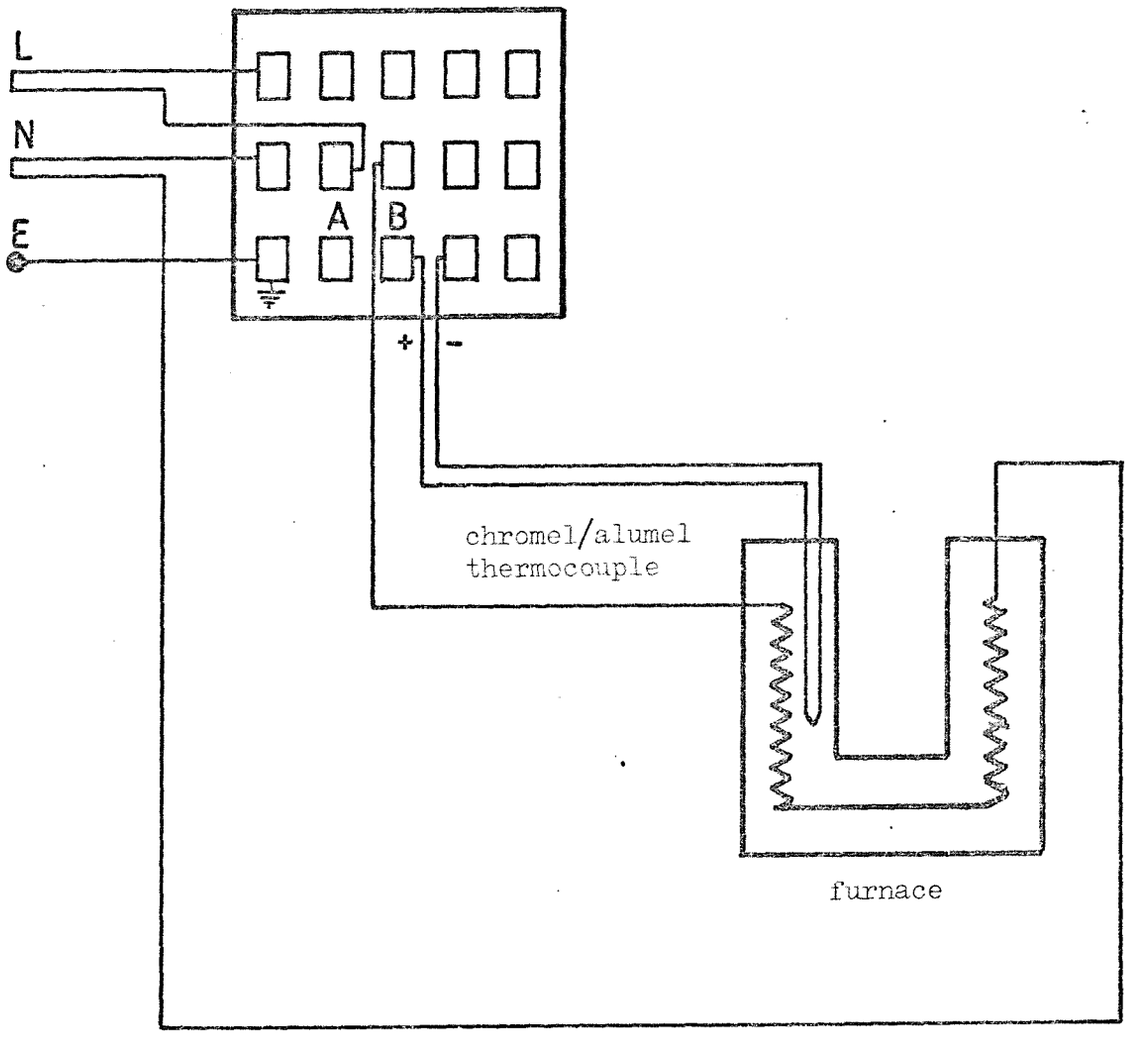

Figure 5.3 Temperature control system.

by resistor R. The working electrode was grounded, thus the voltage developed across a cell could be measured by connecting the reference electrode to a signal averager which would process the resulting signals and give an output potential-time transient, as before, displayed on X-Y recorder or oscilloscope.

5.2 Molten salts system

5.2.1 Furnace: This was a common type of high temperature apparatus essentially the same as previously described by Johnson[106] and by Thompson[107]. The furnace was made by a Nichrome heating element of 100 ohms resistance wound on a silica envelope and embedded in thermal insulant, e.g., kieselguhr. The whole cell was encased in a thin steel tube earthed through a nickel wire. The top part of the furnace was attached to a water-cooled copper collar which supported the flange joint of the cell assembly.

5.2.2 Temperature control system: The temperature of the furnace was controlled by an Ether 'Digi' temperature controller (Pye Ether Ltd.) with digital set-point. It operated directly from a chromel/alumel thermocouple contacted to the furnace winding. The operation was switched by relay (Figure 5.3), so that all the energy was cut off when the desired control temperature was reached. When the furnace temperature was below the preset temperature, the relay was in position A and the AC main supply was then passed through the furnace winding as shown by the front panel control lamp. The furnace was heated until it reached a preset temperature then the relay would automatically change to position B and the control lamp was now 'off'. This system offered a reliable and accurate method of controlling temperatures within $\pm 2^{\circ}C$ at $275^{\circ}C$ and $450^{\circ}C$.

The furnace temperature was certainly not equal to that of the melt temperature. However, the preset temperature could be adjusted to give the desired temperature of the melt. By means of a separate chromel/alumel thermocouple inserted in a glass tube, sealed at one end and immersed in the melt and with a cold junction maintained at $0^{\circ}C$ in mixture of ice and water and connected to a digital micro-voltmeter (Solartron LM1604), the e.m.f. and hence the melt temperature could then be measured.

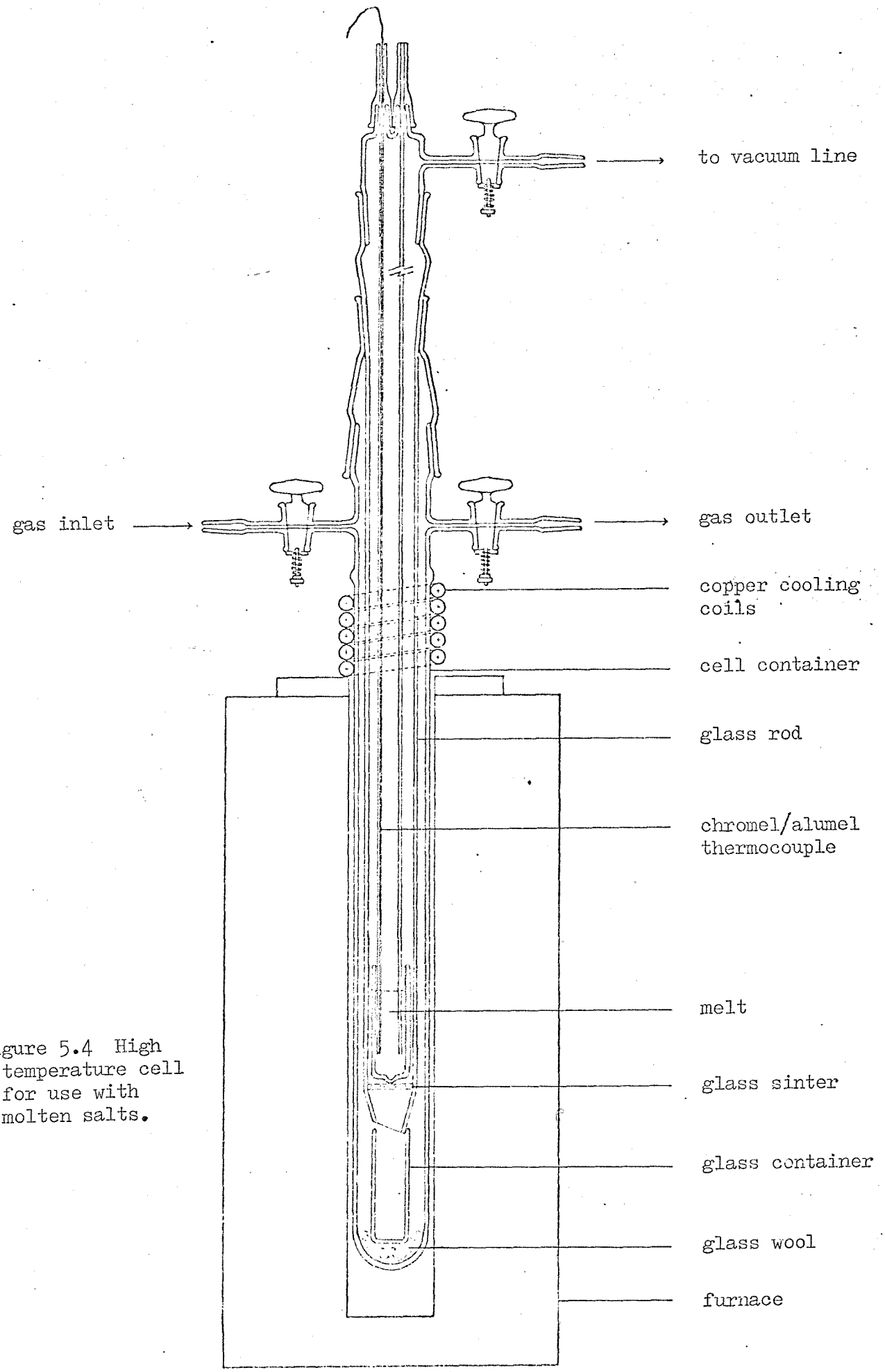

Figure 5.4 High temperature cell for use with molten salts.

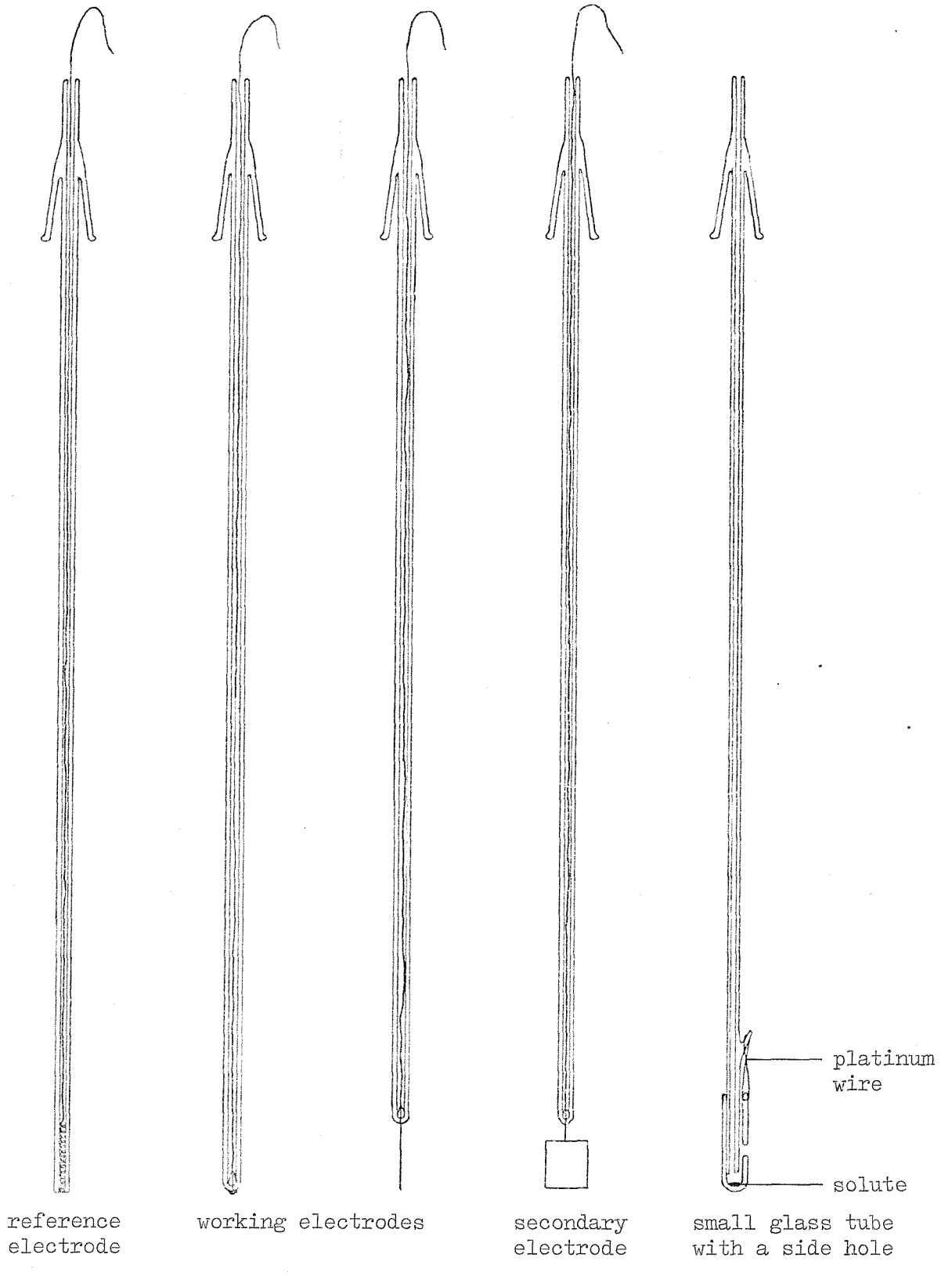

Figure 5.5 The range of working electrodes, reference electrode and solute insertion device.

5.2.3 Nitrate melts

5.2.3.1 Preparation and purification of the $NaNO_3$-KNO_3 eutectic: The preparation of pure melts can be made by fusing 'Analar' grade sodium nitrate together with potassium nitrate (BDH Ltd.) in the mole radio 1:1. Both salts were dried in an electric oven for several hours before being weighed and ground together. The nitrate mixtures were weighed accurately (100 g) and put in the filter unit of the cell assembly. The sample was heated to 200°C under vacuum (10^{-3}-10^{-4}mm Hg) for 15 hr before the temperature was raised above the melting point (228°C) under the atmosphere of 'oxygen-free' nitrogen gas previously dried by calcium chloride and molecular sieve. The subsequent filtration of the melt was carried out through fritted glass. By breaking the thin seal of melt container using a glass rod (inserted through a socket at the top of the cell) to tap at the bottom, the melt would drop directly into a glass container placed below (Figure 5.4). The filter unit was rapidly removed and a new head glass cell was inserted. Thus a chromel/alumel thermocouple already in the glass tube and nitrogen gas bubbling tube were introduced into the melt. The cell and the melt were then purged with purified nitrogen for three hours and an atmosphere of nitrogen was maintained above the melt throughout the course of experiment. The reference electrode, secondary electrode and working electrode were immersed in the melt for voltammetric measurements. This melt was considered pure enough when the resulting voltammogram showed a residual current of 0.04 mA at an applied potential of -0.8 V vs Ag/Ag(I)(0.01M) using platinum working electrode of geometric area of 0.154 cm^2.

5.2.3.2 Preparation and introduction of solutes: Solutions of silver ions were prepared by either in situ anodisation of silver metal wire (Johnson and Matthey Ltd.) or by adding silver nitrate salt directly into the purified melt. Anodisation was carried out by applying a constant current of ~ 10 mA using a silver wire in a sintered compartment separated from the bulk melt as a cathode. The number of coulombs used for silver dissolution was accurately checked by an electronic digital integrator. In the case of high concentrations of solute, the silver salt could be weighed accurately and added to the melt by means of a small glass container with a side hole, attached to a nitrogen tube by a platinum wire (Figure 5.5). After the glass container was put under the

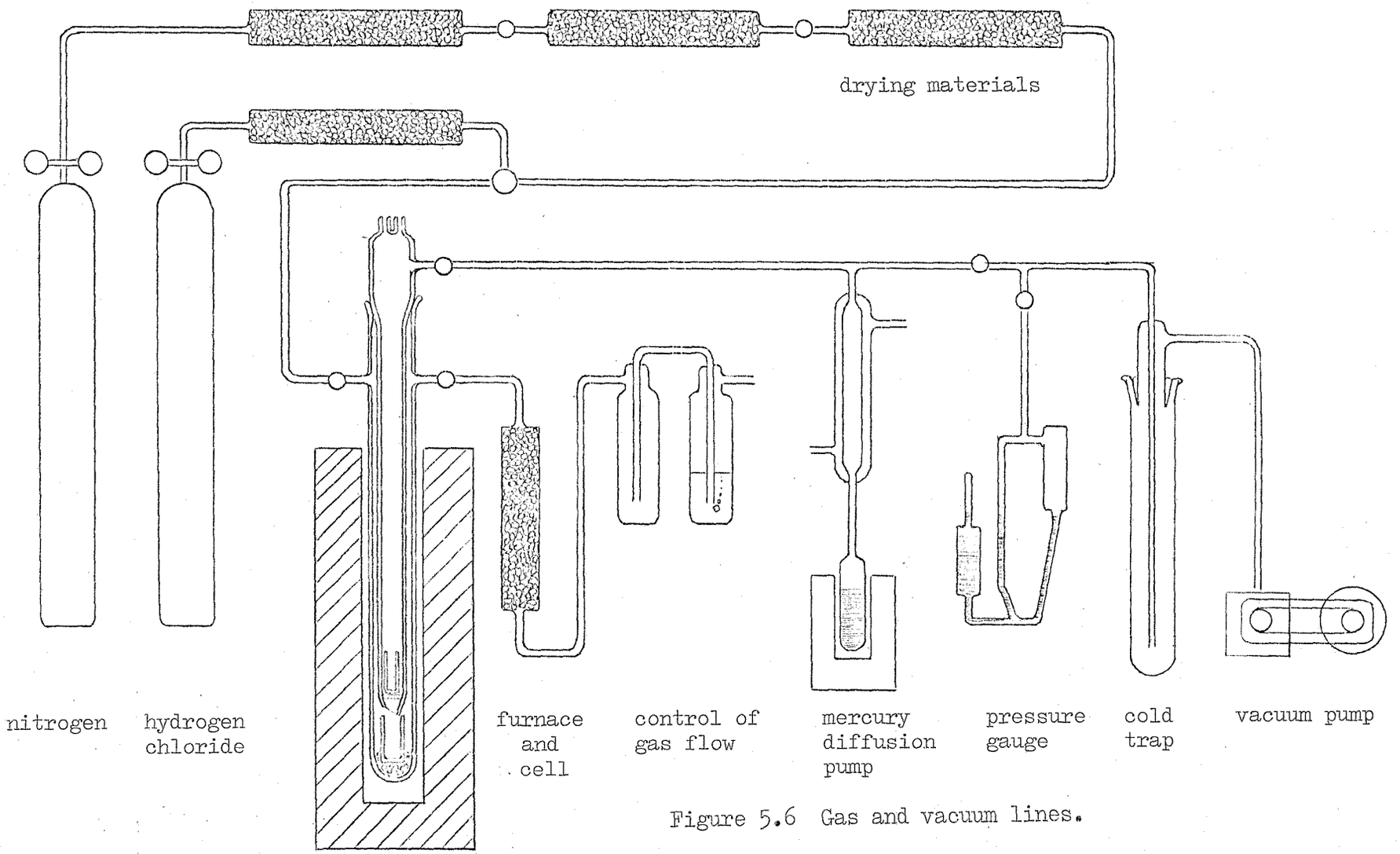

Figure 5.6 Gas and vacuum lines.

melt level, nitrogen was bubbled to homogenize the silver salt with the bulk melt.

Anhydrous $Cd(NO_3)_2$, $Cu(NO_3)_2$, $Co(NO_3)_2$, and $Ni(NO_3)_2$ were prepared from their hydrate salts by heating under vacuum at the temperature $\sim 140^{\circ}C$. Lead nitrate was used after vacuum drying at $200^{\circ}C$ for several hours.

5.2.3.3 Electrodes (Figure 5.5): The working electrodes were constructed by using a small platinum wire (diameter 0.04 cm, length ~1.0 cm) in a glass tube. This is convenient and useful for platinum is readily available with high purity. By careful construction, it can be used properly in low temperature molten nitrates without any seepage of melt into the seal during a short course of investigation. Electrode areas were measured by using a travelling microscope (Beck, London).

The secondary electrode was a large platinum foil (~ 2 cm^2) and the reference electrode was a silver wire inserted in a separated sintered compartment. The standard solution of silver salt (e.g. 0.01 M) was prepared *in situ* by coulombic anodic dissolution of silver metal into a known volume of melt. For convenience, the standard silver salt solution was the same concentration as that in the bulk melt.

5.2.3.4 Electrode pretreatment: The same electrical pretreatment was used as for aqueous systems, but the pretreated electrode was quickly dried in an oven before being introduced into the melt.

5.2.4 Chloride melts

5.2.4.1 Preparation and purification of the LiCl-KCl eutectic: Lithium containing salts such as LiCl holds water tenaciously, thus special care must be taken to ensure a complete dehydration of the solid salts of LiCl-KCl as well as to minimise the absorption of water of the fused salts from moist air. The method of preparation and purification of LiCl-KCl eutectic was similar to that used by Laitinen *et al*[49].

Anhydrous LiCl and 'Analar' grade KCl were mixed together in the proportion 59:41 mole%. The proper amount of the mixture was immediately placed in a glass vessel under vacuum (Figure 5.6). The eutectic was dried *in vacuo* for over fifteen hours at a temperature below its melting point (i.e. $< 352^{\circ}C$). Hydrogen chloride in a stream of dry nitrogen (99% B.D.H. Ltd.) was slowly passed through the drying agent, e.g., anhydrous calcium chloride, then into the evacuated cell until the pressure

exceeded atmospheric. The solid eutectic mixture was then fused under the excess dry hydrogen chloride atmosphere and then filtered as described earlier for nitrates. After the filtration was complete, the cell was evacuated and nitrogen was admitted. Nitrogen was bubbled into the melt for three hours to remove traces of water and the remaining gas. The evacuation procedure was then repeated once more so that the fused salts were completely free from hydrogen chloride gas. The purified solvent was kept in dry nitrogen atmosphere throughout the course of measurement. The purity of the solvent was considered acceptable when the residual current proved to be negligibly small compared to the subsequent voltammetric currents.

5.2.4.2 Preparation and introduction of solutes: Copper(I) was prepared by coulometric anodic dissolution of copper wire using graphite electrode in an isolated compartment as a cathode. Other solutes such as cobalt chloride hydrate were dehydrated in hydrogen chloride atmosphere at the temperature of $\sim 120^{o}C$. Silver ions were introduced to the melt by either anodisation of silver metal *in situ* or dissolution of silver nitrate salts.

5.2.4.3 Electrodes: Tungsten wire was sealed in a glass bead and then into a glass tube exposing a short wire from the seal. Electrical contact was made by winding a tungsten wire with nickel wire.

Copper and nickel foils were used to prepare flag-shaped electrodes using small platinum wire as a flag pole sealing in the glass tubings.

The preparation of reference electrodes for the chloride melts was similar to that in nitrate melts. A glass tube with a sintered glass disc was immersed into the melt and allowed it to pass into the tube until the melt level inside was equal to the outside. A silver wire was inserted and a known concentration of silver ions (e.g. 0.01 M) was generated coulometrically using a graphite electrode in a separate glass tube as a cathode. A side hole of the Ag/Ag(I) reference electrode maintained the equilibration of the internal nitrogen atmosphere and the external atmospheric pressure; the rate of mixing with the bulk solvent was slow.

5.3 Electron micrographs: Electron micrographs were taken by a Cambridge Stereoscan Electron Microscope.

6. VOLTAMMETRIC STUDIES OF PLATINUM ELECTRODES

6.1 Introduction

Platinum is probably the most widely used electrode for electrochemical studies. Its surface resists corrosion in many electrolyte solutions and it serves as a catalytically active metal for various chemical reactions. In addition, electrodes can conveniently be constructed from it by proper sealing in soft glass or by using other insulating materials (such as epoxy resins) to support it.

On the other hand, there are certain disadvantages to its use, especially in electrochemical studies of high sensitivity, i.e. those sensitive to its surface state. Thus, as with other metals in aqueous solution it is known to form an oxide film and similar films are also formed when platinum is exposed to molten nitrates[108].

The existence of an oxide film on platinum is often overlooked because the film thickness is invariably small and the electrode remains visually bright. Even so, many studies of the formation and of the nature of the film have been made, some by indirect electrochemical procedures and others by means of surface optical techniques, such as specular reflectance, ellipsometry and Auger spectroscopy. Much of this work has been reviewed by Damjanovic and Ward[109]. Although many uncertainties concerning the film remain, it is generally agreed that a definite oxide phase is formed at potentials above a critical value which in aqueous solutions is $\pm$ 1.0 V (w.r.t. the normal hydrogen electrode) whilst below this value the film is chemisorbed oxygen. The latter may be conceptually distinguished from the former in that it is composed of metal ions and oxygen atoms in separate planes unlike a phase oxide in which platinum atoms have left their regular positions in the platinum lattice to form a regular array with oxygen ions. The supporting evidence for phase oxides corresponds to the first direct 'chemical' evidence found earlier by Anson and Lingane[110] under conditions normally employed in voltammetry. They pointed out that the surface oxides contain mostly divalent platinum.

It should be emphasised that the anodic film on platinum is very thin, i.e. 0.1-0.2 nm in the early stages and invariably less than 1.5 nm even under the influence of a high electric field. Under this condition, however, the film is normally compact, non-porous but easily removed.

The mechanism and growth of the film can be well described by the theory of metal oxidation of Cabrera and Mott[111,112]. The theory proposed that the film grows by a process of ionic migration, normally the migration of metal ions from the metal-metal oxide interface to the metal oxide surface where they react with chemisorbed oxygen. In the case of platinum oxide, the main process is one of anionic transport whereby the oxide film is formed at the metal surface by a 'place exchange'[113] mechanism. Both processes have a high activation energy.

The rate of growth of the oxide film depends upon the number of interstitial cations initiated at the metal-metal oxide interface and also on the probability of the interstitial cations migrating through the film to the metal oxide-electrolyte interface. This is a function of position and the electric field strength in the oxide layer. As mentioned above, the oxide film is very thin and, generally speaking, its growth is a slow process and even after, say, 1000 sec or at high potential, there is no limiting coverage of the oxide layer. In fact the thickness increases in a continuous manner and in the same structure regardless of whether the electrode was initially treated thermally or mechanically.

The presence of surface oxide affects significantly electrochemical reactions taking place at the surface and many electrode reactions are inhibited by the oxide film. For example, Damjanovic[109] reported that the rate of O_2 reduction on 'oxide free' surface at the potential below $\sim$ 1.0 V is about one-hundred times higher than on 'oxide covered' platinum electrodes. It is found, furthermore, that the mechanism of this reaction is also affected. Bixler and Bruckenstein[114] have prepared 'oxide free' platinum electrode by successive anodic and cathodic polarisation and observed that the 'oxide free' electrode allows complete deposition and dissolution of silver. Toschev and Mutaftschiew[115] pretreated a platinum electrode in nitric acid of different concentrations and for various times before using it as a substrate for the electrochemical nucleation of mercury. The results show an increasing number of mercury nuclei formed on the surface as the acid concentration is increased and as the duration of the electrode treatment is prolonged. In view of catalytic activity of the surface oxide, it is likely that following its removal the platinum electrode becomes more 'active' and thus provides more nucleation sites for mercury.

This research has confirmed that the surface oxide does impose a barrier to charge transfer reaction, in this case to the deposition and dissolution of silver. It greatly retards the rate of nucleation and gives rise a nucleation overpotential of $\sim$ 70 mV in aqueous solution. Moreover, the anodic dissolution of silver in aqueous system is found to be incomplete. A detailed explanation of this is offered in terms of the rectifying properties of the surface arising from partial ionic and electronic conductivities of oxides not only of the platinum substrate but also of the deposited metal.

The corresponding system in molten salts was chosen for study for two reasons. Firstly, it is apparently a well established system, particularly when investigated by voltammetric techniques. Because the ohmic resistivity of the melt is low and the charge transfer reaction is fast or controlled by the rate of mass transfer of electroactive species to the electrode-melt interface, electrode reactions in molten salt systems exhibit little or no activation overpotential. Furthermore, the systems are completely ionic and the complicating influences of water molecules and hydrogen bonding are absent. Secondly, it is evident that many of electrodeposition studies in molten salts have been mostly concerned with the determination of diffusion coefficients, although Hills *et al*[1] have noted large discrepancies in the values of diffusion coefficients because of the neglect the formation and growth of a new phase. It is, therefore, interesting now to focus attention to the nature and role of the substrate surface. This study gives results similar to those obtained from aqueous systems.

The study of electrodeposition and dissolution of metals on solid substrates is often complicated by the complex variation of surface activity with time of electrolysis, and in the case of platinum its real area may become less with time due to oxide film formation or adsorption of impurities. Indeed, it is found that the platinum used in this work illustrates a clear case of this surface complication. Hence platinum is by no means a suitable substrate as far as the study of heterogeneous electrochemical nucleation is concerned. The intervention of its surface oxide in the early stages of metal deposition (i.e. the stages before a uniform deposit is formed) make this common electrode material less attractive and because of this, other electrode materials have also been chosen for comparison.

At this stage, therefore, it is clear that the catalytic activity of many types of electrochemical reactions depends on the thickness of the anodic oxide film. Strictly speaking, the thicker is the film, the less will be the catalytic activity. With this picture in mind, provided one wants to obtain 'reproducible' results, the oxide layer must be removed by means of pretreatment prior to each experiment. The methods of cleaning are varied, depending on the purpose for which the electrode is to be used. The total procedure includes chemical and electrical pretreatment, both of which give an 'active' surface.

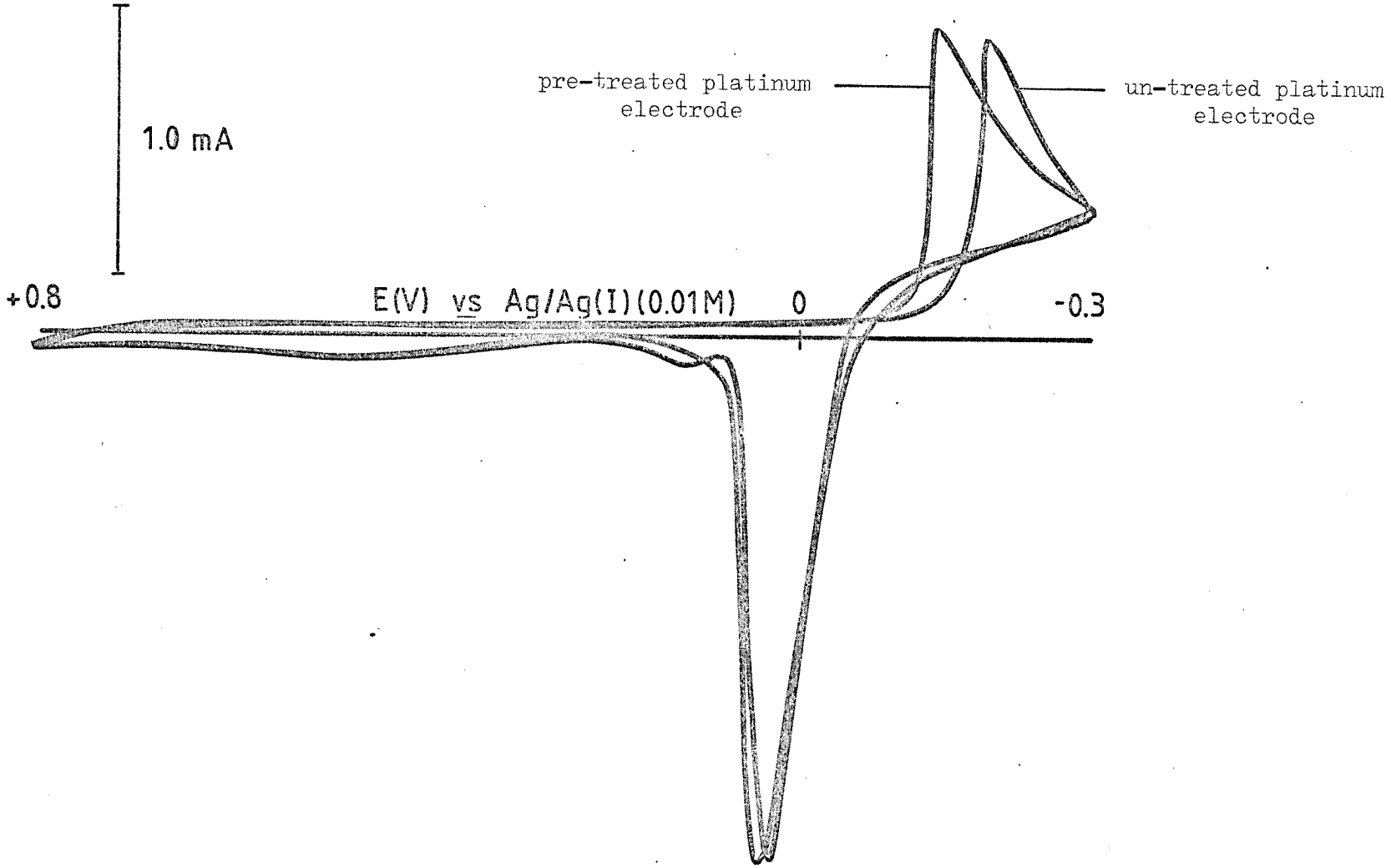

Figure 6.1 Cyclic voltammogram for the deposition of 10 mM $AgNO_3$ in 1 M KNO_3 onto pre-treated and un-treated platinum (A = 0.189 cm^2), v = 0.1 V sec^{-1}.

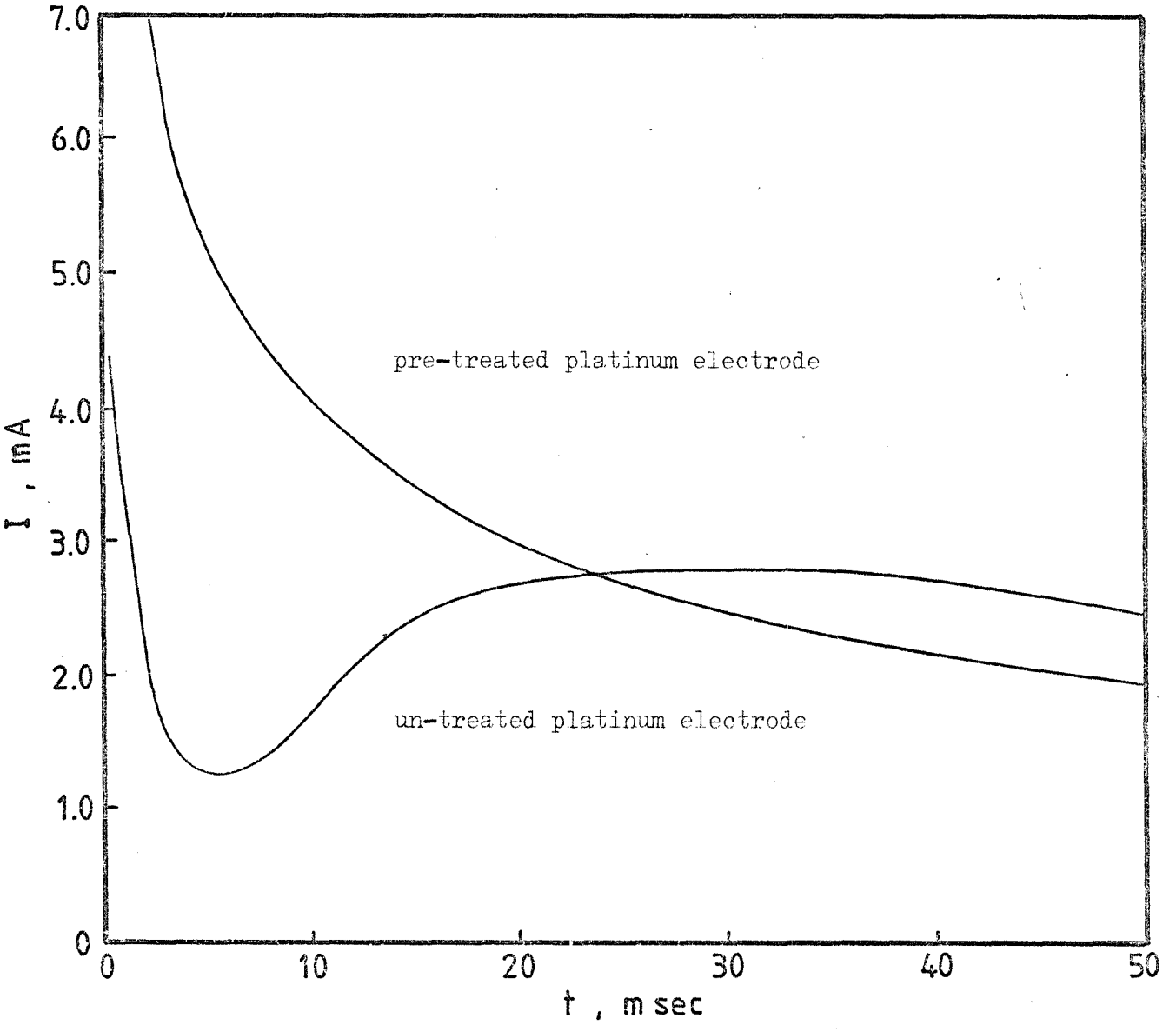

Figure 6.2 Potentiostatic transients for the reduction of 10 mM $AgNO_3$ in 1 M KNO_3 onto pre-treated and un-treated platinum (A = 0.189 cm^2) at an overpotential of 120 mV.

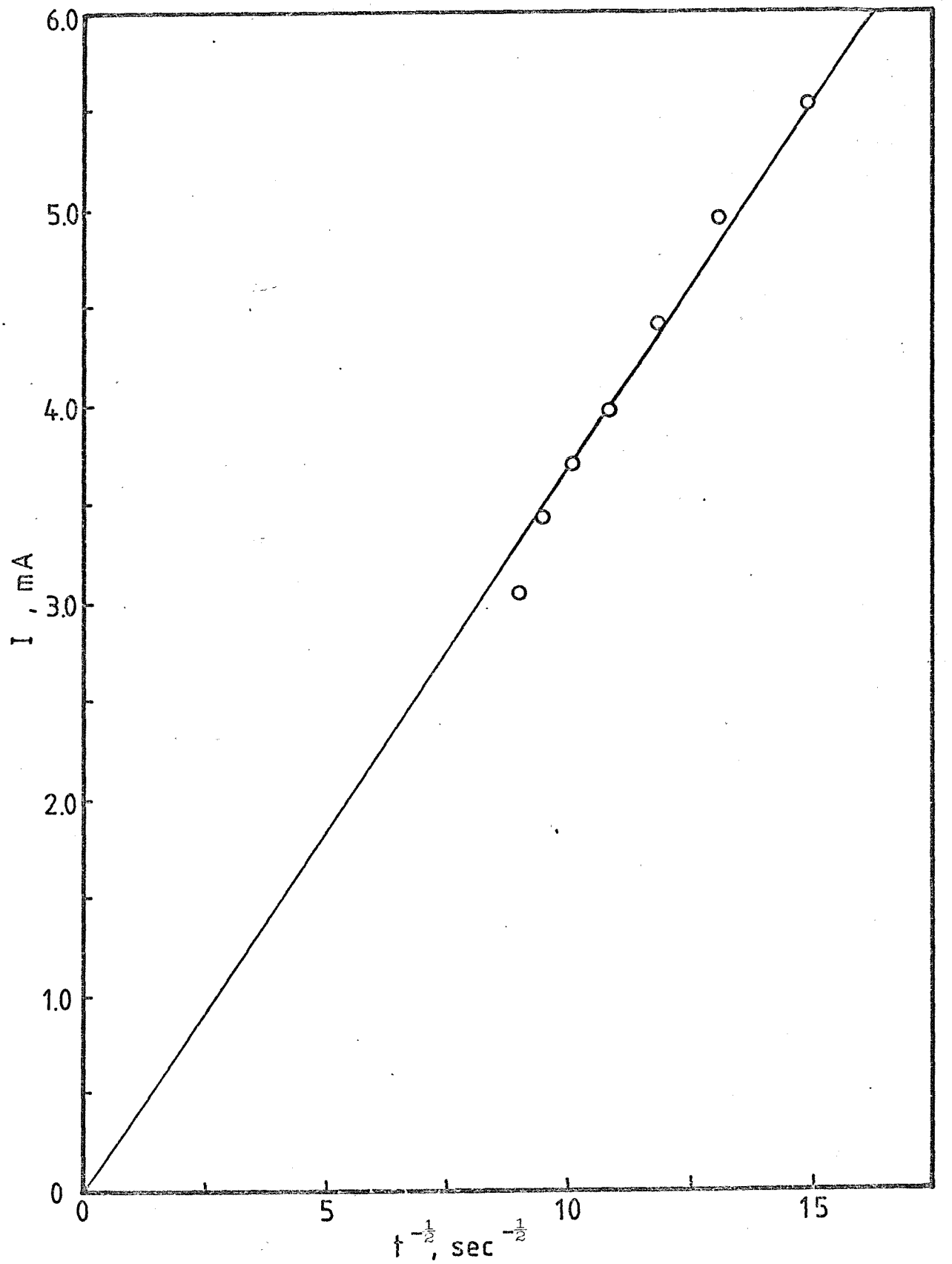

Figure 6.3 Current-time relationship for the deposition of 10.9 mM $AgNO_3$ in 1 M KNO_3 on pre-treated platinum (A = 0.189 cm^2).

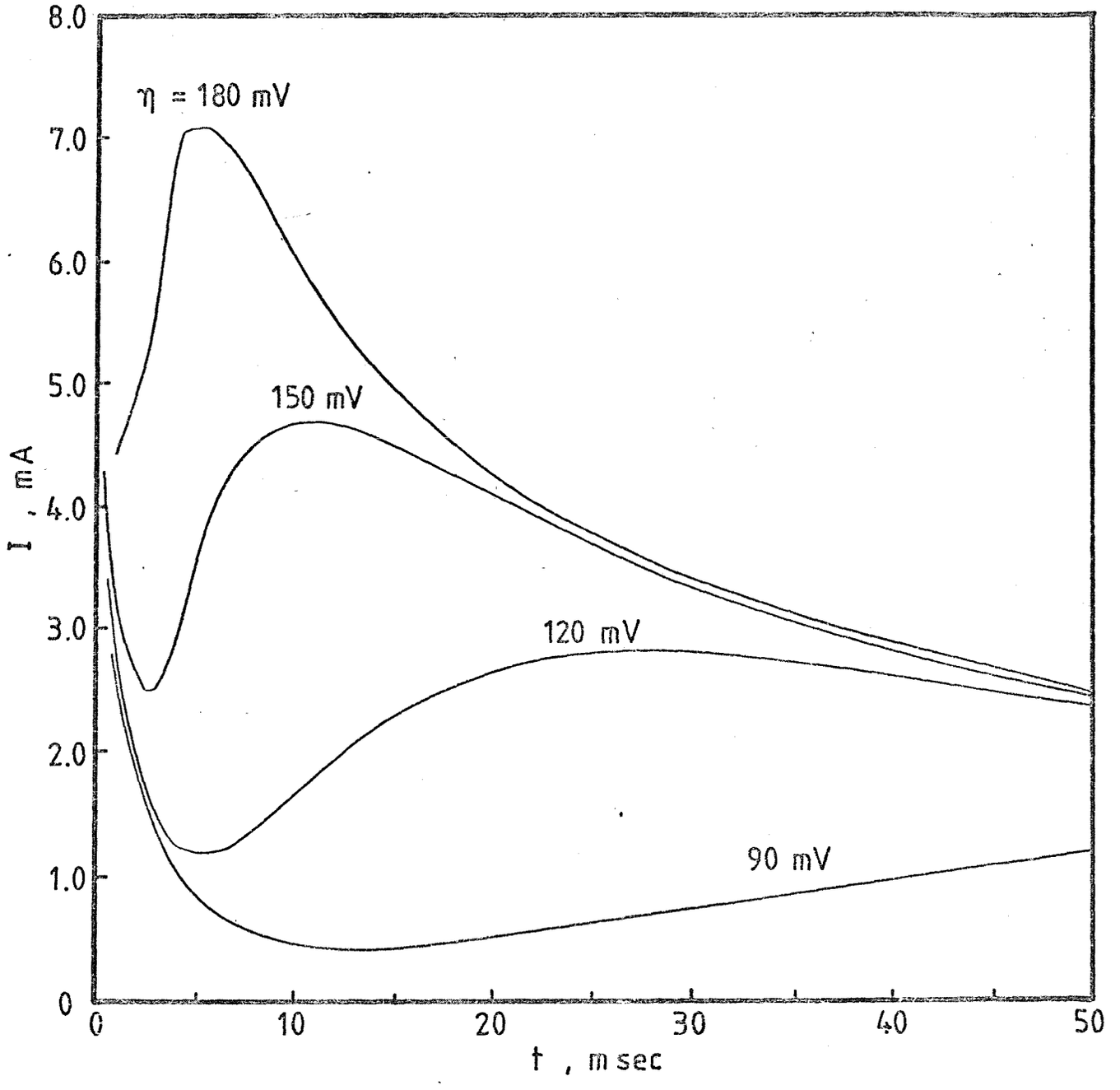

Figure 6.4 Current-time transients for the discharge of 10 mM $AgNO_3$ in 1 M KNO_3 on un-treated platinum (A = 0.189 cm^2) at the overpotentials indicated.

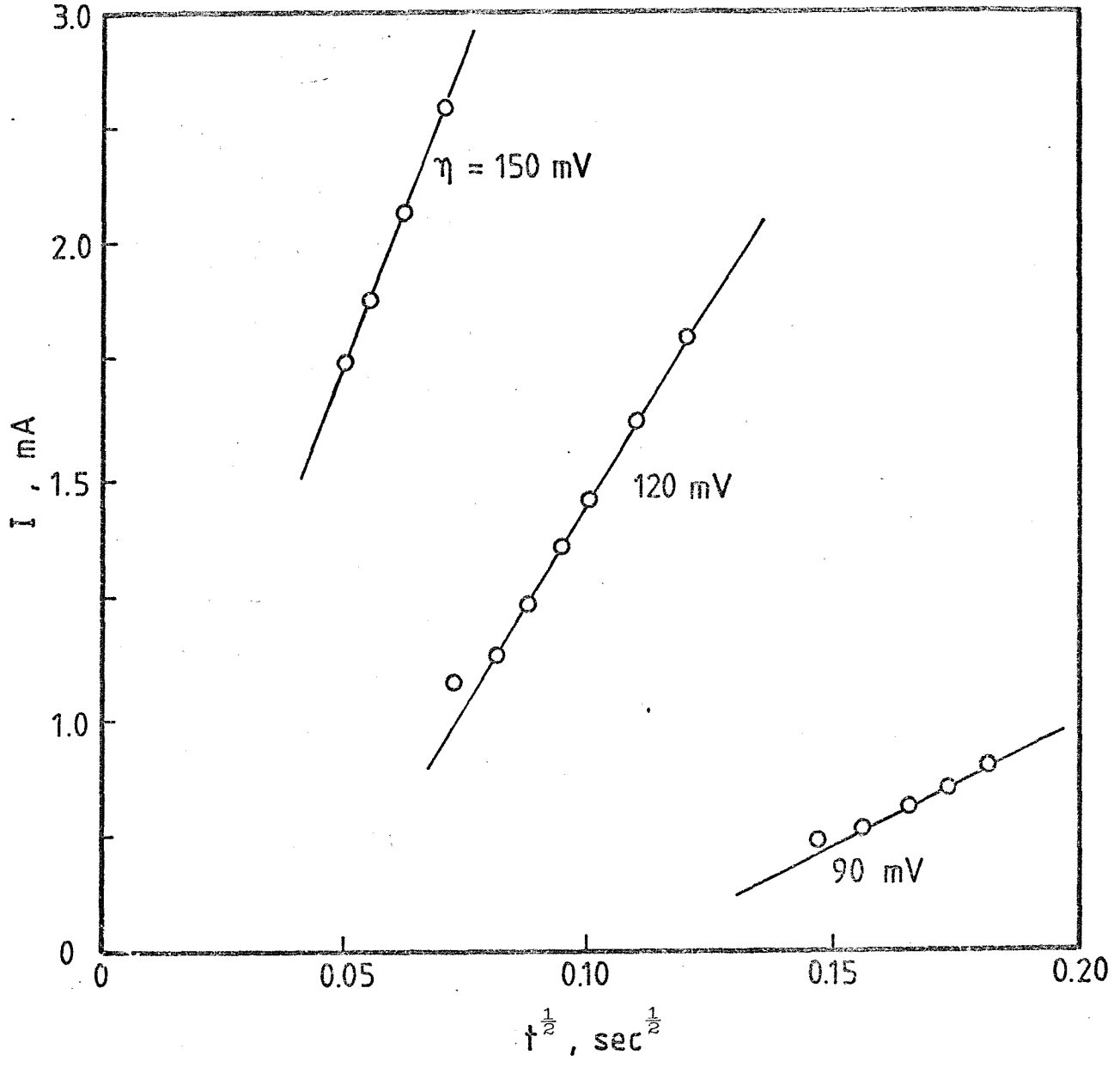

Figure 6.5 Current-time$^{\frac{1}{2}}$ plots for the silver deposition at the overpotentials indicated. (Data from Figure 6.4)

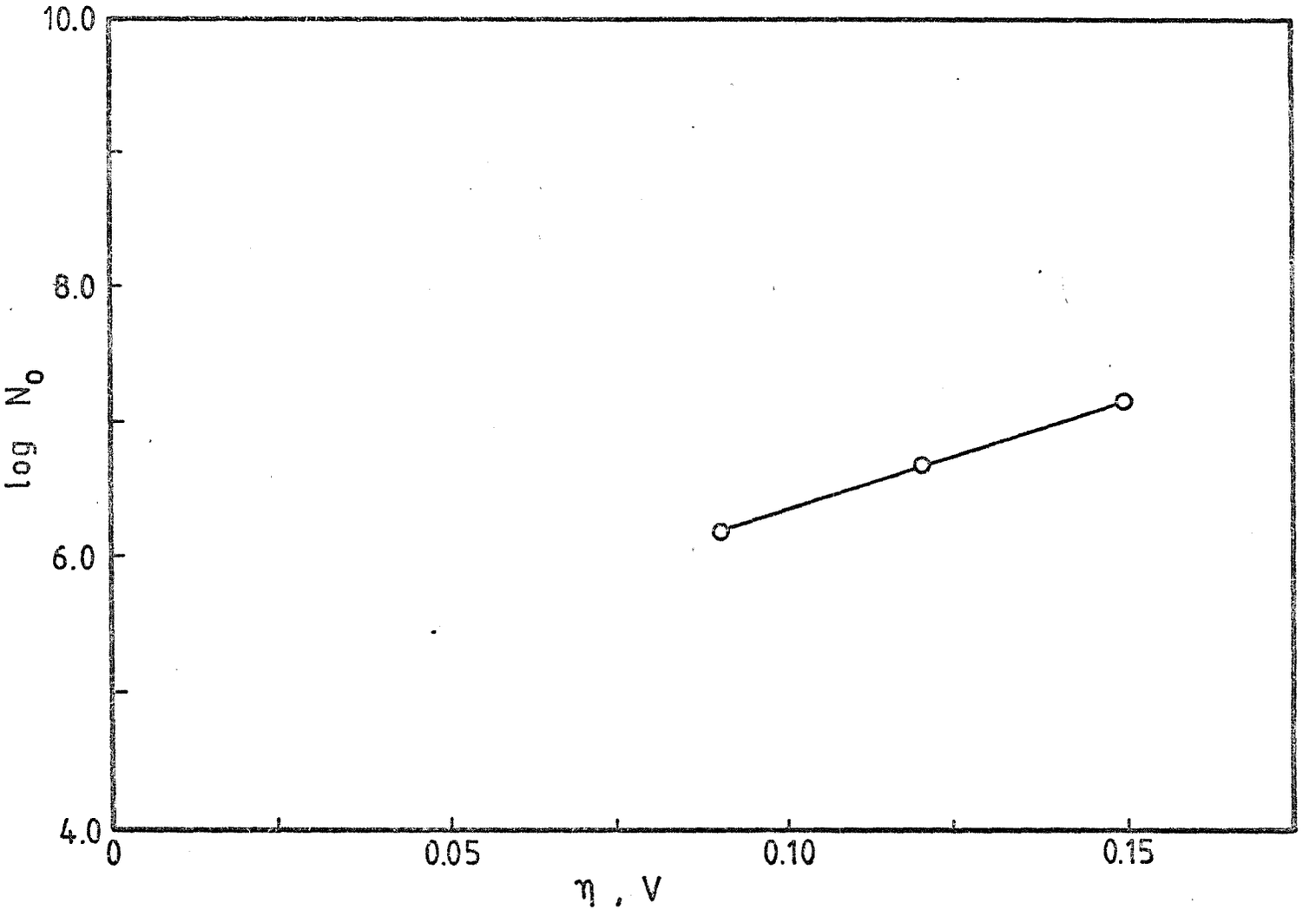

Figure 6.6 Logarithmic plot of N_o vs η (Data from Figure 6.4)

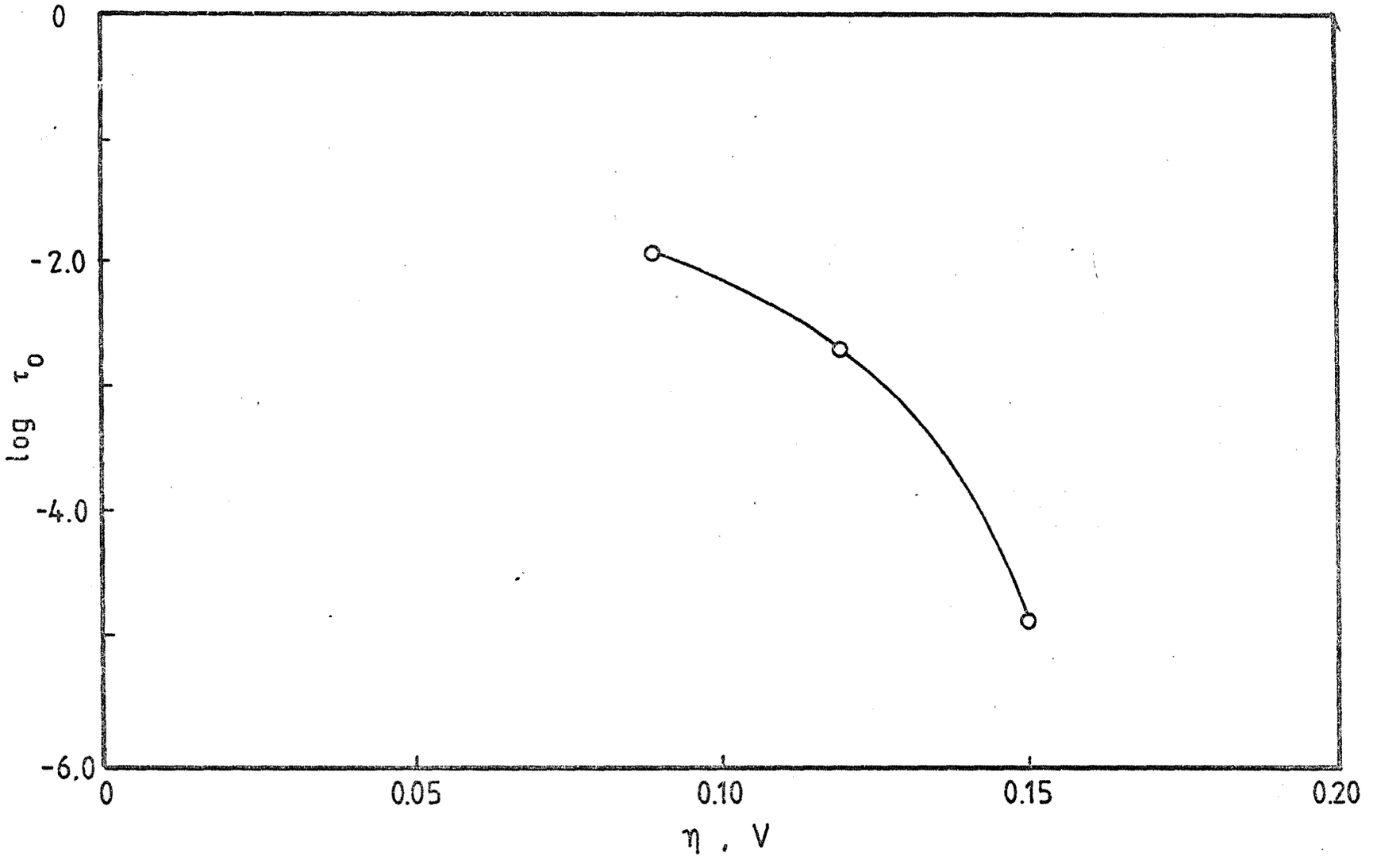

Figure 6.7 Logarithmic plot of intercept τ_o vs η (Data from Figure 6.5)

TABLE 6.1 Successive peak potential separation vs Ag/Ag(I)(0.01 M) and relative cathodic and anodic charges for the reduction and re-oxidation of 0.01 M $AgNO_3$ in 1.0 M KNO_3 solution onto (a) pre-treated Pt electrode and (b) un-treated Pt electrode of area 0.189 cm^2 and at the sweep rate of 0.1 V sec^{-1}, start cycling from +0.8 V to -0.3 V

$E_p^{cathodic}$ / mV	E_p^{anodic} / mV	ΔE_p / mV	$C^{cathodic}$ / mC	C^{anodic} / mC	$C^{cathodic}/C^{anodic}$
(a) pre-treated Pt electrode					
120	67	187	2.1360	2.0787	1.0274
161	67	228	2.1591	2.1557	1.0015
174	67	238	2.1741	2.1608	1.0062
177	64	241	2.1700	2.1421	1.0136
183	61	244	2.1700	2.1292	1.0191
(b) un-treated Pt electrode					
216	36	252	2.1111	1.2929	1.6328
200	36	236	2.0202	1.1717	1.7241
194	29	223	1.9393	1.0101	1.9199
194	25	219	1.8585	0.8686	2.1396
187	22	216	1.7575	0.7474	2.3514

6.2 Results and discussion

6.2.1 Aqueous systems

This part of the work is concerned with further investigation of the effect of oxide films on the voltammetric behaviour of platinum in dilute aqueous silver nitrate solution (0.01 M $AgNO_3$ in 1 M KNO_3). Typical cyclic voltammograms for (i) pre-treated and (ii) un-treated platinum electrodes are shown in Figure 6.1. The steep rise of the cathode current-time transient, the displacement of the peak to cathodic overpotentials as evidenced by the peak separation and the cross-over of the rising and falling cathodic currents are all evidence of the onset of nucleation as the rate-determining process.

Evidently, silver does not 'wet' platinum oxide and 3D nucleation (assumed to be hemispherical) occurs: the same evidence is apparent from potentiostatic experiments which give rise to (i) normal falling current-time transients and (ii) initially rising transients (Figure 6.2). In the first case, electrodeposition of silver onto the entire platinum surface area (assumed to be, on average, planar) gives (according to equation (3.2)) a linear regression line between current and $t^{-\frac{1}{2}}$ passing through the origin. From Figure 6.3 this is clearly so and the corresponding value of D_{Ag^+} (= $1.67 \times 10^{-5} cm^2\ sec^{-1}$) is in good agreement with literature values (= $1.57 \times 10^{-5} cm^2\ sec^{-1}$).[116] On the other hand, the un-treated, oxide-covered platinum electrodes give rise to rising current-time transients the shape of which are markedly dependent on the applied overpotential (see Figure 6.4). As predicted by equation (4.52) the rising currents are linear functions of $t^{\frac{1}{2}}$ (see Figure 6.5), the slopes of which may be used to calculate the nuclear density as a function of overpotential. This is invariably an exponential function and Figure 6.6 shows a logarithmic plot of N_o *vs* η and also of I *vs* $t^{\frac{1}{2}}$ the intercepts of the regression lines in Figure 6.7. The detailed consideration of these aspects is a matter for later consideration. Here, we are concerned with the role and the properties of the oxide layer.

Some of these properties are most evident from the cyclic voltammograms. As we have seen, pre-treated, oxide-free electrodes give rise to normal diffusion-controlled transients and to normal stripping peaks. Peak potential separations and relative cathode and anode current efficiencies under a variety of conditions are shown in Table 6.1 and

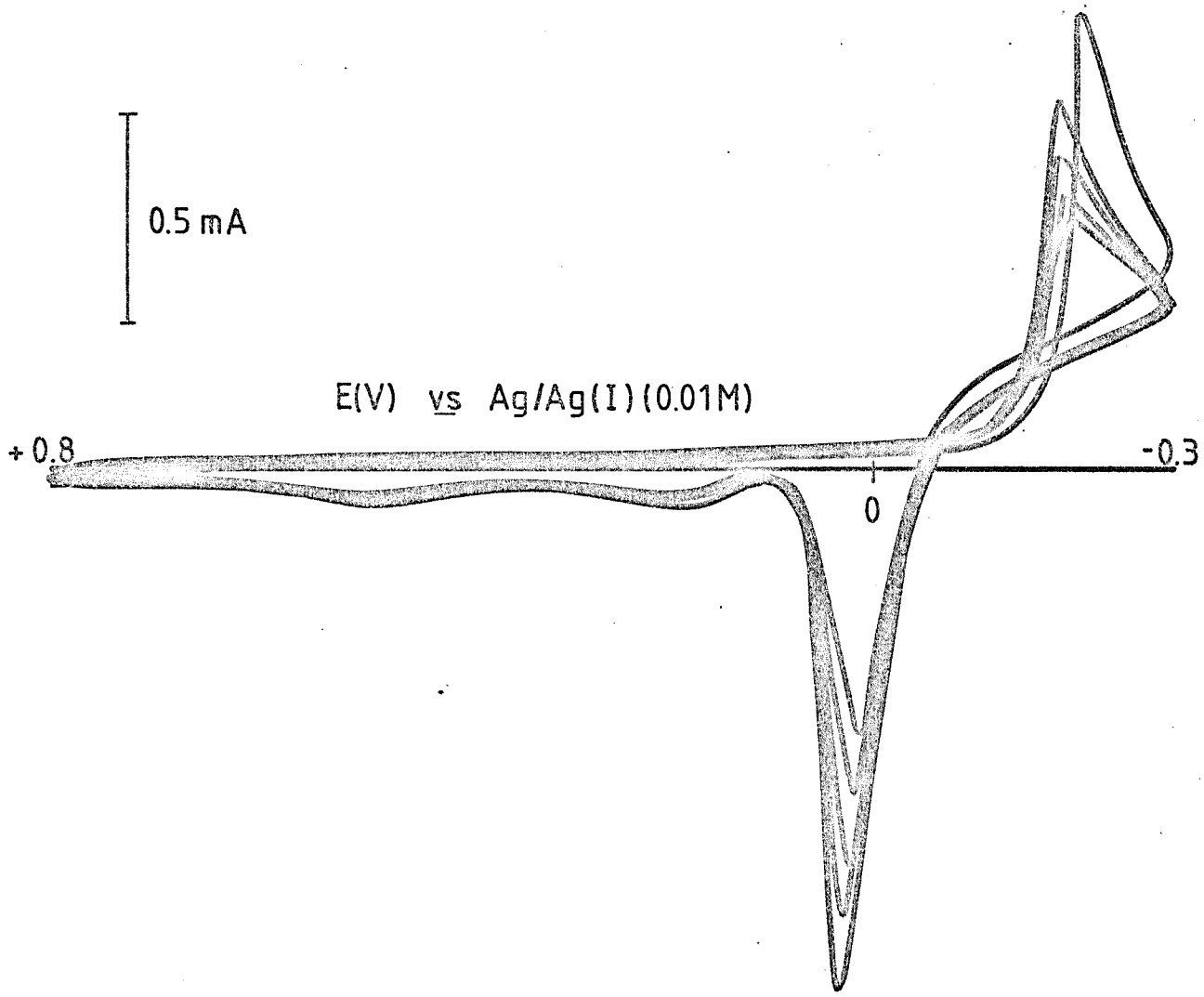

Figure 6.8 Multisweep voltammogram for the reduction of 10 mM $AgNO_3$ in 1 M KNO_3 on un-treated platinum (A = 0.189 cm^2), v = 0.1 V sec^{-1}.

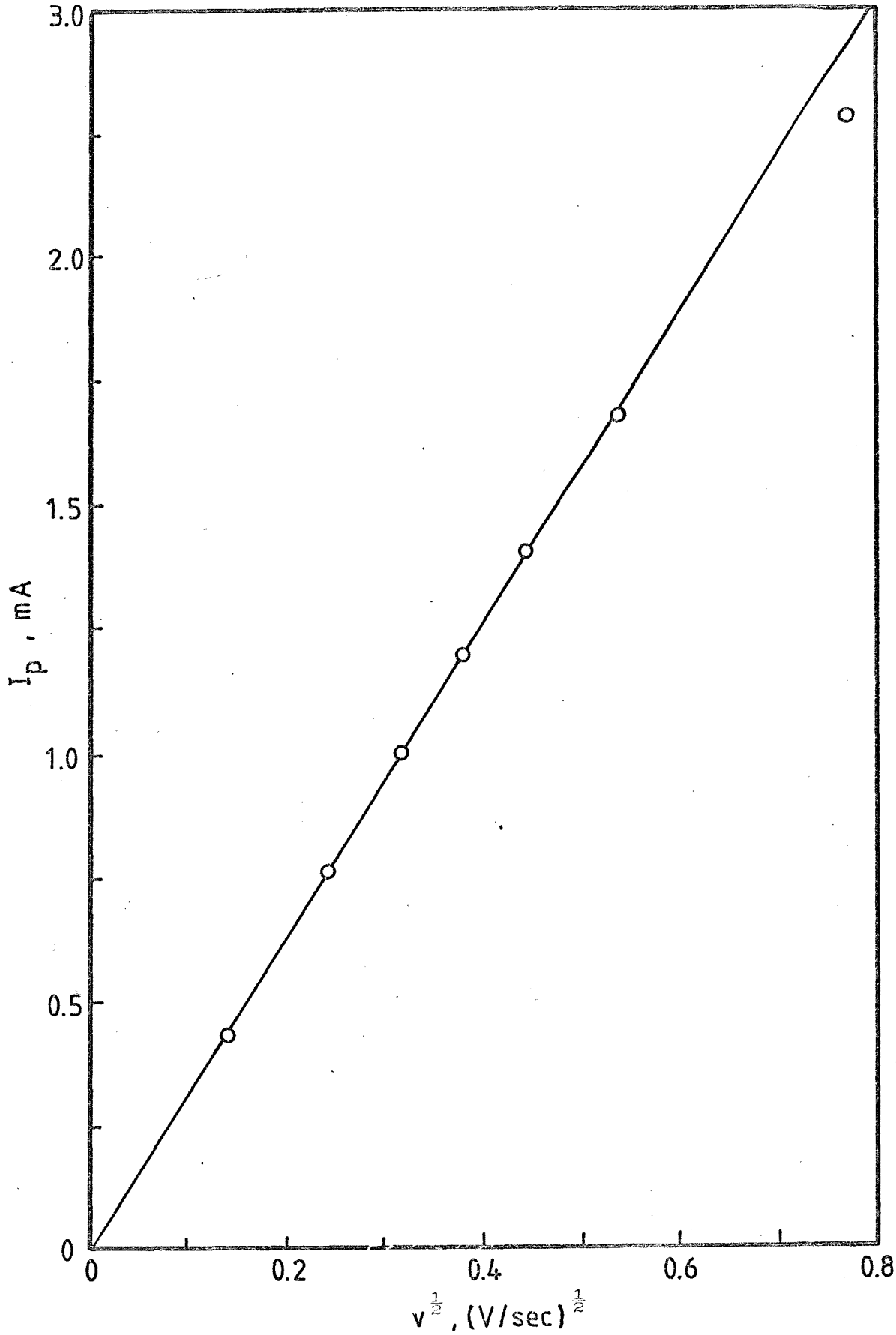

Figure 6.9 Linear relationship between I_p and $v^{\frac{1}{2}}$ for the reduction of 10.2 mM $AgNO_3$ in 1 M KNO_3 on pre-treated platinum (A = 0.189 cm^2).

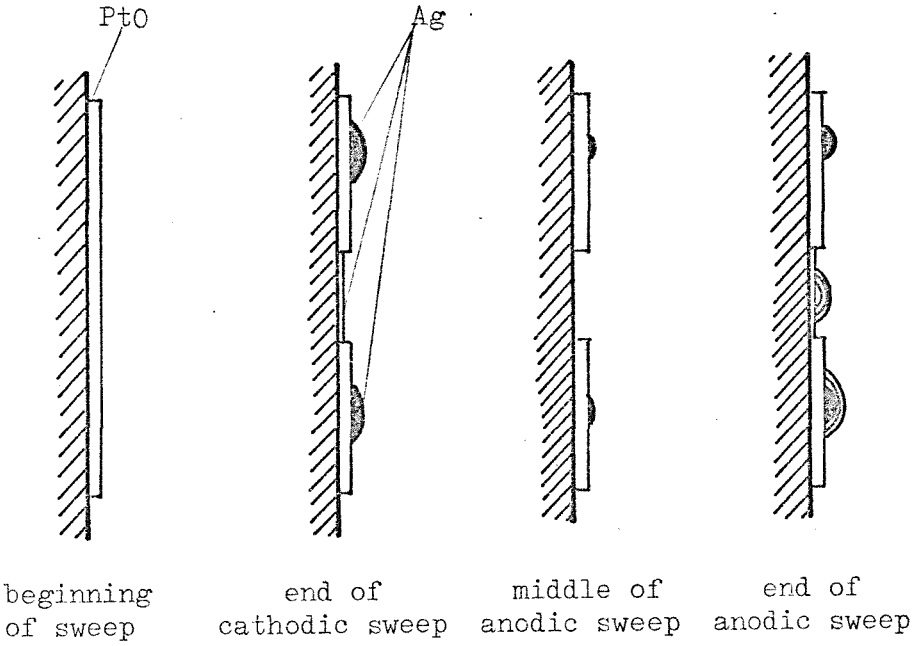

Figure 6.10 A proposed mechanism for the electrodeposition and dissolution of silver onto platinum.

confirm the findings of Bixler and Bruckenstein[114]. On the other hand, un-treated, oxide covered electrodes give rise to different behaviour and on repeated cycling (Figure 6.8) it is immediately evident that the stripping peak height progressively decreases with successive cycling. Other features may also arise depending on the experimental conditions such as pH, scan amplitude, etc.

Figure 6.9 (I_p *vs* $v^{\frac{1}{2}}$ for $AgNO_3$(0.0102 M) in 1 M KNO_3) shows a straight line passing through the origin, and the diffusion coefficient calculated from the slope is $D = 2 \times 10^{-5} cm^2\ sec^{-1}$.

The decrease in stripping current peak height is reflected in the progressive decrease in relative anode current efficiency (Table 6.1) and it must be concluded that the platinum oxide layer is asserting its n-type semi-conductor properties and that some rectification of the triangular sweep function is occurring. The rectification is not complete and this may be because the oxide film is incomplete or that the thin oxide layer is not an efficient semi-conductor.

The general picture, however, can be summarised in Figure 6.10 as in Figure 6.8.

Repetition of the cycle invariably shows that the second cathodic peak potential is shifted anodically because some nuclei are preserved which undercut the otherwise higher nucleation overpotential.

The persistence of the oxide layer might be thought to be dependent on pH but the effect of added nitric acid (0.1 M) is small.

As noted above the rates of formation and dissolution of platinum oxide are slow, at least in aqueous solutions and at room temperatures. In Figure 6.10, an attempt is made to show qualitatively that the original Pt-O film would normally decrease in thickness or extent during the cathodic half-cycle. However, the potential range in which this occurs overlaps strongly with the range of silver deposition potentials and it is likely that silver will be deposited readily as fresh platinum surface is uncovered. Such silver is likely also to dissolve readily during the anodic half-cycle. On the other hand, Pt-O covered with silver is now protected (at least partially) from the cathodic dissolution process. It will therefore persist under both cathodic and anodic conditions and can be imagined progressively to build up, leaving less and less of the platinum surface free for the normal deposition and dissolution of silver.

The limiting state of the anodic 'passivation' of the electrode will no doubt depend on the rate of the formation and dissolution of the oxide as well as on the p-type electrical leakage through the oxide film.

Although these phenomena were the main features of the voltammetric behaviour of treated and un-treated platinum electrodes, there were others. These arose when the amplitude of the linear sweep was increased either anodically or cathodically. Thus, if the electrode is polarised to +800 mV anodic a second anodic current peak progressively appears. The same peak appears if the cathodic limit is increased and it must be assumed that at high cathodic overpotentials the dissolution of the oxide layer can continue possibly along the line of the platinum-platinum oxide interface. If it 'undercuts' the Pt-O and the silver on top of it, then this process would contribute to the subsequent anodic inefficiency and it might also lead to the underpotential deposition of silver on cathodically cleaned platinum. If this were so, then the second anodic peak could be due to the dissolution of silver from a monolayer of silver partially 'reacted' with platinum, i.e. deposited at an underpotential. Certainly, the number of coulombs in the second peak was never more than 0.9 of a total monolayer.

Alternative explanations of the second peak include

(a) surface oxidation of the Ag to Ag_2O (but the second peak persists in acid solution)

(b) the oxidative dissolution of Ag more firmly incorporated into the surface (other than as a monelayer) or

(c) the catalytic oxidation of the platinum at the Ag-Pt boundary, perhaps to a higher oxidation state.

Any such explanation needs also to be related to the promotion of the second anodic peak by extended anodic polarization, the second peak arises of course at the end of the first cycle, and increases in intensity with successive cycles. It is therefore connected with the interaction of deposited silver with the PtO system. The silver may catalyse the anodic oxidation of platinum so as to interfere with its integrity, thereby allowing subsequent access of silver ions to the platinum surface. If undissolved Ag is oxidized to Ag_2O and incorporated

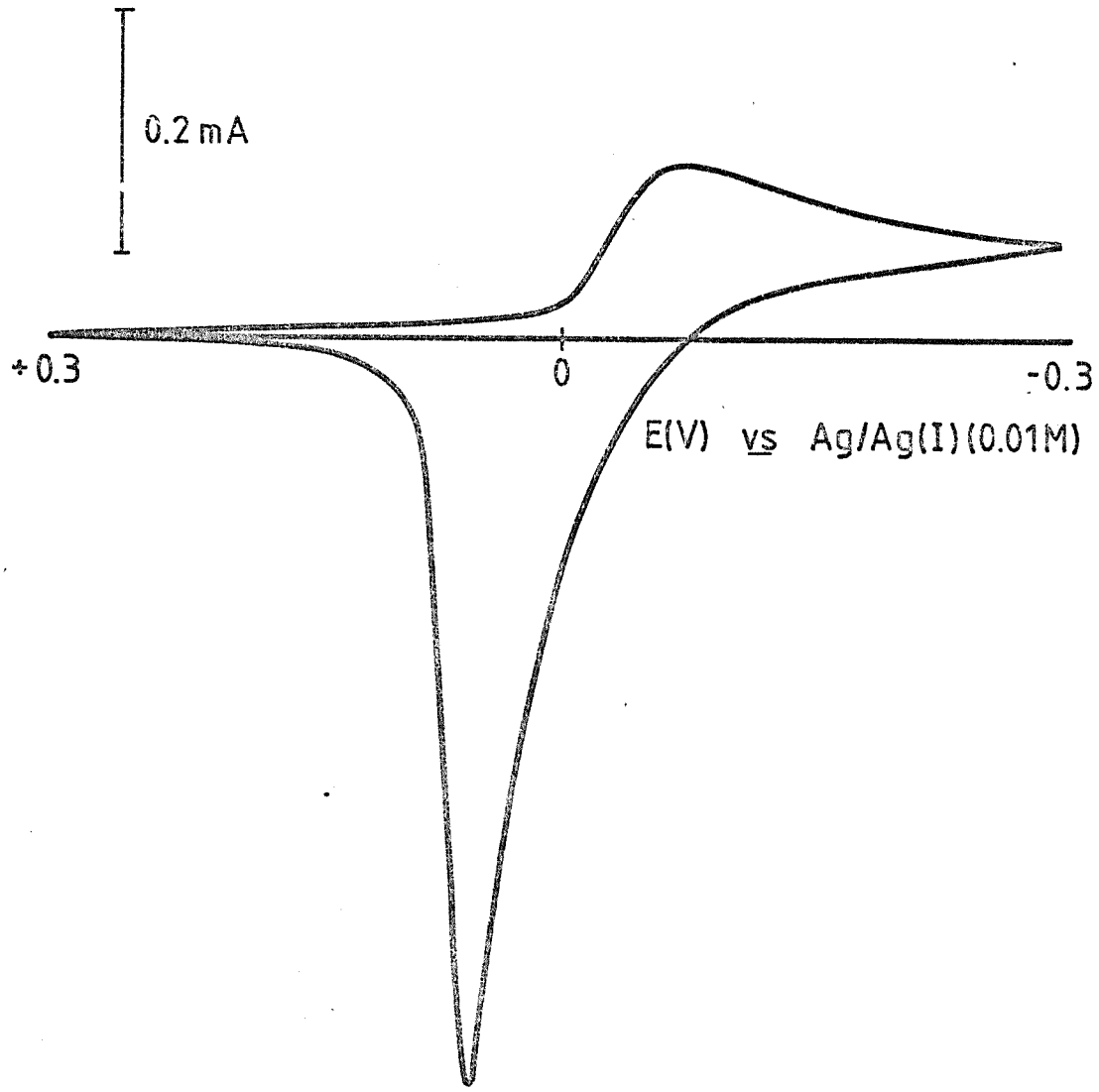

Figure 6.11 A typical voltammogram for the reduction of 6.10 mM $AgNO_3$ in $NaNO_3$-KNO_3 eutectic at 275°C on un-treated platinum (A = 0.143 cm^2), v = 0.1 V sec^{-1}.

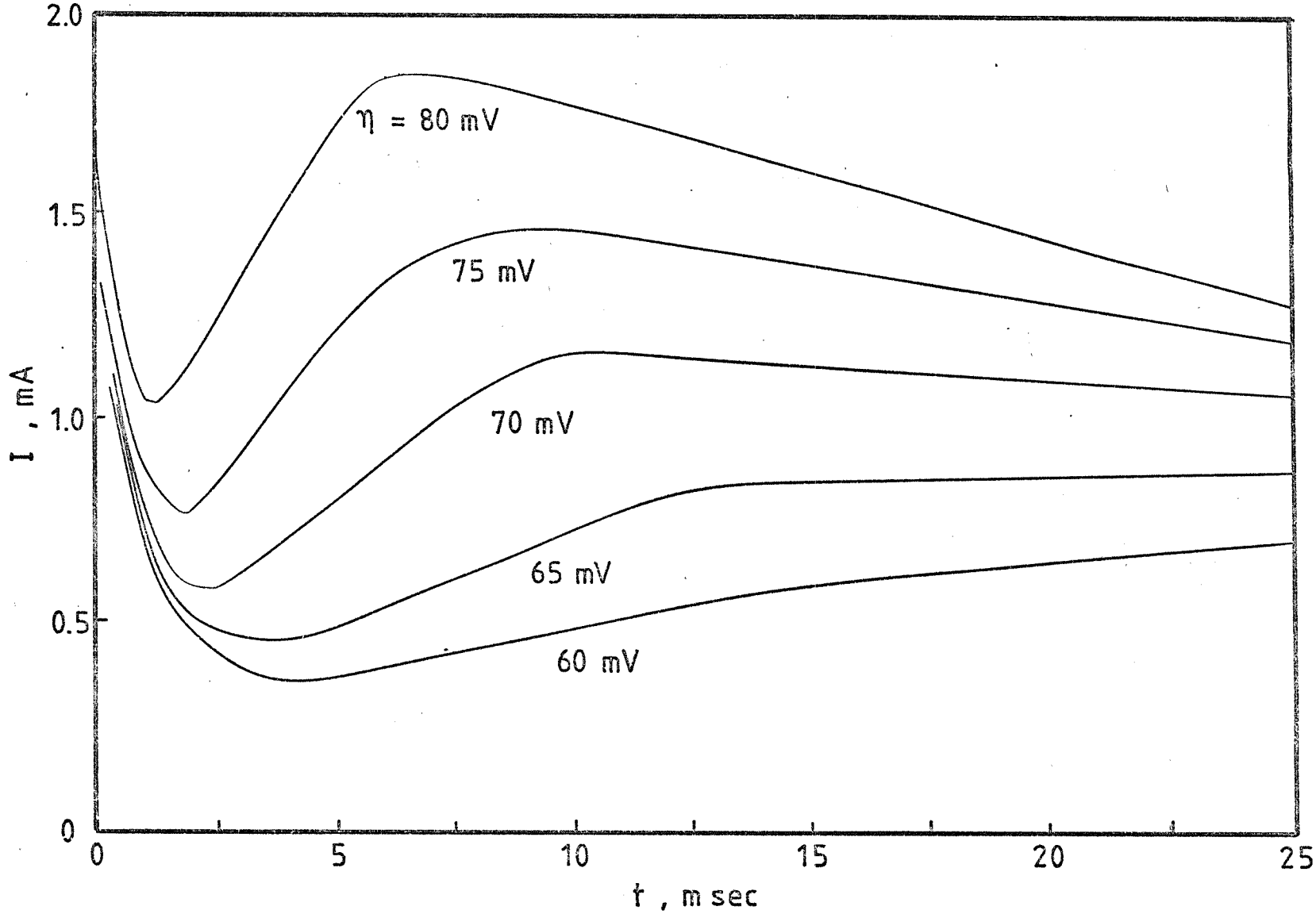

Figure 6.12 I-t transients for the deposition of 11.20 mM $AgNO_3$ on un-treated platinum (A = 0.129 cm^2) at a range of overpotentials indicated.

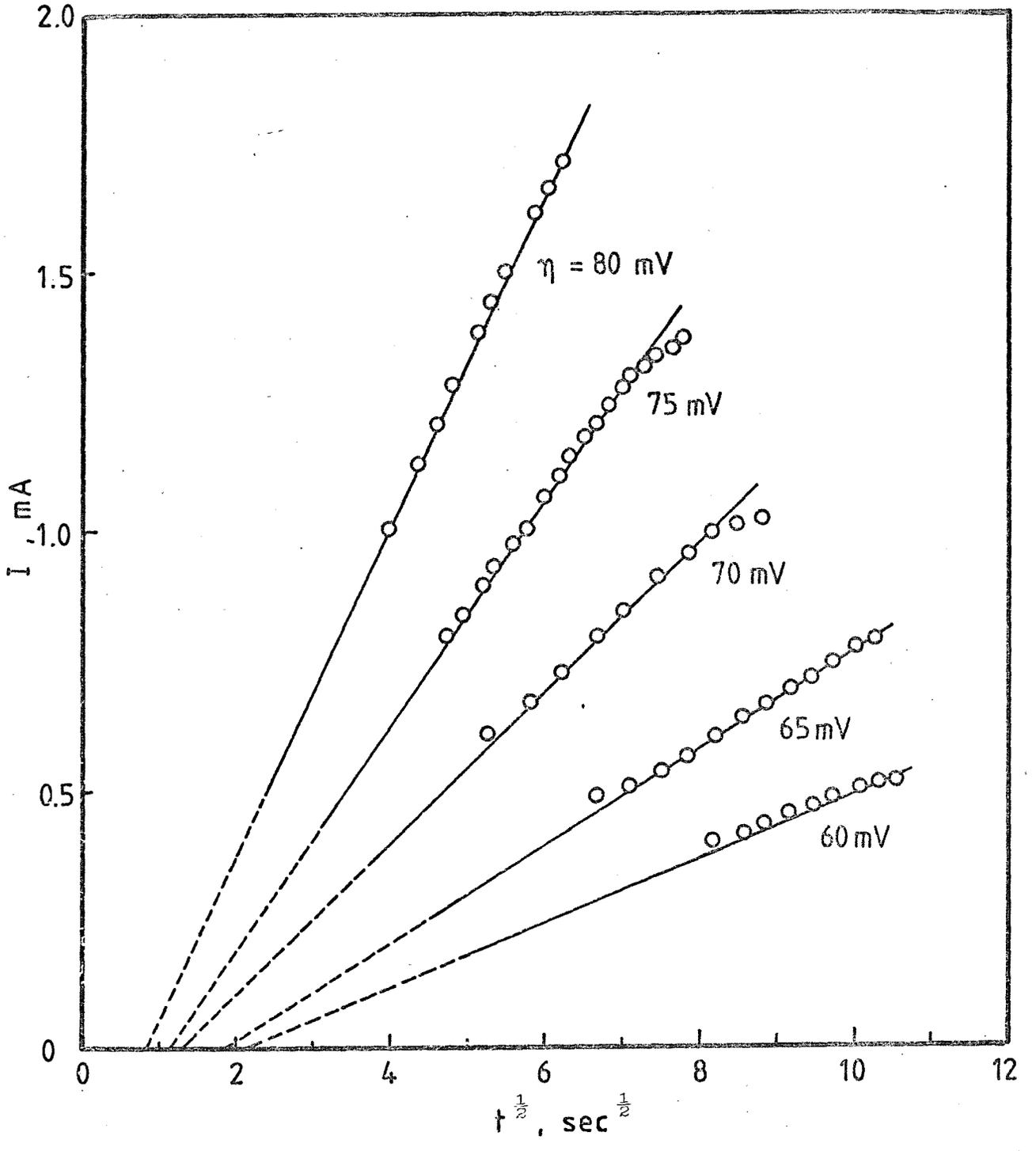

Figure 6.13 I vs $t^{\frac{1}{2}}$ plot for the deposition of silver from $NaNO_3$-KNO_3 eutectic at 275°C (Data from Figure 6.12).

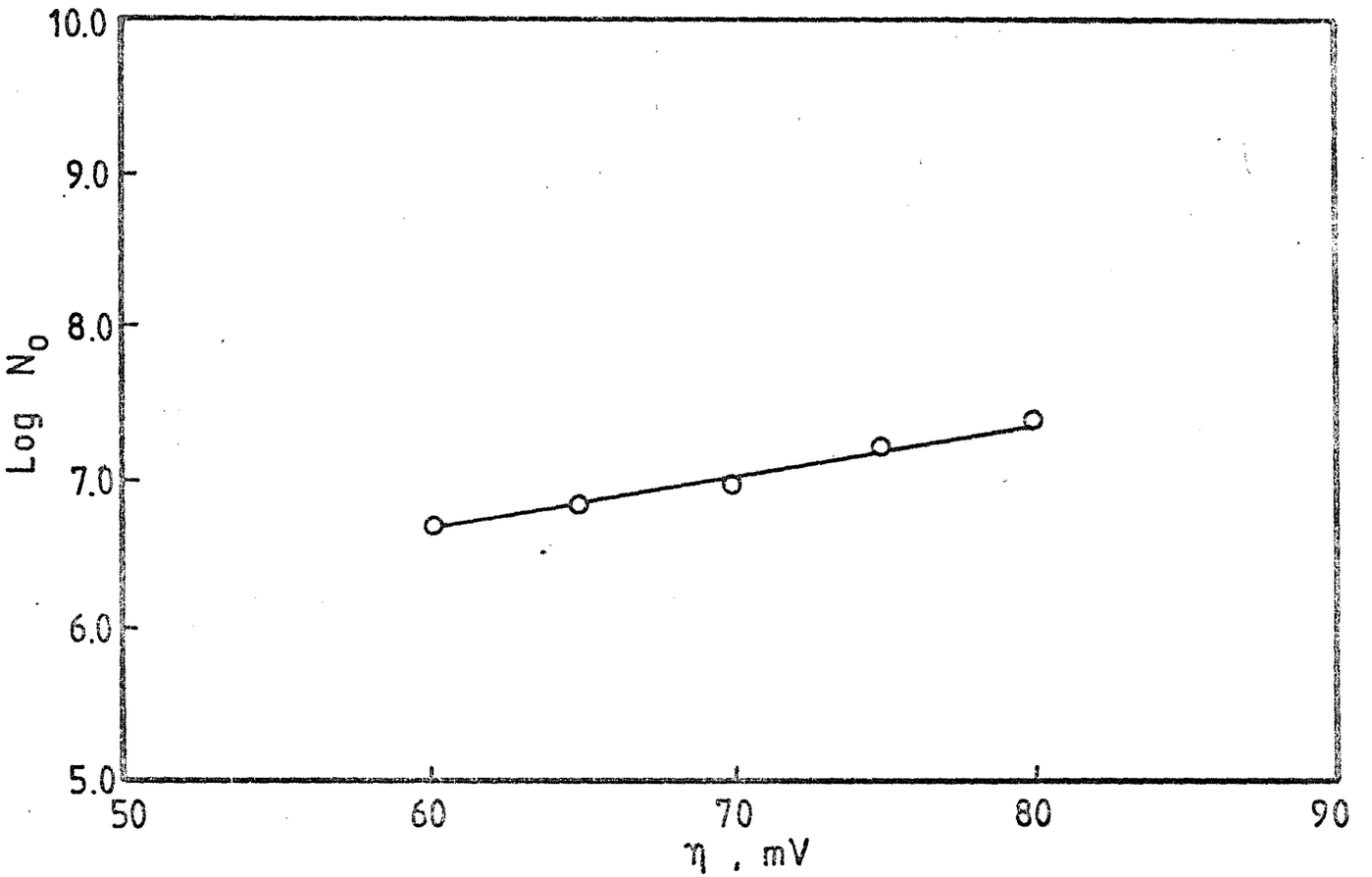

Figure 6.14 The relationship between log N_o and η (Data from Figure 6.12).

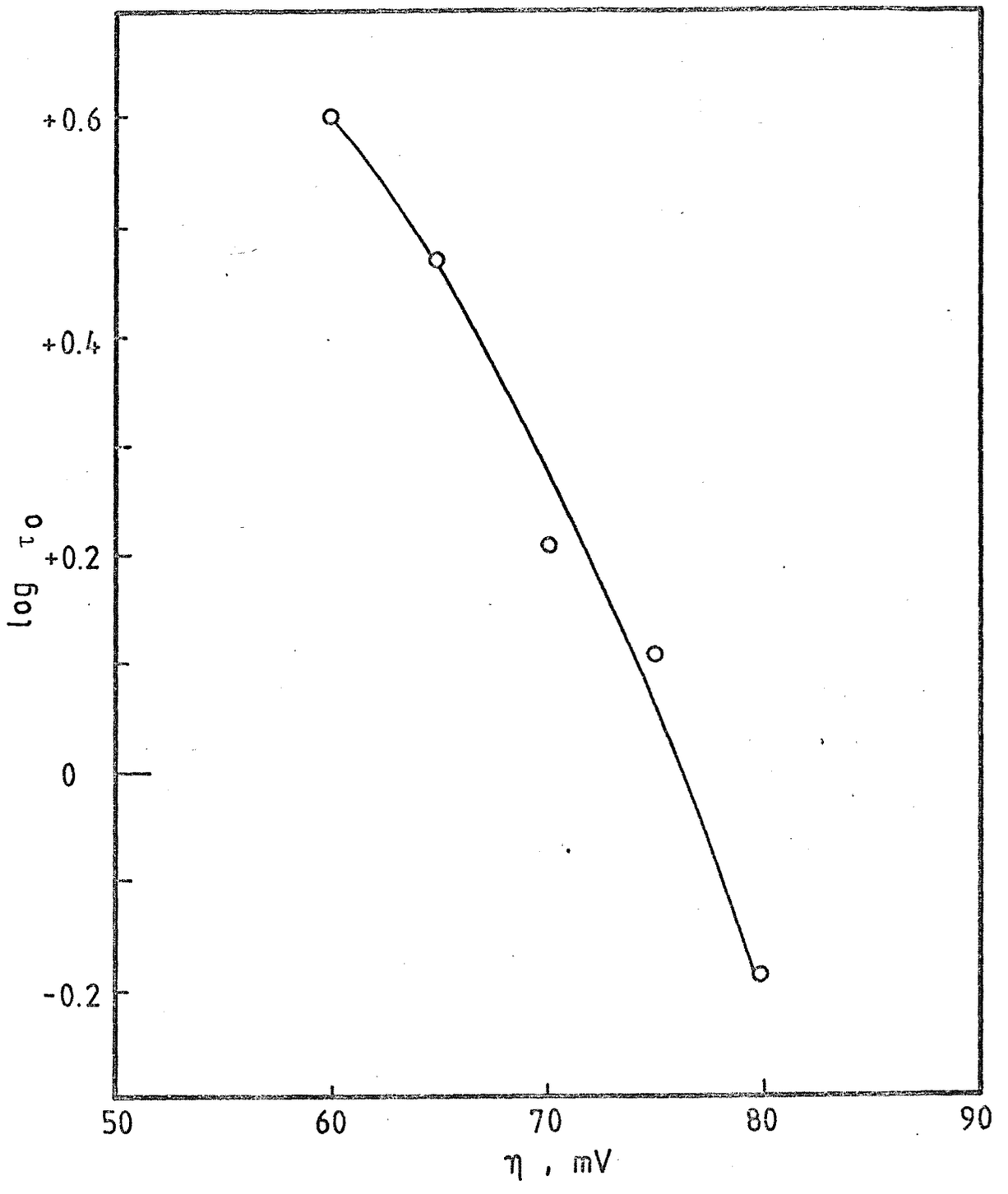

Figure 6.15 The relationship between log τ_o and η (Data from Figure 6.13).

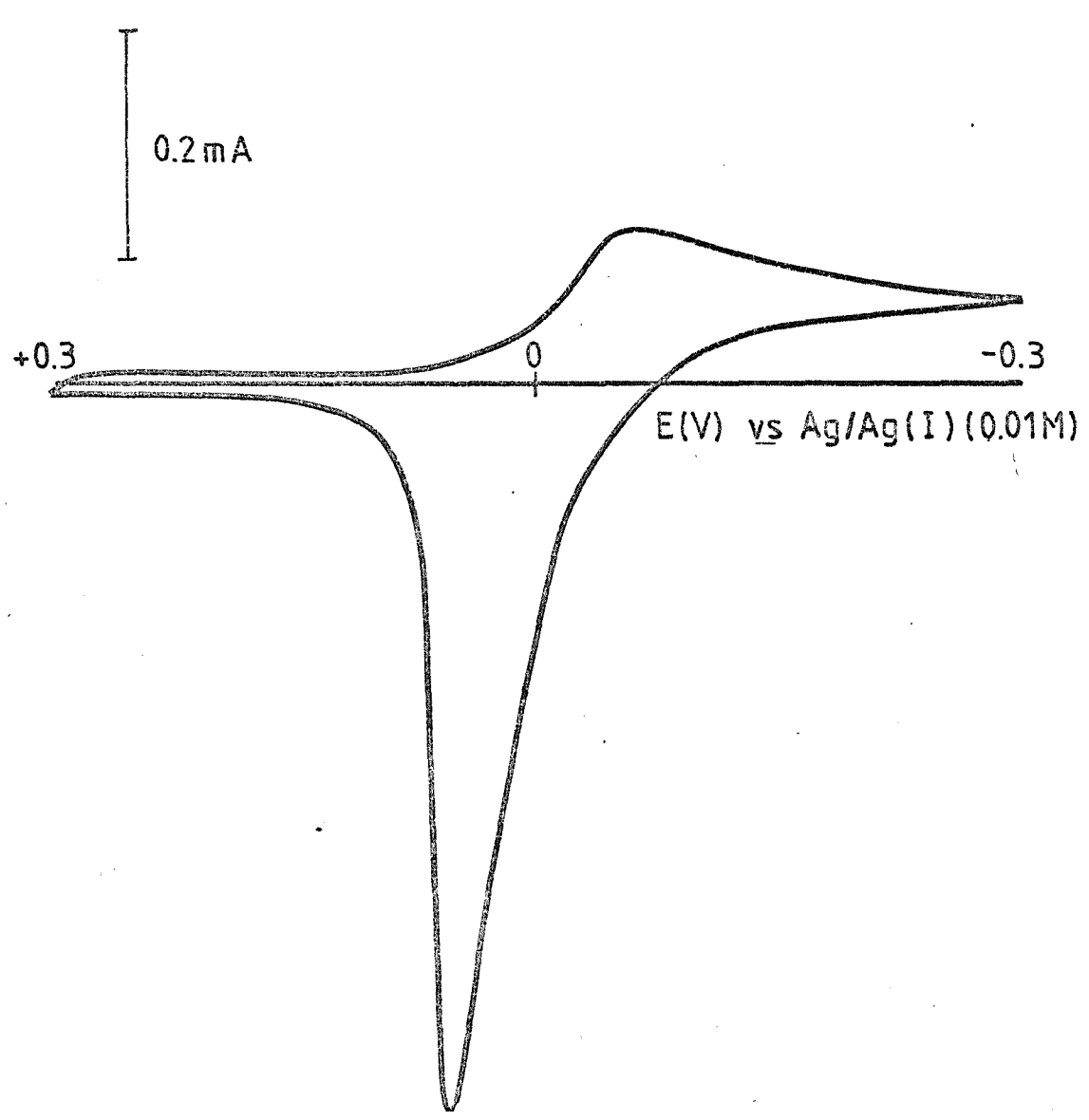

Figure 6.16 A typical voltammogram for the reduction of 6.10 mM $AgNO_3$ in $NaNO_3$-KNO_3 eutectic at 275°C on pre-treated platinum (A = 0.143 cm^2), v = 0.1 V sec^{-1}.

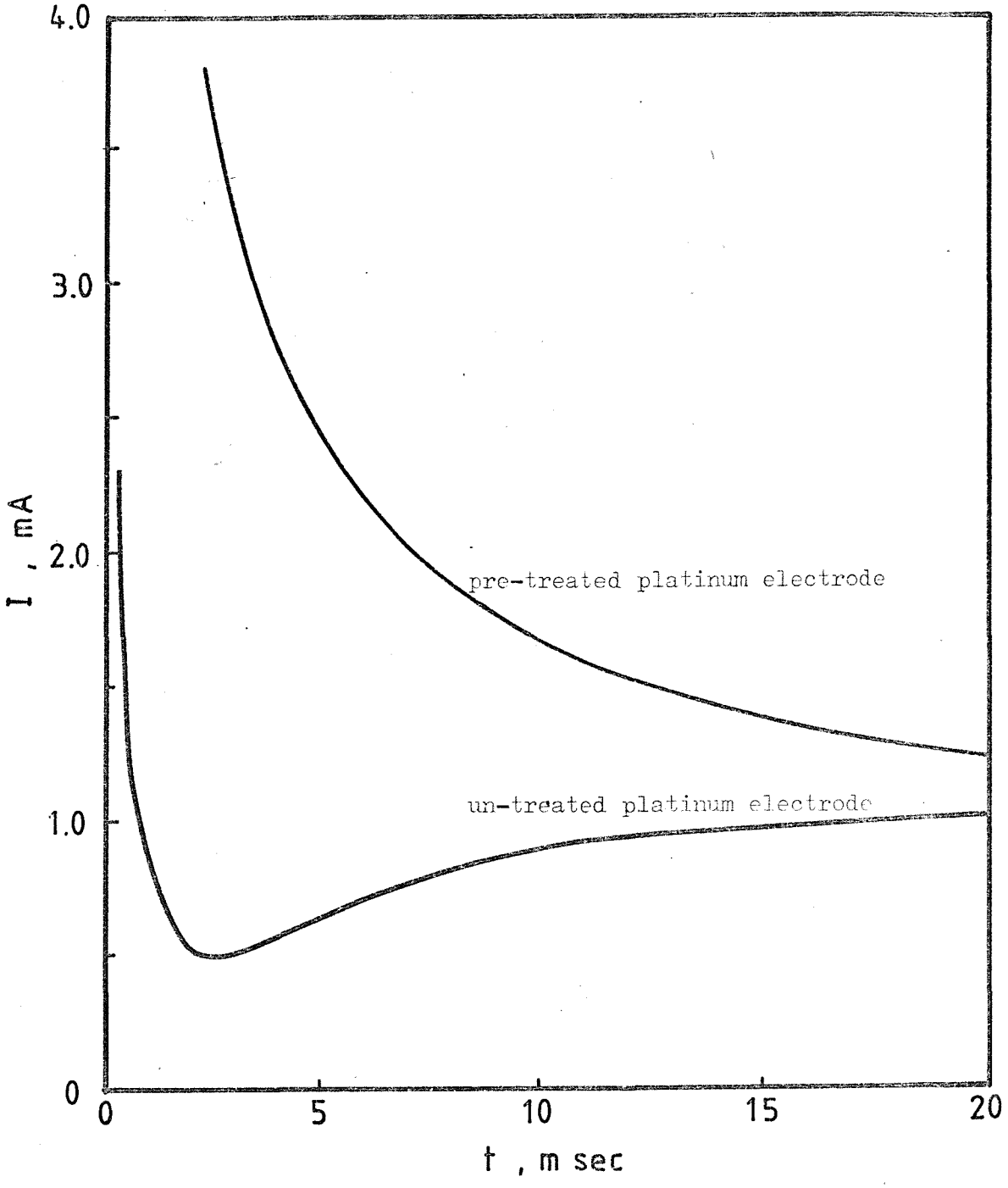

Figure 6.17 I-t transients for the discharge of 11 mM $AgNO_3$ in $NaNO_3$-KNO_3 eutectic at 275°C on pre-treated and un-treated platinum (A = 0.143 cm^2; η = 80 mV).

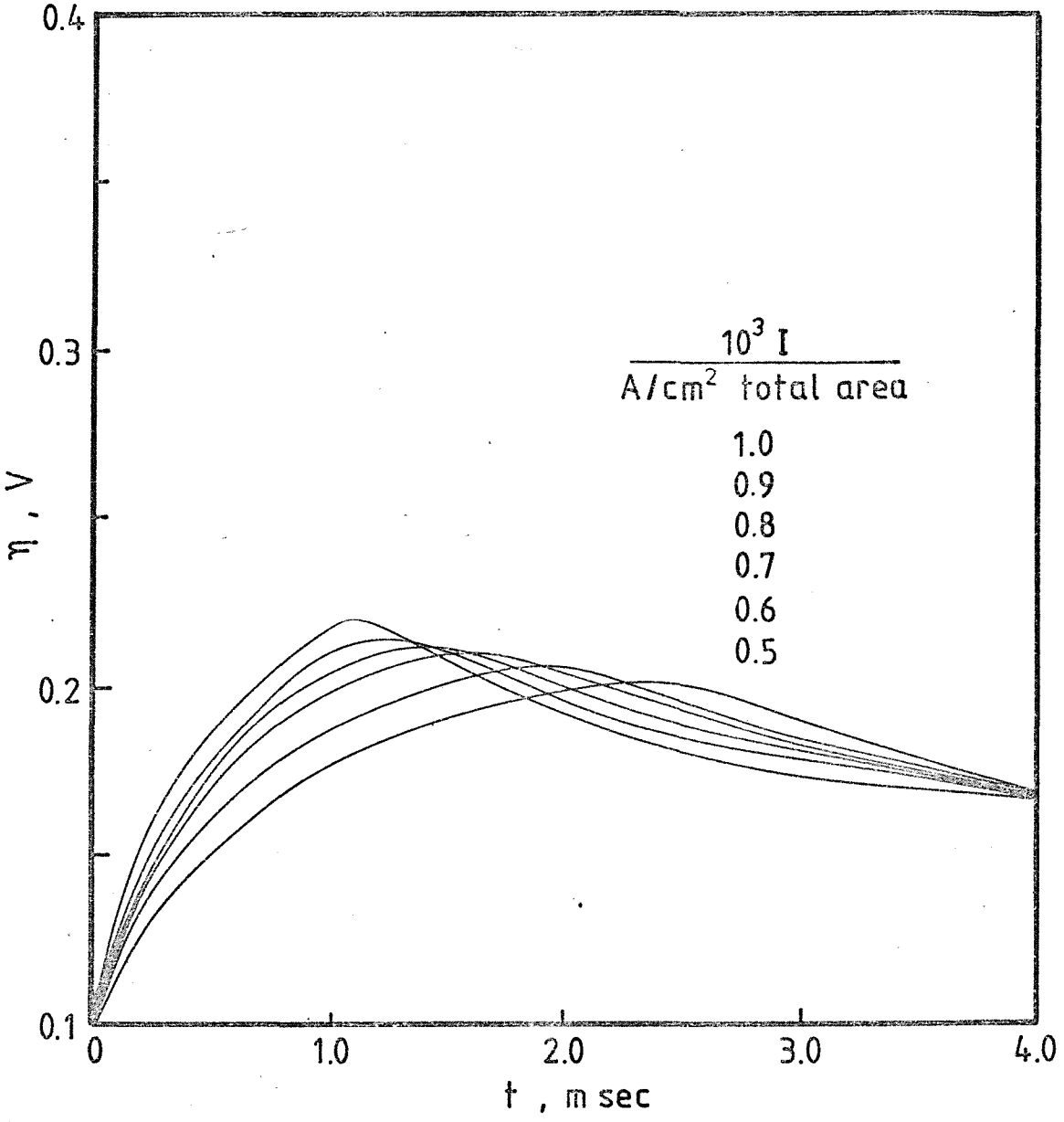

Figure 6.18 Galvanostatic transients for the reduction of 12.3 mM $AgNO_3$ on un-treated platinum (A = 0.029 cm^2) in 1 M KNO_3 at the applied constant currents indicated.

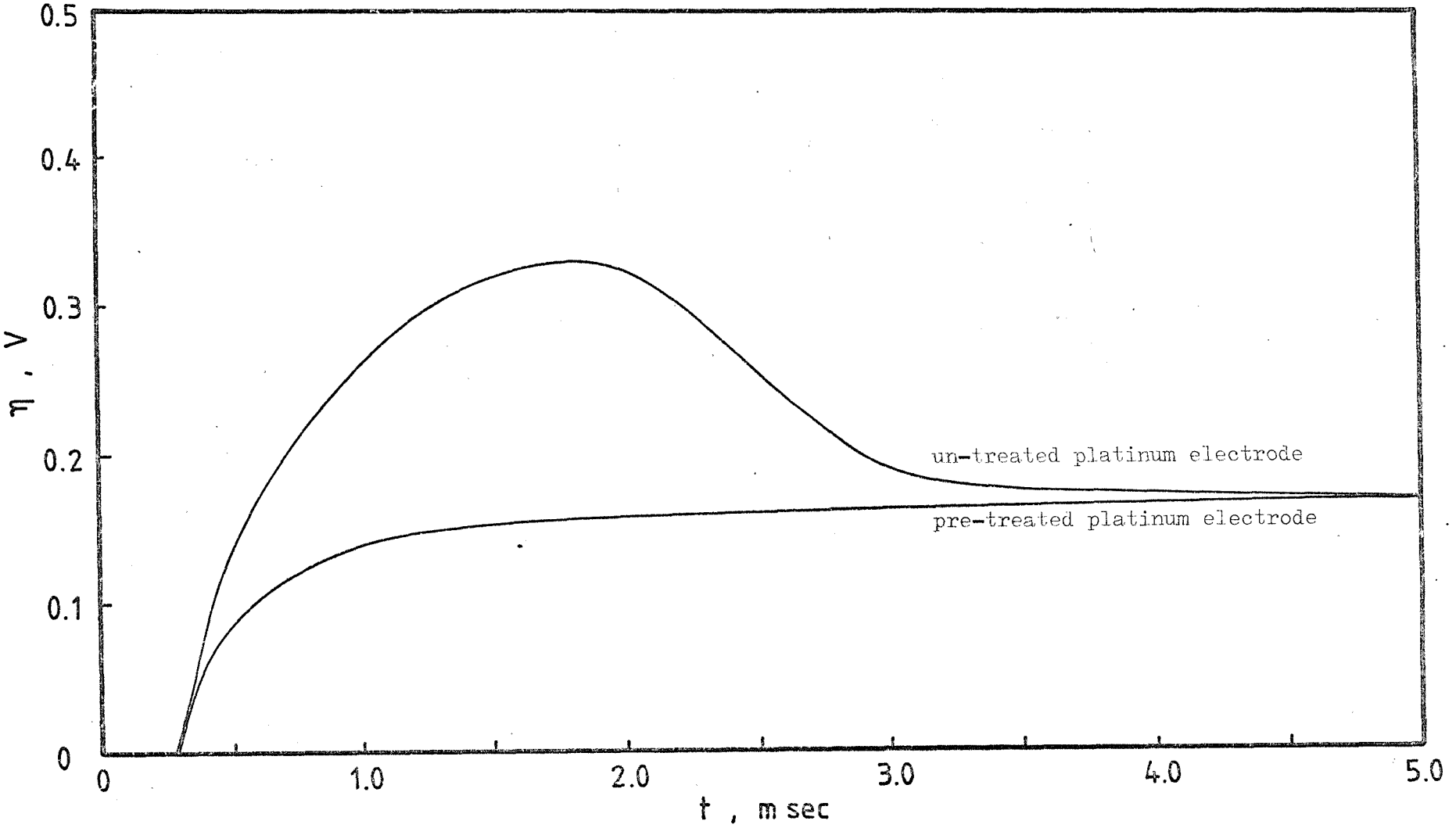

Figure 6.19 Galvanostatic transients for the reduction of 10 mM $AgNO_3$ in 1M KNO_3 on pre-treated and un-treated platinum at the constant current of 5 mA. (A = 0.189 cm^2)

into the underlying PtO then, perhaps, this might be promoted by extremes of anodic polarization and by the cathodic formation of an intermetallic surface Pt-Ag compound. However, all of these suggestions are speculations and the evidence we have, albeit faithfully recorded, is not sufficiently discriminating for us to postulate further.

6.2.2 Nitrate melts

The aqueous work was a precursor to the main research which is to study further the electrodeposition of metals from molten salts. Here we record that part of the molten salt work which bears on the properties of platinum as a working electrode. Hills et al[1,54] used platinum extensively in their study of molten nitrates and molten chlorides and found that the deposition of silver from nitrates was controlled entirely by the kinetic of nucleation. With hind-sight it might not be concluded that in molten $NaNO_3$-KNO_3 at 275°C, the surface of platinum is readily oxdized and that linear sweep and potentiostatic step experiment on platinum would give results similar to those found on un-treated platinum in aqueous solution. This is certainly the case as is seen in Figures 6.11, 6.12, 6.13, 6.14 and 6.15 but perhaps what is remarkable is that by using pre-treated electrodes one can, even in molten nitrates, also observe the behaviour of oxide free electrodes. Results from such systems are shown in Figures 6.16, 6.17 and 6.19. With time, however, the results reverted to those corresponding to oxide covered electrodes and it can simply be concluded that even 275°C, the rate of oxidation of platinum is slow.

6.2.3 Galvanostatic experiment

The theory of nucleation envisages that each nucleus grows at a rate which is influenced by its size and by the overpotential at its surface. The interplay of these two terms gives use to the form of the observed linear sweep voltammogram and to that of the potentiostatic current-time transient. In both cases, however, the main features of the current-time transient are those deriving from (a) the onset of diffusion control and (b) the increase in mass transfer arising from the growth of nuclear area. The effects of nuclear size and of nuclear overpotential on the kinetics of nucleation itself, i.e. on the rate of the charge transfer step, are not so easily discerned.

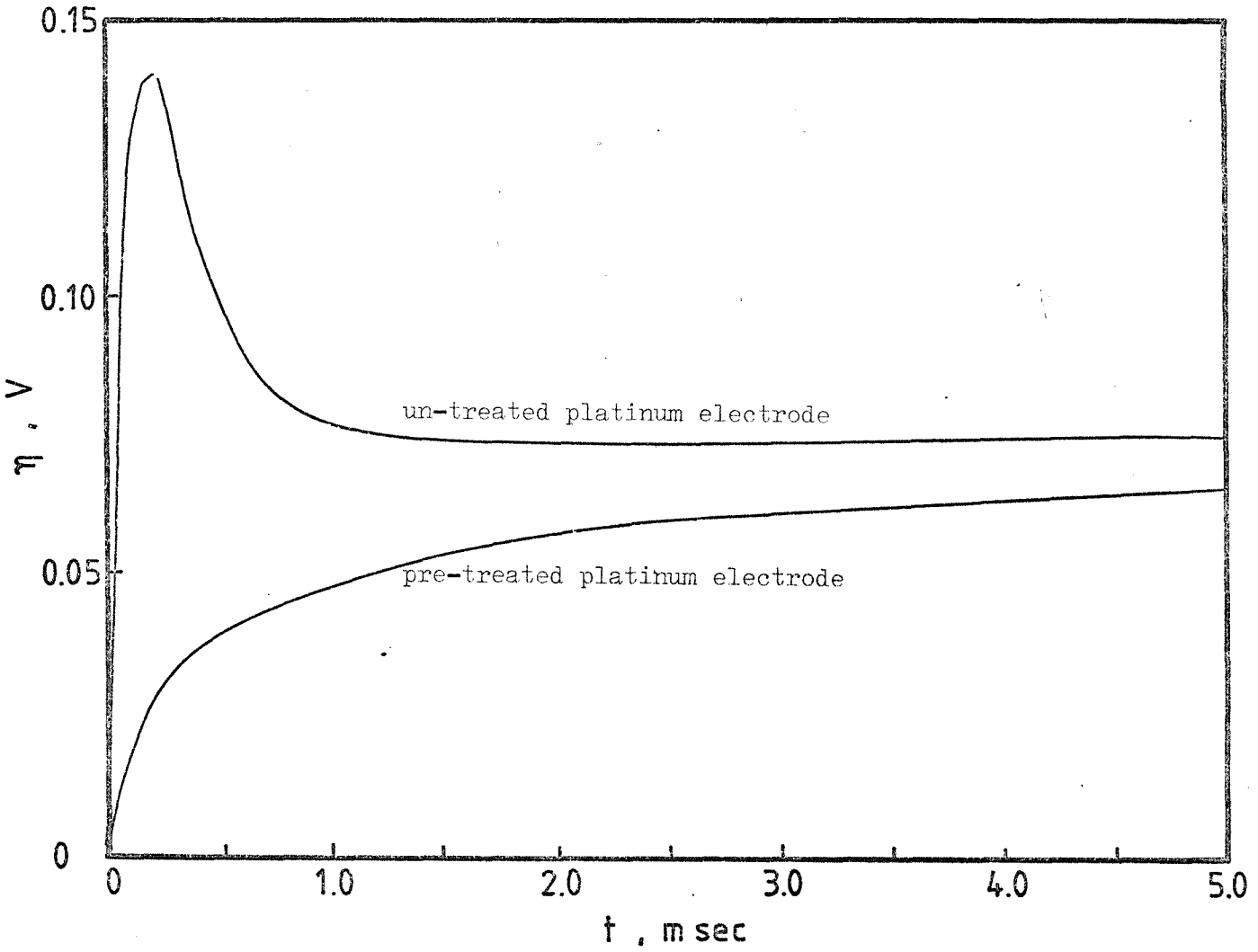

Figure 6.20 Potential-time transients for the reduction of 44.8 mM $AgNO_3$ in $NaNO_3$-KNO_3 eutectic at 275°C on pre-treated and un-treated platinum at the constant current of 10 mA. (A = 0.154 cm^2)

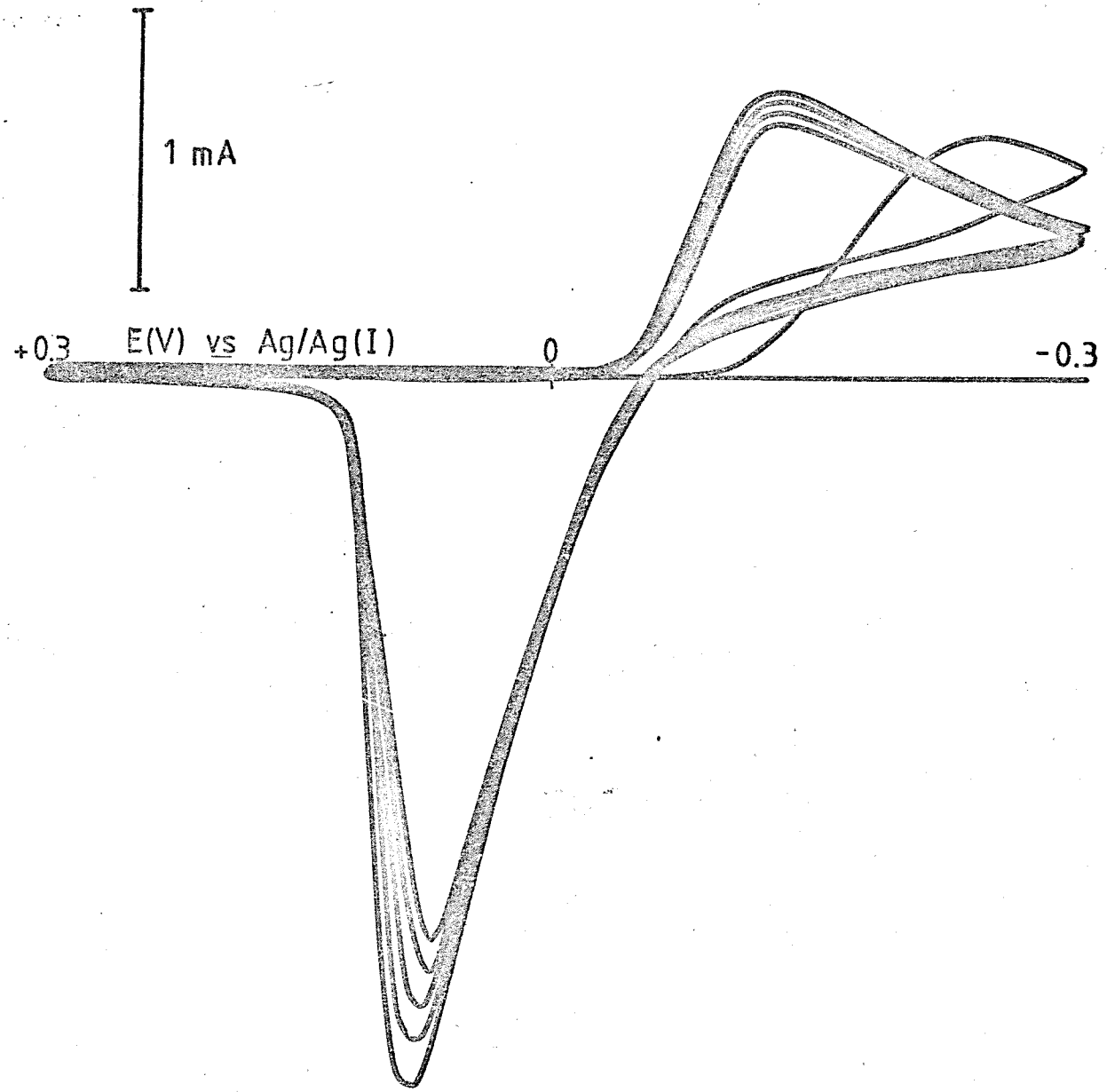

Figure 6.21 Typical current-potential curves for the deposition of 10 mM $AgNO_3$ in 0.1 M HNO_3 on vitreous carbon. (A = 0.316 cm^2; v = 0.1 V sec^{-1})

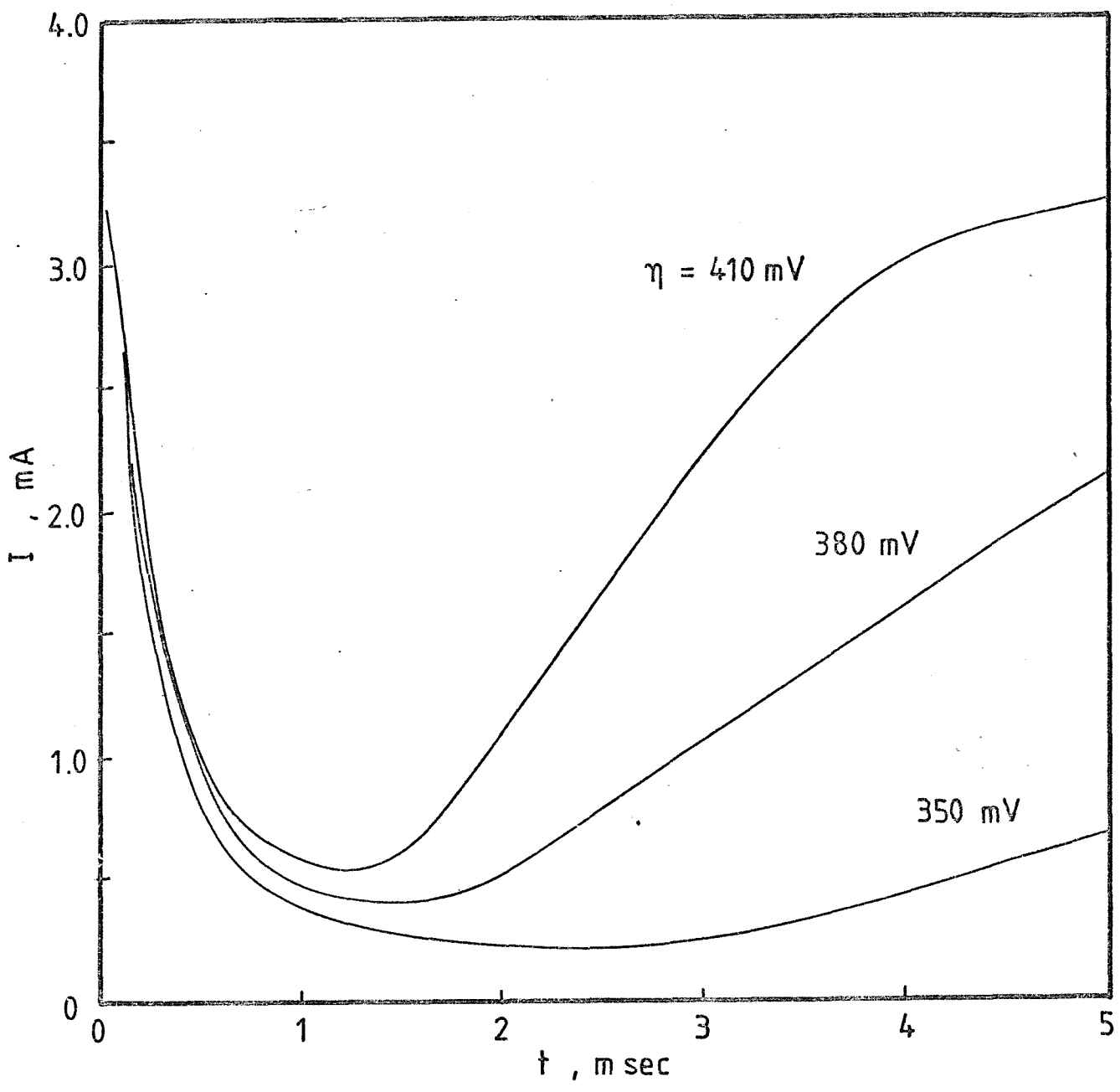

Figure 6.22 I-t transients of the reduction of 10 mM $AgNO_3$ in 1 M KNO_3 on vitreous carbon (A = 0.316 cm^2) at the over-potentials indicated.

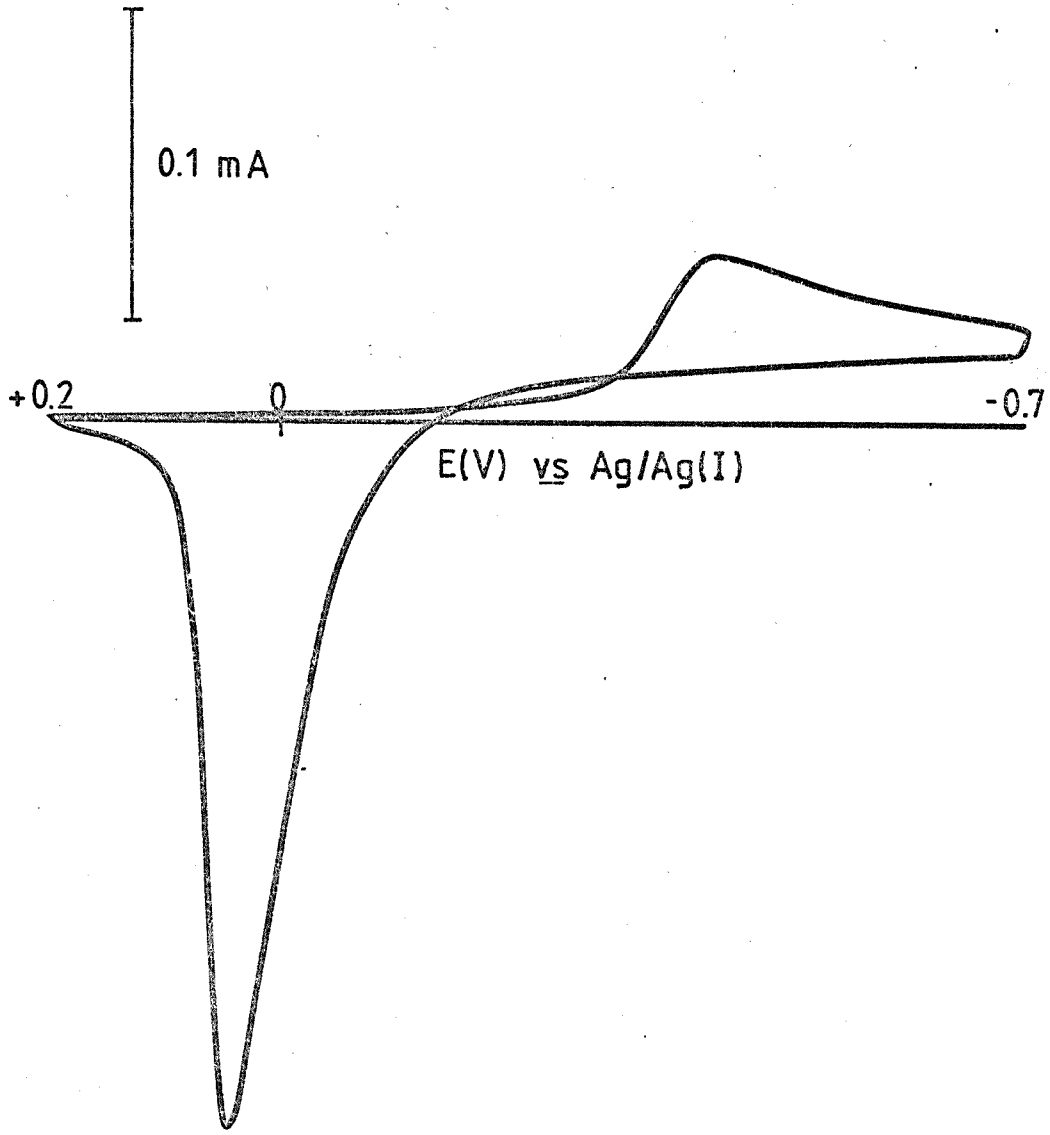

Figure 6.23 Voltammogram for the deposition of 10.6 mM $AgNO_3$ on graphite in $NaNO_3$-KNO_3 eutectic at 275°C. (A = 0.063 cm^2; v = 0.1 V sec^{-1})

However, in the galvanostatic experiment, these effects are vividly apparent in the small but systematic potential peak which is seen at the beginning of the transition time. Such peaks (which have been noted previously and not always ascribed to overshoot) are direct evidence for nucleation. The enforced growth of nuclei under galvanostatic conditions causes the overpotential to rise as the surface energy term increases until the sizes of a sufficient number of nuclei exceeds the critical values corresponding to the overpotential at that point in time. The activation overpotential can then relax whilst still allowing nuclei to grow under charge-transfer control. The height of potential maximum is systematically related the applied current density as shown in Figure 6.18 and can be made the basis of the determination of the charge transfer rate constants. The application of this method to molten salt systems and to high temperature rate constants is an important part of the larger research. Here, we simply show how the method immediately differentiates between nucleation controlled growth and reversible, "epitaxial" growth. Figures 6.19 and 6.20 compare two potential-time transients recorded under identical conditions using the same electrode before and after treatment for the removal of platinum oxide both in aqueous solutions and in nitrate melts.

6.2.4 Graphite

From the forgoing it is plain that the use of platinum as a working electrode may introduce uncertainties into the study of electrode reactions. The degree of oxidation is not easily known or controlled and it has proved more convenient to use graphite in the form of polished discs sealed into glass. The surface of vitreous carbon is probably in an even more complex state of oxidation than platinum. It may well be covered in the chemical groups derived from the oxidation of carbon. Nevertheless, its electrochemical properties are reproducible. It is not easily wetted by metals and their electrodeposition is invariably attended by nucleation. Some examples of the use of graphite both in aqueous solutions and in molten nitrates are shown in Figures 6.21, 6.22 and 6.23. The use of graphite in molten salts is new and, dependent on the success of the seal, it may be possible to use it in molten chlorides. If this is so, then the way is open not only for a wider range of nucleation studies but also for the widespread use of the galvanostatic method for the determination of electrochemical rate constants.

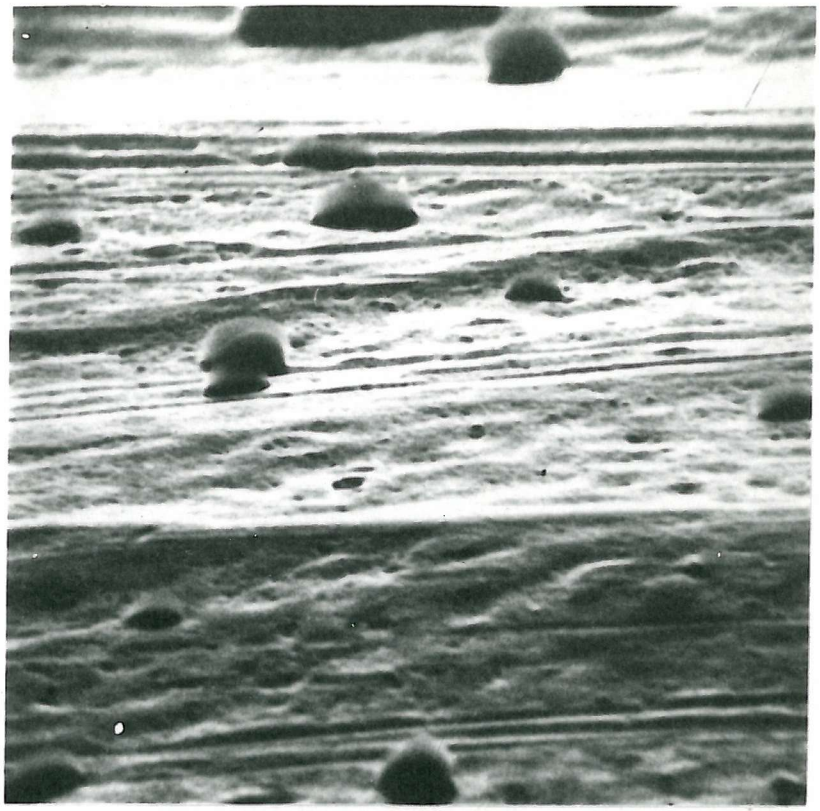

Figure 6.24 Scanning electron micrograph of silver deposited on platinum : magnification 1000 x

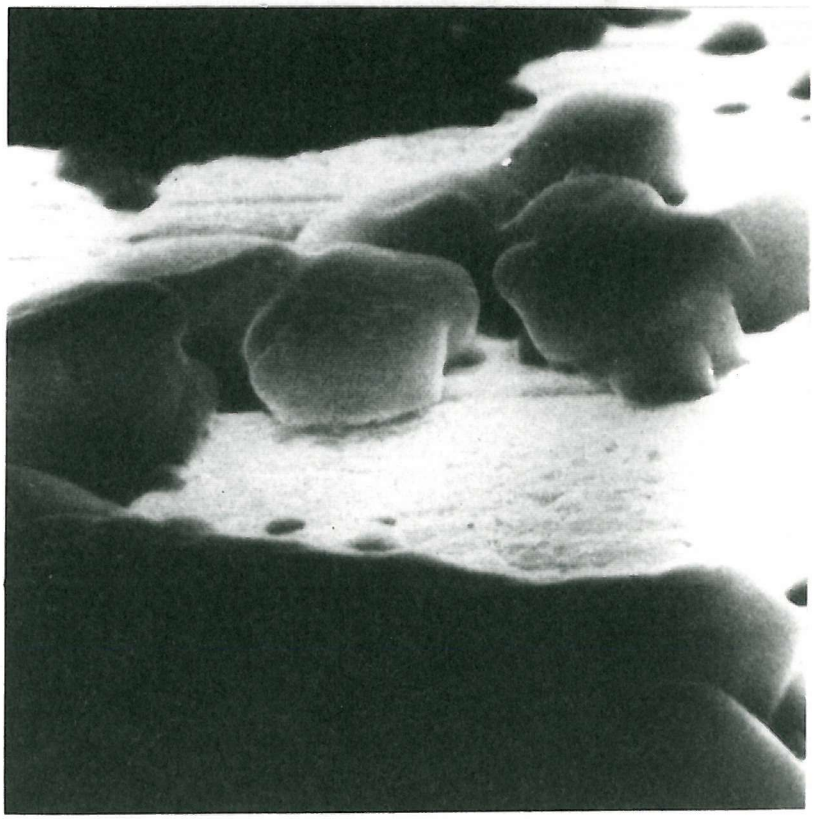

Figure 6.25 Same as Figure 6.24 : magnification 5000 x

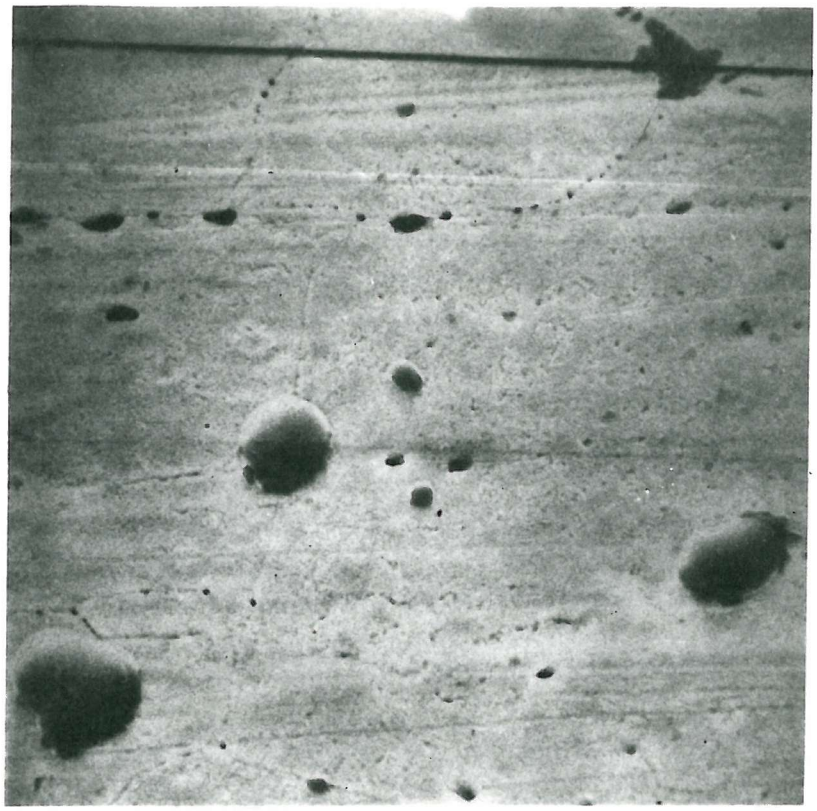

Figure 6.26 Same as Figure 6.24 : magnification 5000 x

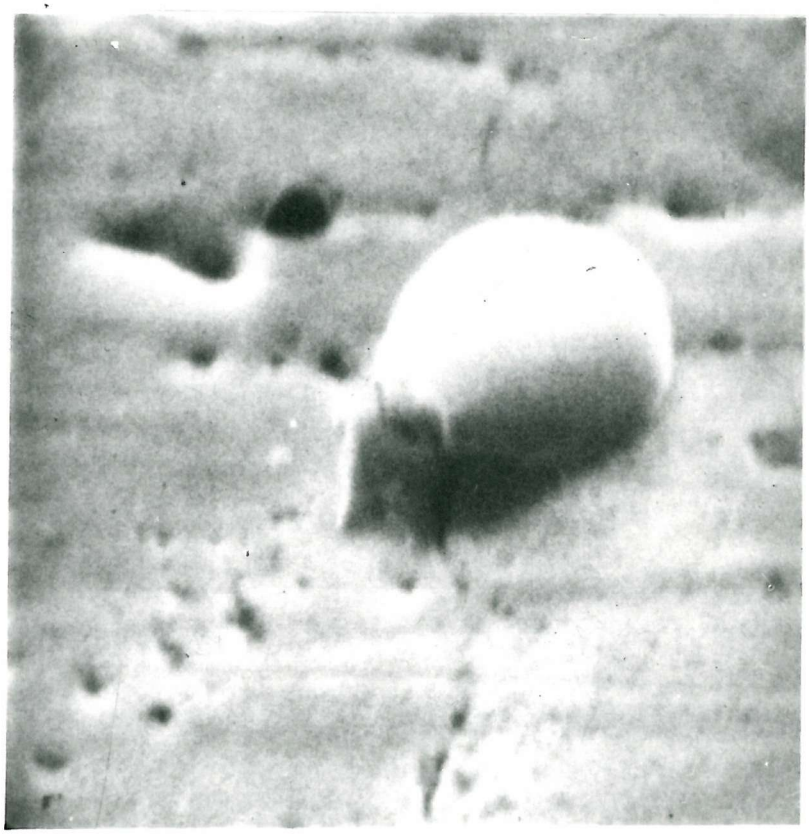

Figure 6.27 Same as Figure 6.24 : magnification 20,000 x

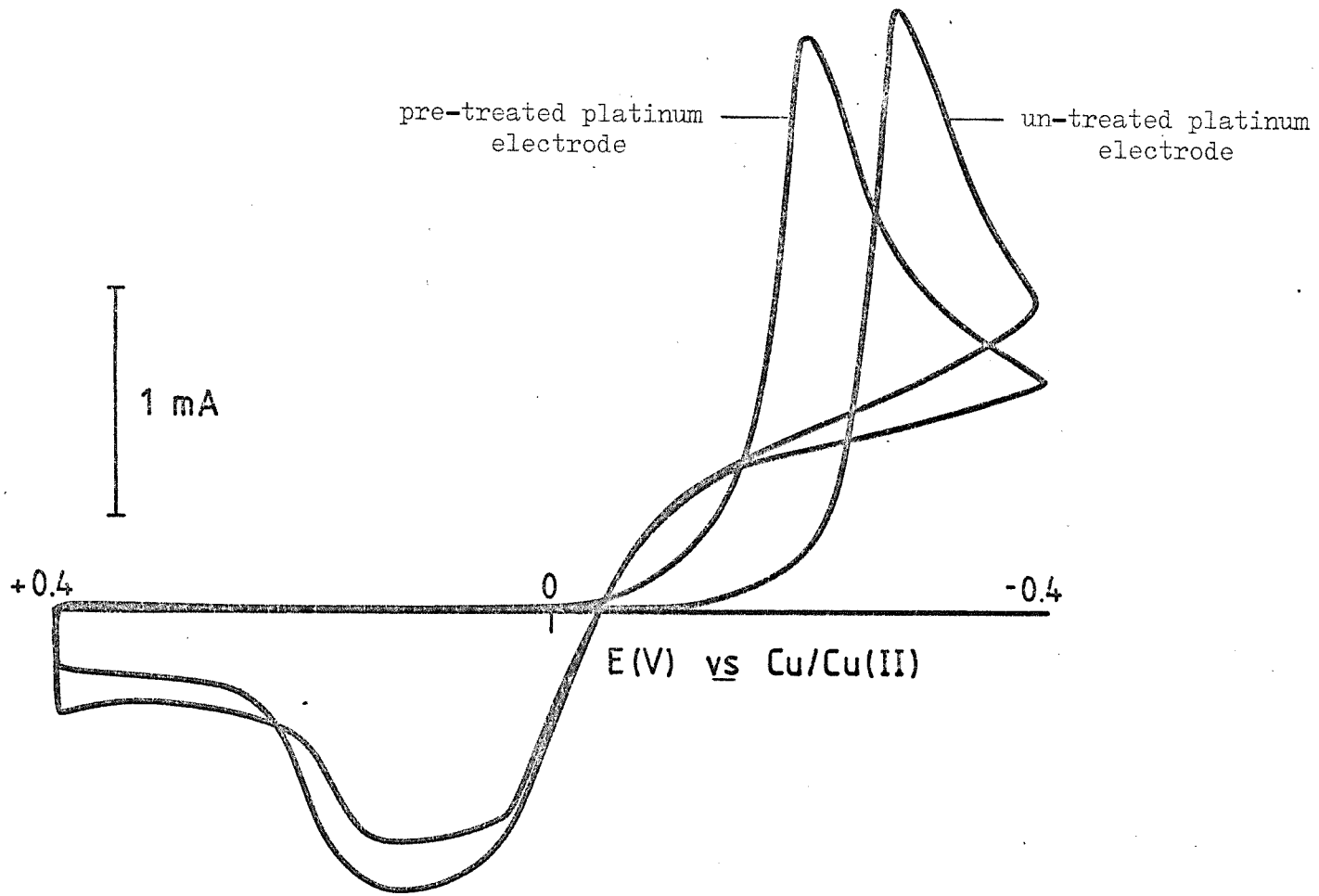

Figure 6.28 Voltammogram for the reduction of 56.98 mM $Cu(NO_3)_2$ in 1 M KNO_3 on pre-treated and un-treated platinum. (A = 0.029 cm^2; v = 0.3 V sec^{-1})

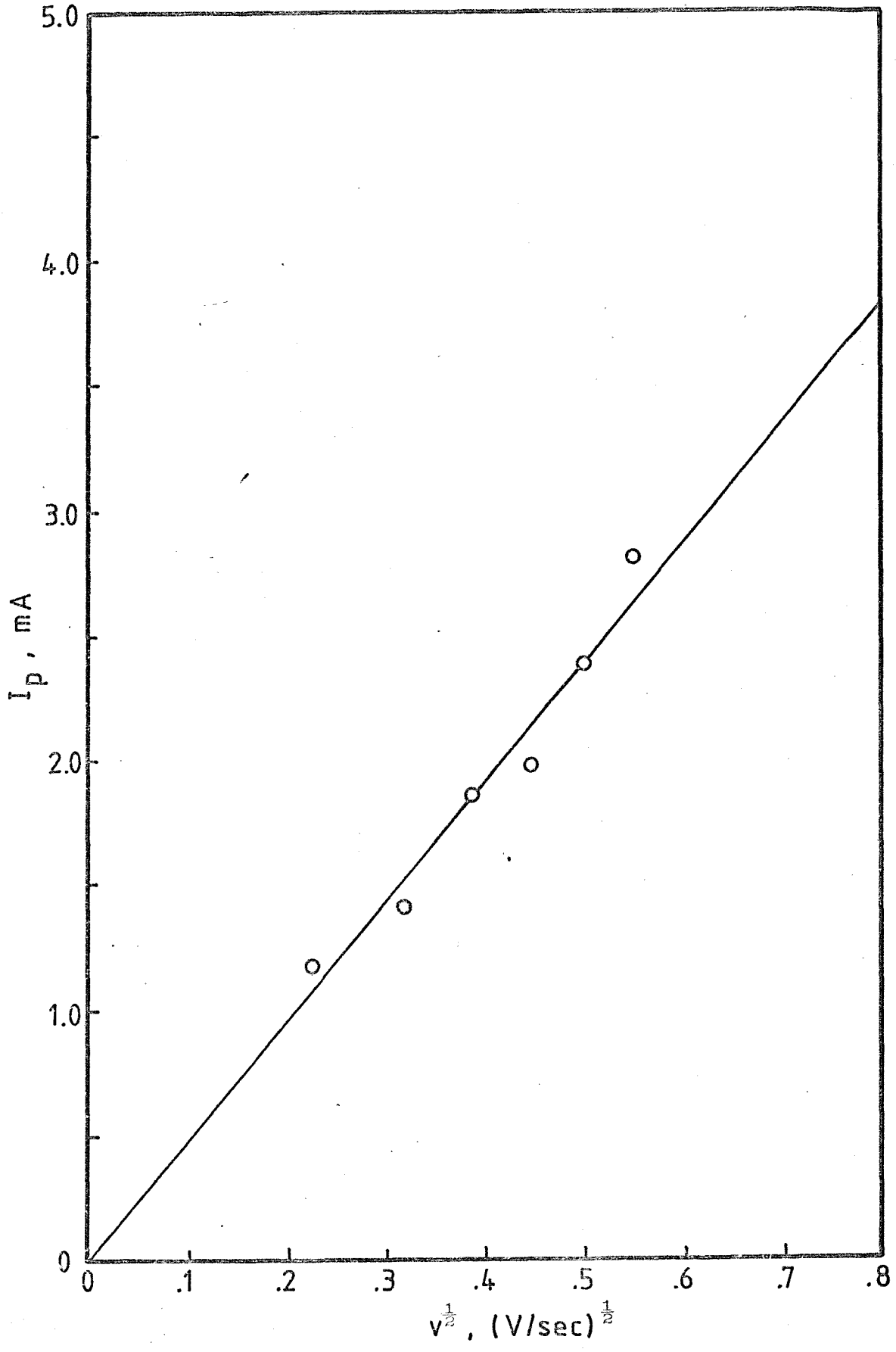

Figure 6.29 I_p vs $v^{\frac{1}{2}}$ plot for the deposition of copper from 56.98 mM $Cu(NO_3)_2$ in 1 M KNO_3 on pre-treated platinum. (A = 0.029 cm^2)

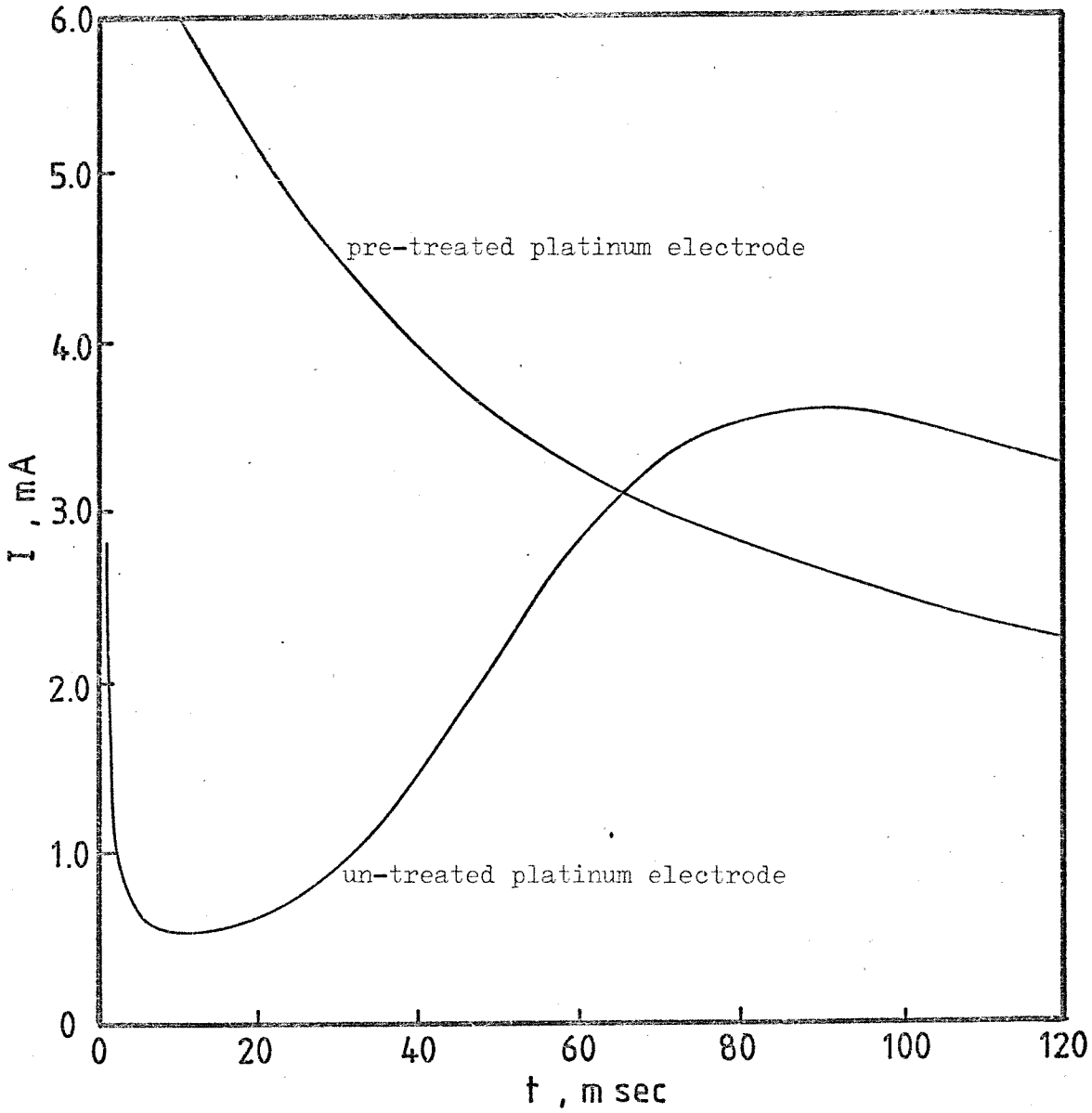

Figure 6.30 I-t transients for the deposition of copper from 56.98 mM $Cu(NO_3)_2$ in 1 M KNO_3 on pre-treated and un-treated platinum at η = 300 mV vs Cu/Cu(II). (A = 0.029 cm^2)

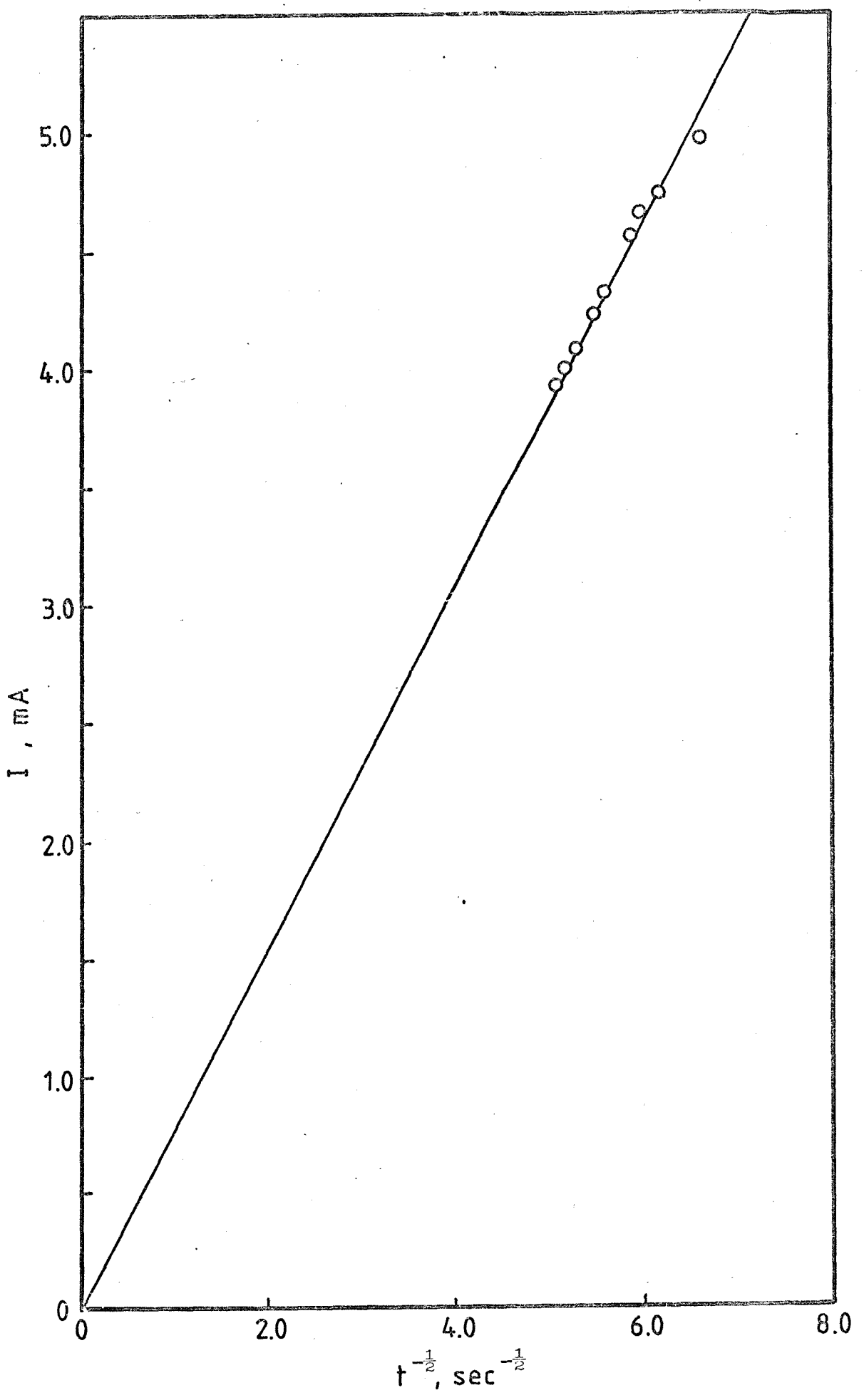

Figure 6.31 I-$t^{-\frac{1}{2}}$ plot for the deposition of copper (Data from Figure 6.30).

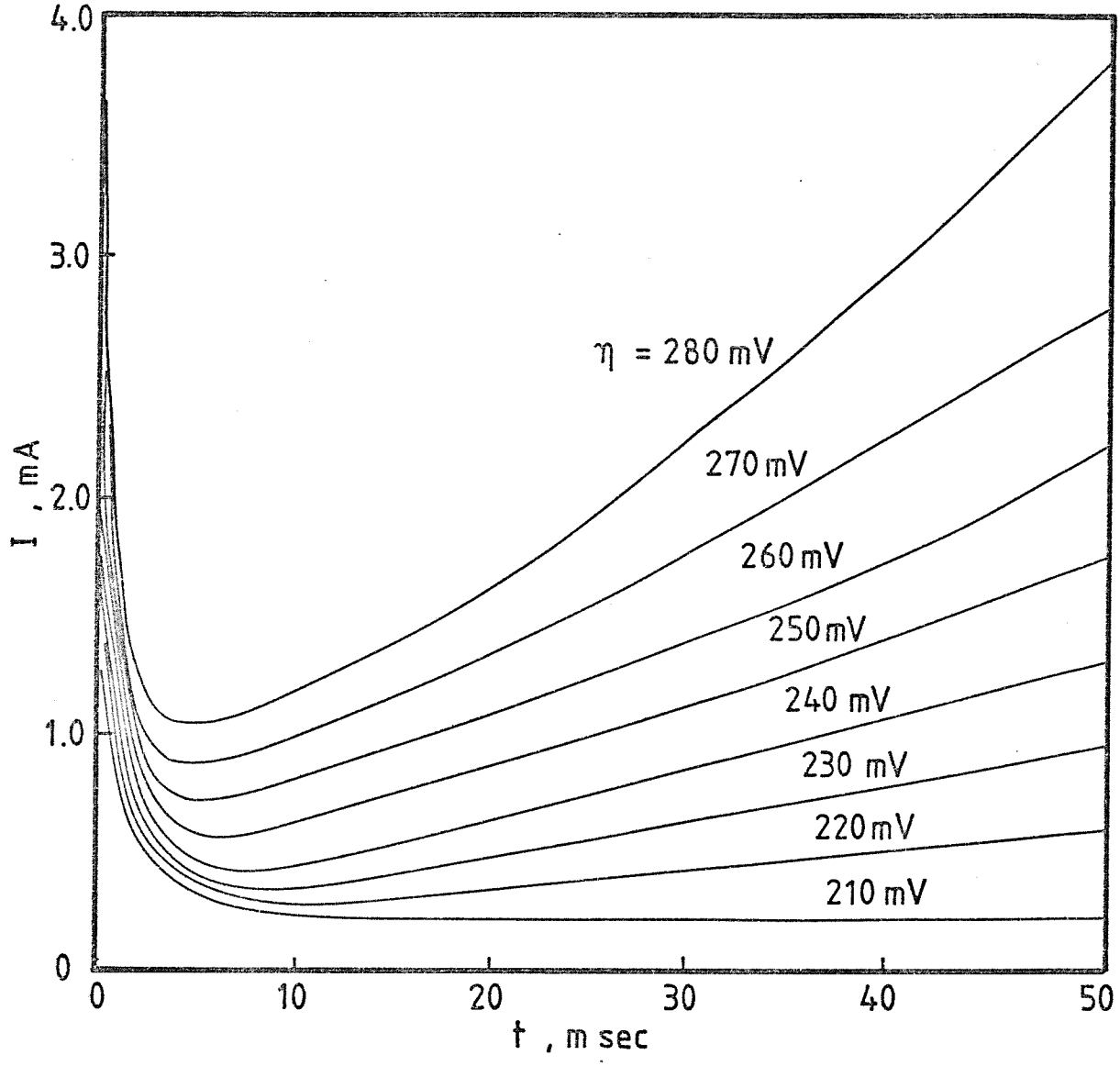

Figure 6.32 Potentiostatic transients for the deposition of copper from 56.98 mM $Cu(NO_3)_2$ in 1 M KNO_3 on un-treated platinum at various overpotentials indicated. (A = 0.029 cm^2)

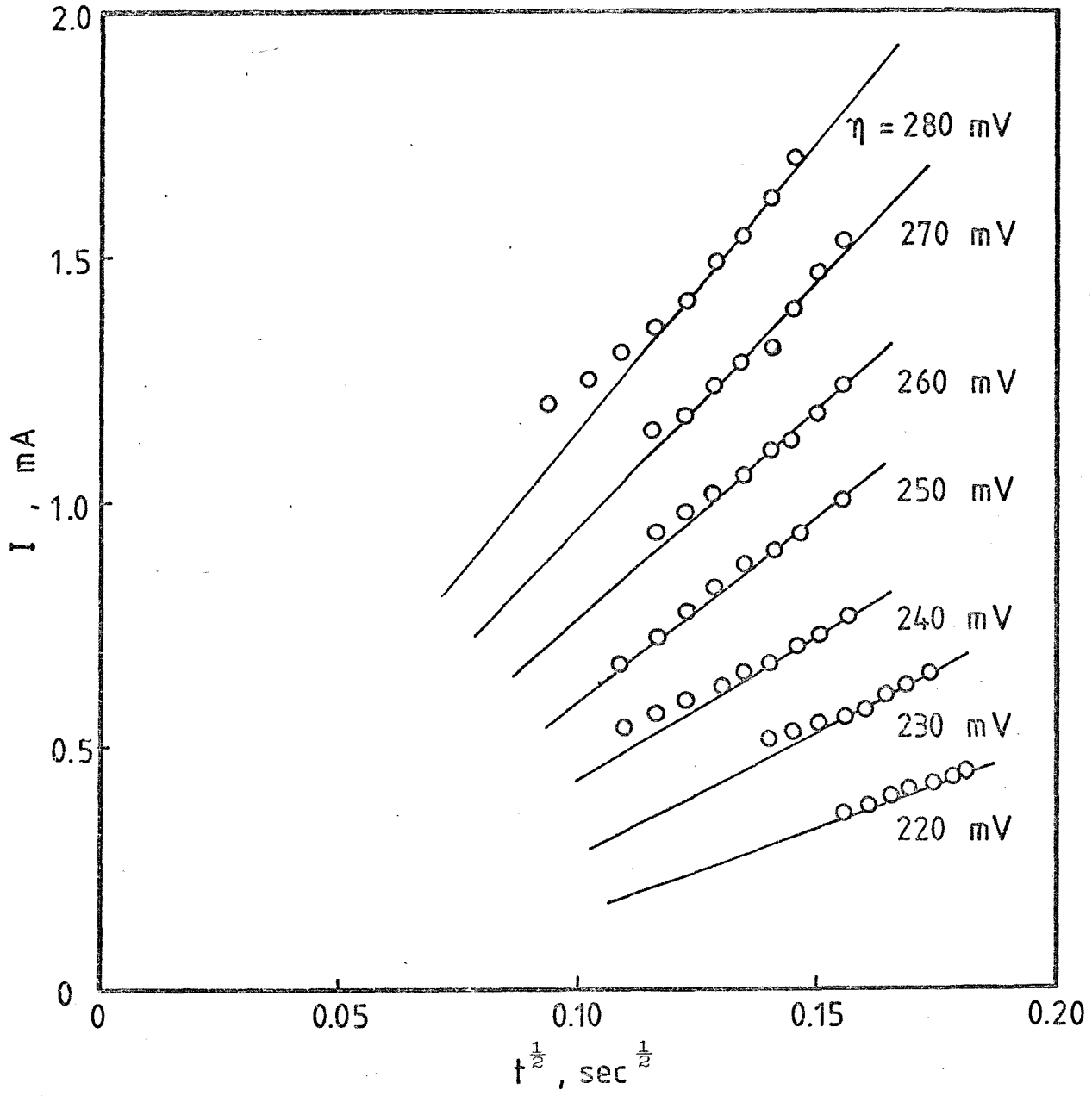

Figure 6.33 I-$t^{\frac{1}{2}}$ plot for the deposition of copper (Data from Figure 6.32).

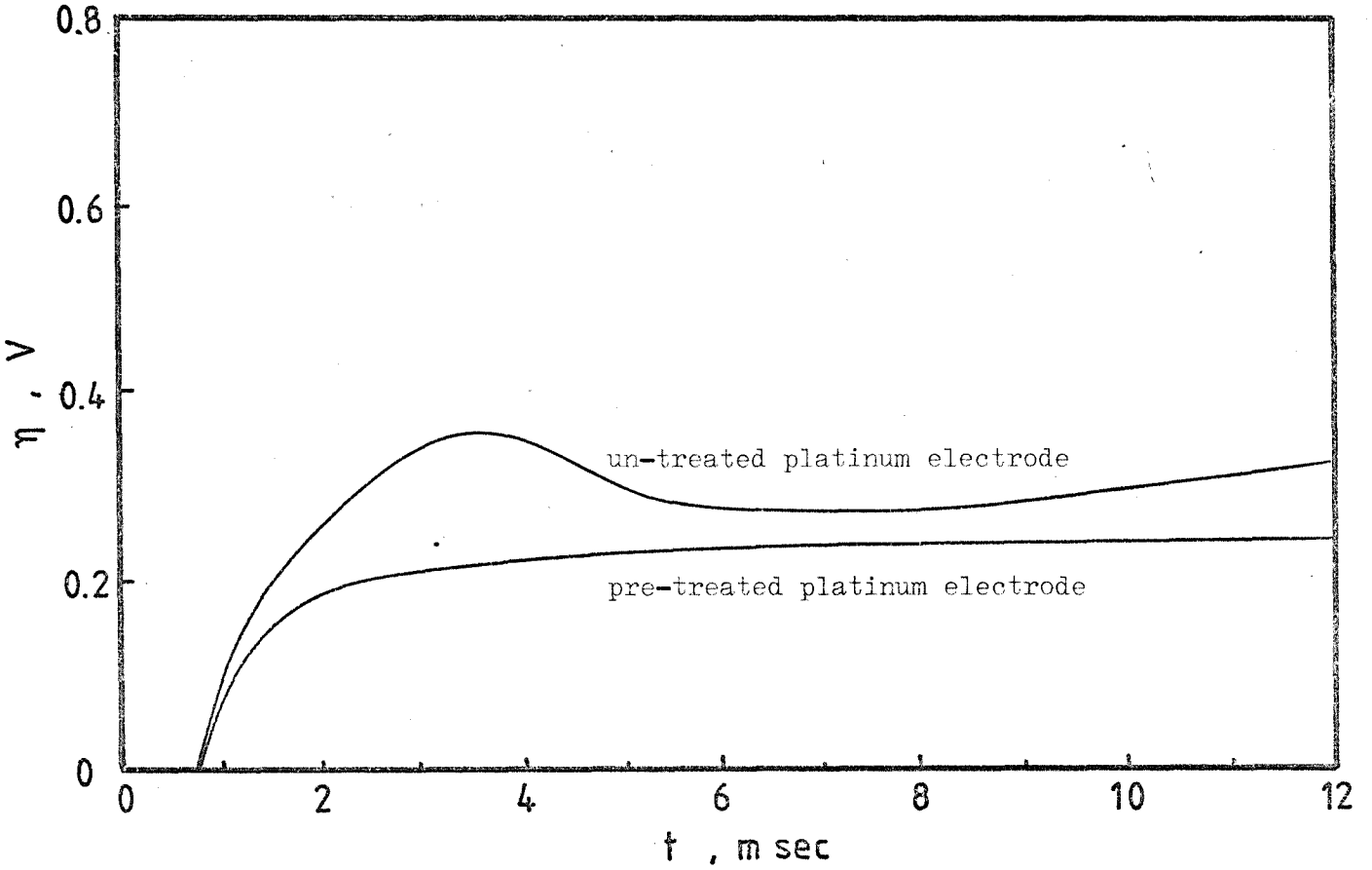

Figure 6.34 Galvanostatic potential-time transients for the reduction of 56.98 mM $Cu(NO_3)_2$ in 1 M KNO_3 at pre-treated and un-treated platinum at constant current of 20 mA. ($A = 0.029\ cm^2$)

TABLE 6.2 Nuclear densities of copper on platinum in 1 M KNO_3 aqueous solutions at various overpotentials. ($A = 0.029\ cm^2$)

η/mV	c = 56.98 mM	
	$\frac{10^3(dI/dt^{\frac{1}{2}})}{A/sec^{\frac{1}{2}}}$	$10^{-4}N_o$
220	3.48	2.32
230	4.90	3.26
240	6.14	4.09
250	7.43	4.95
260	8.52	5.68
270	10.10	6.73
280	11.64	7.76

6.2.5 Electron micrographs

Micrographs of silver deposit on platinum wire electrode in alkali molten nitrates were obtained using a scanning electron microscope and are shown in Figures 6.24, 6.25, 6.26 and 6.27. At a potential of 50 mV, silver nuclei were formed on platinum surface and the electrode was taken from the nitrate melt, rinsed with distilled water to remove any adherent melt before surface observation. Widely separated spherical silver nuclei of approximately uniform size were observed in support of the proposed model of 3D instantaneous nucleation and growth.

6.2.6 The electrodeposition of copper onto platinum in aqueous potassium nitrate solution

The effect of platinum oxide upon the early stages of the metal deposition was further investigated in aqueous solutions containing cupric ions using triangular potential sweep and square pulse technique. It is seen in Figure 6.28 that the rate of nucleation of copper onto platinum oxide is greatly inhibited and it requires the much greater nucleation overpotential (> 80 mV) than that on the bare platinum. Peak currents from the pre-treated electrode vary linearly with the square root of the sweep speed (Figure 6.29) and regress through the origin. The slope $dI_p/dv^{\frac{1}{2}}$ leads to a diffusion coefficient of $8.7 \times 10^{-6} cm^2\ sec^{-1}$, in agreement with the polarographic values of $7.0 \times 10^{-6} cm^2\ sec^{-1}$ reported by Kolthoff[117].

Potentiostatic investigations gave rise to normal falling current-time transients for platinum and rising current-time curves for platinum oxide electrode as is shown in Figure 6.30. In the former case the corresponding I vs $t^{\frac{1}{2}}$ plot yields a straight line passing through the origin (Figure 6.31) and the slope $\frac{dI_1}{dt^{\frac{1}{2}}}$ was used to evaluate the diffusion coefficient of cupric ions, i.e. $1.8 \times 10^{-5} cm^2\ sec^{-1}$.

Over a certain range of pulse amplitudes a family of potentiostatic current-time transients is observed (Figure 6.32). A plot of I vs $t^{\frac{1}{2}}$ from the middle part of such transients gives straight lines (Figure 6.33) and the slope of the lines lead to number nuclear densities at each overpotential given in Table 6.2.

A galvanostatic potential maximum is observed for the un-treated platinum but not on the pre-treated, oxide free electrode (Figure 6.34). Removal of the oxide film has reduced the potential barrier for charge transfer (nucleation) reaction, thus no potential maximum is required.

6.3 Conclusion

In summary it might be concluded that much work has been carried out on the state and mechanism of surface oxidation of platinum,[109,113,118] but a clear understanding of the subject is not reached. There are many uncertainties and hence controversies concerning the exact nature of the protective film, the rate-controlling step of the film formation and the properties and role of the film on the reaction reacting upon it. Electrochemical studies of the oxidation of metals have provided useful detailed and quantitative information. It is apparent, however, that further supporting evidences from other techniques, e.g., ellipsometry and optical reflectance are required. Any such sensitive studies will be achieved only when the solid surface is highly purified and the surface activity throughout the investigation is maintained. Indeed, it would appear unrealistic to prepare a genuine 'oxide free' platinum electrode, simply because any surface exposed even for an instant to the atmosphere or surrounding solvent must be assumed contaminated. Ultimately, we probably can judge a cleaning procedure only on the efficiency and reproducibility from the resulting surface. The present studies have simply confirmed the effectiveness of the electrical pretreatment for the surface preparation of platinum used for metal deposition and the effect of such electrode pretreatment upon the initial stages of the metal deposition is easily discerned.

7. VOLTAMMETRIC STUDIES IN NITRATE MELTS

7.1 Electrochemical nucleation of silver onto vitreous carbon in alkali molten $NaNO_3$-KNO_3 eutectic at 250°C

7.2 Electrodeposition of Pb(II), Cd(II), Co(II), Ni(II) and Cu(II) onto platinum in molten $NaNO_3$-KNO_3 eutectic at 250°-308°C

7.2.1 The system $Pb(NO_3)_2/NaNO_3$-KNO_3 at 250°C

7.2.2 The system $Cd(NO_3)_2/NaNO_3$-KNO_3 at 308°C

7.2.3 The system $Co(NO_3)_2/NaNO_3$-KNO_3 at 255°C

7.2.4 The system $Ni(NO_3)_2/NaNO_3$-KNO_3 at 255°C

7.2.5 The system $Cu(NO_3)_2/NaNO_3$-KNO_3 at 250°C

7.1 Electrochemical nucleation of silver onto vitreous carbon in alkali molten $NaNO_3$-KNO_3 eutectic at 250°C

The processes of electrodeposition of metals onto inert substrates involve the consecutive stages: (i) the initiation of a newly-formed phase, (ii) the subsequent phase growth and (iii) the eventual overlap of the new phase particles to form a compact deposit. The geometry, kinetics and mechanism of such electrolytic deposits and their dependence on the conditions of electrocrystallisation have been the subject of extensive investigations.

In the present study, the potential pulse and current pulse techniques were used for the analysis of the nucleation and growth processes, their morphology and the nature of the rate-determining step.

The present concepts of the mechanism of nucleation and growth on electrodes are varied but are mostly concerned with two fundamental theories. The first theory is concerned with the formation of nuclei at preferred sites and these active sites are normally regarded as having an arbitrary activity distribution. The production of macroscopic structure begins from the first atoms depositing directly onto the active centres followed by the aggregation of further single atoms by direct discharge or adatoms from surface diffusion or a combination of both mechanisms. The second theory is concerned with the deposition of adatoms onto a uniform surface and their incorporation by further direct deposition or by surface diffusion or by a combination of both processes into clusters of perhaps widely varying size. Stable nuclei will form when the aggregate of adatoms exceeds the critical value for that particular overpotential or when the rate constant for the random addition of clusters to form sufficiently large nuclei is approximately equivalent to the equilibrium rate constant for the bulk metal $\rightleftharpoons$ metal ion reaction. On this basis, it is possible experimentally to determine the charge transfer rate constant for the overall metal deposition reaction.

As pointed out earlier, the delineation of a metal deposition reaction onto a foreign substrate is frequently difficult owing to the complexities introduced by the underlying substrate. It is clearly important that electrochemical investigations should be made while the surface state of the electrode is well defined and uncontaminated by adsorbable impurities. This is difficult to control experimentally.

Usually if metal is deposited onto an inert electrode, the current flows and the deposit grows outward into the solution and/or laterally on the surface and can then be removed without adversely affecting the substrate surface. The linear potential sweep and pulse measurements are particularly useful means of detecting although the electrode surface which has normally been brought back to a standard condition, i.e. to an anodic starting potential before the next measurement, may be roughened by its previous treatment giving rise to uncertainties particularly at short time polarisations.

Experience in studying electrocrystallisation in both aqueous solutions and molten salts has clearly indicated the importance of the nature of the substrate surface, especially in relation to the earliest stages of cluster formation and crystal growth, i.e. during the nucleation process. Evidently, some nucleation processes on solid substrate have been limited by the number of discrete centres since the number of nuclei formed at an elapsed time cannot exceed the number of discrete centres. It is possible that a large simplification in analysis of nucleation together with an improvement of reproducibility of results can be made by using single-crystal substrates whereby these active sites appear to be nearly identical. On the other hand, a polycrystalline metal gives rise to a large variation in sites and hence the deposited nuclei are distributed. It is found in general, that only a small proportion of the surface is available for nucleus formation. On the other hand, the fluctuation theory of nucleation and the supporting experimental data suggests that nucleation is actually a random process. The number of nuclei formed in a supersaturated solutions within a finite time interval as well as the time required for the first visible nucleus to appear are also random quantities. Paradoxically, the choice of a suitable electrode material for this study is also important.

Platinum has been seen to be not well suited for studies of the nucleation of metals because of the complicating effects of its surface oxides. For general electrochemical studies liquid electrodes are probably the best but they are not convenient for investigations in molten salts. From the viewpoint of high-temperature systems, the prospects of using other solid electrode materials is also not encouraging. It was therefore decided that vitreous carbon, which has been successfully employed for nucleation studies of silver in aqueous solutions, would be used in

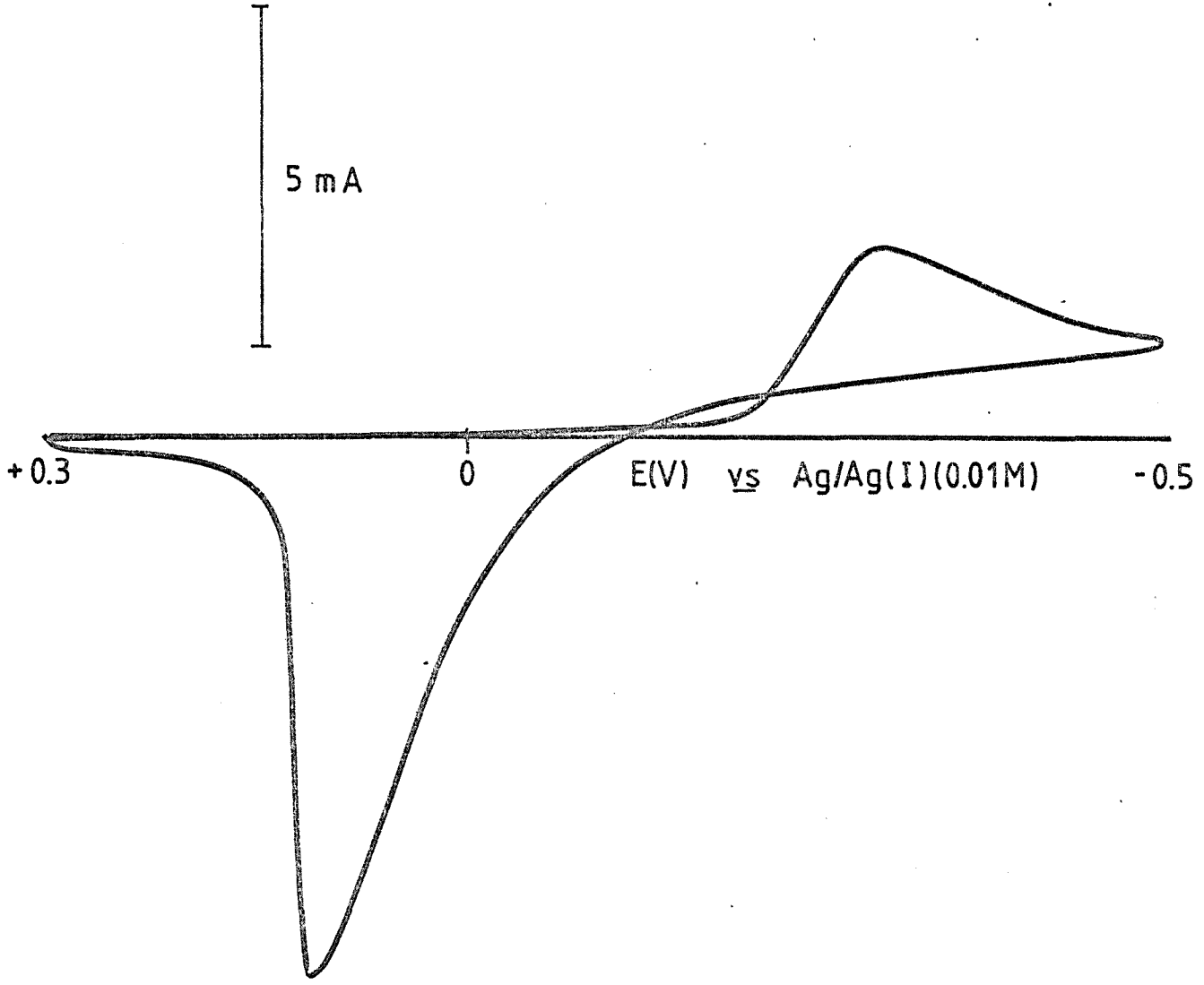

Figure 7.1 A typical voltammogram for the electrodeposition-dissolution of silver from 29.21 mM $AgNO_3$ on a vitreous carbon in $NaNO_3$-KNO_3 eutectic at 250°C, V = 0.1 V sec^{-1}. (A = 0.312 cm^2)

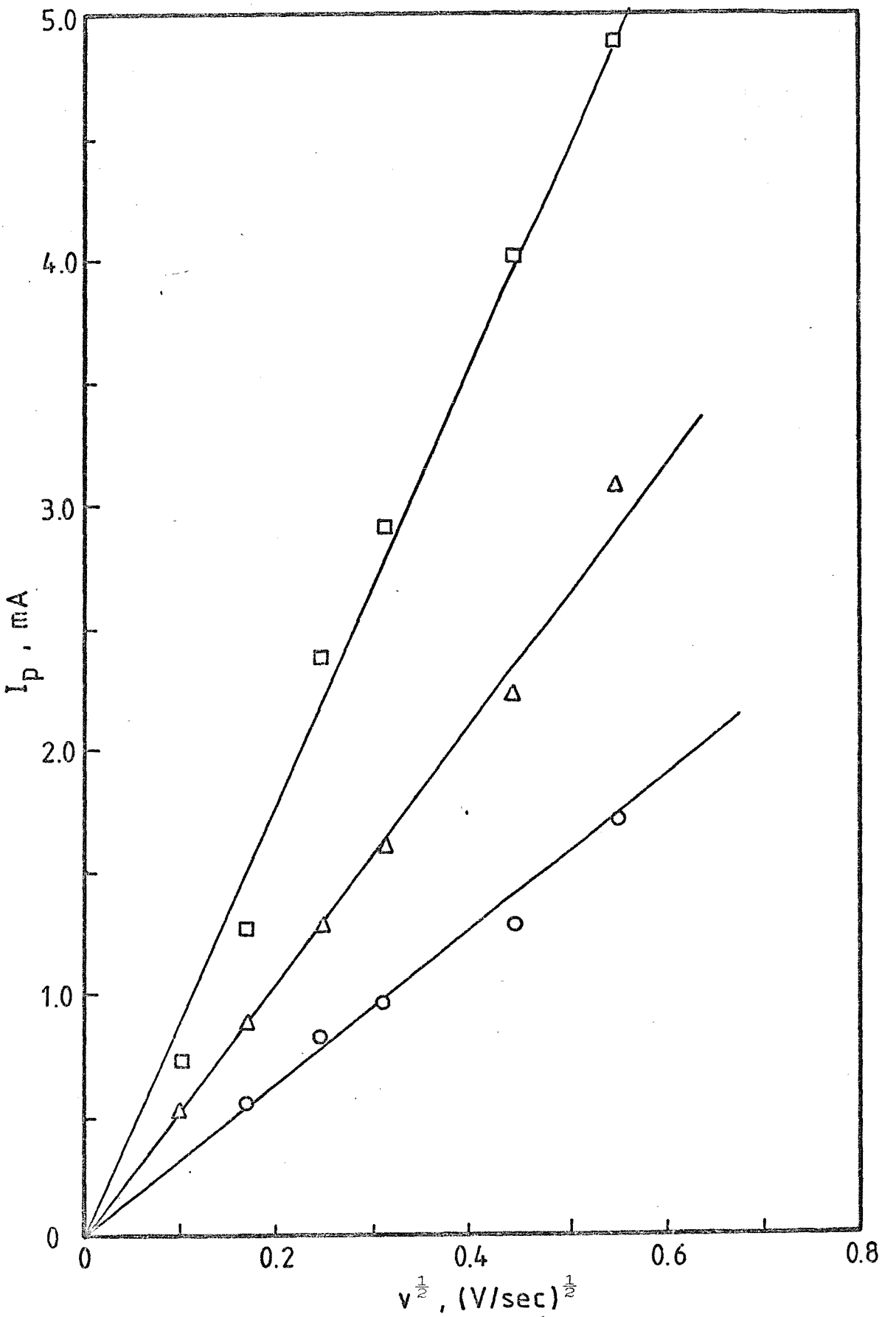

Figure 7.2 The linear relationship of I_p vs $v^{\frac{1}{2}}$ for the reduction of 13.15(○), 23.03(△) and 29.21(□) mM of $AgNO_3$ on vitreous carbon in $NaNO_3$-KNO_3 eutectic at 250°C.

TABLE 7.1 Diffusion coefficients of various metal ions in the $NaNO_3$-KNO_3 eutectic at 250-308°C.

electroactive species	t °C	$10^6 c$ mol/cm^3	$10^6 D/cm^2\ sec^{-1}$ cyclic voltammetry	potential step	literature values
Ag(I)	250	13.15	7.7	15	4.0(250°C),(40)
		23.03	6.5	16	
		44.80	12.3	15	
			Mean: 8.8	Mean: 15.3	
Pb(II)	250	4.88	2.51		
		10.22	2.69	4.76	2.3(263°C),(40)
		15.00	2.20		
			Mean: 2.46		
Cd(II)	308	11.88	6.11		5.1(263°C),(40)
		17.09	4.59		
		22.48	5.56	3.18	
			Mean: 5.42		
Co(II)	255	22.49	0.68	1.4	0.8(148°C),(39)
Ni(II)	255	6.72	0.3	2.23	0.35(143°C),(39)
Cu(II)	250	18.17	0.15	0.05	-

TABLE 7.2 Cyclic voltammetric peak potentials, peak separation potentials over a range of sweep rates for the electrodeposition-dissolution of Ag(I) onto vitreous carbon electrode at the concentrations indicated in $NaNO_3$-KNO_3 eutectic at 250°C. (Electrode area = 0.312 cm^2)

$\frac{v}{mV/sec}$	$\frac{E_p^c}{mV}$	$\frac{E_p^a}{mV}$	$\frac{\Delta E_p}{mV}$
	vs Ag/Ag(I)(0.01M)		
(a) c = 13.15 mM			
30	285	85	370
60	290	95	385
100	320	90	410
200	335	90	425
300	345	95	440
(b) c = 23.03 mM			
10	290	175	465
30	280	170	450
60	310	160	470
100	330	150	480
200	320	140	460
300	370	125	495
(c) c = 29.21 mM			
10	225	105	330
30	265	95	360
60	270	110	380
100	290	115	405
200	310	105	415
300	330	105	435

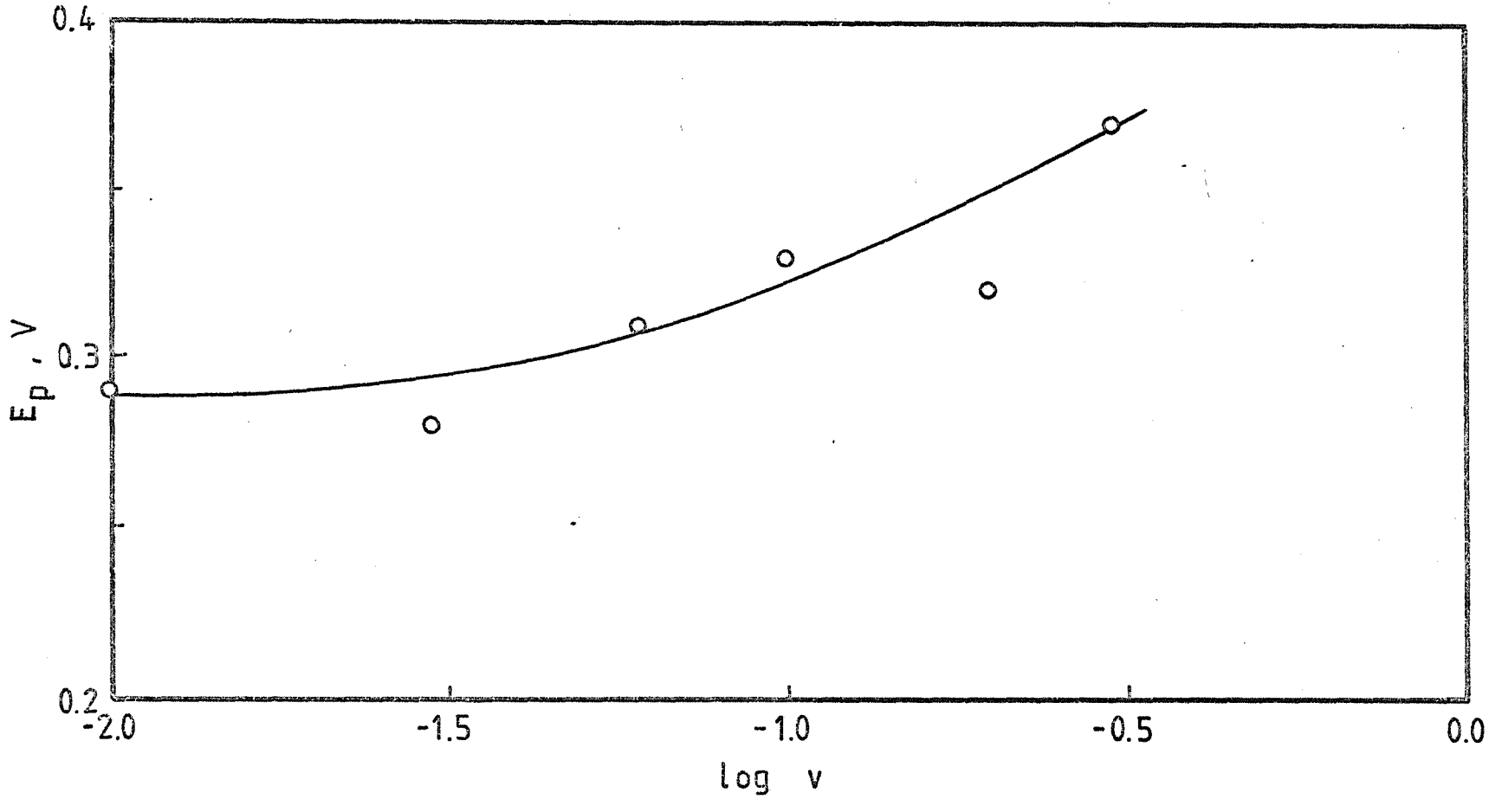

Figure 7.3 E_p vs log v for the reduction of 23.03 mM $AgNO_3$ and vitreous carbon from $NaNO_3$-KNO_3 eutectic at 250°C. ($A = 0.312\ cm^2$)

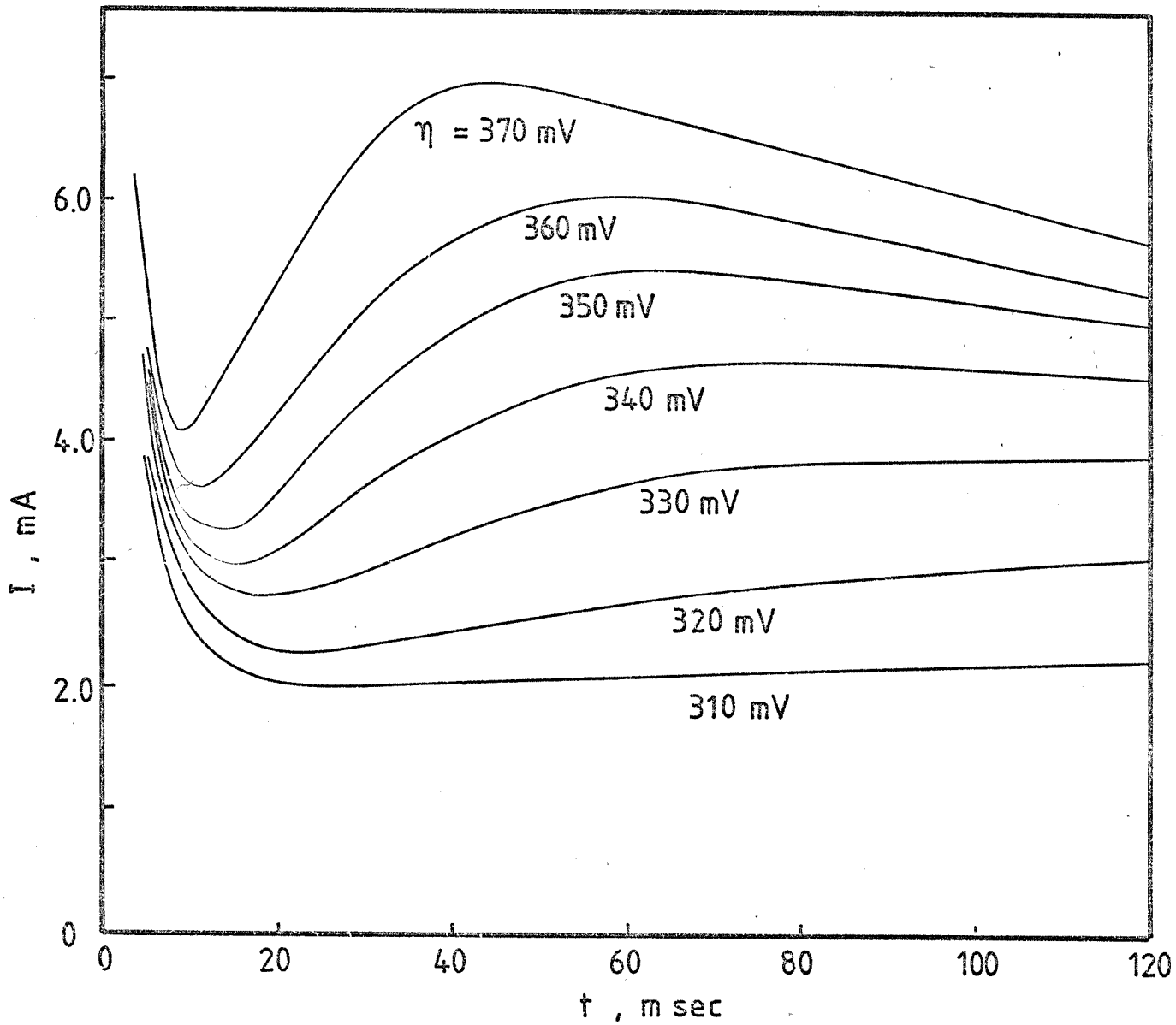

Figure 7.4 I-t transients for the reduction of 29.21 mM $AgNO_3$ on vitreous carbon in $NaNO_3$-KNO_3 eutectic at 250°C at the overpotentials indicated. (A = 0.312 cm^2)

molten salts. It seemed appropriate that the use of vitreous carbon should be first explored in the low melting nitrate solvent, particularly for the silver deposition which is evidently simple and certain a reproducible reaction so far as heterogeneous nucleation studies are concerned.

Voltammetric studies were therefore made of the reduction of silver ions onto a mechanically well polished circular electrode of vitreous carbon in fused alkali nitrates at concentrations of 23.03×10^{-3}M, 29.21×10^{-3}M and 44.80×10^{-3}M. The potential sweep method, potential pulse method and current pulse methods were separately applied to the system. Potentials were measured against the Ag/Ag(I)(0.01 M) reference electrode. All measurements were carried out at the temperature of 250°C.

A typical linear sweep voltammogram for the electrodeposition-dissolution of silver is shown in Figure 7.1. Well-defined deposition and dissolution peaks are observed. The special characteristics of the voltammogram is the cross-over between the rising and falling cathodic current which is invariably evidence for the formation of nuclei. Coulometric studies revealed that the charge under the silver deposition peak is equal to that of the dissolution peak so that all the nuclei once formed readily redissolved.

Cathodic peak currents were plotted against the square root of the sweep rate and found to be linear (Figure 7.2). The slope of the lines, which pass through the origin, lead, via equation (3.14), to diffusion coefficients for Ag^+. The mean value was found to be $0.88 \times 10^{-5} cm^2\ sec^{-1}$ as is shown in Table 7.1.

The cathodic and anodic peak potentials and the peak separation potentials as a function of the sweep speed are shown in Table 7.2. In each case the peak separation is well over $\frac{2.2RT}{nF}$ ($\sim$ 100 mV) indicating some degree of irreversibility. The cathodic peak potential was found to increase (i.e. become more cathodic) almost linearly with log v (Figure 7.3).

Potential step experiment was also carried out to study the deposition reaction of silver onto vitreous carbon. The result for one concentration of silver ions is shown in Figure 7.4 and similar observations were made at the other concentrations. Over the range of controlled overpotentials, a family of rising current-time transients

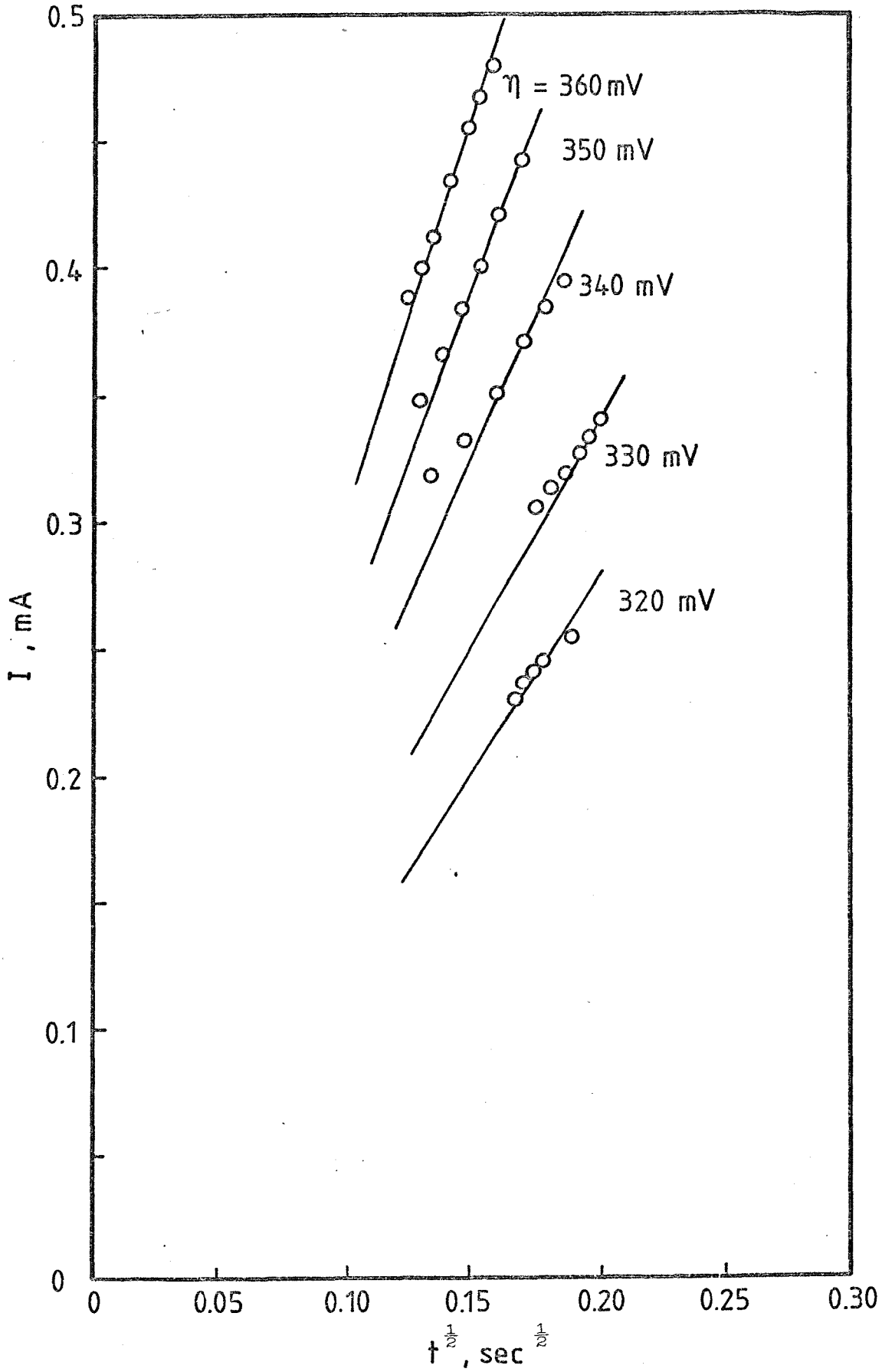

Figure 7.5 I-$t^{\frac{1}{2}}$ plot for the reduction of silver on vitreous carbon (Data from Figure 7.4).

TABLE 7.3 Nuclear number densities of silver on a vitreous carbon electrode in $NaNO_3$-KNO_3 eutectic at 250°C and at the overpotentials and concentrations indicated. (Electrode area = 0.312 cm^2)

	c = 18.63 mM		c = 23.03 mM		c = 29.21 mM		c = 44.80 mM	
η/mV	$10^3 dI/dt^{\frac{1}{2}}$ / $A/sec^{\frac{1}{2}}$	$10^{-5}N_o$	$10^3 dI/dt^{\frac{1}{2}}$ / $A/sec^{\frac{1}{2}}$	$10^{-5}N_o$	$10^3 dI/dt^{\frac{1}{2}}$ / $A/sec^{\frac{1}{2}}$	$10^{-5}N_o$	$10^3 dI/dt^{\frac{1}{2}}$ / $A/sec^{\frac{1}{2}}$	$10^{-5}N_o$
320					15.73	6.22	17.91	3.72
330	5.81	4.52	28.27	16.0	17.70	7.00	21.37	4.44
340					22.22	8.79	24.34	5.06
350	8.16	6.34	35.54	20.1	26.92	10.66	26.61	5.54
360	9.35	7.27	38.05	21.5	31.01	12.27	28.86	6.00
370	11.05	8.59						
380	13.04	10.14	46.46	26.2				
390			50.53	28.5				

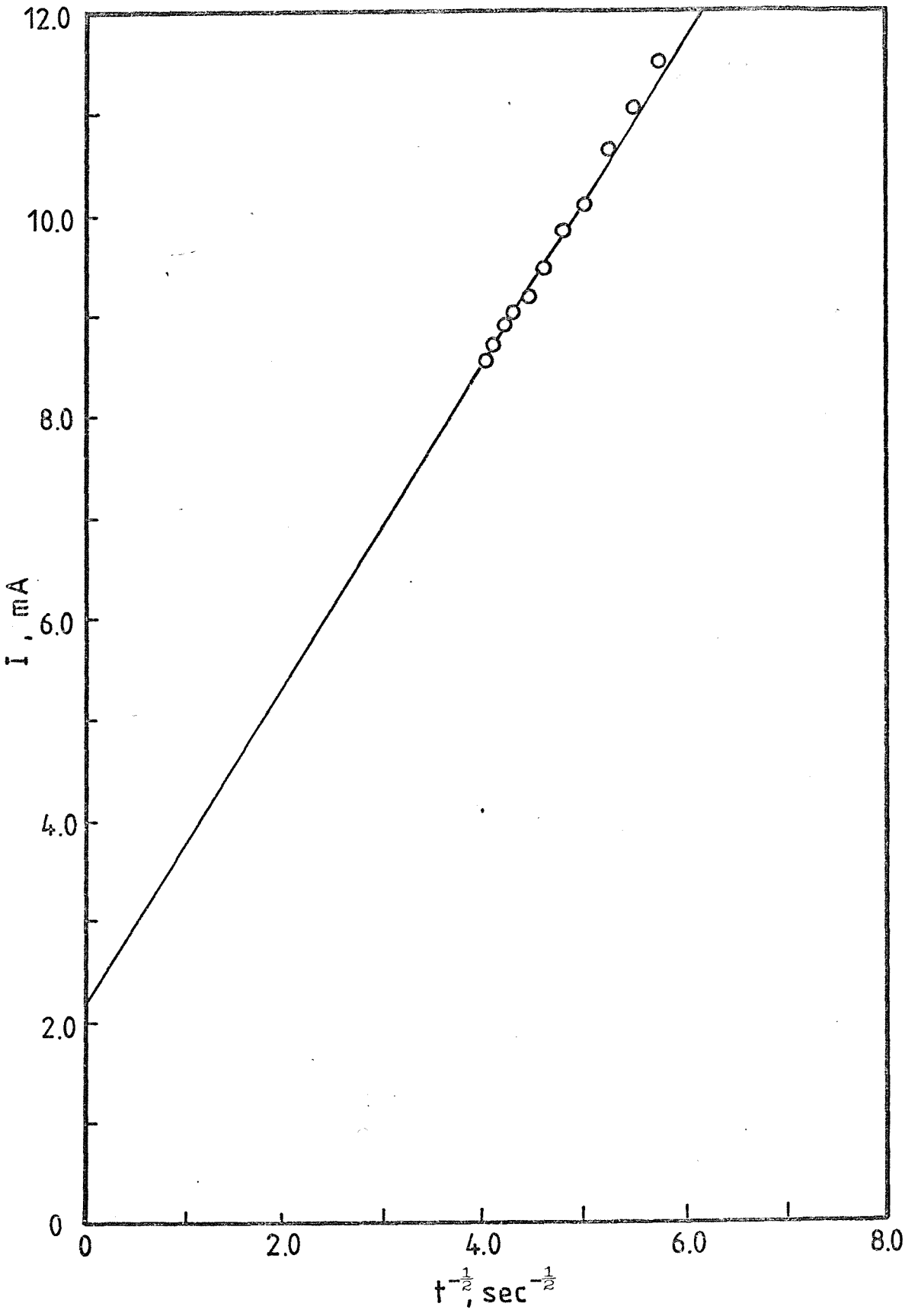

Figure 7.6 $I\text{-}t^{-\frac{1}{2}}$ plot for the reduction of 23.03 $AgNO_3$ on vitreous carbon in $NaNO_3$-KNO_3 eutectic at 250°C. ($A = 0.312\ cm^2$)

was obtained. The initial sharp rise of the resulting current is associated with the charging current of the interfacial capacitance and possible of ad-atom formation which decays effectively to zero before the onset of the faradaic process which is eventually controlled by mass transfer. The middle part of each transient shows the increase of current related to the growth of nuclear size of established silver nuclei and hence of the total electroactive area of silver surface. The later part of the transients reflects the overlap of the diffusion zones of neighbouring hemispherical nuclei which ultimately give rise to a continuous layer of silver. It follows that the recorded current finally falls with time according to the laws of planar (linear) diffusion. From a knowledge of the current density, the nuclear density at various degree of supersaturation can be calculated using equation (4.52) and from the total electrode area of the vitreous carbon disc. Visual counting of silver nuclei formed on the electrode surface in molten salts at particular overpotential might also be possible if a suitably designed furnace (e.g. with a window) were employed

Figure 7.5 shows plots of I vs $t^{\frac{1}{2}}$ for the rising portion of the curves in Figure 7.4. A linear relationship between I and $t^{\frac{1}{2}}$ at each applied overpotential is observed. It can therefore be concluded that the silver deposition onto vitreous carbon proceeds by the mechanism of 3D instantaneous nucleation followed by growth controlled by the hemispherical diffusion of silver ions from the melt. The number of nuclei calculated from the slope $\frac{dI}{dt^{\frac{1}{2}}}$ using equation (4.52) is shown in Table 7.3. It should be noted that according to the equation for 3D instantaneous nucleation, there is no parameter which is dependent upon the nucleation driving force, i.e. the applied overpotential. However, it would appear that the number of nucleation sites N_o is actually proportional to the pulse amplitude. This is evident from the increasing nuclear density with pulse height as shown in Table 7.3.

At high degrees of supersaturation (high overpotentials), silver is widely nucleated and covers the whole electrode surface giving rise to the falling current-time curve. The corresponding plot of I vs $t^{-\frac{1}{2}}$ is linear but does not pass through the origin (Figure 7.6). The slope of the line leads to diffusion coefficient of silver ions which is $1.55 \times 10^{-6} cm^2 sec^{-1}$ as estimated by equation (3.2).

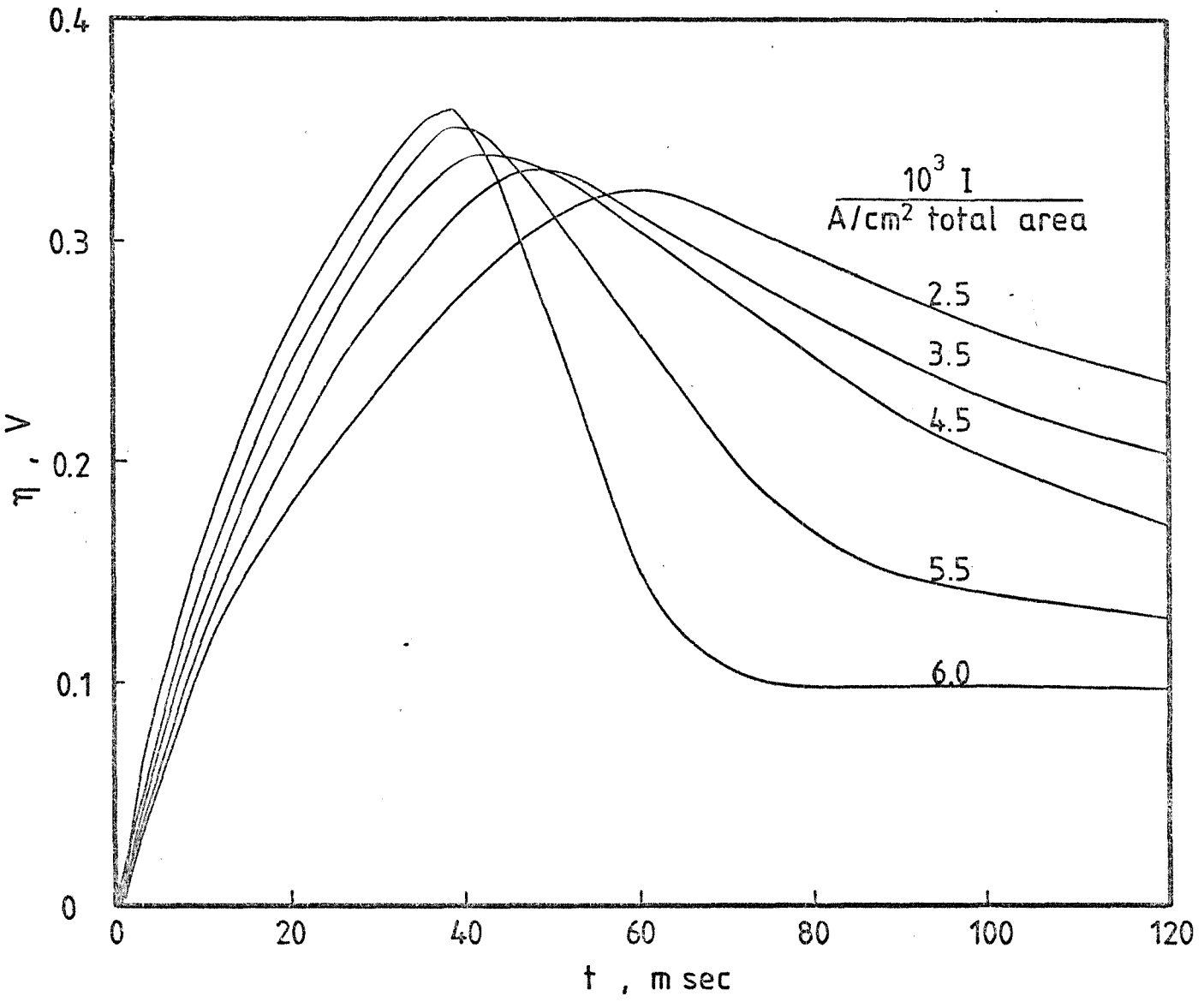

Figure 7.7 Galvanostatic transients for the reduction of 29.21 mM $AgNO_3$ on vitreous carbon in $NaNO_3$-KNO_3 eutectic at 250°C at various constant currents indicated. (A = 0.312 cm^2)

TABLE 7.4 Calculated capacity at different galvanostatic constant current densities.

$10^3 I$ / A/cm^2	$10^6 C_{dl}$ / F/cm^2
8.01	518
11.21	564
14.42	547
17.62	569
19.23	544

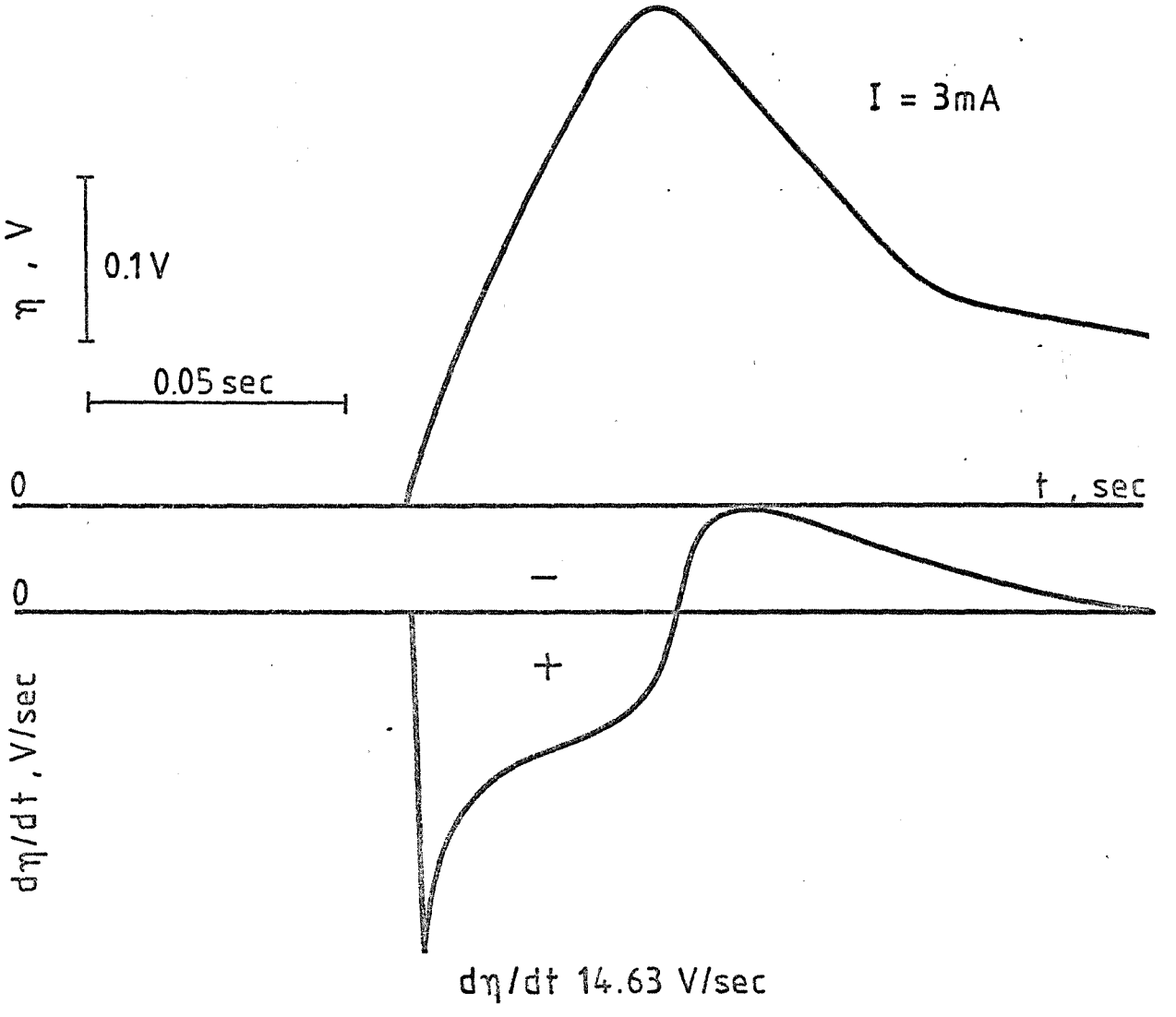

Figure 7.8 Galvanostatic η-t transient and its derivative.

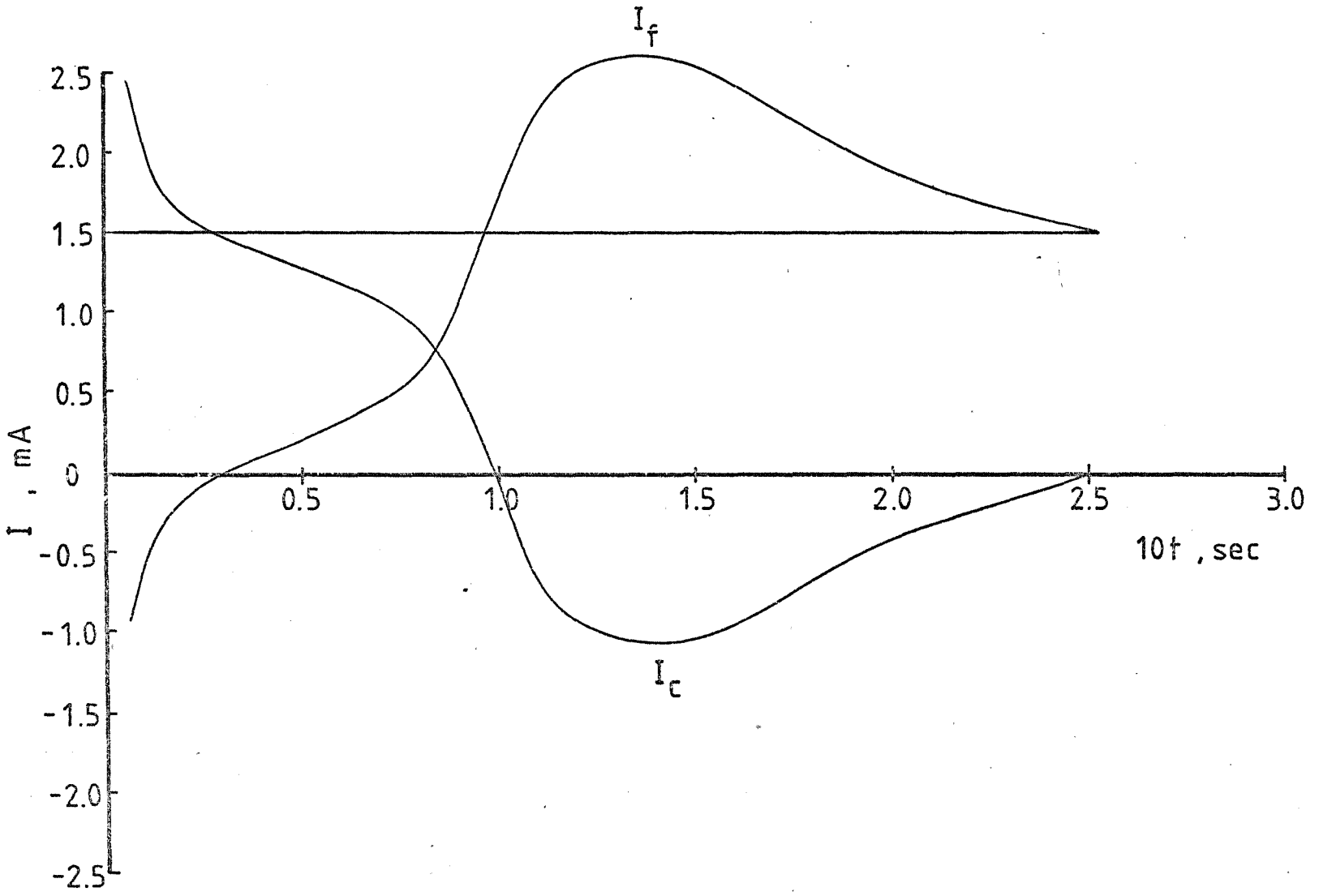

Figure 7.9 Typical deconvolution for the faradaic current from the galvanostatic transient.

Galvanostatic transients at various constant currents were also recorded at different concentrations of silver ions and the result for one concentration is presented in Figure 7.7. In each case, a pronounced potential maximum at the beginning of the transition time is observed. Increasing the applied current densities results in an increase of the potential maximum and a corresponding decrease in the interval from the starting of the current pulse to the maximum. A maximum on the η-t curves is indicative of the formation of critical clusters of elemental silver which takes place before a continuous deposit is laid down. The aim of this study is to utilize the maximum as a basis for the determination of the apparent rate constant of the charge transfer process.

It may be noted that at the start of the galvanostatic transients, the current is principally consumed in the charging of the electrical double layer. At $t = o$, the current may be assumed to be entirely capacitative in nature. In terms of this assumption the initial potential/time slope can be extrapolated to zero time and the limiting slope used to evaluate the interfacial capacitance by means of equation (4.56). The resultant value was found to be independent of the applied current densities as is shown in Table 7.4. A separate experiment for the evaluation of the capacitance was also carried out using a differentiator to determine the slope $\frac{d\eta}{dt}$ (Figure 7.8) and again in terms of equation (4.56) the capacity can be calculated. Both the extrapolation and instrumental differentiation methods give similar results. The magnitude of the effective capacity ($of \sim 600\,\mu F\ cm^{-2}$) is rather large and can be attributed to a parallel combination of the double layer capacity and the pseudo-capacity involving adsorbed silver ions or silver adatoms. Using this value, the charging current can be computed and deconvoluted from the total current to give the faradaic current as a function of time along the entire transients. A typical deconvolution is shown in Figure 7.9. It follows that at the potential maximum the charging current is by definition zero and the total current is then solely faradaic. Because of the high rate of mass transfer to a small nucleus, it is also assumed that it is entirely charge-transfer controlled.

The determination of the nuclear density up to the potential maximum of the galvanostatic transient and hence the faradaic nuclear

TABLE 7.5 Analysis of the galvanostatic potential maxima observed at a vitreous carbon electrode at the concentrations of $AgNO_3$ indicated in molten $NaNO_3$-KNO_3 eutectic at 250°C. (Electrode area = 0.312 cm^2)

η	$10^3 I$	$10^4 Q_{faradaic}$	$10^{-5} N_o$	$10^5 \bar{r}_{max}$	η^σ	$\eta_{corrected}$	nuclear current densities
mV	amp	coulomb		cm	mV	mV	amp/cm^2
	(a)	c = 23.03 mM					
333	2.5	2.24	16.1	1.92	1.66	331.34	0.67
345	3.0	2.51	20.1	1.85	1.72	343.28	0.69
364	4.0	2.68	21.5	1.85	1.72	363.28	0.86
376	5.0	2.65	26.2	1.72	1.85	374.15	1.02
394	6.0	2.81	28.5	1.71	1.86	392.14	1.14
	(b)	c = 29.21 mM					
324	2.5	2.46	6.22	2.72	1.17	322.83	0.86
334	3.5	3.11	7.00	2.82	1.13	332.87	1.00
344	4.5	3.33	8.79	2.68	1.19	342.81	1.13
354	5.5	3.96	10.66	2.66	1.19	352.81	1.16
362	6.0	3.82	12.27	2.51	1.27	360.73	1.23
	(c)	c = 44.80 mM					
315	2.0	2.79	3.72	3.36	0.94	314.06	0.75
326	3.0	2.71	4.44	3.14	1.01	324.99	1.09
338	3.5	2.65	5.06	2.98	1.07	336.93	1.23
356	4.5	2.45	5.54	2.82	1.13	354.87	1.62
375	6.0	2.62	6.00	2.81	1.14	373.87	2.01

current density can be made either by optical or potentiostatic techniques. Practically, it is more convenient to use the latter procedure because of the uncertainties attaching to visual counting method. A separate potentiostatic experiment at potentials identical to those of the galvanostatic maximum gives a series of rising current-time curves as shown earlier in Figure 7.4 and from which the number of nuclei in each case can be determined (Table 7.3). Knowing the number density of nuclei and by inserting appropriate numerical values of other variables and constants in equation (4.60) the average nuclear radius at the potential maximum, $\bar{r}_{max}$, can be found together with the average nuclear area, $2\pi\bar{r}_{max}N_o$. Thus it is also necessary to know the nuclear area. This is readily obtained from the nuclear volume which in turn is obtained from the mass, density and molecular weight of the deposited metal together with the nuclear number density, i.e.

$$\frac{2}{3}\pi\bar{r}^3_{max}N_o = \frac{Q_{max}M}{nF\rho} \quad , \tag{7.1}$$

where Q_{max} is the faradaic charge consumed up to the potential maximum,

$$Q_{max} = \int_0^{t_{max}} Idt \quad . \tag{7.2}$$

From this electroactive area the faradaic current densities at each overpotential maximum were calculated and listed in Table 7.5. The table also presents the calculated values of N_o, $\bar{r}_{max}$ and the excess interfacial energy term $\frac{3\sigma M}{zF\rho\bar{r}_{max}}$ used to correct the nucleation overpotential values so long as the interfacial energy term, σ, of a doubly heterogeneous process remains valid in physical meaning, i.e. the nuclear size is not too small.

It should be emphasized here that the 'σ' term is undoubtedly complex in nature and hence its experimental determination is inevitably subject to error particularly when dealing with microscopic clusters. This is obviously the weak point of the thermodynamic theory of nucleation process although in general it is acceptable that the theory is sound in principle. In this study we simply take the value from the surface tension of silver at its melting point.

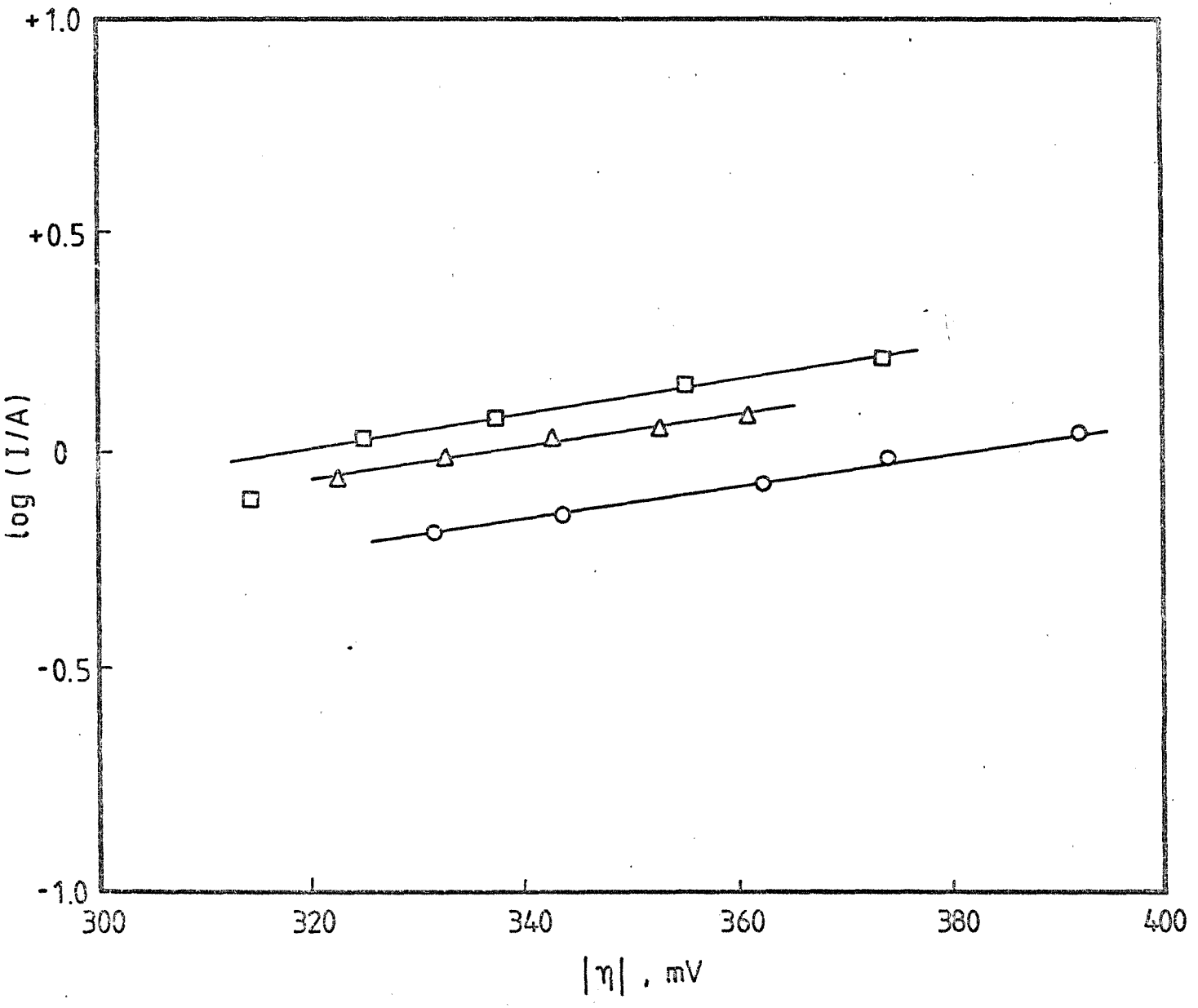

Figure 7.10 The current density-potential relation for deposition of silver from 23.03(○), 29.21(△) and 44.80(□) mM $AgNO_3$ on vitreous carbon in $NaNO_3$-KNO_3 eutectic at 250°C. (A = 0.312 cm^2)

TABLE 7.6 The apparent charge transfer rate constant of the system $AgNO_3/NaNO_3$-KNO_3 eutectic at 250°C on vitreous carbon

$10^6 c$ mol/cm^3	$10^2 I_o$ amp/cm^2	α	$10^4 k^o$ cm/sec
23.03	3.86	0.39	2.7
29.21	4.86	0.40	2.7
44.80	5.62	0.41	2.2
			Mean: 2.53

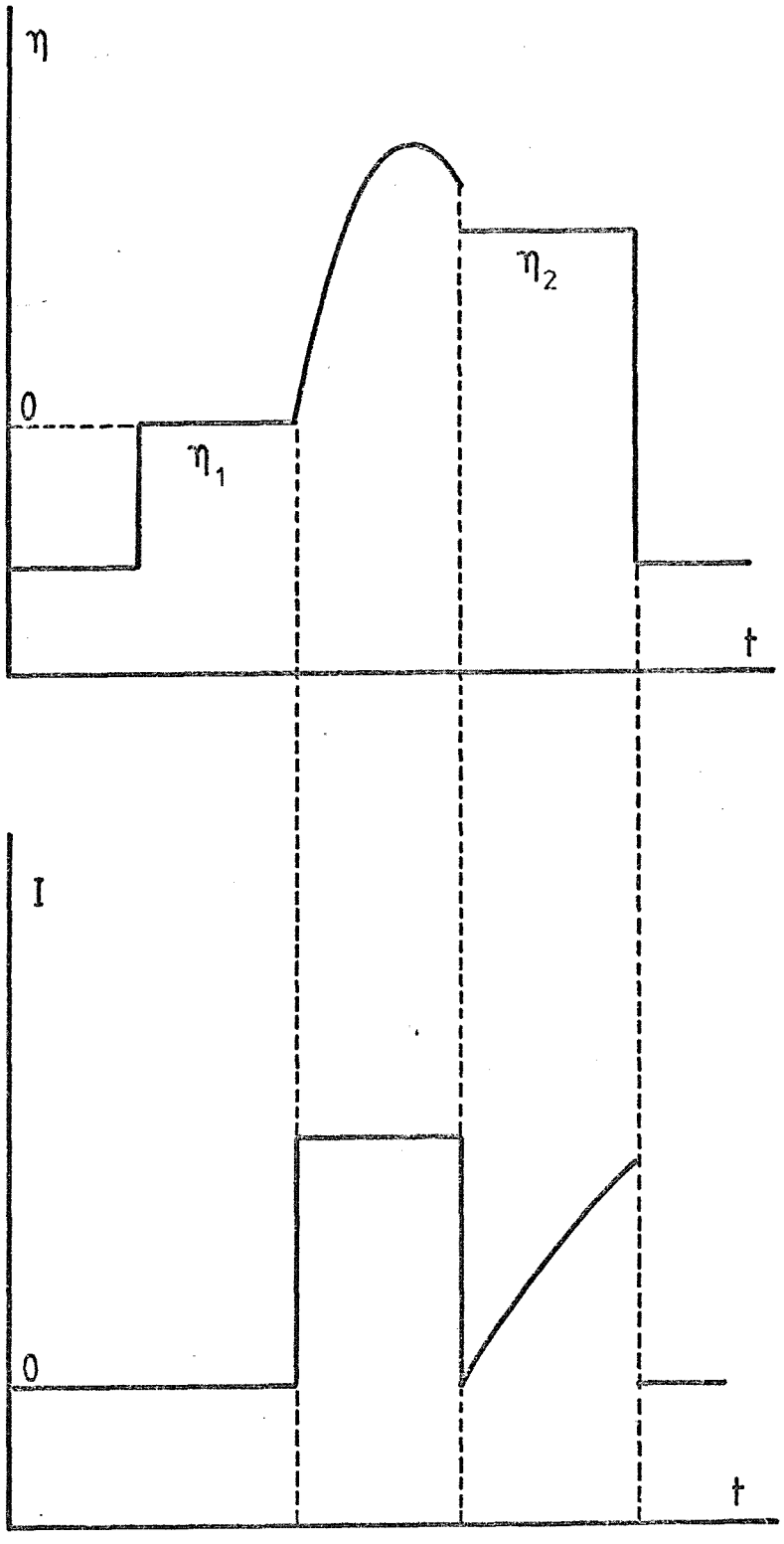

Figure 7.11 Potentiostatic-galvanostatic-potentiostatic pulse train and the resulting current-time transient.

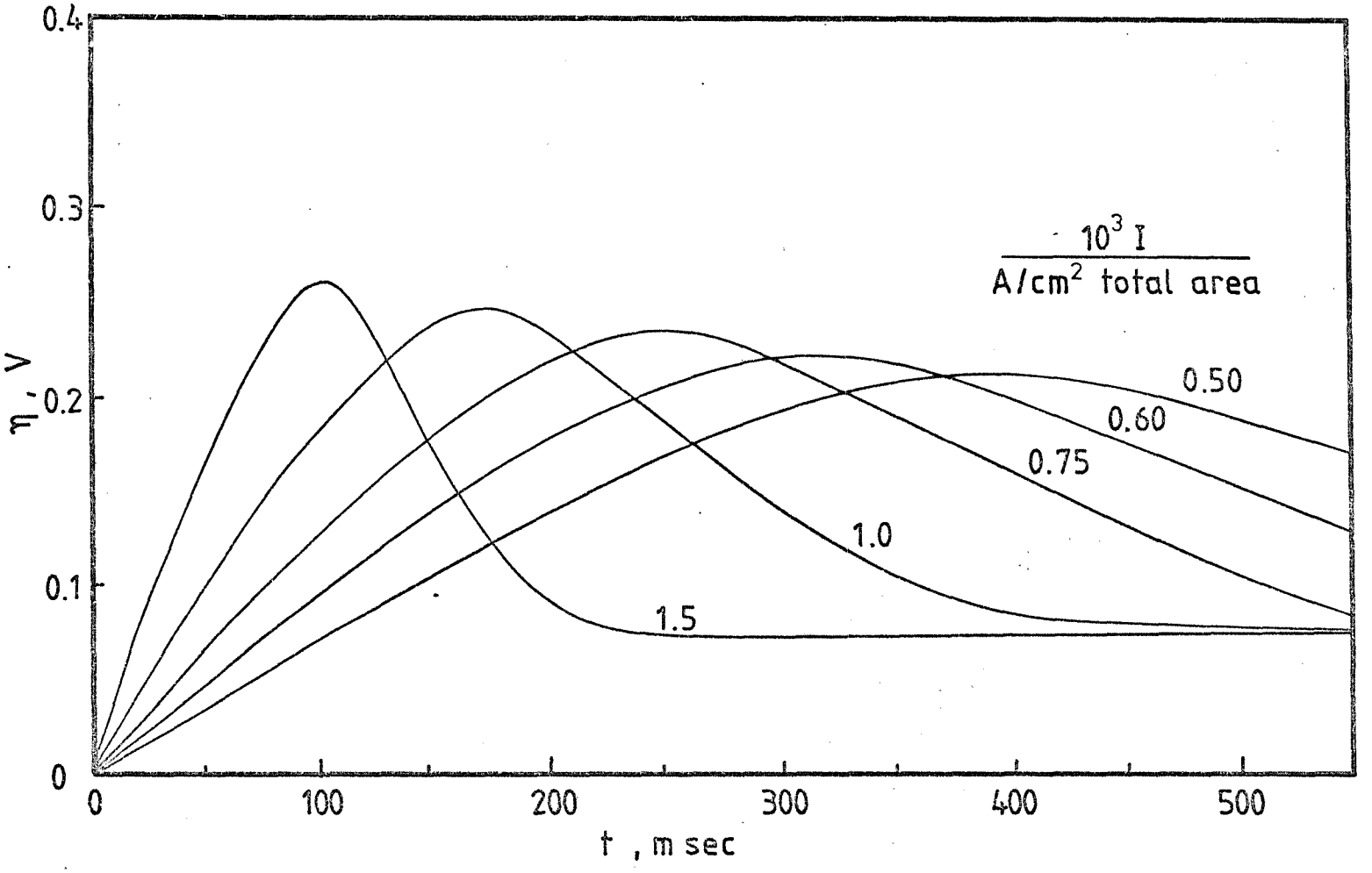

Figure 7.12 Galvanostatic transients for the reduction of 24.15 mM $AgNO_3$ on vitreous carbon in $NaNO_3$-KNO_3 eutectic at 250°C at various constant currents indicated. (A = 0.312 cm^2)

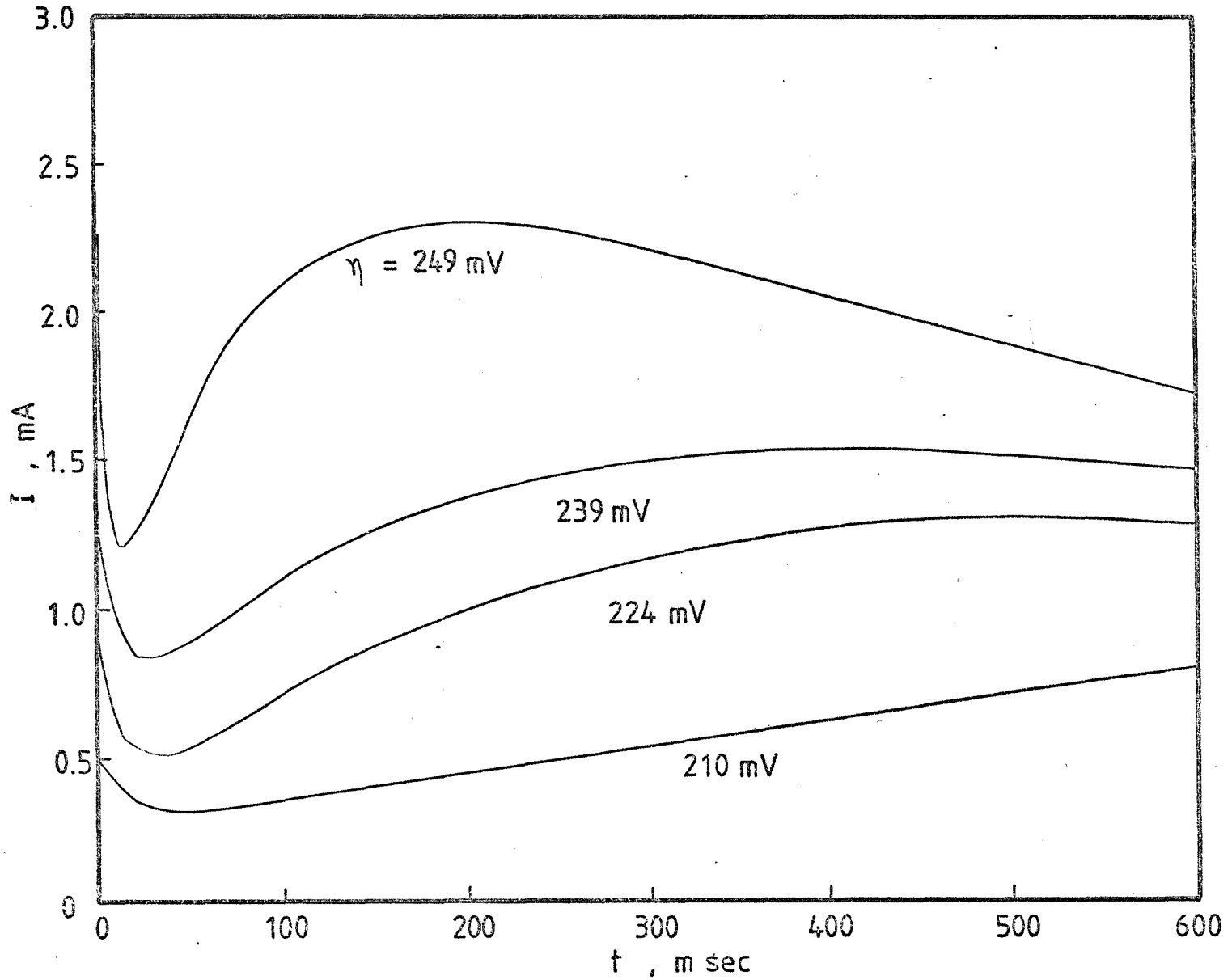

Figure 7.13a Potentiostatic transients at the galvanostatic potential maxima from Figure 7.12.

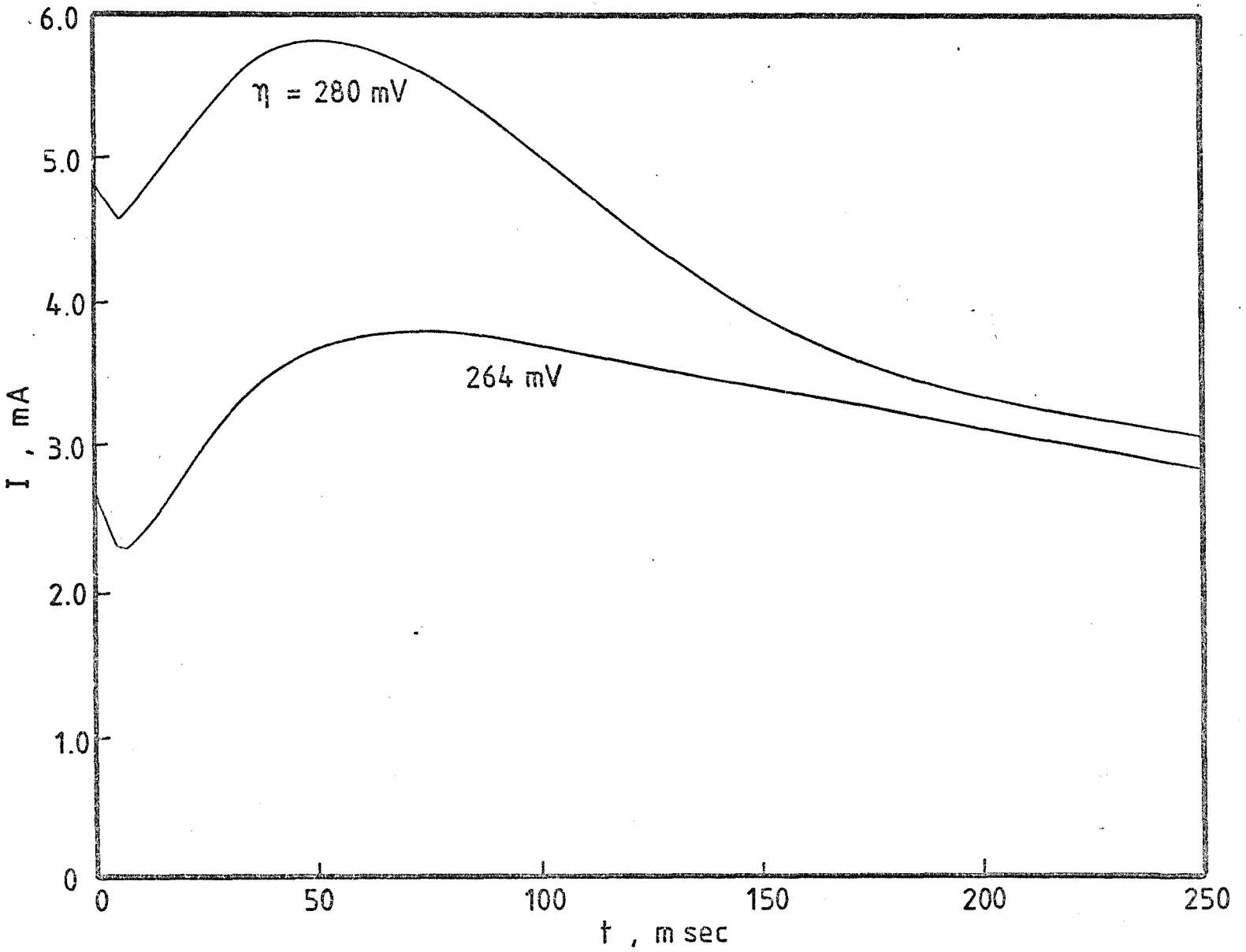

Figure 7.13b Potentiostatic transients at the galvanostatic potential maxima from Figure 7.12.

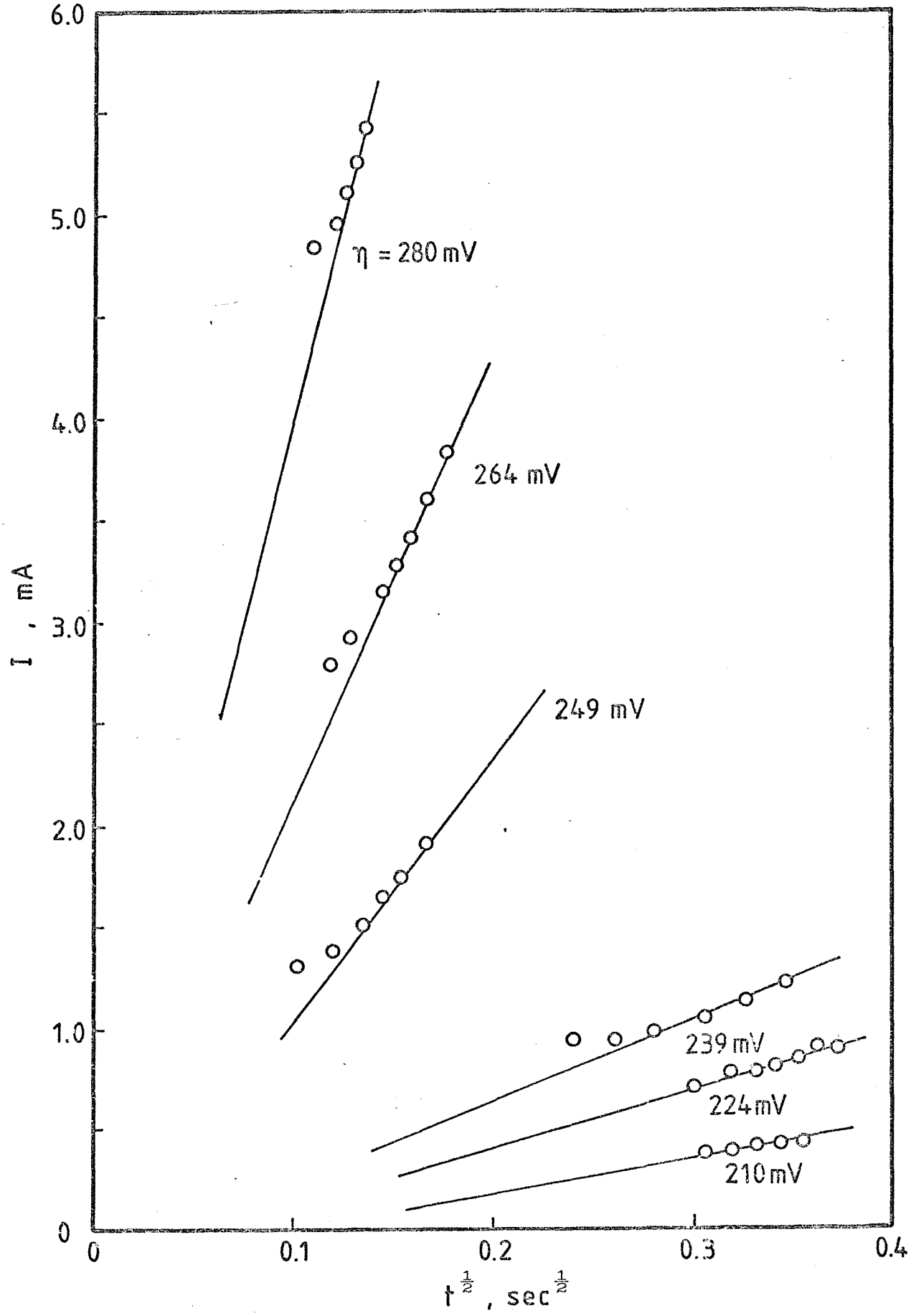

Figure 7.14 I-$t^{\frac{1}{2}}$ plot for the reduction of silver on vitreous carbon.
(Data from Figure 7.13a & b)

TABLE 7.7 Analysis of the galvanostatic potential maxima observed at a vitreous carbon electrode in 24.15 mM solution of $AgNO_3$ in molten $NaNO_3$-KNO_3 eutectic at 250°C. (Electrode area = 0.312 cm^2)

η	$10^3 I$	$10^4 Q_{faradaic}$	$10^{-5} N_o$	$10^5 \bar{r}_{max}$	η^σ	$\eta_{corrected}$	nuclear current densities
mV	amp	coulomb		cm	mV	mV	amp/cm^2
210	0.5	1.58	0.85	4.56	0.70	209.3	0.45
224	0.6	1.47	1.46	3.72	0.86	223.14	0.47
239	0.75	1.37	2.07	3.23	0.99	238.01	0.55
249	1.0	1.22	7.04	2.06	1.55	247.45	0.53
264	1.5	1.03	14.60	1.53	2.08	261.92	0.69

$\alpha = 0.42$

$I_o = 5.95 \times 10^{-2}$ amp/cm^2

$k^o = 3 \times 10^{-4}$ cm sec^{-1}

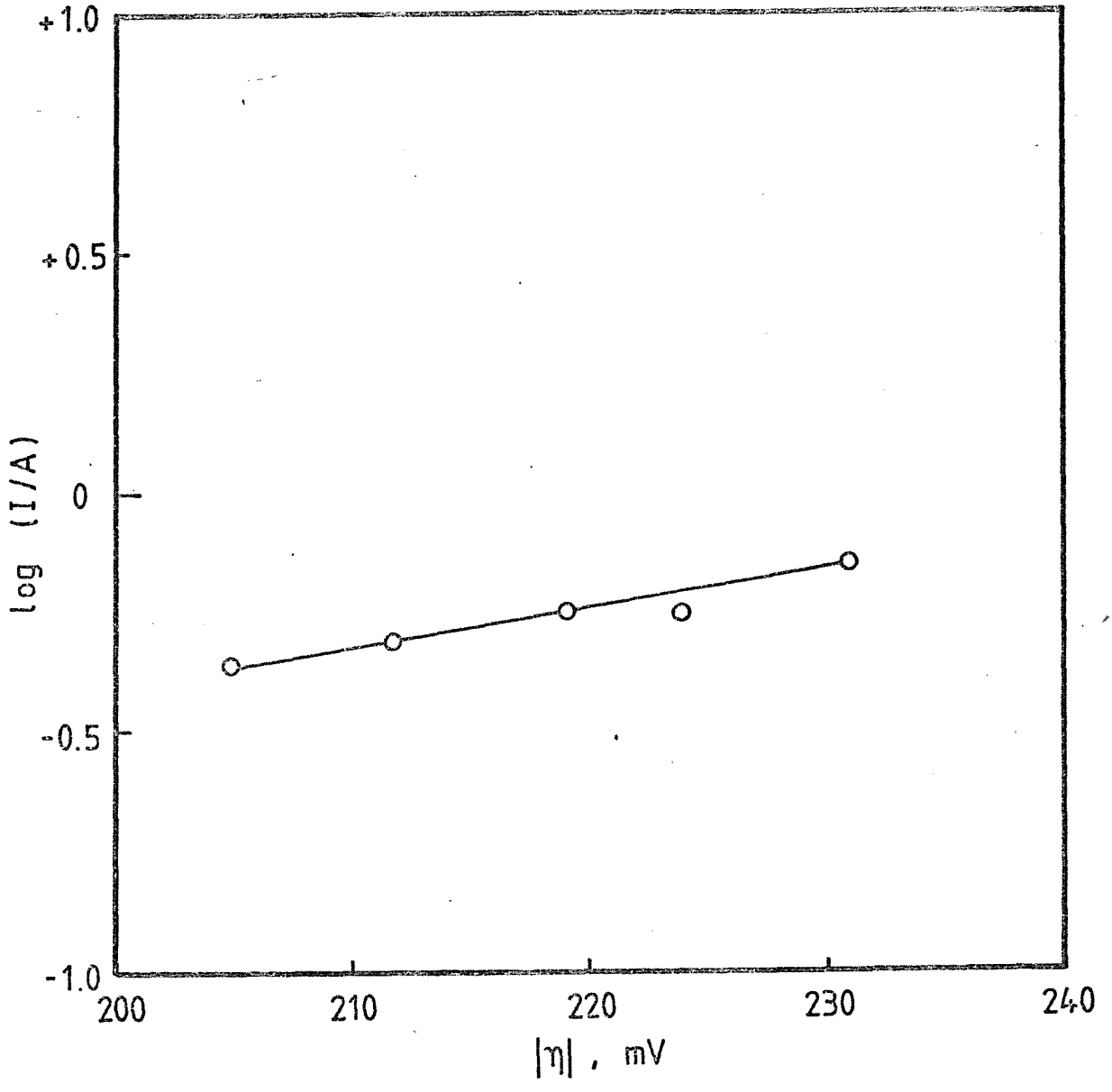

Figure 7.15 Tafel plot for the deposition of silver on vitreous carbon in $NaNO_3$-KNO_3 eutectic at 250°C.

Figure 7.10 shows Tafel plots of $\log \left[\frac{I_{faradaic}}{2\pi \bar{r}^{2}_{max} N_o} \right]$ vs $\left| \eta_{max} - \frac{3\sigma M}{zF\rho \bar{r}_{max}} \right|$ for three concentrations of silver ions. The slope of each straight line gives consistent values of the transfer coefficient, i.e. 0.40 ± 0.01, as is shown in Table 7.6. The Table 7.6 also includes the values for the exchange current density determined from the intercept and also the corresponding average standard rate constant for the silver $\rightleftharpoons$ silver ion deposition reaction of 2.53×10^{-4} cm sec^{-1}.

There is another method which is called a potentiostatic-galvanostatic-potentiostatic pulse train which has been used for the determination of the charge-transfer rate constant. This method is invariably concerned with the renewal of the electrode surface and the application of a driving force to initiate and grow a number of stable nuclei. A combination of potentiostatic and galvanostatic techniques is relevant for this purpose. The stimulus pulse and corresponding response are shown schematically in Figure 7.11. The first potentiostatic pulse is used to bring the electrode surface back to a certain anodic starting potential to remove any previous deposit and allow the subsequent metal deposition reaction to be carried out on a reproducible substrate. The second galvanostatic pulse gives rise to potential-time transients at different constant currents and the result is shown in Figure 7.12. All measurements show potential maxima and, at these maxima, the galvanostatic transient can be interrupted and switched to the potentiostatic pulse circuit giving rise to a series of rising current-time transients in Figure 7.13 (a & b). The slope of I vs $t^{\frac{1}{2}}$ plot in Figure 7.14 gives the number of nuclear density and, as before, the nuclear current density included in Table 7.7.

A plot of $\log \left[\frac{I_{faradaic}}{2\pi \bar{r}^{2}_{max} N_o} \right]$ vs $\left| \eta_{max} - \frac{3\sigma M}{zF\rho \bar{r}_{max}} \right|$ gives a straight line (Figure 7.15). The slope of a Tafel line leads to the transfer coefficient value of 0.42. The exchange current density can be found from the intercept and the calculated rate constant value is of 3.0×10^{-4} cm sec^{-1} both are given in Table 7.7.

The rate constant values evaluated from both separate potentiostatic, galvanostatic methods and the so-called P-G-P pulse trains are in good agreement but lower by approximately a factor of ten

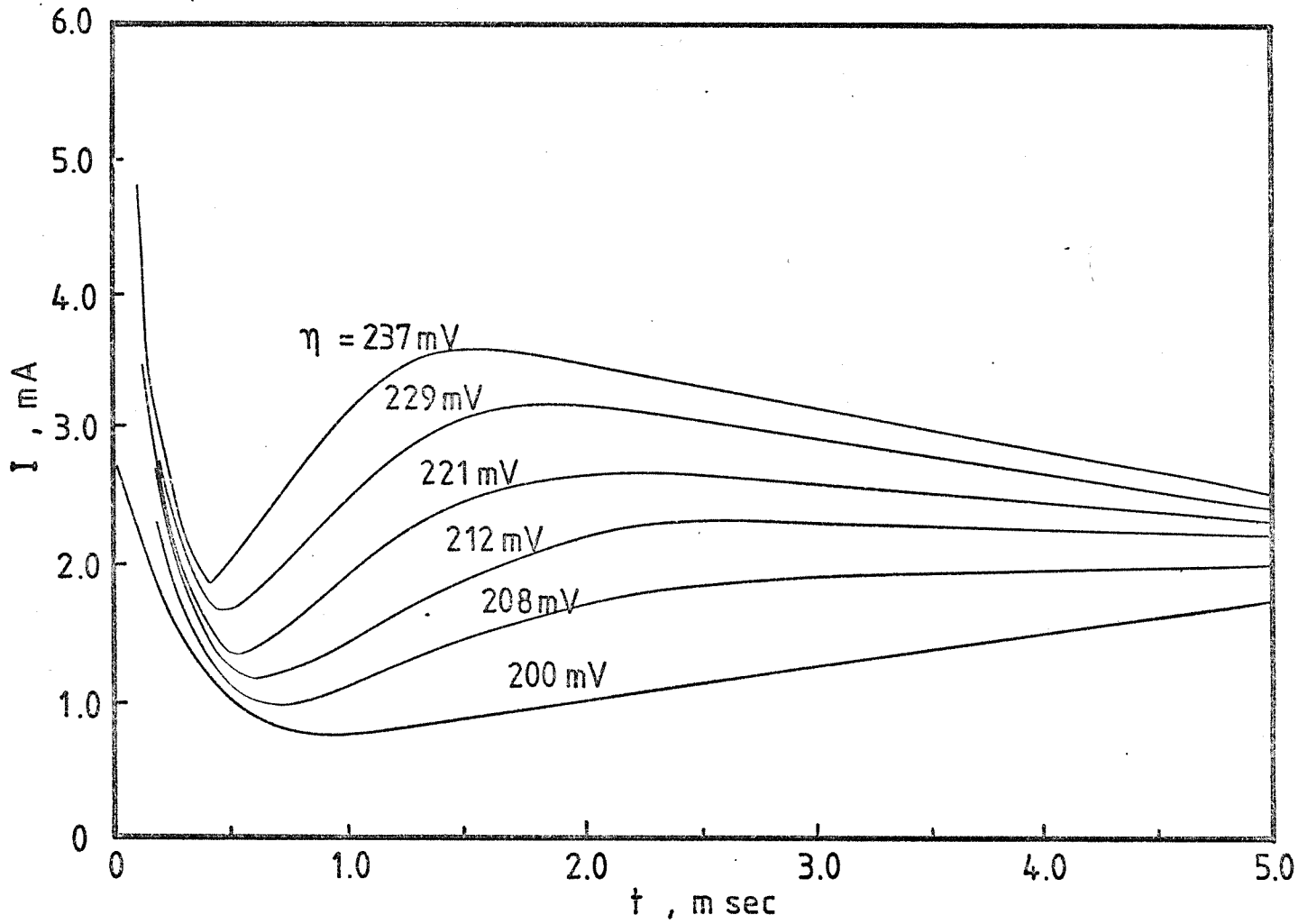

Figure 7.16 Potentiostatic transients at the galvanostatic potential maxima from Figure 6.18 for the deposition of silver from 12.3 mM $AgNO_3$ on platinum in 1 M KNO_3 solution. (A = 0.029 cm^2)

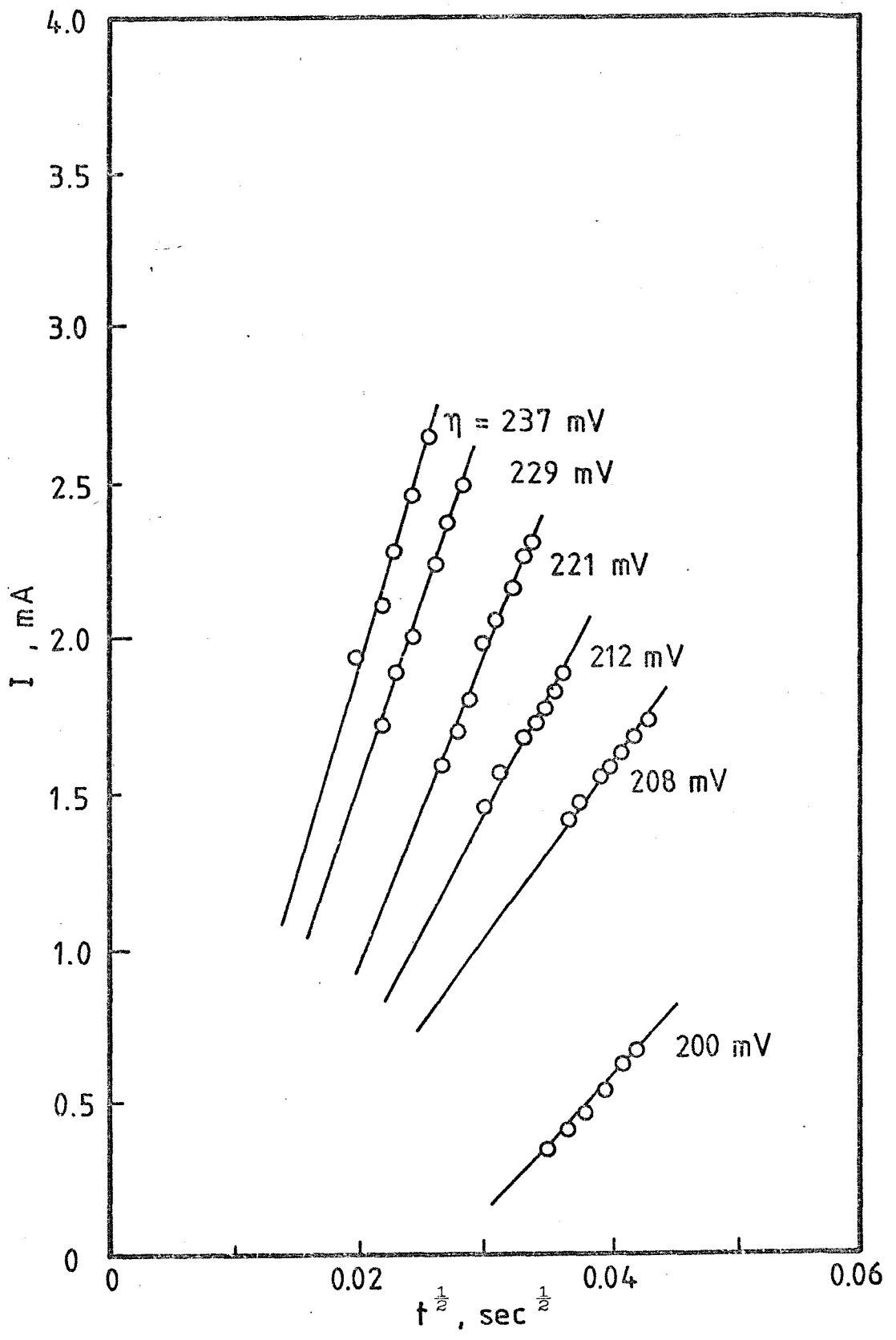

Figure 7.17 I-$t^{\frac{1}{2}}$ plot for the silver deposition on platinum (Data from Figure 7.16).

TABLE 7.8 Analysis of the galvanostatic potential maxima observed at a spherical platinum electrode for 12.3 mM $AgNO_3$ in 1 M aqueous KNO_3 solution. (Electrode area = 0.029 cm^2)

η	$10^3 I$	$10^6 Q_{faradaic}$	$10^{-6} N_o$	$10^6 \bar{r}_{max}$	π^σ	nuclear current densities
mV	amp	coulomb		cm	mV	amp/cm^2
200	0.5	0.9463	6.0	2.00	15.95	0.0331
208	0.6	0.9352	7.8	1.82	17.52	0.0369
212	0.7	0.9551	10.9	1.64	19.45	0.0380
221	0.8	0.9936	14.3	1.52	20.98	0.0385
229	0.9	1.0303	16.9	1.45	22.00	0.0403
237	1.0	1.0730	18.5	1.43	22.30	0.0420

$\alpha = 0.14$

$I_o = 0.013$ amp/cm^2

$k^o = 2.24 \times 10^{-3}$ cm sec^{-1}

TABLE 7.9 Calculated interfacial capacities in aqueous solution at different galvanostatic current densities

$\frac{10^3 I}{A/cm^2}$	$\frac{10^6 C_{dl}}{F/cm^2}$
17.24	41.3
20.68	33.0
24.13	34.6
27.58	39.6
31.03	40.4
34.48	44.9

than the reported value of 5×10^{-3} cm sec^{-1} by Bockris, Inman and Blomgren[48] for a similar system using a single pulse galvanostatic method. The difference may be accounted for by the neglected concentration overpotential or, more likely, by errors in the evaluation of $\bar{r}_{max}$.

It is evident from the potentiostatic current-time relation (equation 3.3) that the rate of mass transfer to small electrode is very high. An estimation of the mass transfer controlled faradaic current to a stationary hemispherical nucleus is found to be large and even much larger for a growing hemisphere which is a more realistic model. These estimated values are high compared to those obtained in Table 7.5 and 7.7 and the potential maximum of the galvanostatic transients is almost certainly largely controlled by charge transfer.

On the other hand, a detailed analysis of the early stages of the metal deposition[119] although in aqueous solutions showed a rapid transition of progressive nucleation to instantaneous nucleation being controlled by mass transfer. This situation takes place at some over-potentials, time scales and average nuclear radius close to the values obtained from the galvanostatic maximum. Hence the beginning part of the potential time transients reflects a mixed contribution of activation overpotential and concentration overpotential and their subsequent decline as the electroactive area increases resulting a corresponding decrease of the current density. However, the faradaic current simultaneously increases non-linearly from zero as shown in Figure 7.9 and the overpotential reaches a maximum then relaxes thereafter, the maximum being characterized by the applied current density and the exchange current density for the charge transfer process.

In view of the paucity of similar work for the evaluation of charge-transfer rate constants for the bulk silver $\rightleftharpoons$ silver ion reaction in molten salts, we may use the corresponding data for the silver deposition reaction on platinum in aqueous solutions (given in the last chapter) as a basis for comparison.

By means of an interruption at the galvanostatic potential maximum (Figure 6.18) and a separate potentiostatic estimation of the nuclear number density (Figures 7.16 and 7.17), the nuclear number density can be found. The nuclear density, the nuclear current density and the nuclear radius are given in Table 7.8. Table 7.9 shows the corresponding

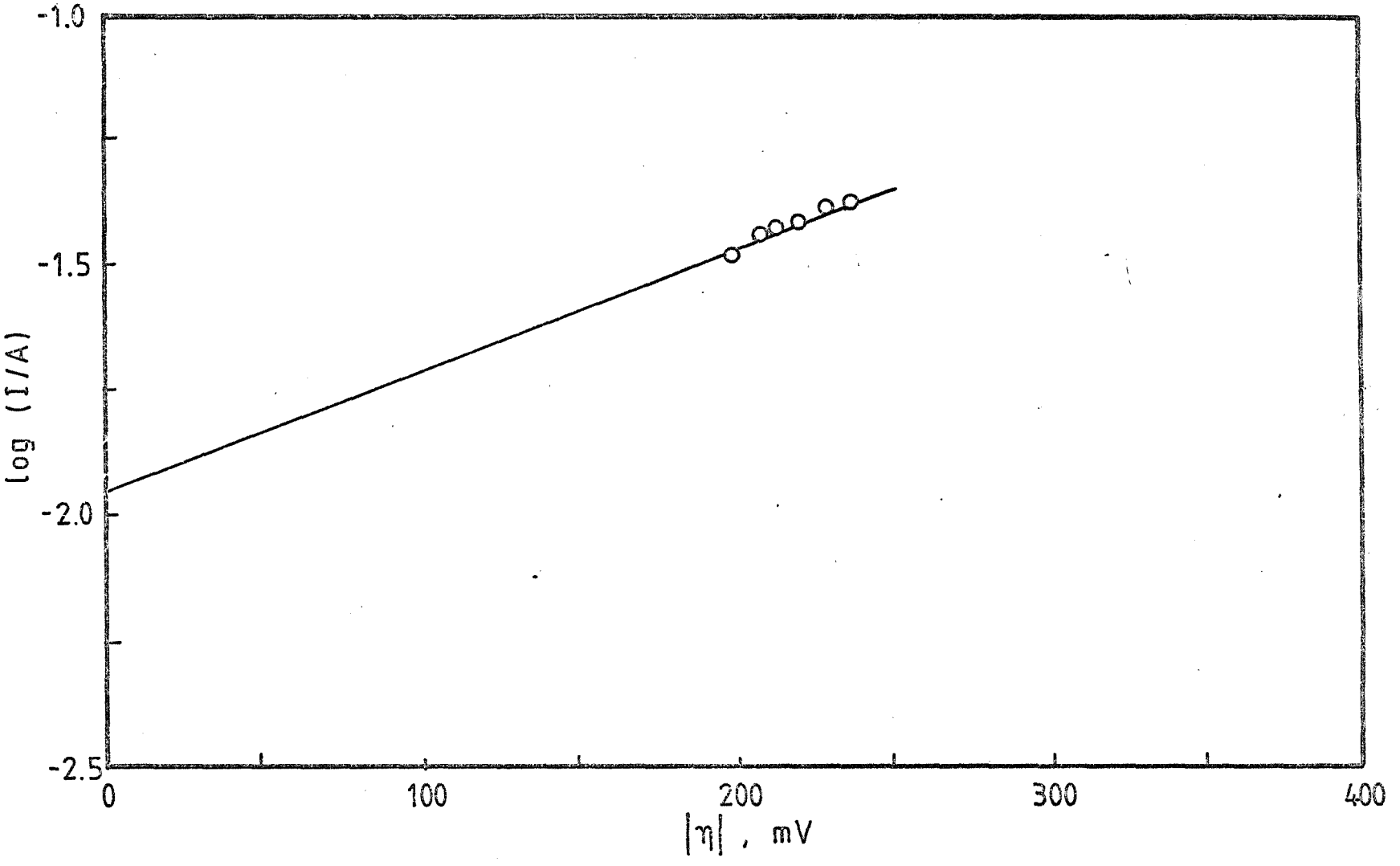

Figure 7.18 Tafel plot for the deposition of silver on platinum in 1 M KNO_3 solution.

capacitance of the platinum-solution interface which is relatively independent on the applied constant current densities.

A Tafel plot of $\log \left[\frac{I_{faradaic}}{2\pi \bar{r}^2_{max} N_o}\right]$ vs $\left|\eta_{max}\right|$ gives a straight line (Figure 7.18) and the slope of the line leads to the transfer coefficient value of 0.14. The intercept leads to the exchange current density for the aqueous solution of 0.01 M $AgNO_3$ in 1 M KNO_3 of 0.013 amp cm^{-2} and the charge-transfer rate constant of 2.24×10^{-3} cm sec^{-1}. The 'I_o' value is in a satisfactory agreement with the reported value by Mehl and Bockris[6] of 0.03 amp cm^{-2} for silver in 0.01 M $AgClO_4$ solution.

It should be noted that the correction term $\frac{3\sigma M}{zF\rho\bar{r}_{max}}$ which ought to be used to substract from the galvanostatic maximum overpotential is highly uncertain since the average nuclear radius is very small, i.e. 10^{-6} cm. On these circumstances the surface energy term, σ, tends to lose its physical meaning. The magnitude of the correction is of the order of ten millivolts and is high enough to affect significantly the shape of the rising current-time transients in potentiostatic experiments and therefore the rate of formation of nuclei.

At this stage, we have established the high temperature rate constant for the bulk silver $\rightleftharpoons$ silver ion reaction. There remains a number of unanswered problems concerning, for example, the intrinsic character of the rate constant itself, the unknown rate constant value for ad-atom formation, the distribution of nuclear size along the transient and the mixed effects of capacity, mass transfer and charge transfer. These are rather complex in nature and subject to further extensive investigations. Nevertheless, we have clearly illustrated that vitreous carbon can properly be used as a substrate for nucleation and growth studies in molten nitrates. In the next chapter, we report on an investigation to establish its usefulness for similar studies of silver in the higher melting chloride solvent, molten LiCl-KCl. Before that, however, we report related studies of several other systems in molten nitrates.

7.2 Electrodeposition of Pb(II), Cd(II), Co(II), Ni(II) and Cu(II) onto platinum in molten $NaNO_3$-KNO_3 eutectic at 250°-308°C

It has been shown that the deposition of silver on platinum and vitreous carbon proceeds by 3D instantaneous nucleation followed by growth controlled by the hemispherical diffusion of silver ions from the melt. The whole process requires a significant overpotential but is uncomplicated by kinetic or chemical complications. It is likely that for this reason that the reduction of Ag(I) ion in molten nitrates has been studied widely. However, this is not the case for the electrodeposition of other metal ions on platinum in the same system.

Many metal deposition reactions in fused alkali nitrates have mechanisms unrelated to considerations of nucleation and growth. There are probably three factors which are likely to be responsible for these additional aspects. Firstly, consideration must be given to the active role of the solvent since it is often evident that the charge-transfer process is followed by the rapid oxidation of the newly-deposited metal by the nitrate melts. Secondly, and as noted above, consideration must be given to the surface state of the platinum substrate. Although its surface is exposed to the oxidising nitrate solvent during the course of the investigation, at some stage of the electrode process, however, the platinum oxide may be reduced, giving rise to normal potential decay-time transients. Thirdly, it is necessary to consider the possibility of intermetallic compound formation between the deposit and the electrode, particularly at high working temperatures.

In view of the presence of these complicating features, it is not surprising that previous voltammetric studies in molten salts were less concerned with metal deposition reactions. However, the aim of the present investigations was to study the early stages of the metal deposition from alkali molten nitrates. Almost certainly because of the high reactivity of the nitrate media towards newly deposited metals no characteristics of the formation of a new phase or of its growth process were detected.

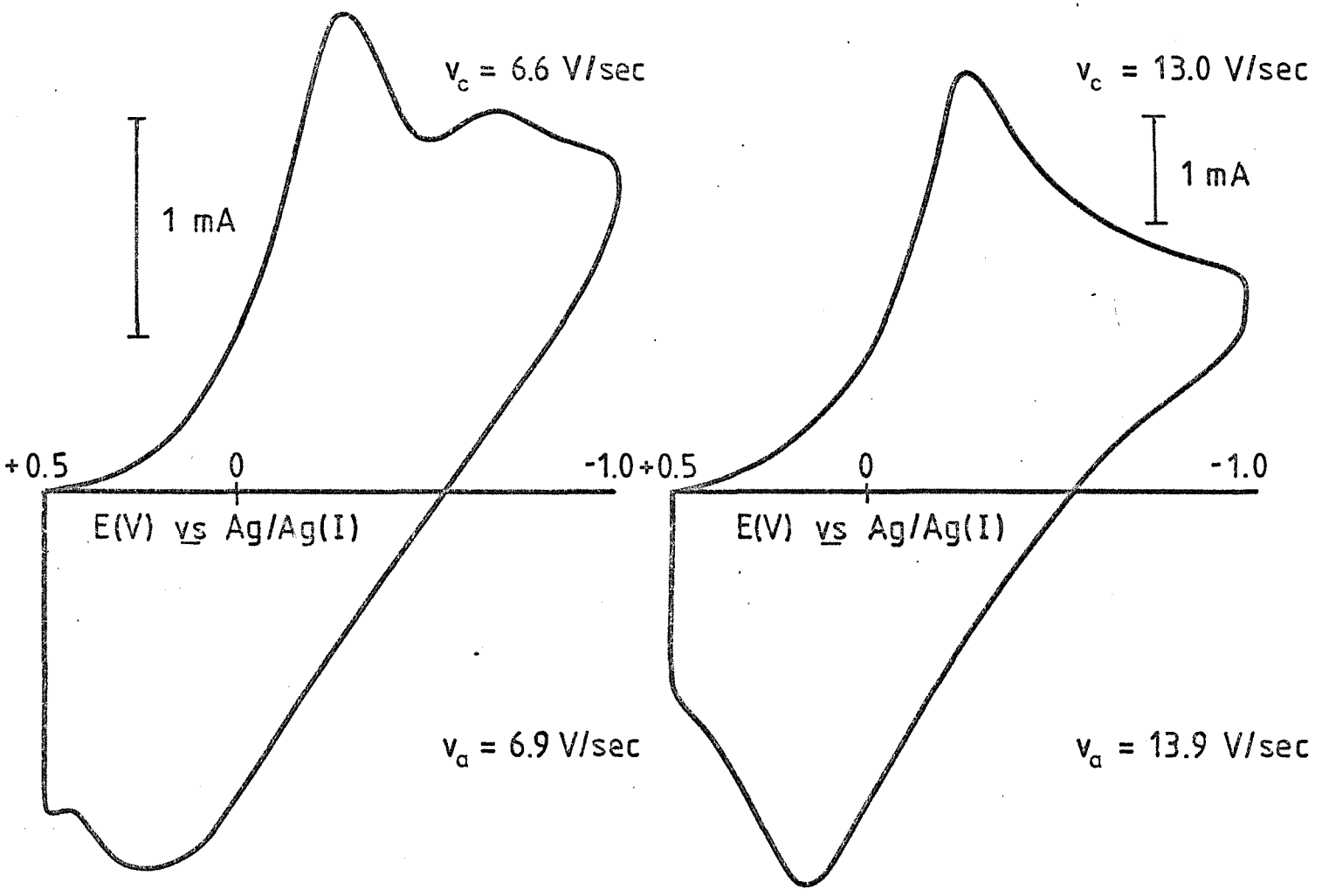

Figure 7.19 Cyclic voltammogram for the reduction of 10.22 mM $Pb(NO_3)_2$ at platinum in $NaNO_3$-KNO_3 eutectic at 250°C. (A = 0.074 cm^2)

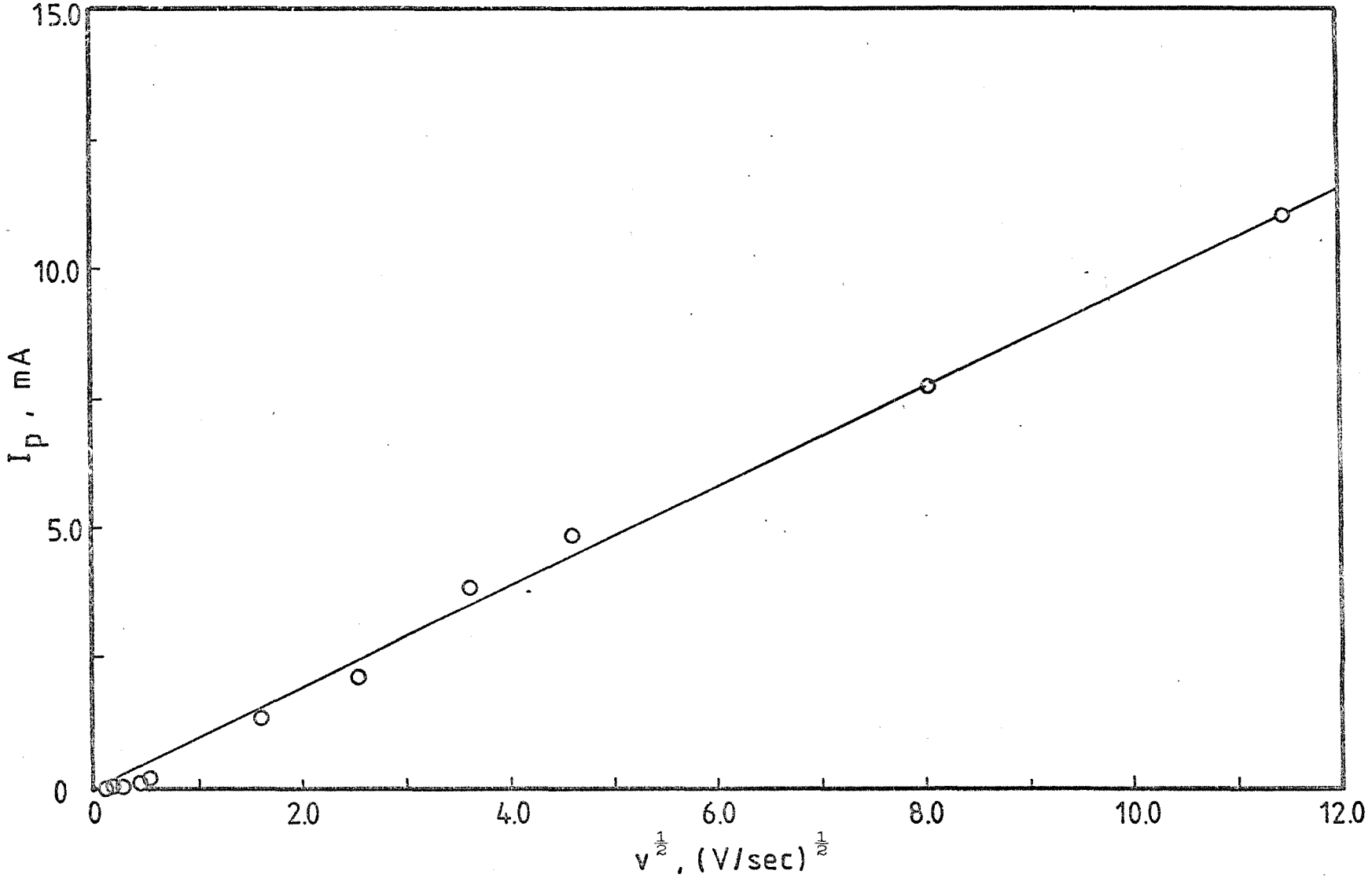

Figure 7.20 I_p vs $v^{\frac{1}{2}}$ relation for the reduction of 10.22 mM $Pb(NO_3)_2$ at pltinum in $NaNO_3$-KNO_3 eutectic at 250°C. (A = 0.074 cm^2)

TABLE 7.10 Peak current constants of the system $Pb(NO_3)_2/NaNO_3$-KNO_3 at 250°C.

$\frac{10^6 c}{mol/cm^3}$	$\frac{10^3(I_p/v^{\frac{1}{2}})}{A/(V/sec)^{\frac{1}{2}}}$	$\frac{A}{cm^2}$	$10^{-3}(K_p = \frac{I_p/v^{\frac{1}{2}}}{Ac})$	literature value
4.88	2.1818	0.036 (spherical)	1.24	
10.22	9.7274	0.074 (cylindrical)	1.28	
15.00	12.9160	0.074 (cylindrical)	1.16	
			Mean: 1.22	1.37(42)

TABLE 7.11 Peak potential as a function of sweep rate for the reduction of Pb(II) on platinum at various concentrations indicated.

$\frac{v}{V/sec}$	$\frac{E_p}{mV}$
c = 4.88 mM, A = 0.036 cm^2	
2.34	350
6.00	343
11.79	236
23.55	221
60.5	157
123.9	150
c = 10.22 mM, A = 0.074 cm^2	
2.52	300
6.6	285
13.05	285
21.36	355
64.8	180
131.1	135
c = 15.00 mM, A = 0.074 cm^2	
2.55	330
7.51	315
13.05	300
23.31	300
64.50	240
130.50	150

7.2.1 The system $Pb(NO_3)_2/NaNO_3$-KNO_3 at 250°C

As noted above, many metals react with molten nitrates to form metal oxides. Lead metal was deposited on platinum and found to react further with the nitrate solvent to form lead oxide. It is possible that the latter oxidation reaction affected the former reduction process and no evidence of phase formation and its growth process was obtained.

Voltammetric studies have been made of the deposition of lead from a range of concentration of $Pb(NO_3)_2$ (4.88, 10.22 and 15 mM) onto cylindrical or spherical platinum electrodes in molten $NaNO_3$-KNO_3 eutectic at 250°C. All measurements were made with respect to the Ag/Ag(I) reference electrode. For linear sweep experiments, the electrode was held at an anodic potential for two minutes to ensure a complete dissolution of any previous deposition product before starting the deposition again.

Cyclic voltammogram for the reduction and re-oxidation reactions in 10.22 mM lead nitrate solution at two sweep rates are shown in Figure 7.19. In each case, well-defined reduction peaks were obtained. It may be noted that, at sweep rates less than ~9 V sec^{-1} there are two peaks but only one peak at faster sweep rates. This was always the case irrespective of the concentration or electrode geometry.

Peak currents from the first wave of the voltammogram recorded between 0.03-131 V sec^{-1} and at different concentrations of lead nitrate were plotted against the square root of the scan rate and found to be linear, the regression line passing through the origin as shown in Figure 7.20 for one concentration. The slopes of the lines enabled the diffusion coefficient to be calculated by using equation (3.14) which for the working temperature of 250°C becomes

$$I_p = 277 z^{3/2} A c v^{\frac{1}{2}} D^{\frac{1}{2}} \quad . \qquad (7.3)$$

The diffusion coefficient was found to be 2.46×10^{-6} cm^2 sec^{-1} in agreement with the previously reported values included in Table 7.1. The peak current constants ($K_p = I_p / v^{\frac{1}{2}} A c$) for each concentration of lead nitrate solution are presented in Table 7.10. The constancy of the K_p values simply illustrates the linear dependence of the current peak height on the lead ion concentration and the electrode area. Peak potentials are shown in Table 7.11 and seen to be independent of

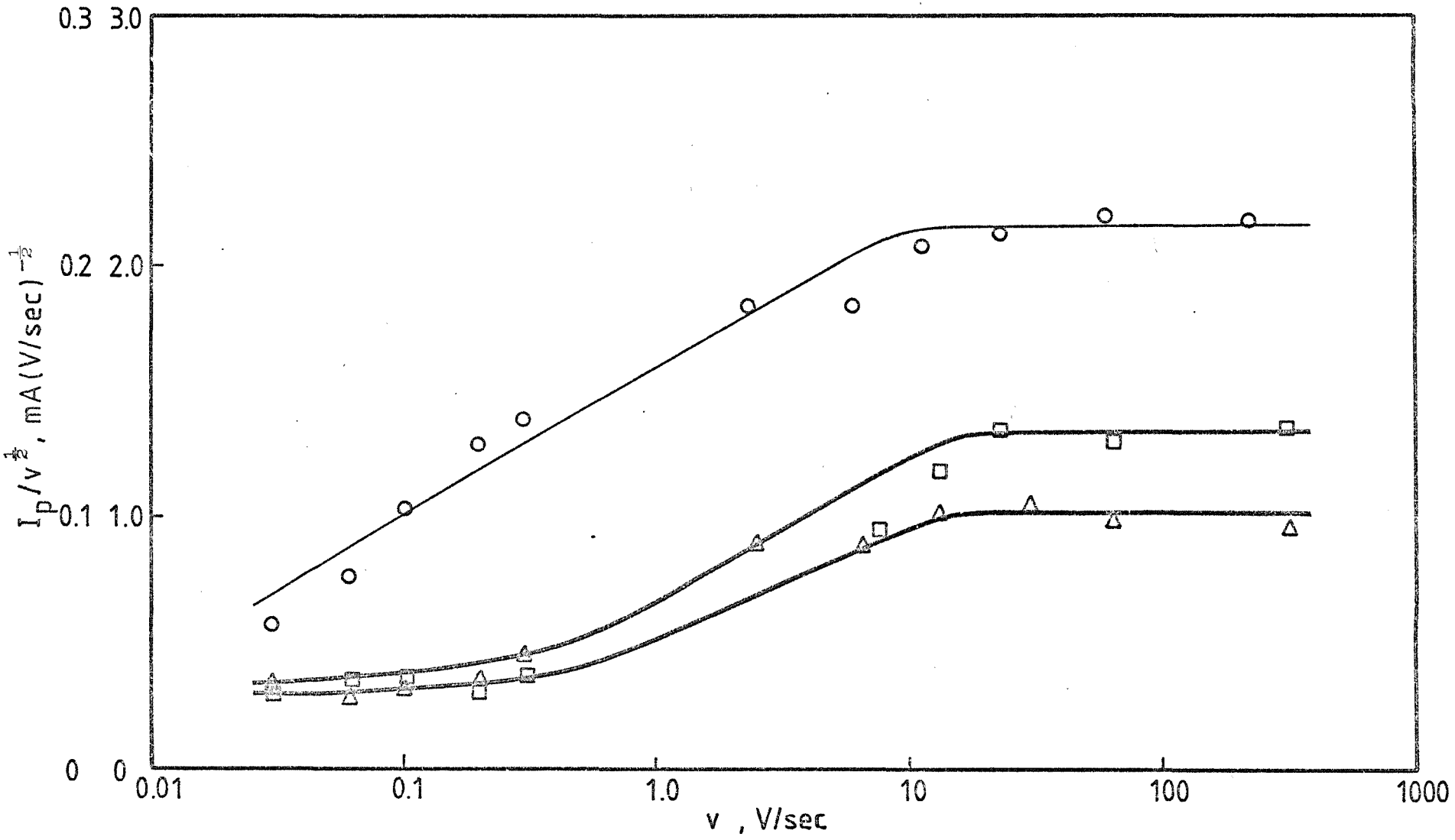

Figure 7.21 $I_p/v^{\frac{1}{2}}$ vs plot for the electrodeposition of $Pb(NO_3)_2$ on platinum in $NaNO_3$-KNO_3 eutectic at 250°C. (O = 4.88 mM; A = 0.036 cm^2), (Δ = 10.22 mM; A= 0.074 cm^2), (□ = 15.00 mM; A = 0.074 cm^2)

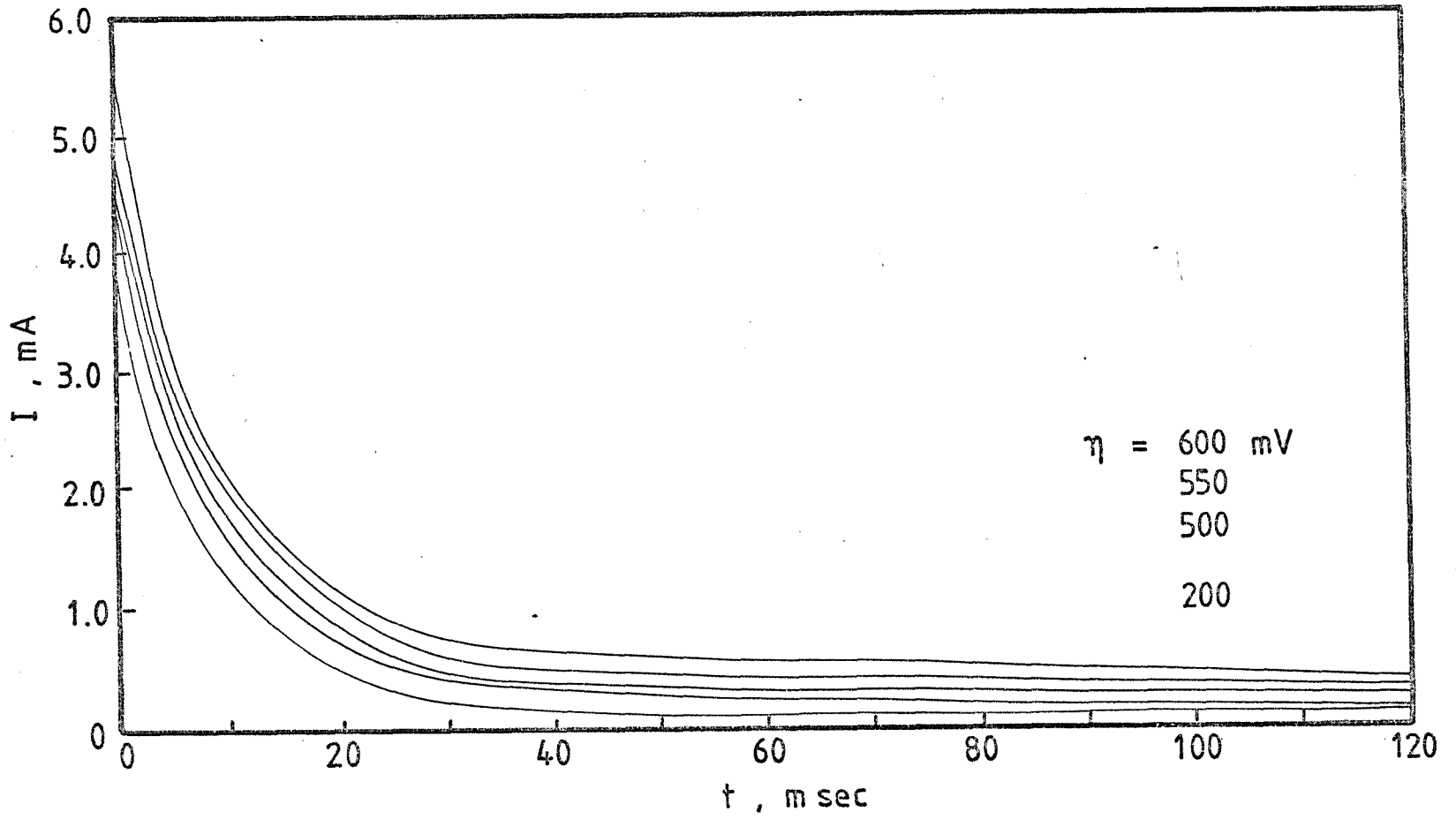

Figure 7.22 I-t transients for the reduction of 10.22 mM $Pb(NO_3)_2$ on platinum at the overpotentials indicated. ($A = 0.148\ cm^2$)

the concentration but not of the rate of polarisation. The present observations are in good agreement with those of Behl and Gaur[42] who used rapid scan voltammetry for the study of lead deposition on platinum from molten $NaNO_3$-$Ba(NO_3)_2$ eutectic at 350°C. The interpretation of the results is as follows.

Lead metal is known to alloy with platinum and also to react with the nitrate melt. Several voltammetric studies[40-42] have confirmed that lead oxide is formed when the reduction of lead ions is carried out in the oxidising nitrate solvent. It follows that the oxidation product on the electrode surface would inhibit the main reduction process resulting in peak currents smaller than those predicted by the theory, i.e. by equation (3.14). Therefore, the $I_p/v^{\frac{1}{2}}$ plots will not be linear in character and this seems to be the case, especially at low sweep rates, i.e. up to ~ 9 V sec^{-1} (Figure 7.20). In this region, a negative deviation is observed corresponding to the effect of the lead oxide. On the other hand, when the rate of potential change is fast, e.g., faster than 9 V sec^{-1}, the reduction of lead oxide was not observed and hence only a single reduction peak was obtained. It is also seen that between 9-131 V sec^{-1}, the peak currents are linearly dependent on the square root of the sweep speed in accord with theoretical expression.

Figure 7.21 shows plots of $I_p/v^{\frac{1}{2}}$ *vs* v for each concentration of lead nitrate solutions. It should be noted that $I_p/v^{\frac{1}{2}}$ increases with increasing sweep velocities to about 10 V sec^{-1} and becomes constant thereafter. The observation corresponds to the assumption that the oxidation reaction between the deposited lead metal and the nitrate melt at fast sweep rates is itself insufficiently fast to affect the voltammogram.

The potentiostatic method was also used to study the lead deposition reaction. The results show the normal falling current-time transients over a range of overpotentials from 200 to 600 mV (Figure 7.22). It is well known that the formation of a new phase gives rise to rising current-time transients which are a function of the number and geometry of the nuclei. In the present observations, however, no rising transients were obtained. Therefore, it can be concluded that the lead deposition was not controlled by nucleation and growth process. The reason for this is probably associated with the intervention of the nitrate solvent in the discharge process.

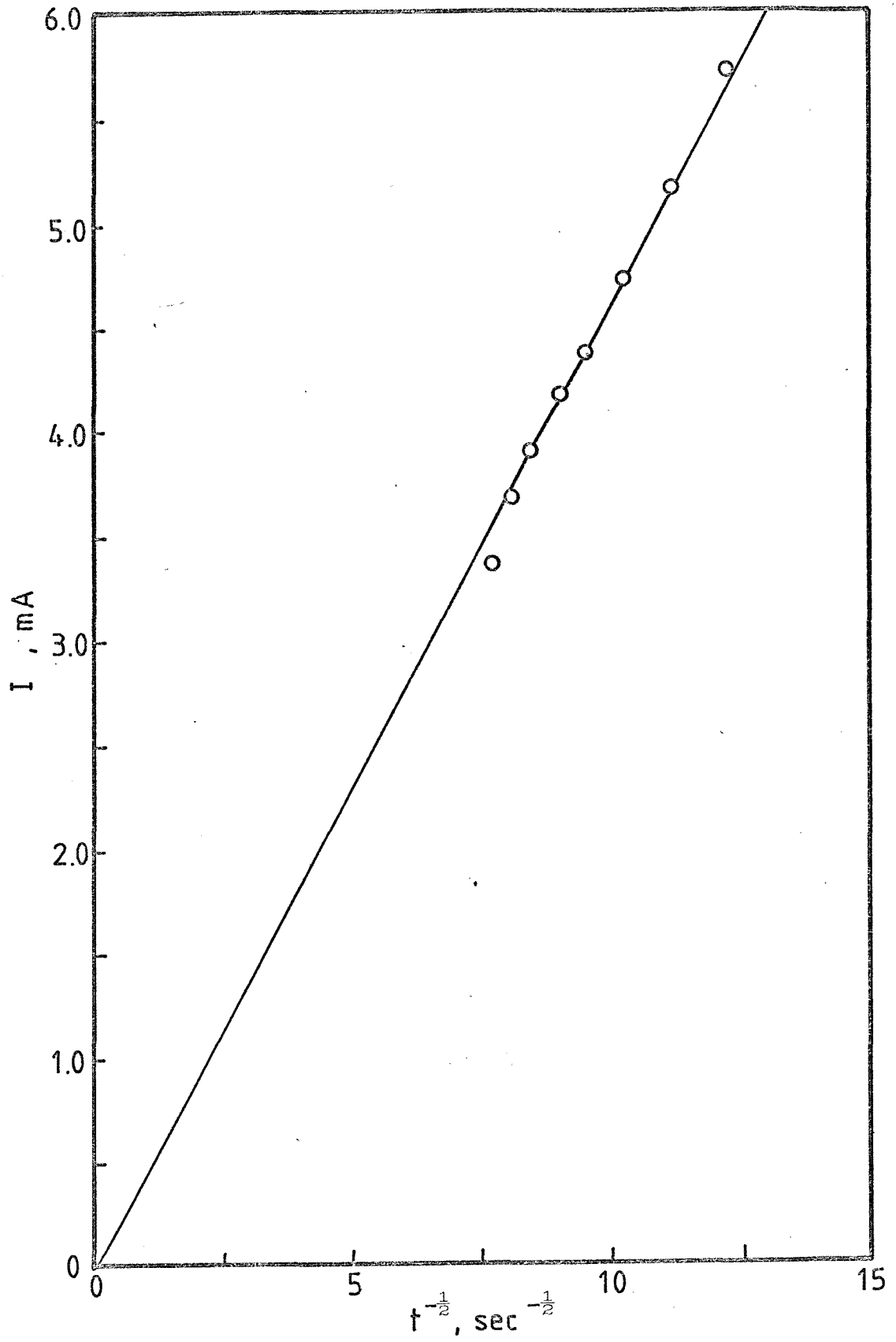

Figure 7.23 $I\text{-}t^{-\frac{1}{2}}$ plot for the reduction of 10.22 mM $Pb(NO_3)_2$ at platinum at η = 500 mV. (A = 0.148 cm^2)

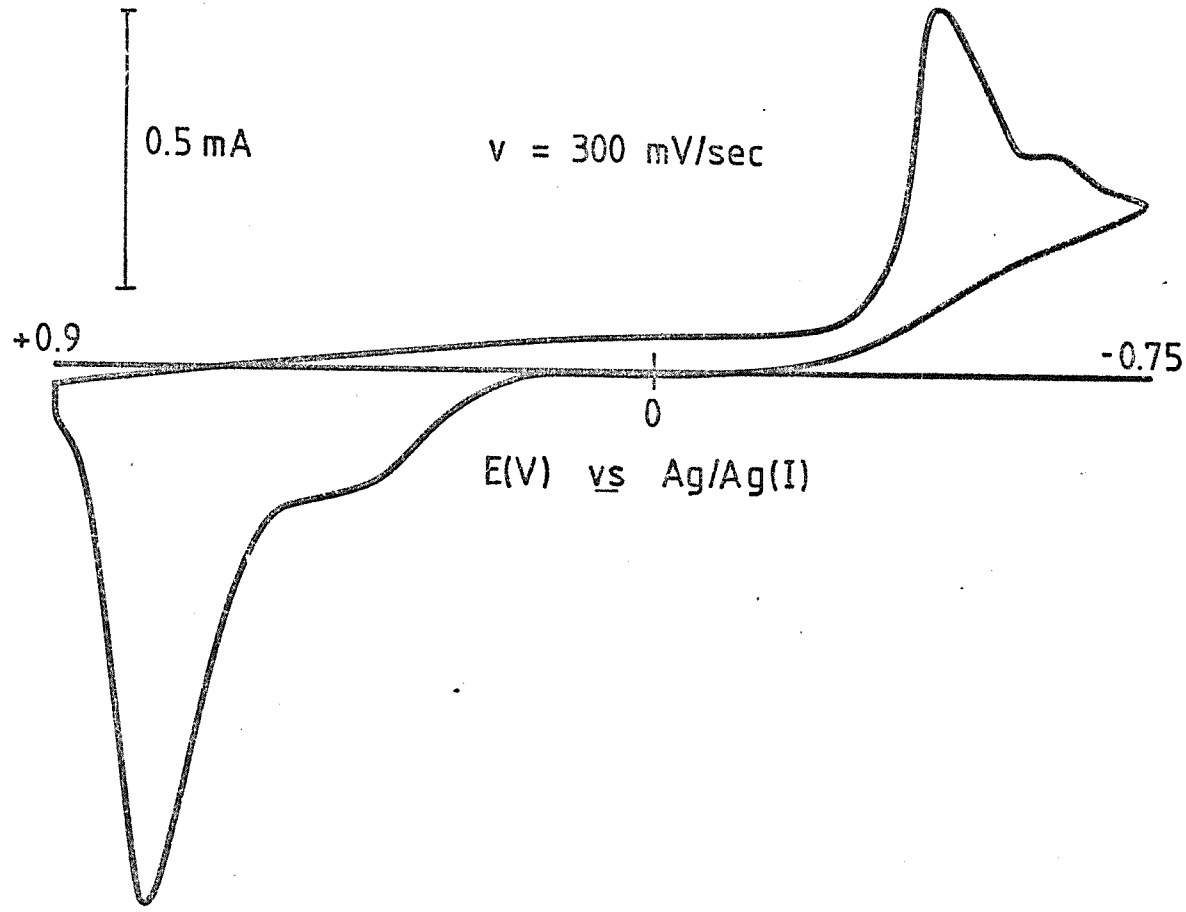

Figure 7.24 Current-potential curve for the deposition of 11.88 mM $Cd(NO_3)_2$ on platinum in $NaNO_3$-KNO_3 eutectic at 308°C. (A = 0.036 cm^2)

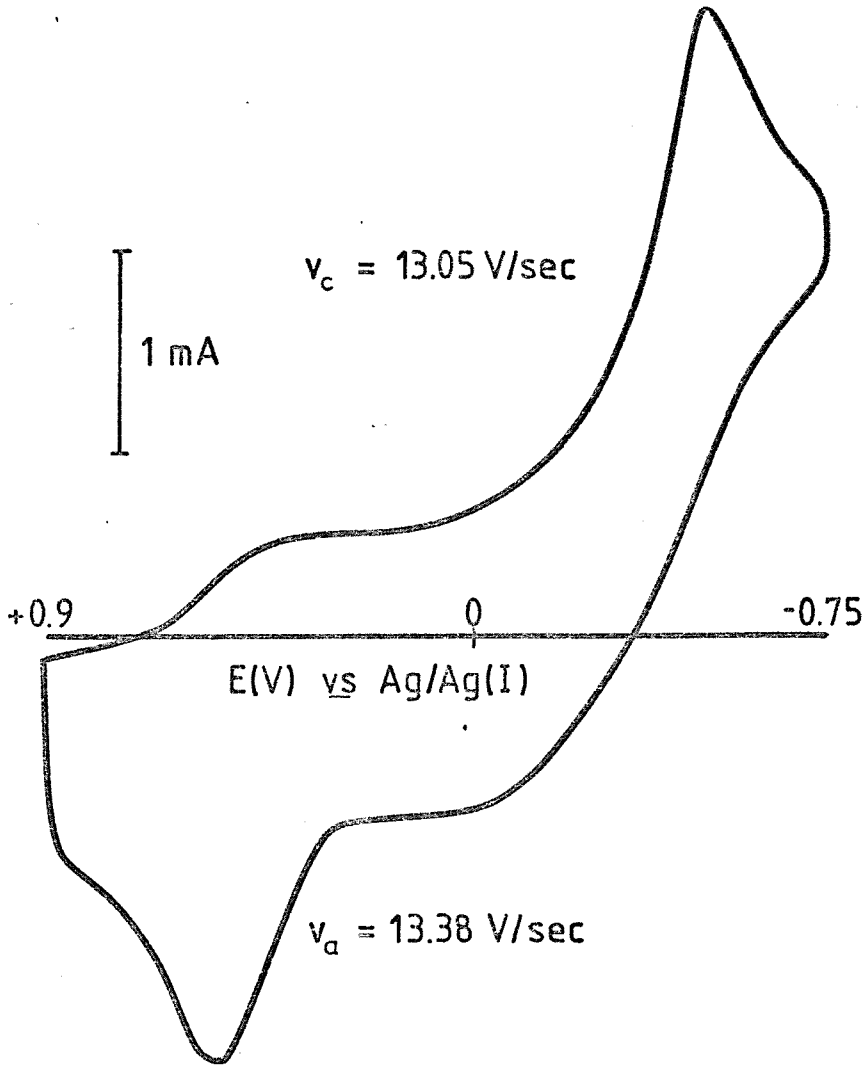

Figure 7.25 As Figure 7.24

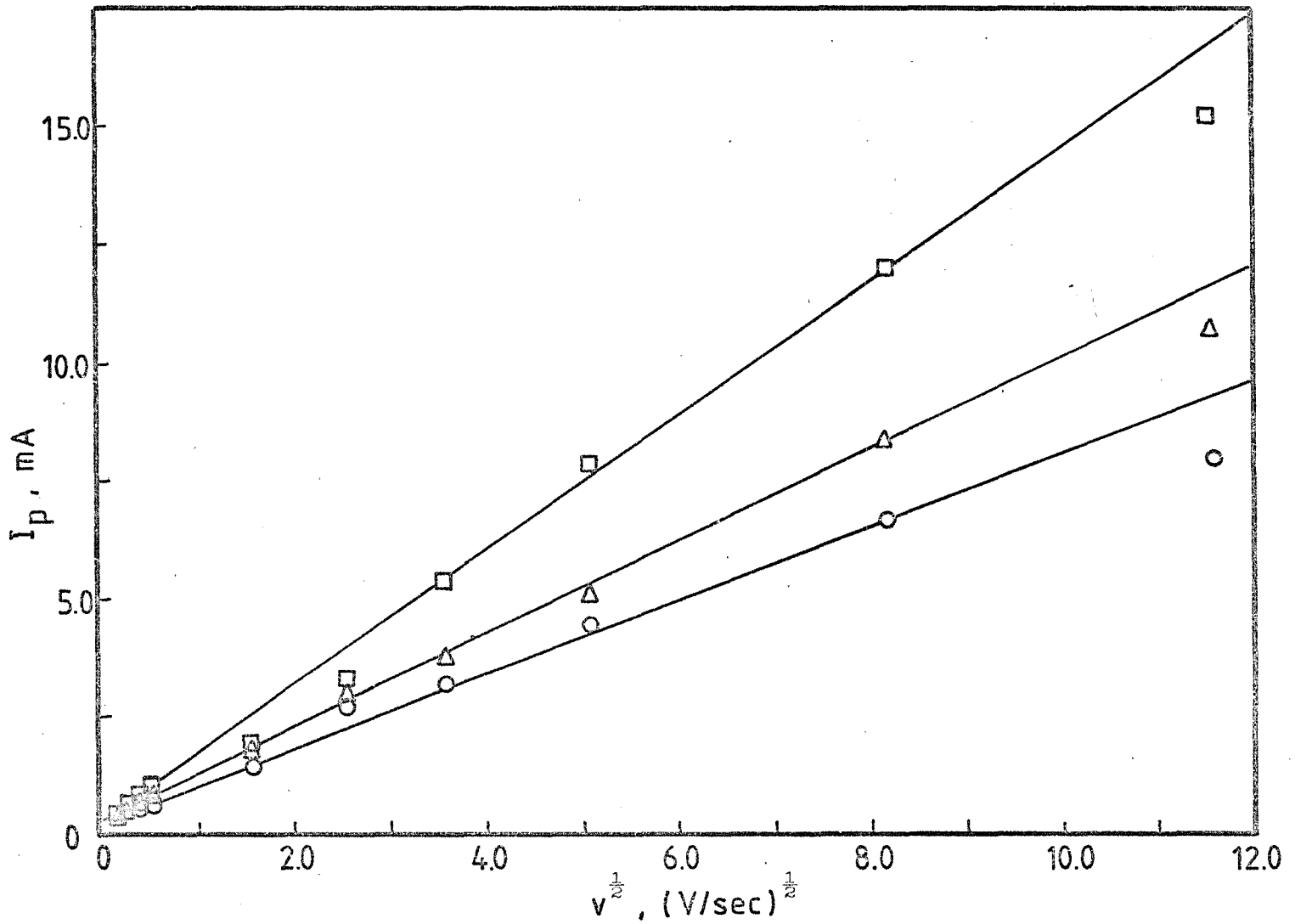

Figure 7.26 Peak current vs (sweep rate)$^{\frac{1}{2}}$ plot for 11.88(O), 17.09(Δ) and 22.48(□) mM $Cd(NO_3)_2$ in $NaNO_3$ -KNO_3 eutectic at 308°C.

TABLE 7.12 Cyclic voltammetric peak potentials, peak separation potentials over a range of sweep rates for the electrodeposition-dissolution of Cd(II) onto platinum at the concentrations indicated in $NaNO_3$-KNO_3 eutectic at 250°C. (Electrode area = 0.036 cm^2)

$\frac{v}{V/sec}$	$\frac{E_p^c}{V}$	$\frac{E_p^a}{V}$	$\frac{\Delta E_p}{V}$
	E vs Ag/Ag(I)		
(a) c = 11.88 mM			
0.030	0.303	0.702	1.004
0.060	0.307	0.727	1.064
0.100	0.372	0.746	1.118
0.200	0.426	0.736	1.112
0.300	0.432	0.741	1.172
2.61	0.445		
6.65	0.511		
13.05	0.478		
26.19	0.503		
67.3	0.461		
135.3	0.519		
(b) c = 17.09 mM			
0.030	0.352	0.795	1.147
0.060	0.333	0.765	1.097
0.100	0.352	0.800	1.152
0.200	0.367	0.805	1.172
0.300	0.382	0.829	1.211
2.61	0.462		
6.65	0.486		
13.05	0.495		
26.19	0.478		
67.3	0.511		
135.3	0.528		
(c) c = 22.48 mM			
0.030	0.318	0.715	1.033
0.060	0.342	0.760	1.102
0.100	0.367	0.780	1.147
0.200	0.382	0.820	1.202
0.300	0.397	0.824	1.221
2.61	0.478		
6.65	0.478		
13.05	0.552		
26.19	0.577		
67.3	0.561		
135.3	0.528		

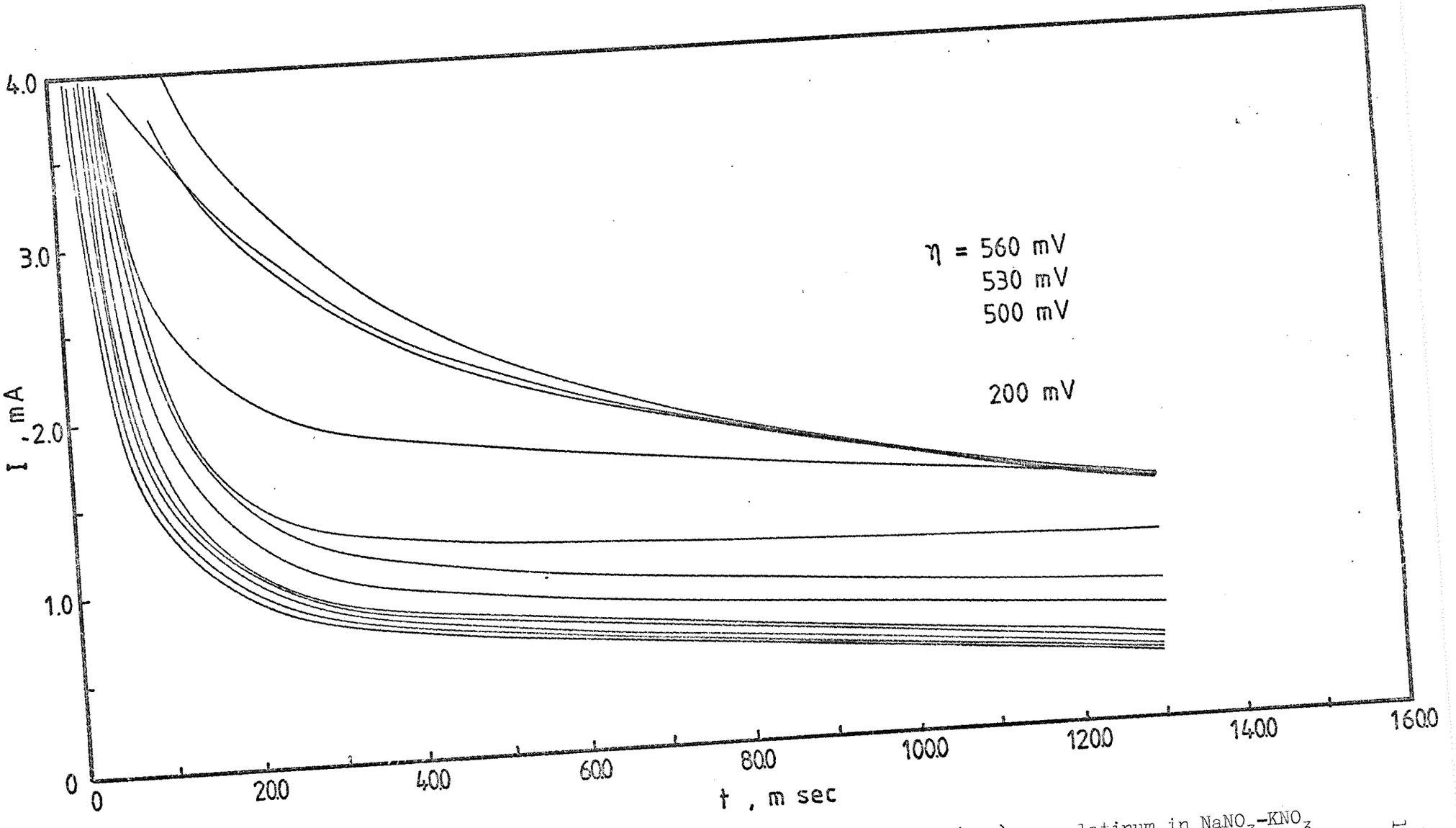

Figure 7.27 Potentiostatic transients for the reduction of 22.48 mM $Cd(NO_3)_2$ on platinum in $NaNO_3$-KNO_3 eutectic at 308°C. (A = 0.036 cm^2)

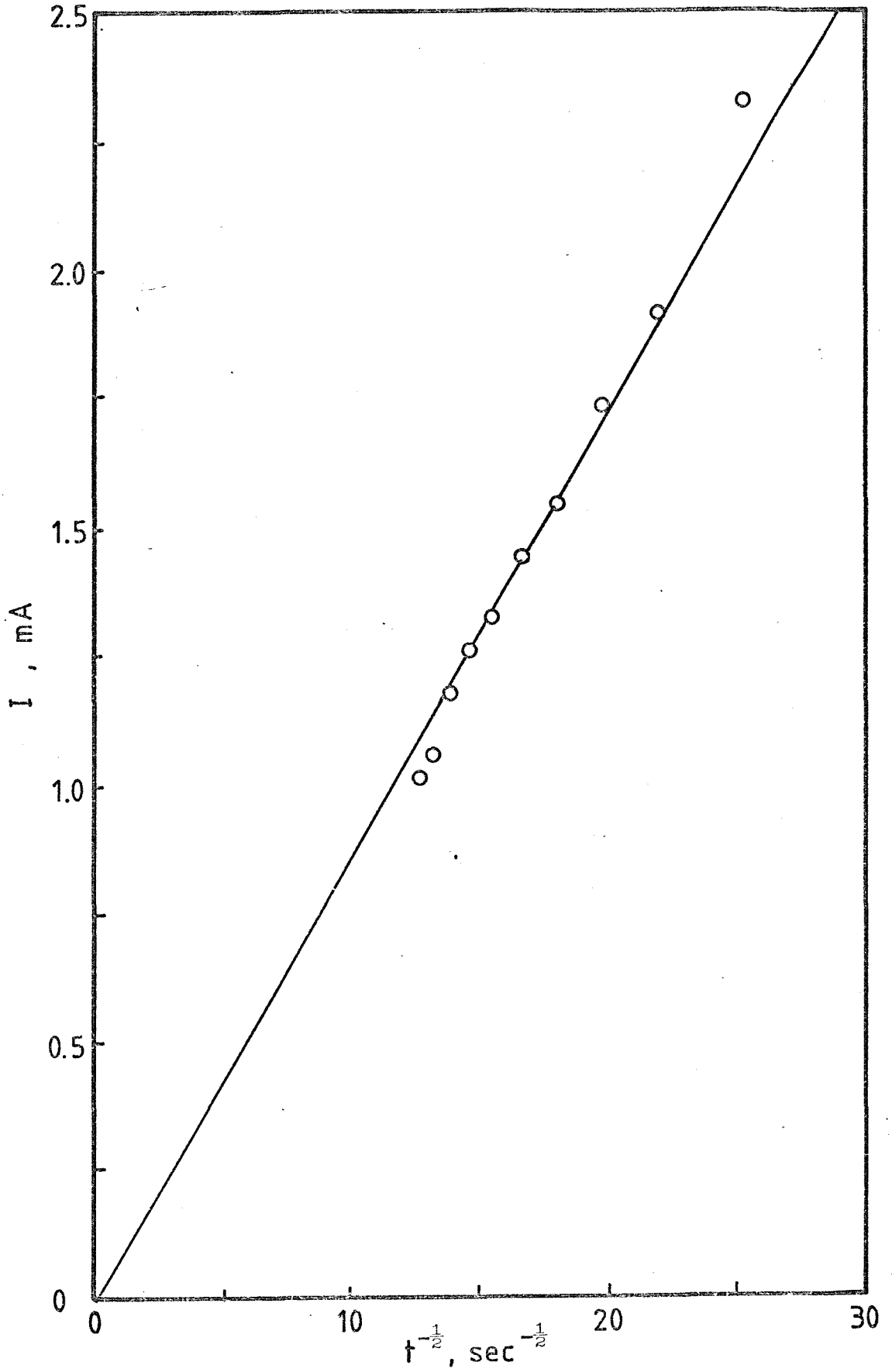

Figure 7.28 I vs $t^{-\frac{1}{2}}$ plot for 22.48 mM $Cd(NO_3)_2$ on platinum in $NaNO_3$-KNO_3 eutectic at 308°C, η = 350 mV. (A = 0.036 cm^2)

A plot of I vs $t^{-\frac{1}{2}}$ predicted by equation (3.5) is shown in Figure 7.23 resulting a straight line passing through the origin. The slope gives the diffusion coefficient value listed in Table 7.1. The D value appears to deviate from that obtained by the linear sweep method.

7.2.2 The system $Cd(NO_3)_2/NaNO_3$-KNO_3 at 308°C

The electrodeposition of cadmium on platinum from alkali molten nitrates is similar in character to that of lead, i.e. appears not to be controlled by nucleation and growth. It was found that the reduction of cadmium was immediately followed by its oxidation by the nitrate solvent. As a consequence, no nucleation reaction takes place.

Voltammograms for the deposition-dissolution of cadmium at low sweep rates show two peaks in the cathodic region (Figure 7.24) and again, the post peak is almost certainly due to the reduction of cadmium oxide. Integration of the area under the cathodic peaks using a digital integrator gave charge values slightly greater than those on the anodic side which is in accord with the intermediate re-oxidation of the metal. On the other hand, the cadmium so deposited may form an alloy with the underlying platinum substrate which would inhibit the dissolution reaction. With increasing scan rate, e.g., higher than 8 V sec^{-1}, the reduction of cadmium oxide becomes competitive with the rate of polarisation and hence the resultant voltammogram shows only one peak (Figure 7.25). The linear dependence of peak height on the scan velocities at various concentrations of cadmium nitrate is shown in Figure 7.26. It is anticipated that at low sweep rates cadmium oxide formation will inhibit the cadmium deposition process giving negative deviations from the I_p vs $v^{\frac{1}{2}}$ plots. However, this effect is not clearly shown. The diffusion coefficient of the cadmium ion was determined from the slope and also included in Table 7.1.

Peak potentials and peak potential separations are shown in Table 7.12 as a function of sweep speeds at different concentrations of cadmium nitrate. It is seen that peak separation potentials are always $> \frac{2.2RT}{nF}$, i.e. far beyond the value for a reversible reaction.

Potentiostatic studies gave rise to usual diffusion controlled falling current-time curves independent of the pulse height (Figure 7.27). The linear plot of I vs $t^{-\frac{1}{2}}$ shown in Figure 7.28 gives the diffusion coefficient value included in Table 7.1.

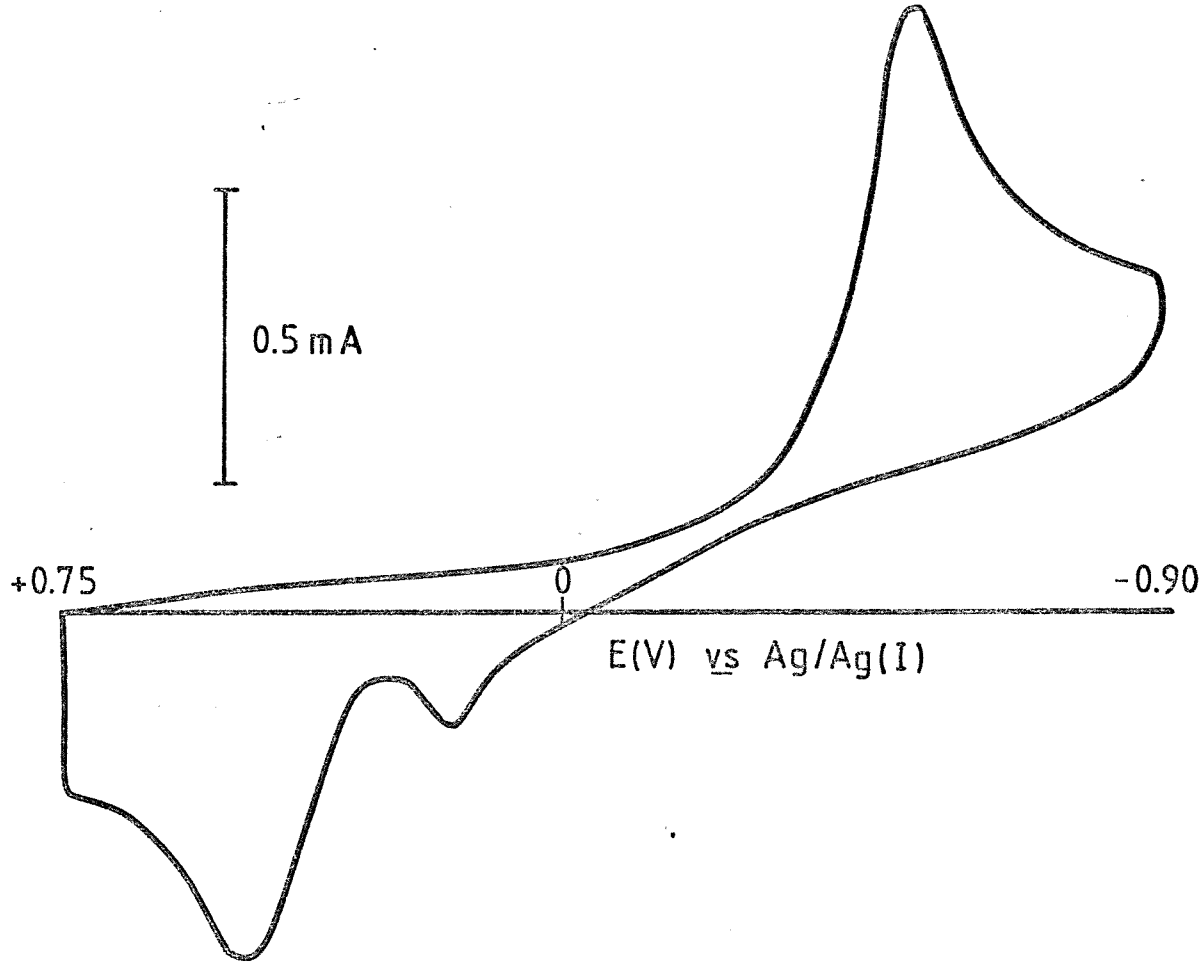

Figure 7.29 Voltammogram for the reduction of 22.49 mM $Co(NO_3)_2$ at platinum in $NaNO_3$-KNO_3 eutectic at 255°C, v = 0.3 V sec^{-1}. (A = 0.157 cm^2)

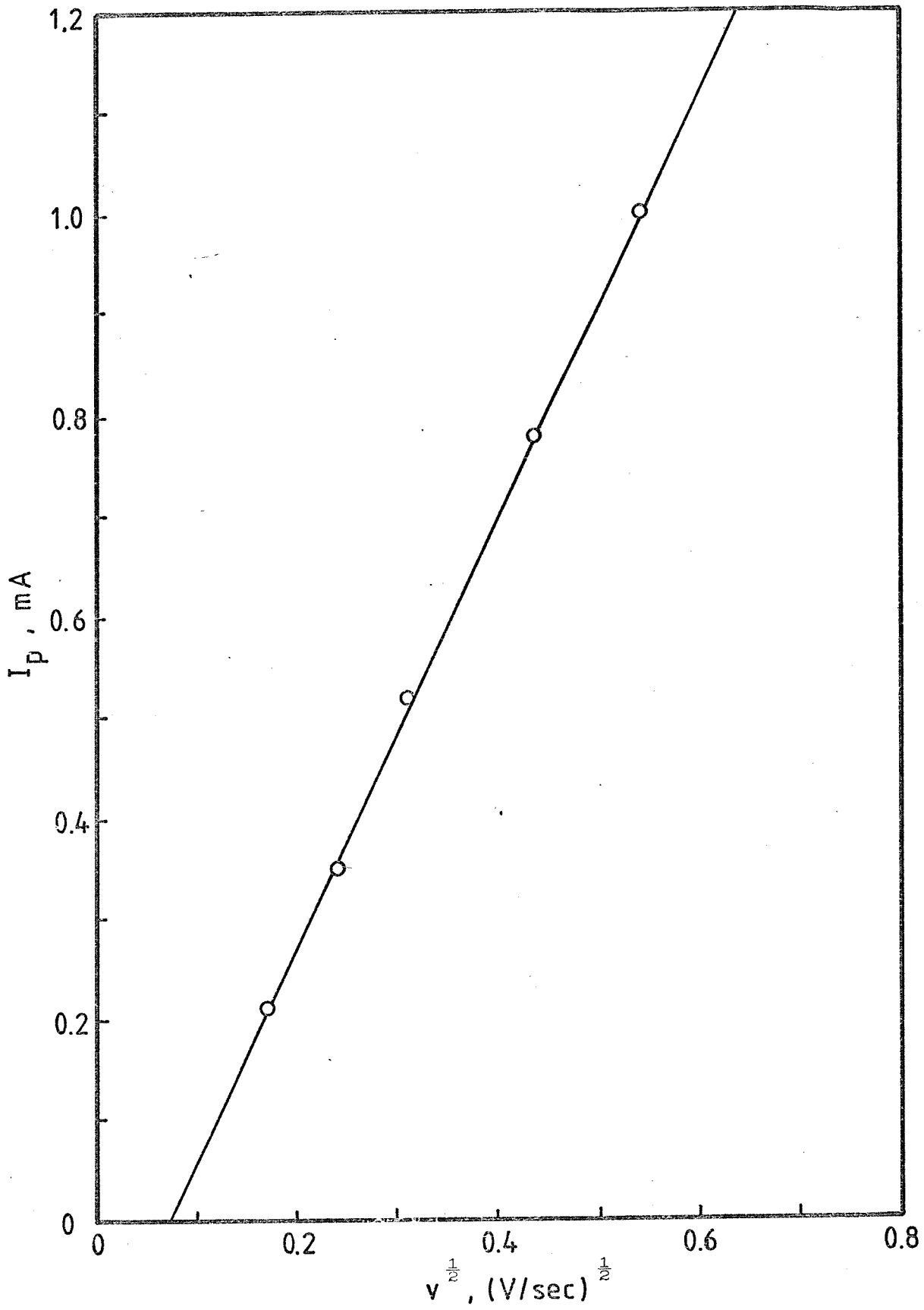

Figure 7.30 Linear plot of I_p vs $v^{\frac{1}{2}}$ for the deposition of 22.49 mM $Co(NO_3)_2$ on platinum in $NaNO_3$-KNO_3 eutectic at 255°C. (A = 0.147 cm^2)

TABLE 7.13 Cyclic voltammetric peak potentials, peak separation potentials over a range of sweep rates for the electrodeposition-dissolution of Co(II) onto platinum at a concentration of 22.49 mM in $NaNO_3$-KNO_3 eutectic at 255°C. (Electrode area = 0.147 cm^2)

$\frac{v}{V/sec}$	$\frac{E_p^c}{mV}$	$\frac{E_p^a}{mV}$	$\frac{\Delta E_p}{mV}$
	E vs Ag/Ag(I)		
0.030	582	481	1063
0.060	462	441	903
0.100	472	441	913
0.200	482	471	953
0.300	482	481	963

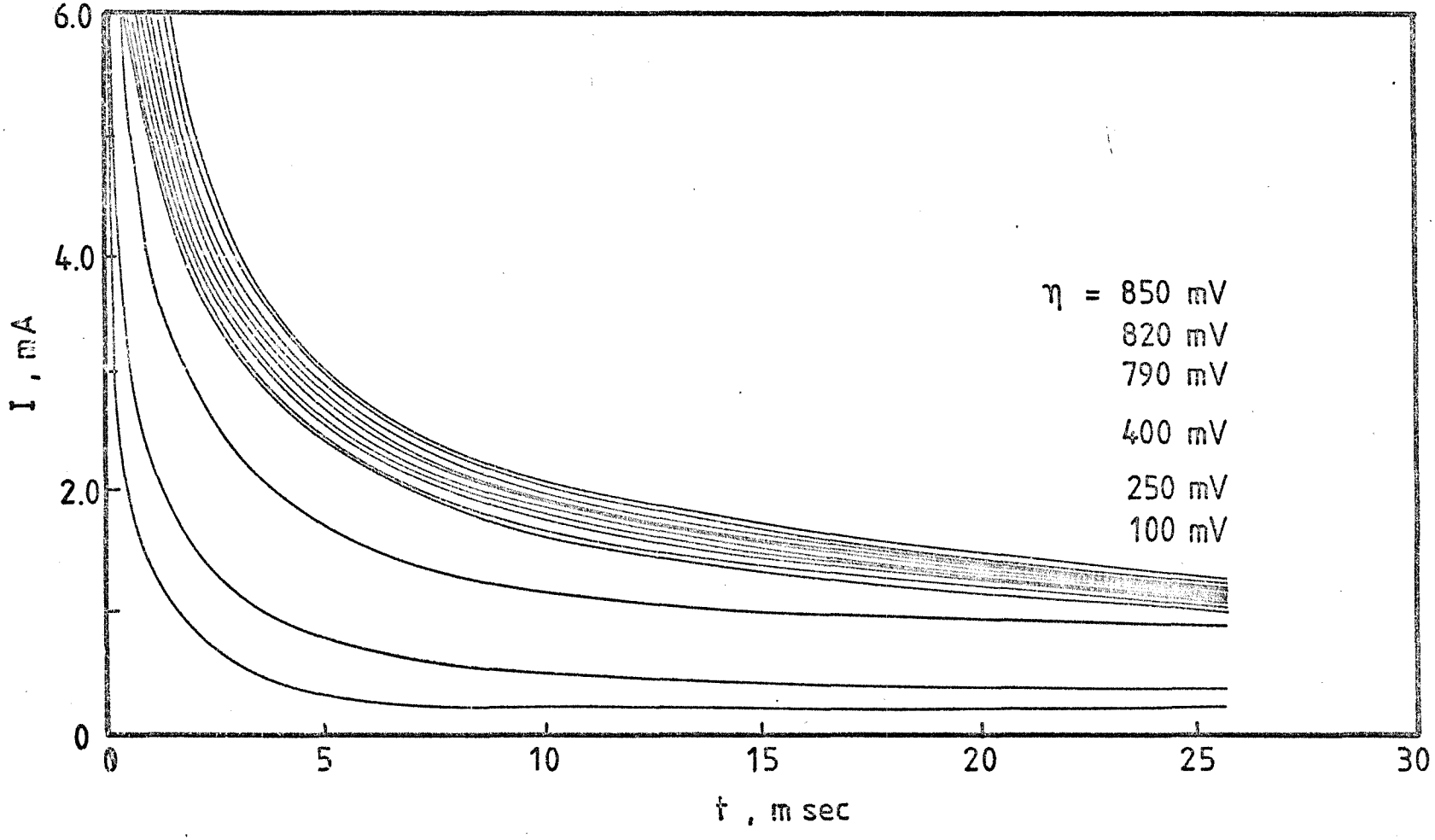

Figure 7.31 I-t transients for the reduction of 22.49 mM $Co(NO_3)_2$ at platinum in $NaNO_3$-KNO_3 eutectic at 255°C at various overpotentials indicated. (A = 0.068 cm^2)

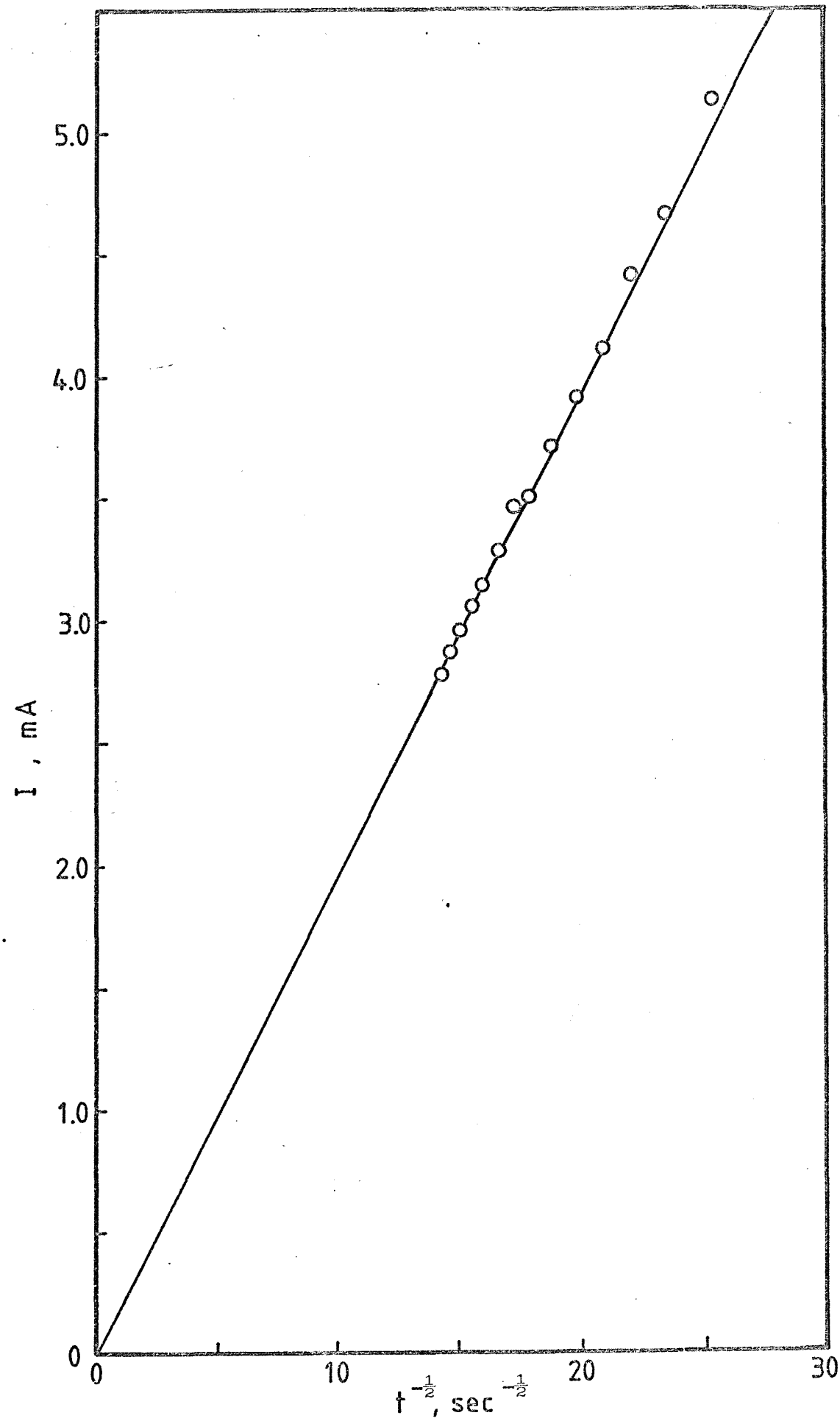

Figure 7.32 I-$t^{-\frac{1}{2}}$ plot for the reduction of 22.49 mM $Co(NO_3)_2$ at platinum in $NaNO_3$-KNO_3 eutectic at 255°C. (A = 0.068 cm^2)

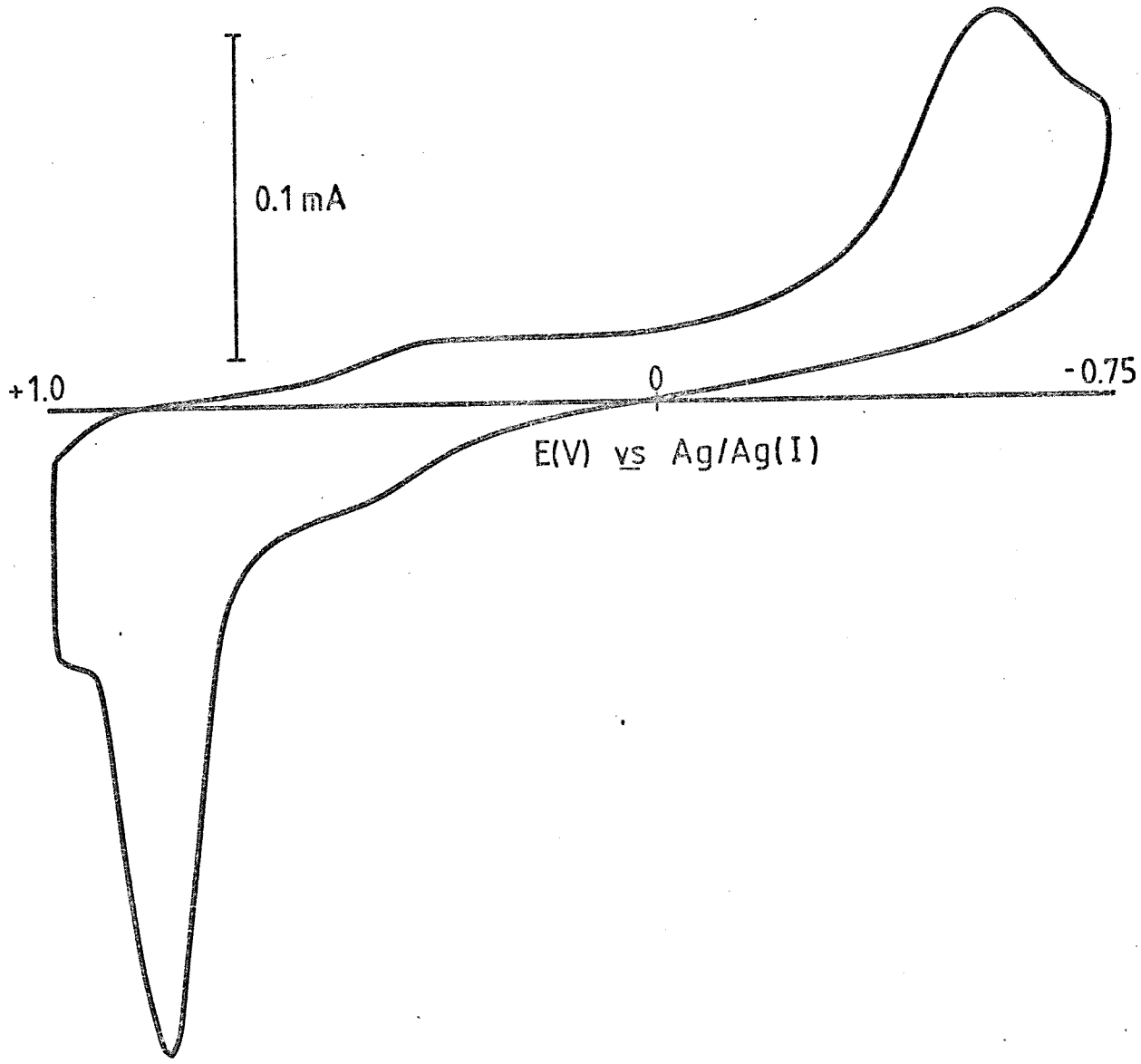

Figure 7.33 Cyclic voltammogram for the reduction of 6.72 mM $Ni(NO_3)_2$ at platinum in $NaNO_3$-KNO_3 eutectic at 255°C, v = 0.3 V sec^{-1}. (A = 0.079 cm^2)

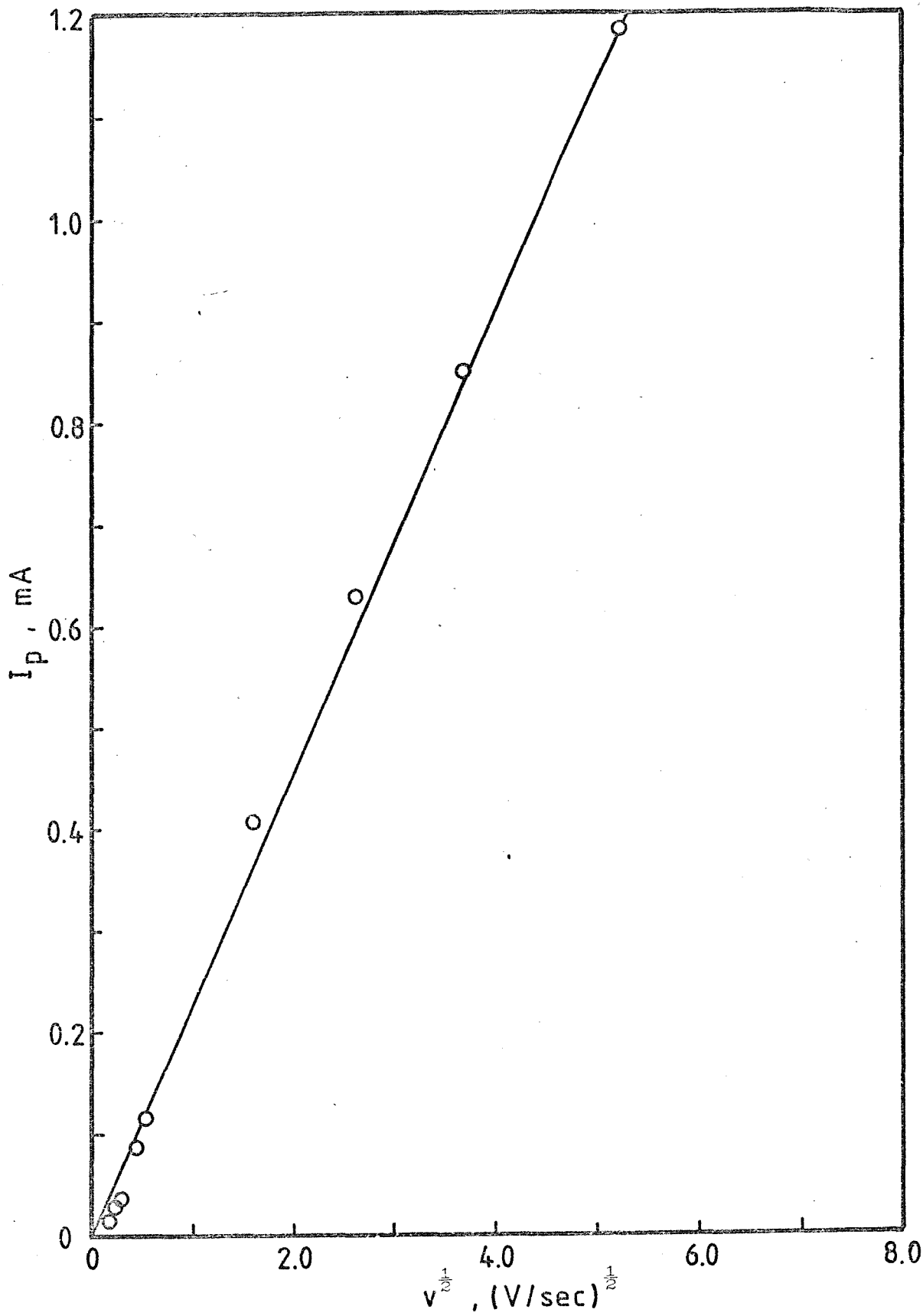

Figure 7.34 I_p vs $v^{\frac{1}{2}}$ plot for the reduction of 6.72 mM $Ni(NO_3)_2$ at platinum in $NaNO_3$-KNO_3 eutectic at 255°C. (A = 0.079 cm^2)

7.2.3 The system $Co(NO_3)_2/NaNO_3$-KNO_3 at 255°C

Cobalt metal reacts very rapidly with the nitrate melt to form a black oxide layer on platinum surface. Evidently, the dissolution of deposited cobalt was incomplete since the charge under the cobalt deposition peak at all sweep rates was much more than required for dissolution. Even though the anodic sweep rate was increased, e.g., thirty-fold faster than the rate of cobalt deposition, the surface of the platinum could not be renewed. Narayan and Inman [43] have, however, employed successfully a rapid current reversal method to strip the cobalt metal from the platinum and its surface remained visually bright for subsequent investigations.

The I/E contour for the system $Co(NO_3)_2/NaNO_3$-KNO_3 at 255°C is shown in Figure 7.29. Result shows a single well-defined deposition peak. Peak currents against $v^{\frac{1}{2}}$ plot gives a straight line but not passing through the origin (Figure 7.30). Instead, it gives a negative intercept which is probably due to change of the surface state of the platinum after each voltammetric scan. Cobalt oxide would inevitably reduce the active area of the bare platinum resulting in peak currents lower than those predicted by the theory. The diffusion coefficient of cobalt ions was determined and is shown in Table 7.1.

Peak potentials and peak separation potentials at each sweep rate are shown in Table 7.13 and found to depart from the reversible value.

Potentiostatic I/t profiles at various pulse heights shown in Figure 7.31 impart no characteristic features of nucleation and growth phenomena. The form of $I/t^{-\frac{1}{2}}$ plot is linear (Figure 7.32) giving the D value listed in Table 7.1.

7.2.4 The system $Ni(NO_3)_2/NaNO_3$-KNO_3 at 255°C

According to Narayan and Inman[43], nickel metal reacts with $NaNO_3$-KNO_3 less rapidly than cobalt. By conventional chronopotentiometry, the satisfactory reproducible transition times in each investigation may be obtained. The present voltammetric studies were, however, complicated by a black oxide film of nickel. Apparently nickel oxide could not readily be removed when the linear sweep method was employed, particularly at low sweep rates (Figure 7.33). This effect invariably reflects a negative departure from linearity of $I_p/v^{\frac{1}{2}}$ plot as shown in Figure 7.34.

TABLE 7.14 Cyclic voltammetric peak potentials, peak separation potentials over a range of sweep rates for the electrodeposition-dissolution of Ni(II) onto platinum at a concentration of 6.72 mM in $NaNO_3$-KNO_3 eutectic at 255°C. (Electrode area = 0.079 cm^2)

$\frac{v}{V/sec}$	$\frac{E^c_p}{mV}$	$\frac{E^a_p}{mV}$	$\frac{\Delta E_p}{mV}$
	E vs Ag/Ag(I)		
0.030	451	801	1252
0.60	501	811	1312
0.100	511	811	1322
0.200	541	840	1381
0.300	551	830	1381
2.77	575	860	1435
7.07	575		
13.86	610		
27.75	627		

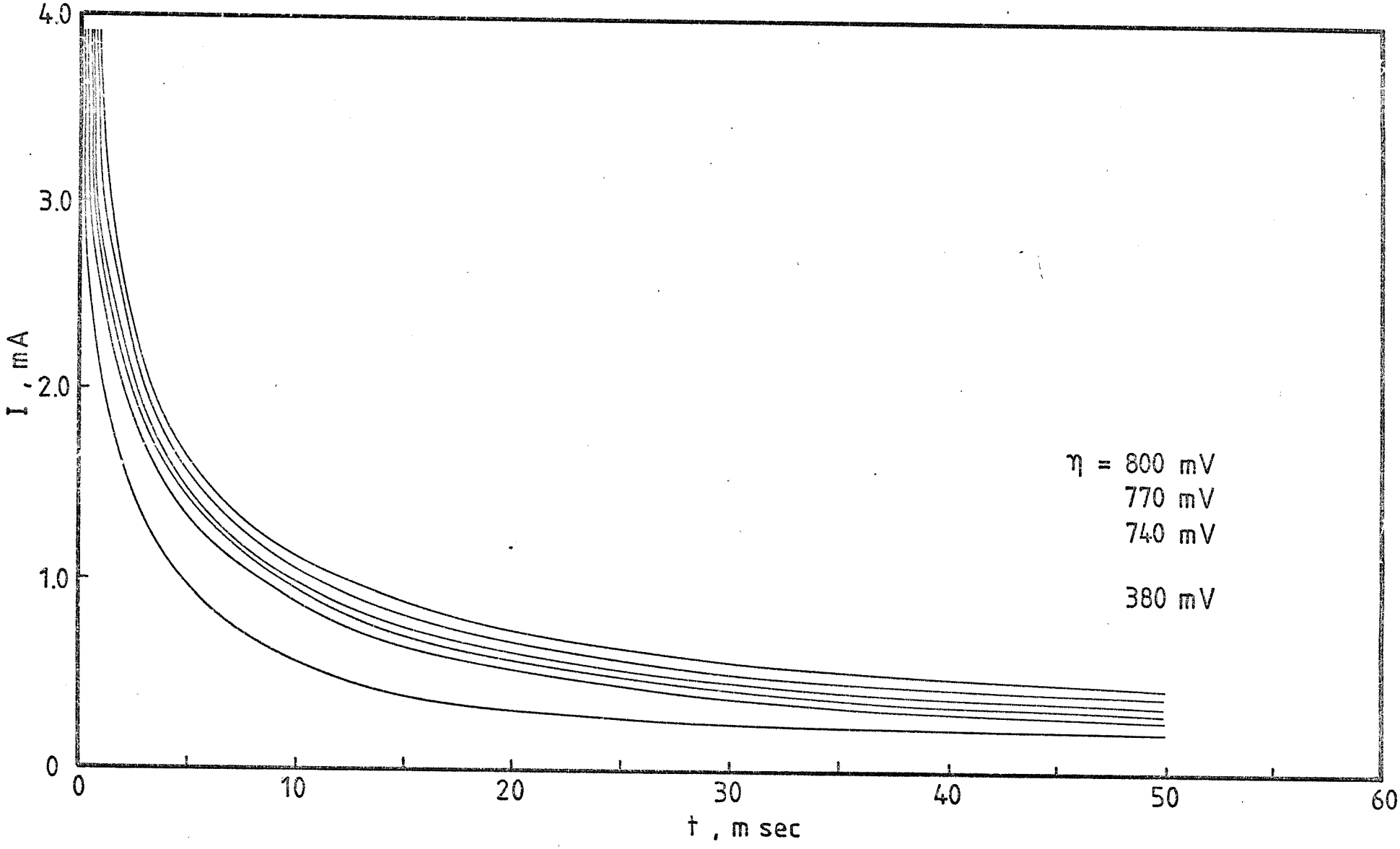

Figure 7.35 Potentiostatic transients for the deposition of 6.72 mM $Ni(NO_3)_2$ on platinum in $NaNO_3$-KNO_3 eutectic at 255°C at the overpotentials indicated. (A = 0.079 cm^2)

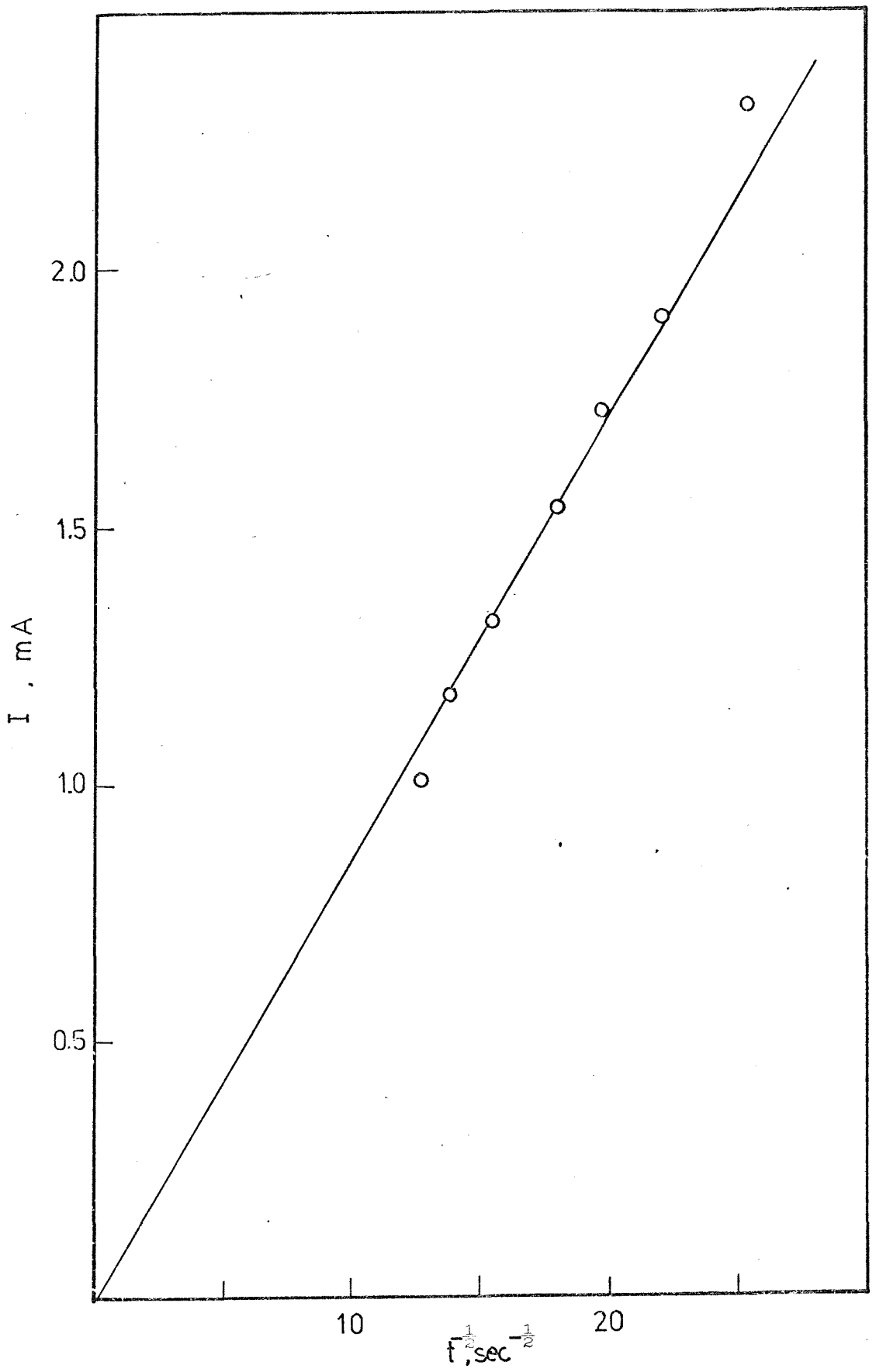

Figure 7.36 $I\text{-}t^{-\frac{1}{2}}$ relation for the reduction of 6.72 mM $Ni(NO_3)_2$ on platinum in $NaNO_3$-KNO_3 eutectic at 255°C at η = 590 mV. (A = 0.079 cm^2)

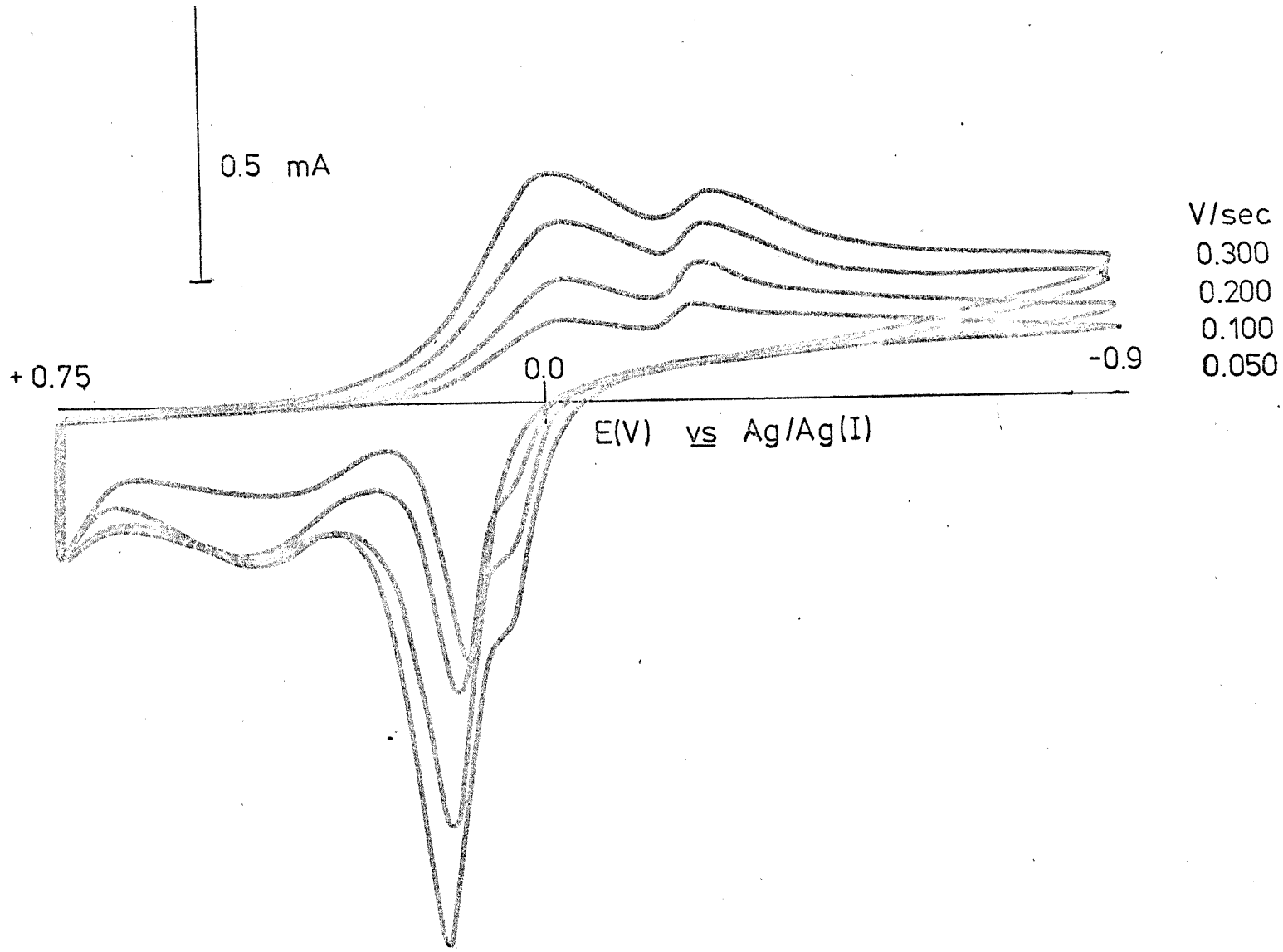

Figure 7.37 Voltammogram for the reduction of 18.17 mM $Cu(NO_3)_2$ at platinum in $NaNO_3$-KNO_3 eutectic at 250°C. (A = 0.156 cm^2)

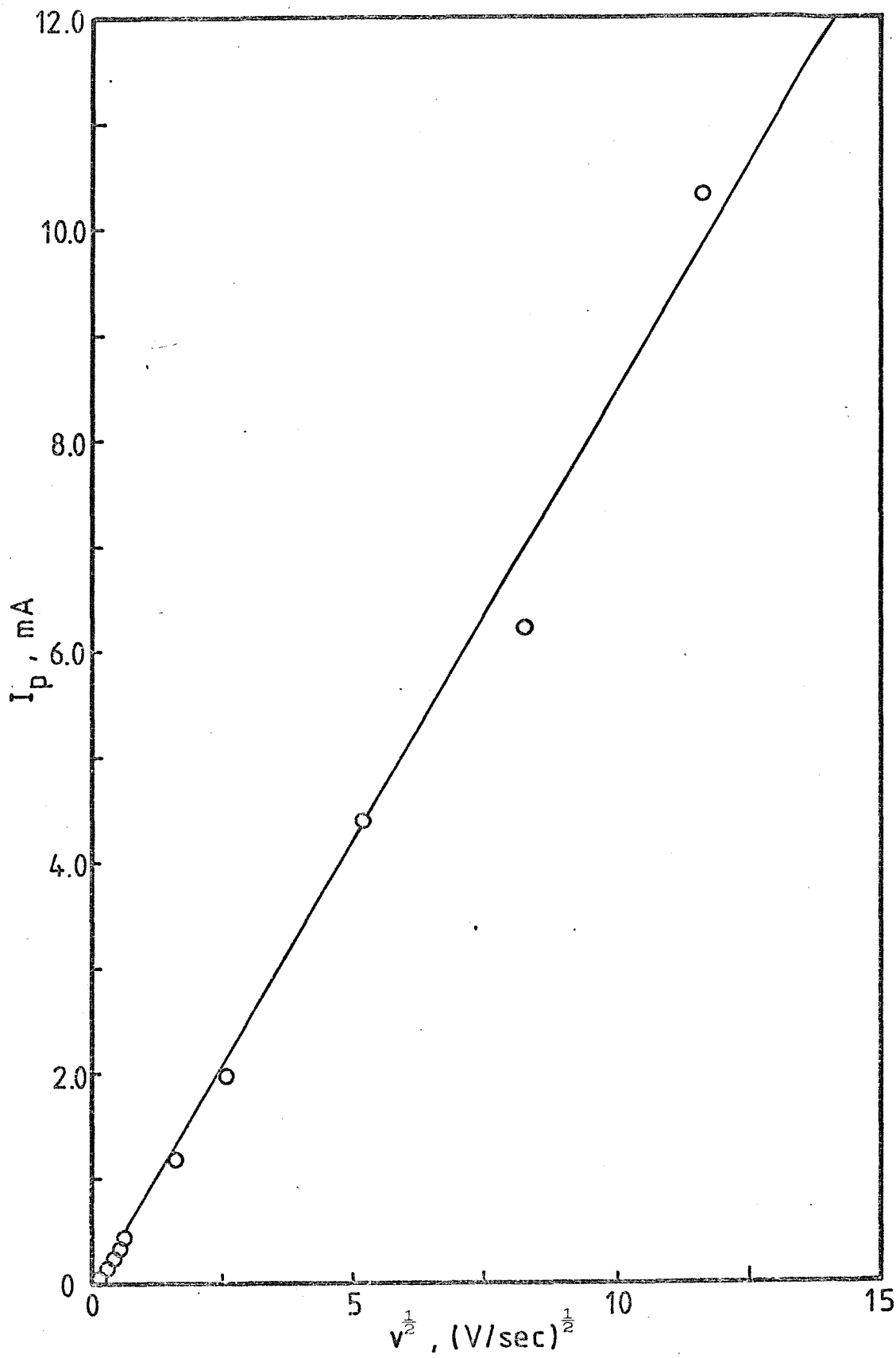

Figure 7.38 Linear relationship of I_p vs $v^{\frac{1}{2}}$ for the reduction of 18.17 mM $Cu(NO_3)_2$ at platinum in $NaNO_3$-KNO_3 eutectic at 250°C. (A = 0.156 cm^2)

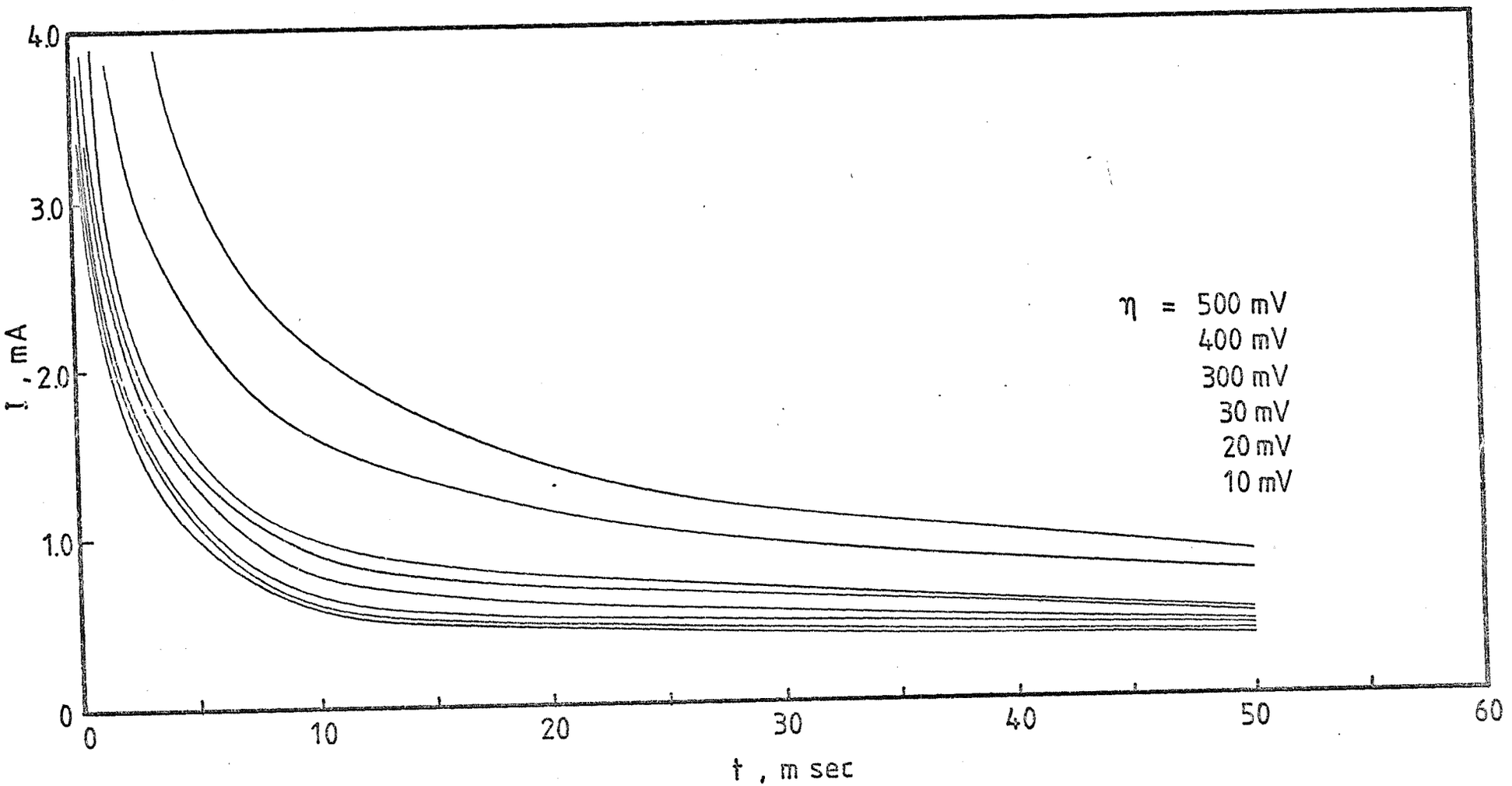

Figure 7.39 I-t transients for the deposition of 18.17 mM $Cu(NO_3)_2$ on platinum in $NaNO_3$-KNO_3 eutectic at 250°C at overpotentials indicated. (A = 0.156 cm^2)

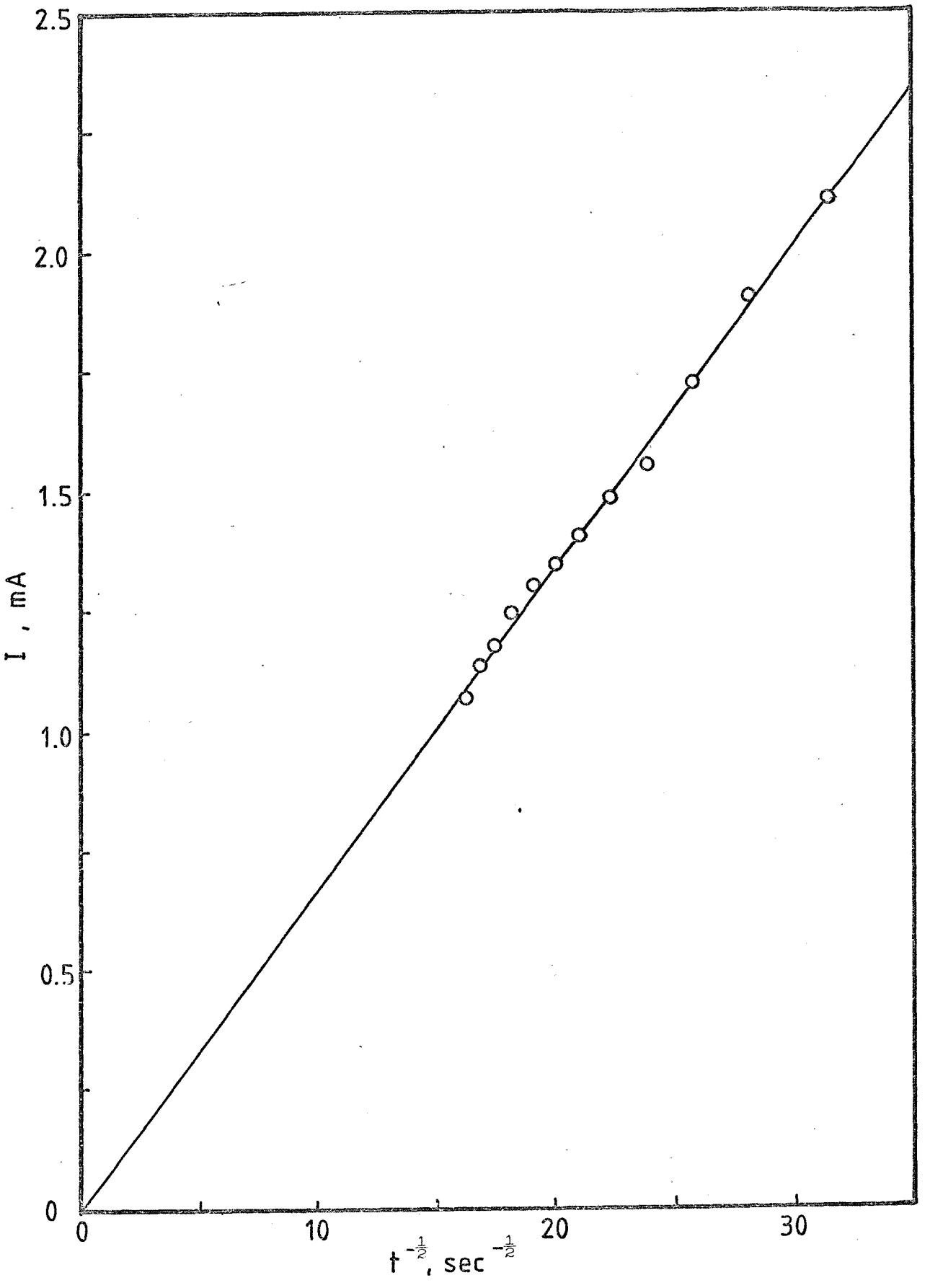

Figure 7.40 I-$t^{-\frac{1}{2}}$ plot for the deposition of 18.17 mM $Cu(NO_3)_2$ on platinum in $NaNO_3$-KNO_3 eutectic at 250°C at η = 50 mV. (A = 0.156 cm^2)

Increasing the rate of potential change, the surface oxide effect becomes less pronounced and normal linear dependence of $I_p/v^{\frac{1}{2}}$ is obeyed. The calculated diffusion coefficient is shown in Table 7.1.

Peak potentials and peak separation potentials at different scan rates are shown in Table 7.14. The data obtained are seen to deviate from reversible electrode process.

Potential step experiment reveals no evidence of new phase generation (Figure 7.35). I *vs* $t^{-\frac{1}{2}}$ plot takes the usual linear form (Figure 7.36) and the D value was computed from its slope.

7.2.5 The system $Cu(NO_3)_2/NaNO_3$-KNO_3 at 250°C

Studies of the discharge of copper (II) ions onto platinum from aqueous solutions clearly exhibits a nucleation reaction which precedes the copper deposition and a following growth process controlled by hemispherical diffusion of the copper ions. In molten nitrates, however, the electrode process behaves in a different manner. The other metal deposition processes in fused nitrates already discussed have suffered from the chemical complication of the nitrate solvent and no evidence of the new phase formation is shown. Again, with the present system the active role of nitrate melt as a reaction media is well-confirmed.

Copper metal reacts with nitrate melt to form oxides. A voltammogram for the reduction of Cu(II) ions at various sweep rates are shown in Figures 7.37 with two peaks on the cathodic region. A linear dependence of the first current peak heights *vs* the square root of the sweep rate is observed (Figure 7.38). The slope of the line leads to a diffusion coefficient of 0.15×10^{-6} cm^2 sec^{-1}.

Potentiostatic current decays with time at different magnitude of overpotential (Figure 7.39). I *vs* $t^{-\frac{1}{2}}$ plot (Figure 7.40) leads the D value of 0.05×10^{-6} cm^2 sec^{-1}.

Both values of the diffusion coefficient are too low to be acceptable and it is likely that all of these metal deposition reactions, other than that of silver, are complicated and therefore spoiled by the secondary chemical oxidation by the nitrate melt.

8. VOLTAMMETRIC STUDIES IN CHLORIDE MELTS

8.1 Electrochemical nucleation of copper onto a vitreous carbon in the molten LiCl-KCl eutectic at 438°C

8.2 Electrochemical nucleation of cobalt onto a vitreous carbon in the molten LiCl-KCl eutectic at 467°C

8.3 Electrodeposition of silver onto platinum, vitreous carbon, tungsten, copper and nickel in the molten LiCl-KCl eutectic at ~ 450°C

8.3.1 The system $AgNO_3$/Pt in the LiCl-KCl eutectic at 400°C

8.3.2 The system $AgNO_3$/vitreous carbon in the LiCl-KCl eutectic at 400°C

8.3.3 The system $AgNO_3$/tungsten in the LiCl-KCl eutectic at 400°C

8.3.4 The system $AgNO_3$/Cu and Ni in the LiCl-KCl eutectic at 450°C

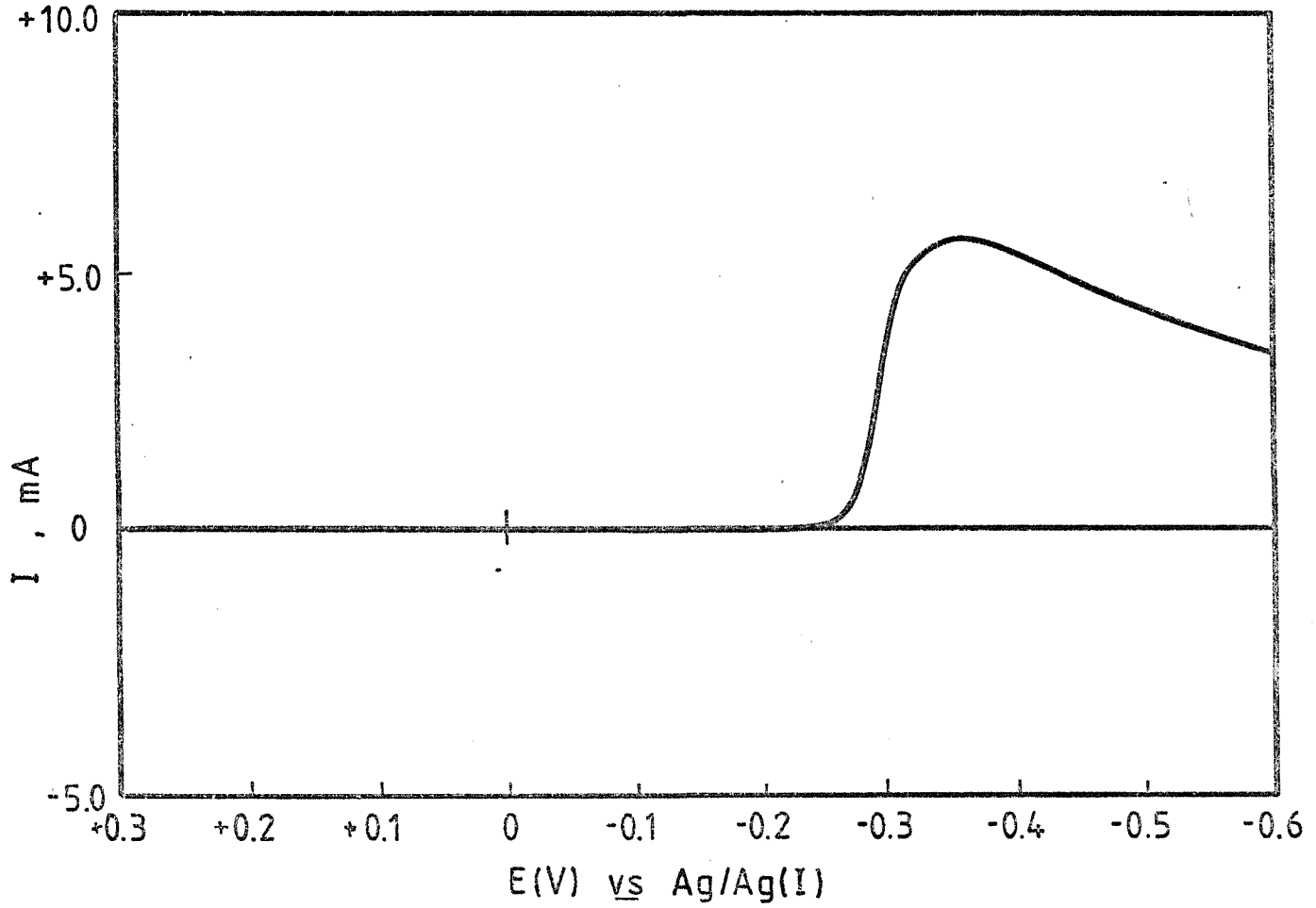

Figure 8.1 A linear sweep voltammogram for the reduction of 48.23 mM Cu(I) on vitreous carbon in LiCl-KCl eutectic at 438°C, v = 0.3 V sec^{-1}. (A = 0.312 cm^2)

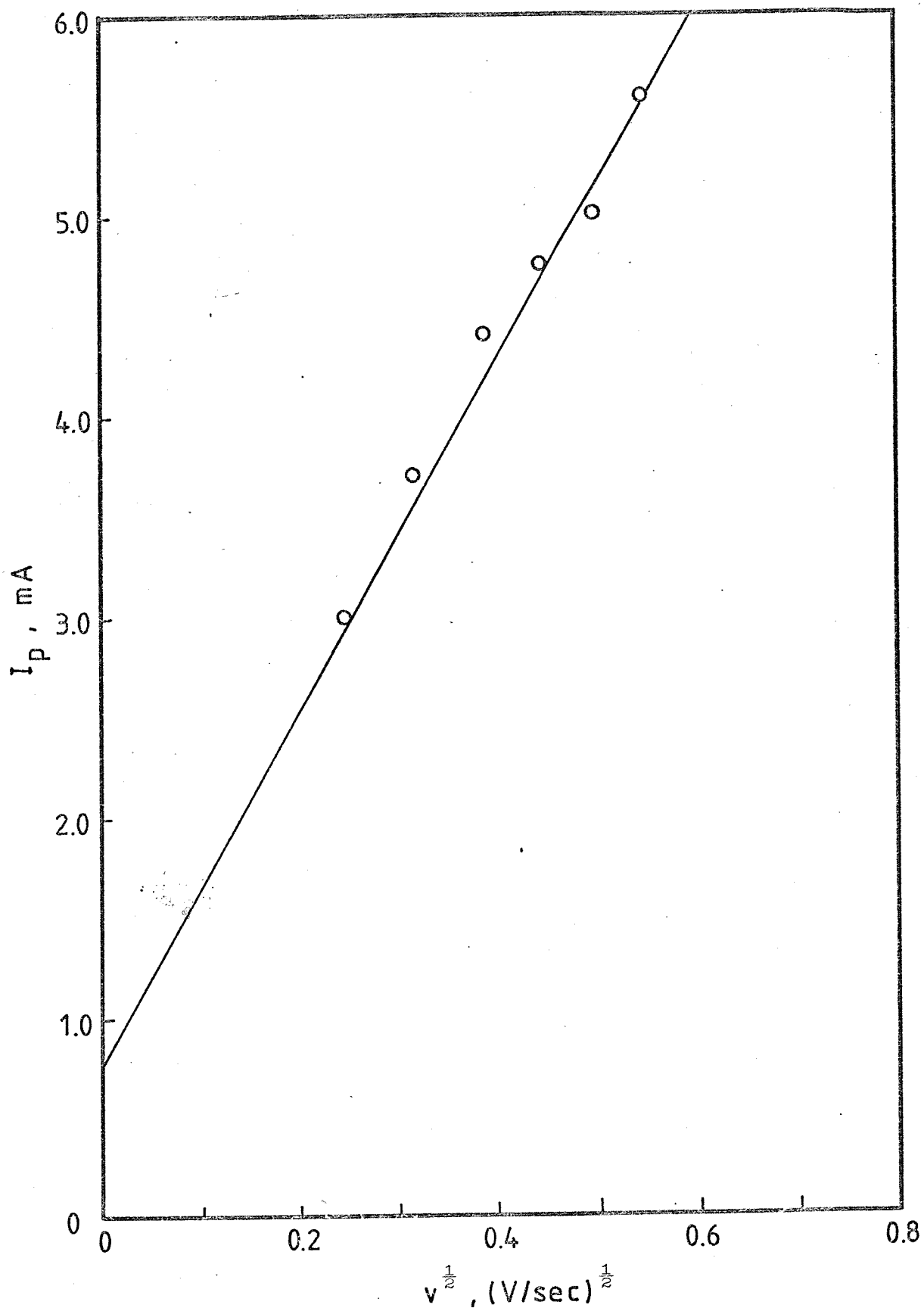

Figure 8.2 I_p vs $v^{\frac{1}{2}}$ plot for the reduction of 48.23 mM Cu(I) on vitreous carbon in LiCl-KCl eutectic at 438°C. (A = 0.312 cm^2)

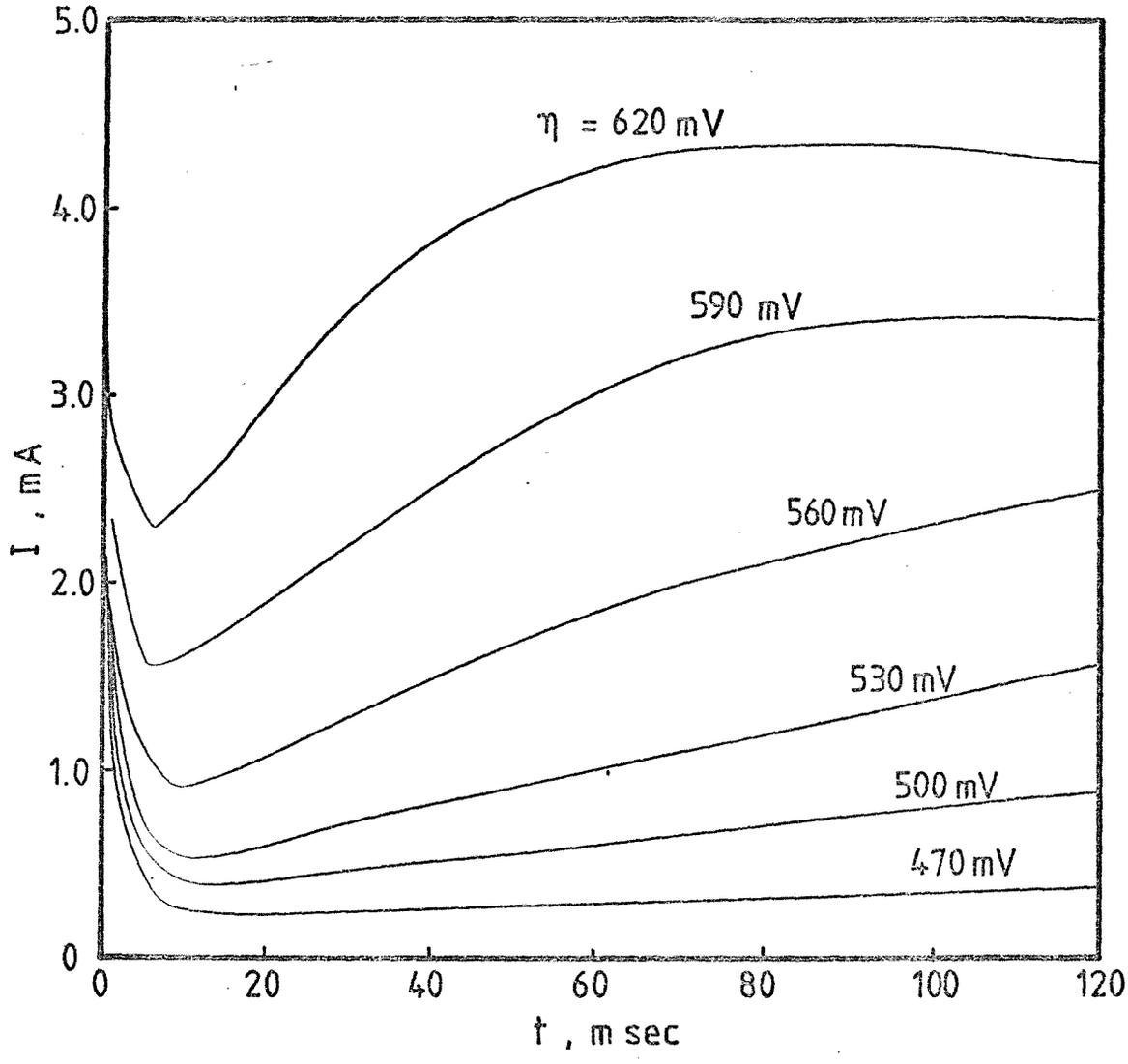

Figure 8.3 Potentiostatic current-time transients for the deposition of copper from 48.23 mM Cu(I) onto vitreous carbon in LiCl-KCl eutectic at 438°C at the applied overpotentials indicated. ($A = 0.312\ cm^2$)

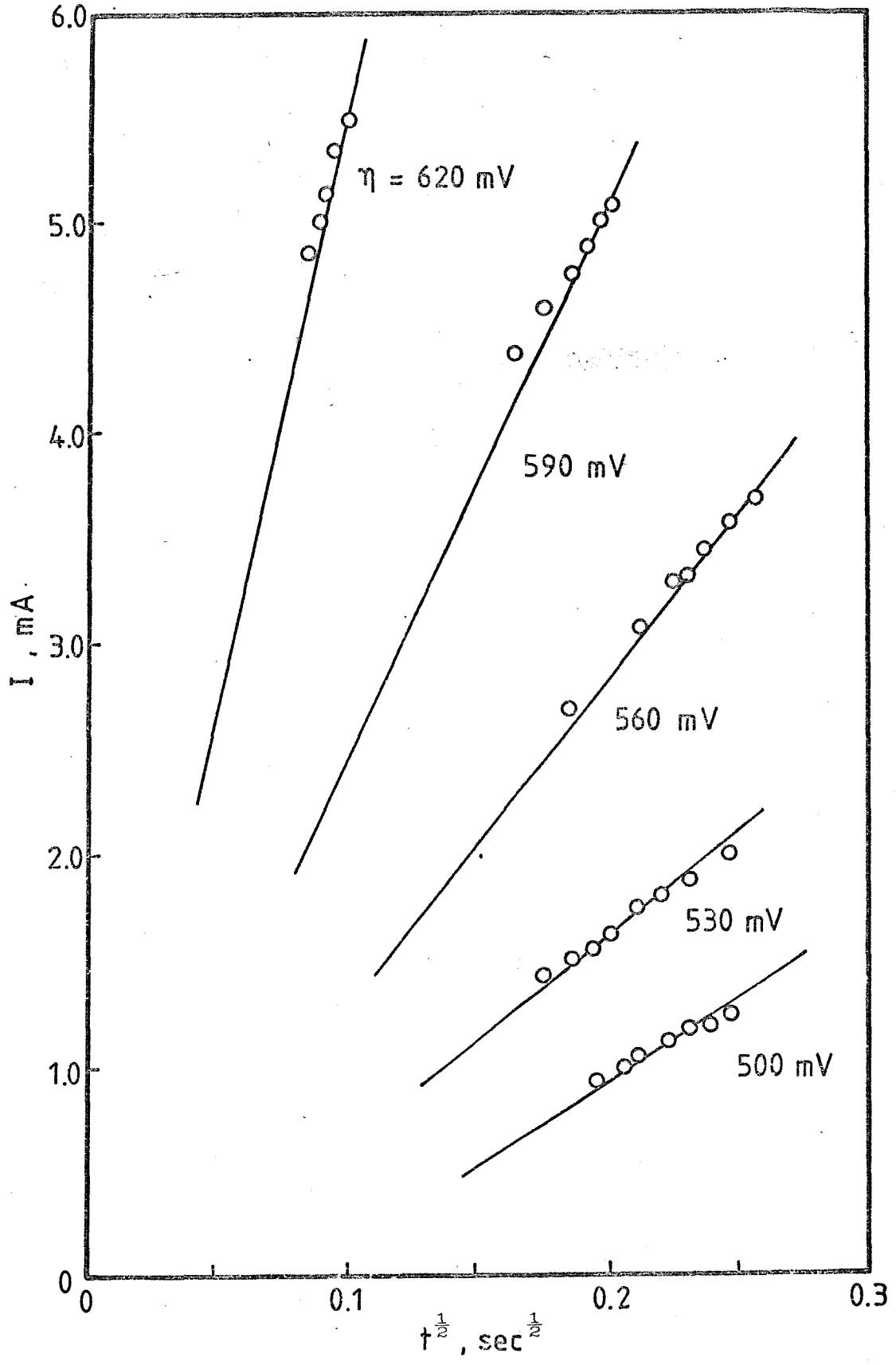

Figure 8.4 I-$t^{\frac{1}{2}}$ relation for the deposition of Cu(I) on vitreous carbon. (Data from Figure 8.3)

TABLE 8.1 Diffusion coefficients of various metal ions in LiCl-KCl eutectic at 400°-467°C.

electroactive species	$\frac{t}{°C}$	$\frac{10^6 c}{mol/cm^3}$	$10^5 D/cm^2\ sec^{-1}$ cyclic voltammetry	potential step	previous values
Ag(I)/vitreous carbon	400	27.95	2.18	2.5	2.6(450°C)(50)
		23.96	2.06		3.3(450°C)(120)
					4.6(480°C)(21)
Ag/Pt(wire)	400	27.95	2.16	2.62	5.1(450°C)(107)
(sphere)		27.95	2.33		
Ag/W	400	27.95	0.13	1.7	
Cu(I)/vitreous carbon	438	48.23	2.24	1.68	2.78(461°C)(58)
Co(II)/vitreous carbon	467	9.81	1.25	0.73	4.39(450°C)(107)
					2.42(450°C)(50)
Co(II)/Pt	467	9.81	-	1.31	

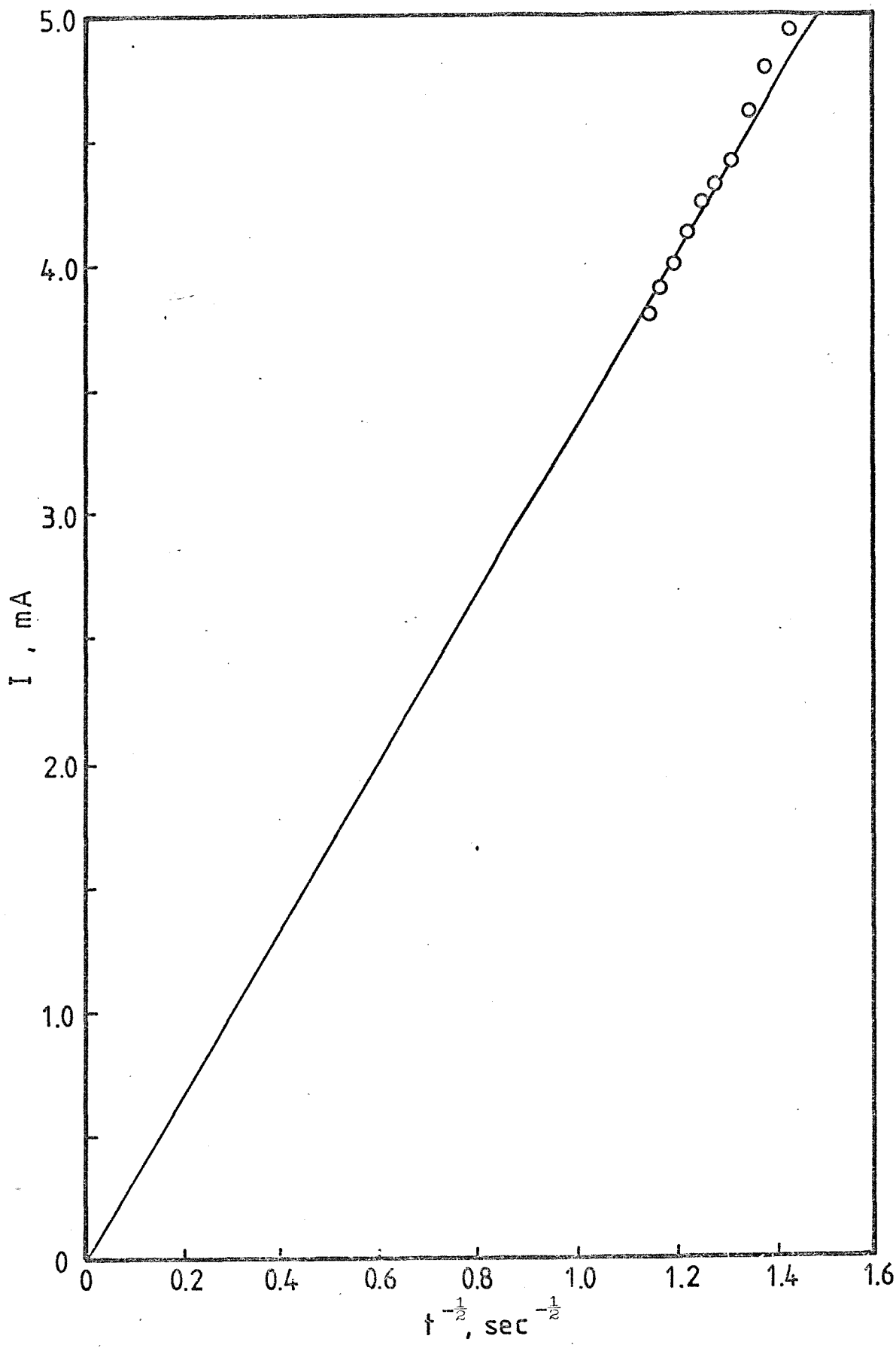

Figure 8.5 $I\text{-}t^{-\frac{1}{2}}$ plot for the reduction of 48.23 mM Cu(II) at vitreous carbon in LiCl-KCl eutectic at 438°C at η = 620 mV. (A = 0.312 cm^2)

TABLE 8.2 Nuclear densities of copper on a vitreous carbon electrode in molten LiCl-KCl eutectic at 438°C. (Electrode area = 0.312 cm^2)

	c = 48.23 mM	
η/mV	$\frac{10^3 dI/dt^{\frac{1}{2}}}{A/sec^{\frac{1}{2}}}$	$10^{-5} N_o$
500	8.17	1.71
530	10.0	2.10
560	16.0	3.36
590	27.0	5.67
620	57.0	11.9

8.1 Electrochemical nucleation of copper onto a vitreous carbon in the molten LiCl-KCl eutectic at 438°C

A wide range of investigations of metal deposition from chloride melts on various electrode materials has been reported[17,21]. In the main, these studies were concerned with the determination of ionic transport properties as was the case for nitrate melts. There have been, however, some recent studies more concerned with the early stages of the metal deposition[54], i.e. the underpotential deposition, but no studies have been reported on overpotential deposition, i.e. on nucleation kinetics. It was therefore considered interesting and challenging to survey the mechanism of metal depositions of this type in molten chlorides. To this end we bagan with voltammetric studies of the electrodeposition of cuprous ions onto a vitreous carbon electrode in the molten LiCl-KCl eutectic at 438°C.

Linear potential sweep and pulse measurements were used to study the cathodic reactions in solutions of Cu(I), 48.29 mM in LiCl-KCl melt, generated by coulometric anodic dissolution of pure coppermetal *in situ*. All potential measurements were made against the Ag/Ag(I) reference electrode in the same solvent.

A voltammogram for the reduction of Cu(I) on vitreous carbon is shown in Figure 8.1. At each scan rate a single, well-defined deposition peak was observed, the peak height and sweep rate being related as theoretically predicted by equation (3.14), although the line does not pass through the origin (Figure 8.2). The slope of the line leads to the diffusion coefficient of cuprous ions in the chloride melt of $2.24 \times 10^{-5} cm^2\ sec^{-1}$ given in Table 8.1.

The positive intercept on the current axis of Figure 8.1 indicates that the electrode process is not entirely straightforward and evidence that once again a nucleation overpotential is involved, may be seen in Figure 8.3 which shows a family of potentiostatic rising current-time transients over a range of applied overpotentials. Evidently also the formation of the new phase requires a high degree of supersaturation and the η values are > 500 mV *vs* Ag/Ag(I). The middle part of the I/t profile gives a linear $I/t^{\frac{1}{2}}$ plot as is shown in Figure 8.4. Its slope $dI/dt^{\frac{1}{2}}$ leads, via equation (4.52), to the number nuclear densities shown in Table 8.2.

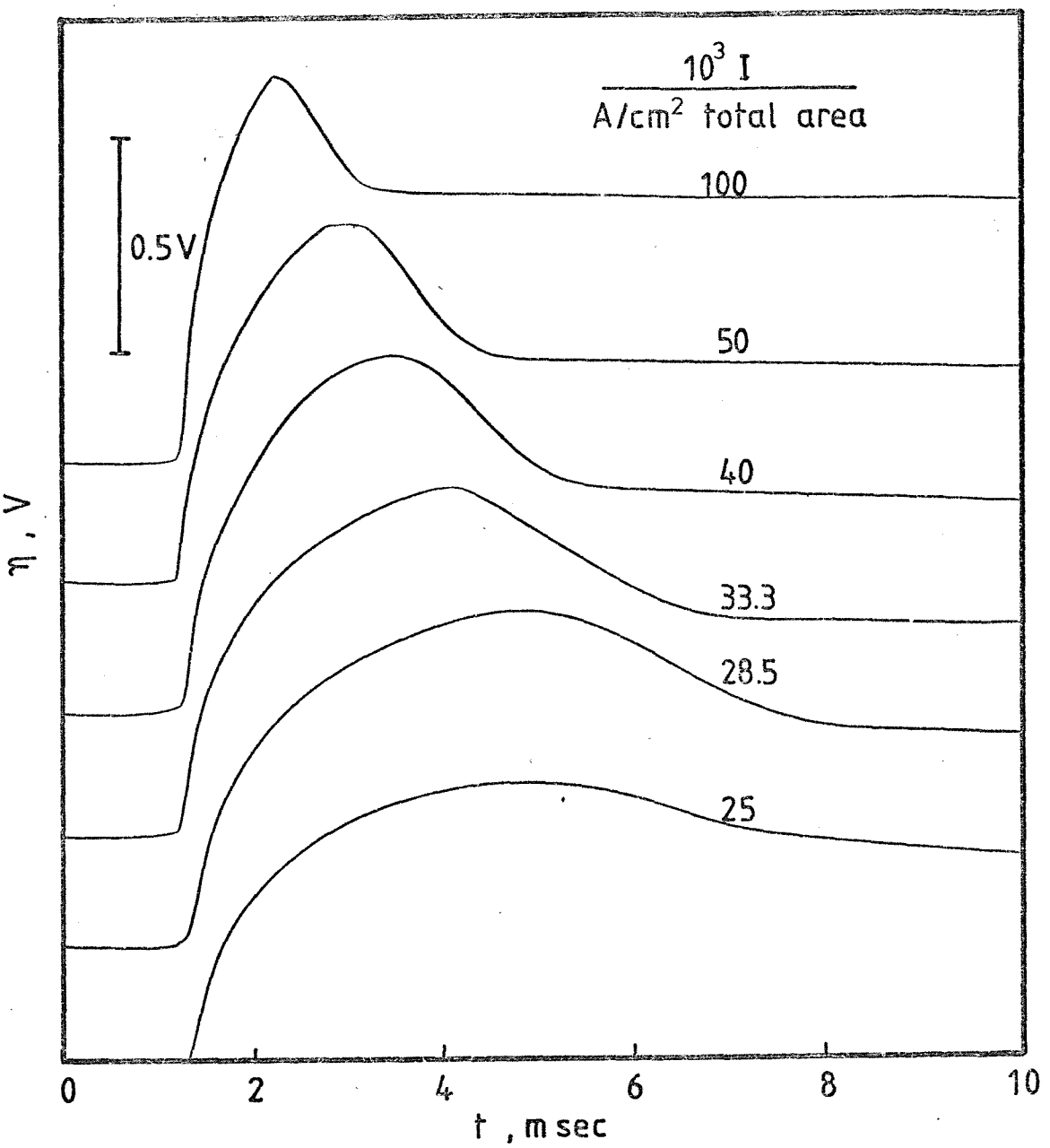

Figure 8.6 Galvanostatic potential-time transients for the deposition of copper from 48.23 mM Cu(I) on vitreous carbon at the constant currents indicated. (A = 0.312 cm^2)

At a high pulse potential, the resulting current follows the normal falling transient associated with linear diffusion and the $I/t^{-\frac{1}{2}}$ plot takes the linear form (Figure 8.5) passing through the origin. The slope of the line leads to the diffusion coefficient of $1.68 \times 10^{-5} cm^2\ sec^{-1}$.

Well-pronounced galvanostatic potential maxima at various applied current densities were also observed as is shown in Figure 8.6. Increasing the constant current densities results in an increase of the potential maximum and a corresponding decrease of the time scale from the beginning of the current pulse to the maximum. The results are in good agreement with those obtained by Lantelme[58] in the same system. It may be thought that the potential at maximum could be used as the basis for the determination of charge transfer rate constant of the bulk copper $\rightleftharpoons$ cuprous ions reaction. However, since the enforced nucleation overpotential at the maximum is even higher than the applied overpotential which gives rise to potentiostatic rising current time transients, a separate potentiostatic evaluation of nuclear density at the galvanostatic maximum is not possible. It is possible that the large constant current pulse required for nucleation and growth processes of copper is partly associated with the large background current of the chloride melt. On the other hand, the vitreous carbon surface may be sensitive to impurities in molten chlorides although the electrode is usually stabilized at a certain anodic potential. Any such effects are likely to have influence on the early stages of the metal deposition and hence on the resulting potential-time transients.

The copper deposition process is, at any rate, seen to be preceded by 3D instantaneous nucleation reaction and growth controlled by hemispherical diffusion of cuprous ions in chloride melt. The whole process is not affected by solvent intervention and is unlikely to be influenced by surface complications due, for example, to oxide formation.

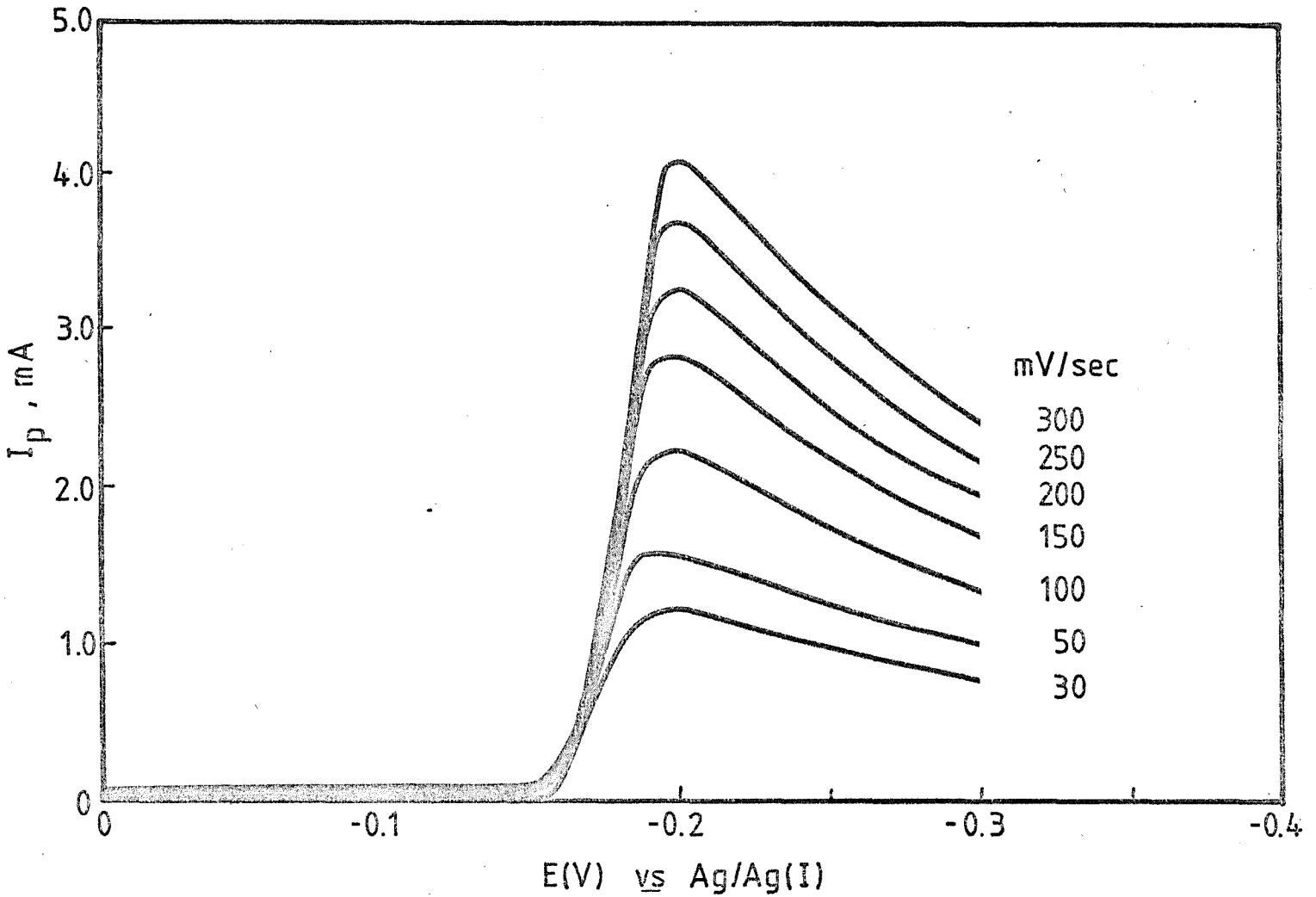

Figure 8.7 Linear sweep voltammogram for the reduction of 9.81 mM $CoCl_2$ on vitreous carbon in LiCl-KCl eutectic, 467°C at the sweep rates indicated. (A = 0.312 cm^2)

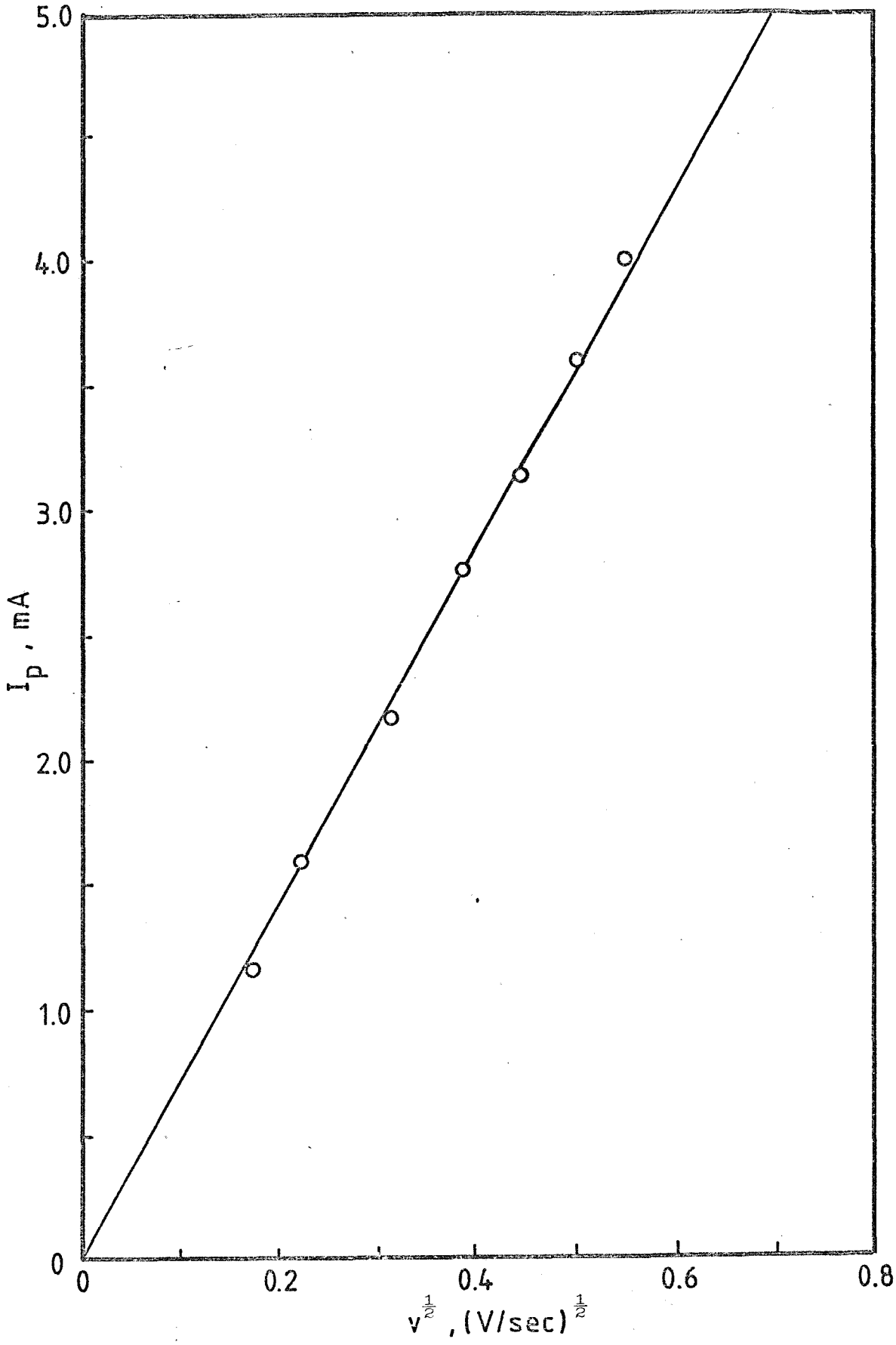

Figure 8.8 Linear plot of I_p vs $v^{\frac{1}{2}}$ for the reduction of 9.81 mM $CoCl_2$ at vitreous carbon in LiCl-KCl eutectic at 467°C. (A = 0.312 cm^2)

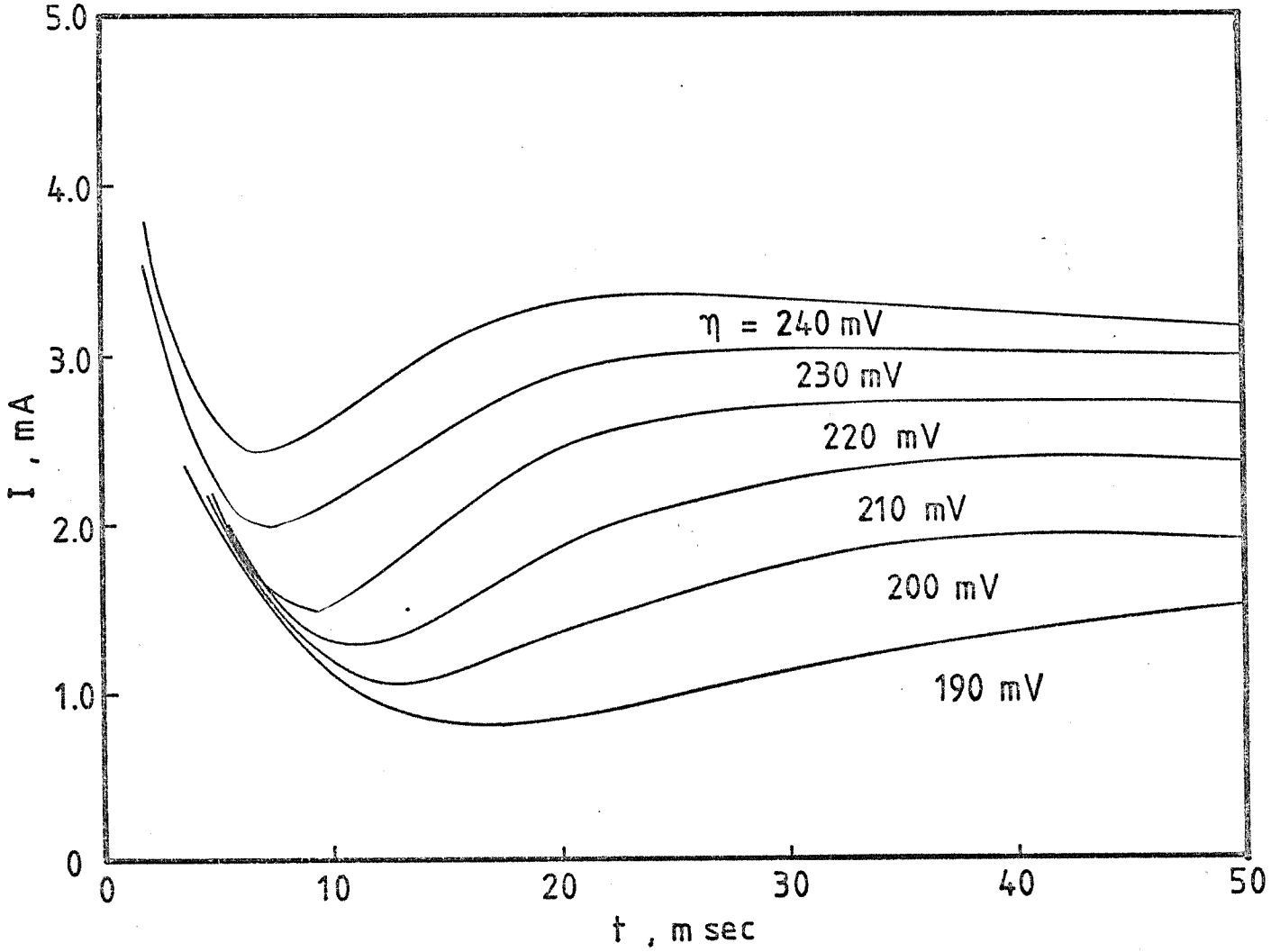

Figure 8.9 Potentiostatic current-time transients for the deposition of cobalt from 9.81 mM $CoCl_2$ on vitreous carbon in LiCl-KCl eutectic at 467°C at the applied overpotentials indicated. (A = 0.312 cm^2)

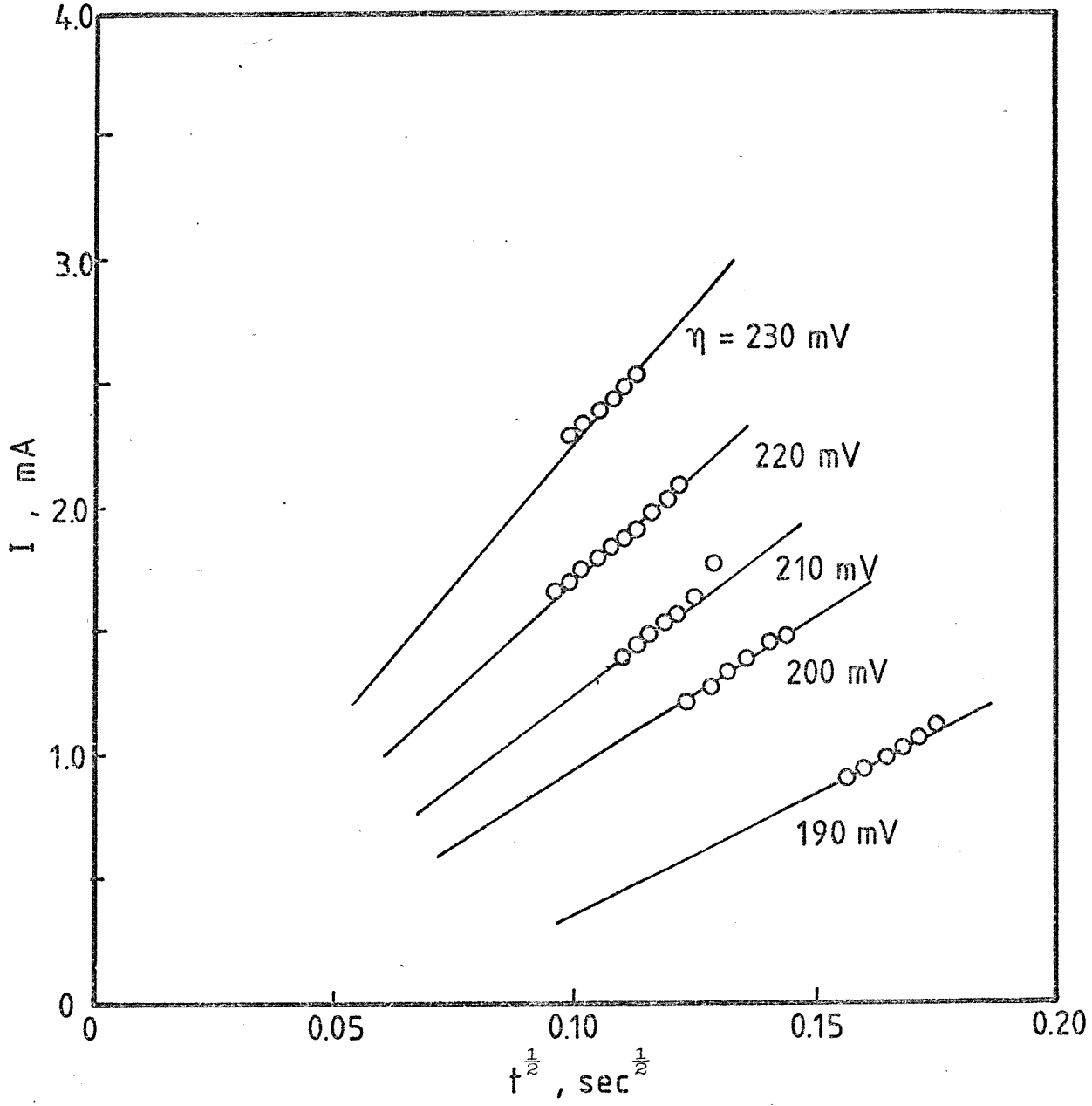

Figure 8.10 I-$t^{\frac{1}{2}}$ plot for the electrodeposition of Co(II) onto vitreous carbon. (Data from Figure 8.9)

TABLE 8.3 Nuclear densities of cobalt on a vitreous carbon electrode in molten LiCl-KCl eutectic at 467°C. (Electrode area = 0.312 cm^2)

	c = 22.49 mM	
η/mV	$\frac{10^3 dI/dt^{\frac{1}{2}}}{A/sec^{\frac{1}{2}}}$	$10^{-5} N_o$
200	10	37.6
210	12.6	47.3
220	14.8	55.6
230	17.9	67.3
240	23.4	87.9

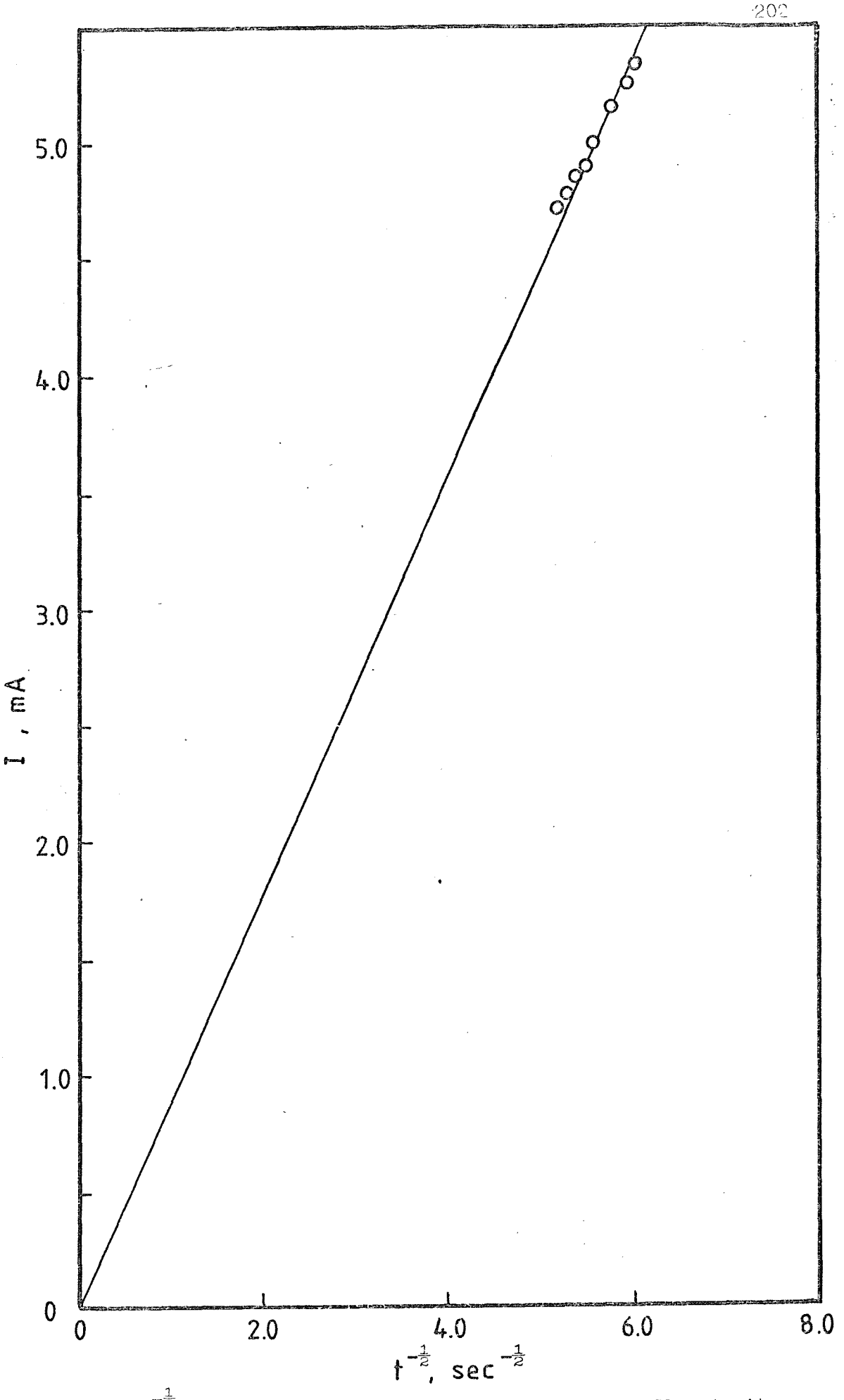

Figure 8.11 $I\text{-}t^{-\frac{1}{2}}$ relation for the reduction of 9.81 mM $CoCl_2$ at vitreous carbon in LiCl-KCl eutectic at 467°C at η = 300 mV. (A = 0.312 cm^2)

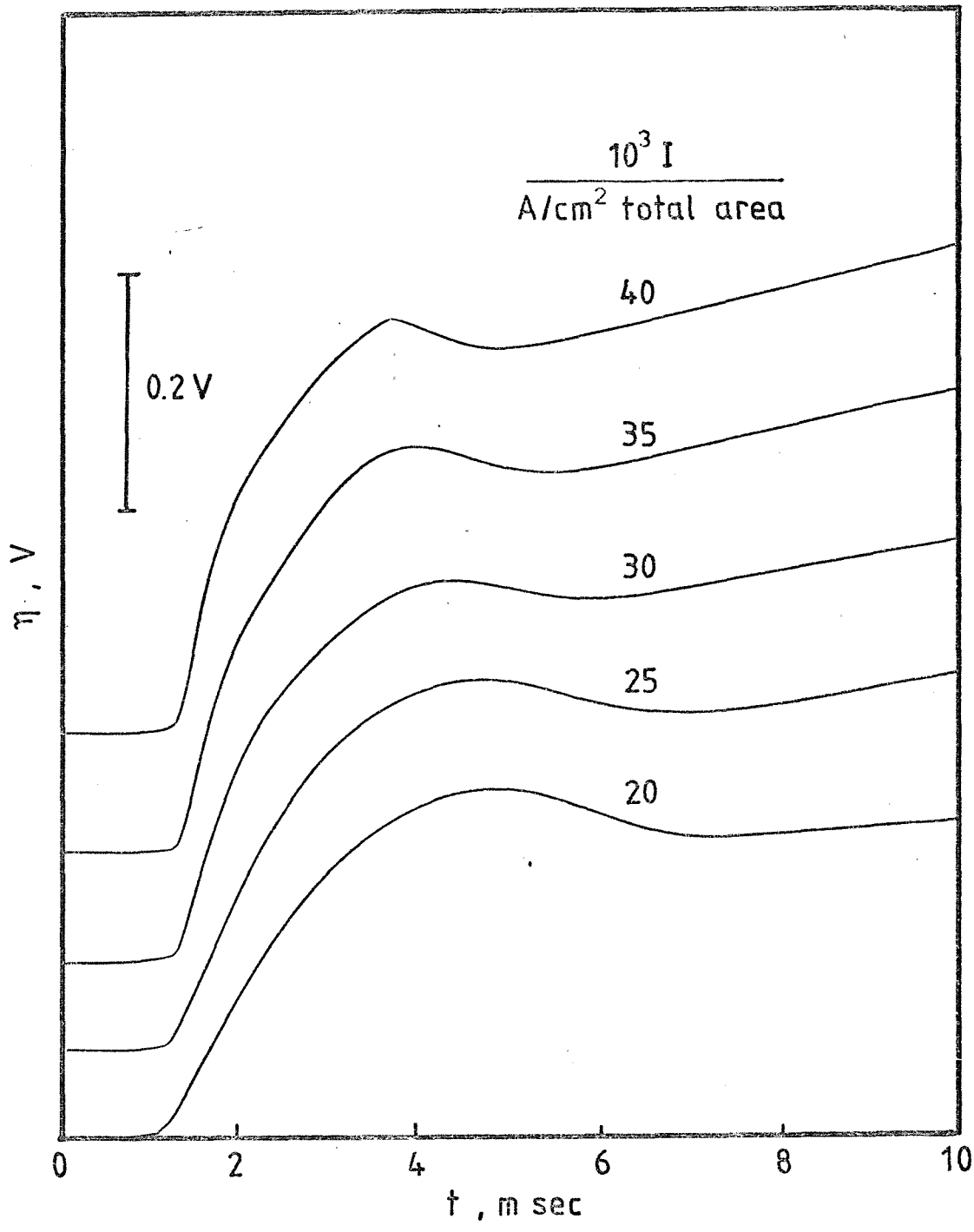

Figure 8.12 Galvanostatic transients for the reduction of 9.81 mM $CoCl_2$ at vitreous carbon in LiCl-KCl eutectic at 467°C at the constant currents indicated. (A = 0.312 cm^2)

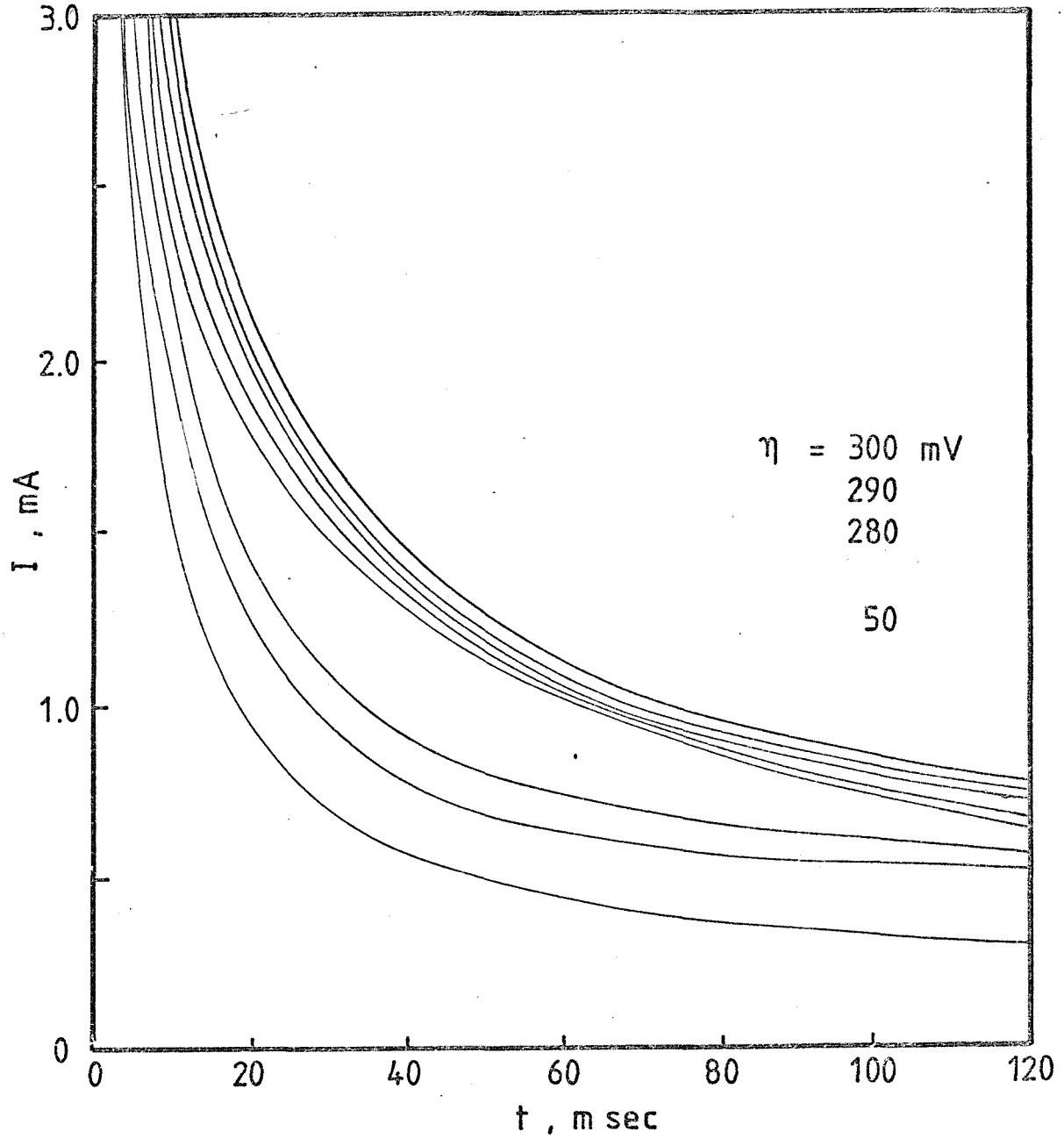

Figure 8.13 Potential-time transients for the electrodeposition of cobalt from 9.81 mM $CoCl_2$ on platinum in LiCl-KCl eutectic at the overpotentials indicated. (A = 0.312 cm^2)

8.2 Electrochemical nucleation of cobalt onto a vitreous carbon in the molten LiCl-KCl eutectic at 467°C

The application of the vitreous carbon electrode to studies of nucleation and growth in chloride melts of the other metals, e.g., cobalt has also been the subject for preliminary investigation.

Typical current/potential contour at different rates of polarisation are shown in Figure 8.7. A single cathodic wave for cobalt deposition is observed and linearity between peak current and the square root of the scan rate is obeyed (Figure 8.8). The evaluated diffusion coefficient from the sweep method is $1.25 \times 10^{-5} cm^2\ sec^{-1}$.

Potentiostatic rising current/time profiles at different degrees of supersaturation shown in Figure 8.9 are direct evidence of nucleation. The slope $dI/dt^{\frac{1}{2}}$ (Figure 8.10) leads to the number nuclear densities at several overpotentials shown in Table 8.3. The latter section of the current-time transient gives a linear plot of I vs $t^{-\frac{1}{2}}$ passing through the origin (Figure 8.11) and the calculated diffusion coefficient is $0.73 \times 10^{-5} cm^2\ sec^{-1}$.

Galvanostatic potential maximum at each current density (Figure 8.12) confirms the nucleation and growth mechanism which takes place before the continuous, bulk deposition of cobalt. An interesting feature of the galvanostatic transients is that the potential maximum is poorly defined in comparison with other nucleation processes both in the same or different ionic solvents. Again, the potential maximum is higher than the corresponding potentiostatic nucleation overpotentials shown to be required in separate potentiostatic experiments. Consequently, the potentiostatic estimation of the number nuclear density at the galvanostatic maximum and also the charge transfer rate constant for the bulk cobalt $\rightleftharpoons$ cobalt ions is not possible. It may be anticipated that all nucleation transients could be refined by using a highly reproducible electrode in highly purified solvent and these are subject to further investigations. Nevertheless, the future use of vitreous carbon as a substrate for nucleation studies of various metals is quite promising and encouraging.

If now we consider the same reaction taking place on platinum, it is seen from potentiostatic studies in Figure 8.13 that the cobalt deposition on it is not preceded by a process of nucleation.

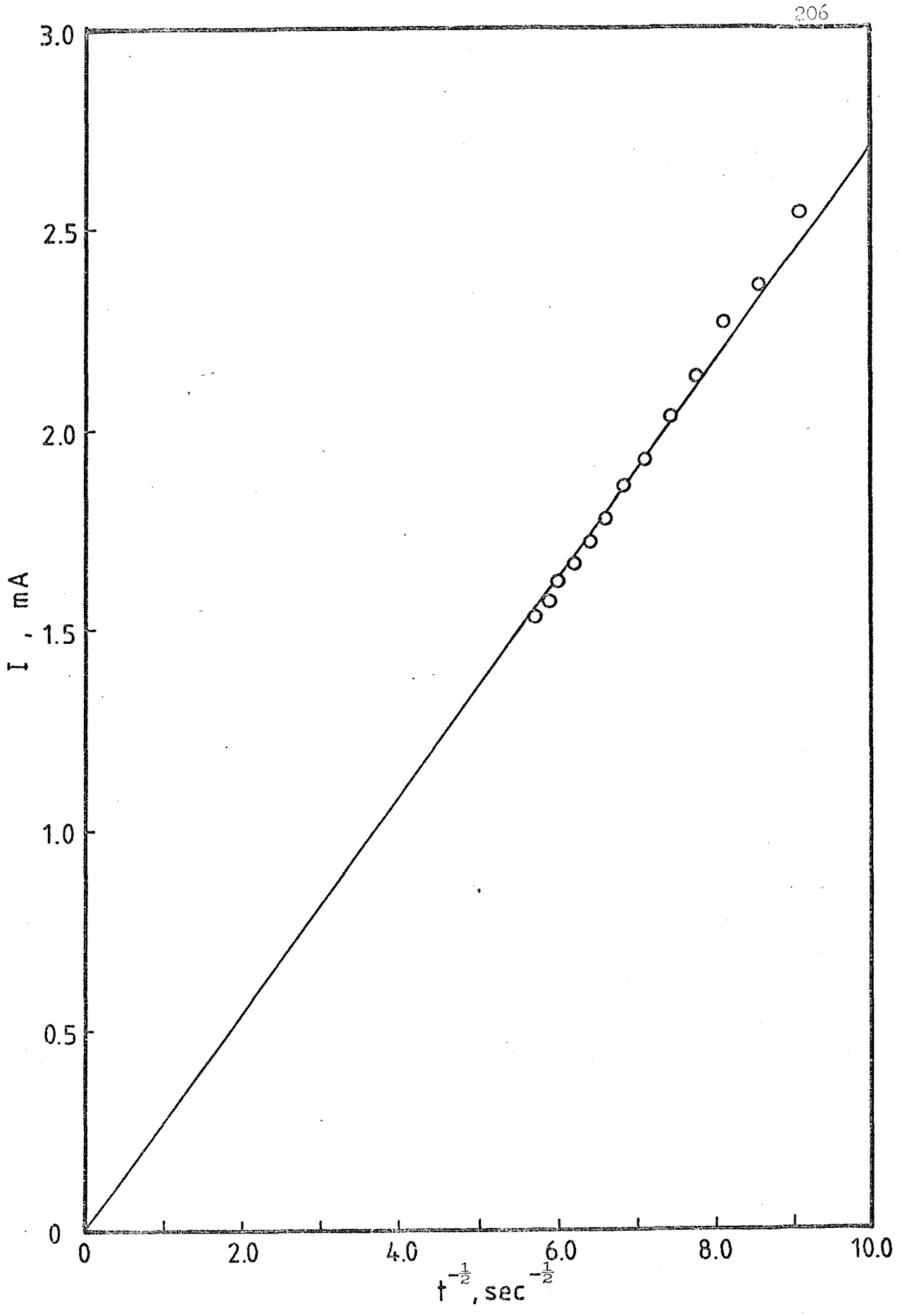

Figure 8.14 $I\text{-}t^{-\frac{1}{2}}$ relationship for the deposition of cobalt from 9.81 mM $CoCl_2$ on platinum in LiCl-KCl eutectic at η = 300 mV. ($A = 0.07 cm^2$)

This is also the case for the copper deposition in the same solvent reported by Baraboshkin *et al*[45] and that for the silver deposition to be discussed in the following section. It is believed that this behaviour is related to the formation of alloy compounds between platinum and the depositing metals in high melting chlorides.

The I *vs* $t^{-\frac{1}{2}}$ plot of the cobalt deposition on platinum (shown in Figure 8.14) is linear passing through the origin, the slope of the line leads to the 'D' value of $1.31 \times 10^{-5} cm^2\ sec^{-1}$.

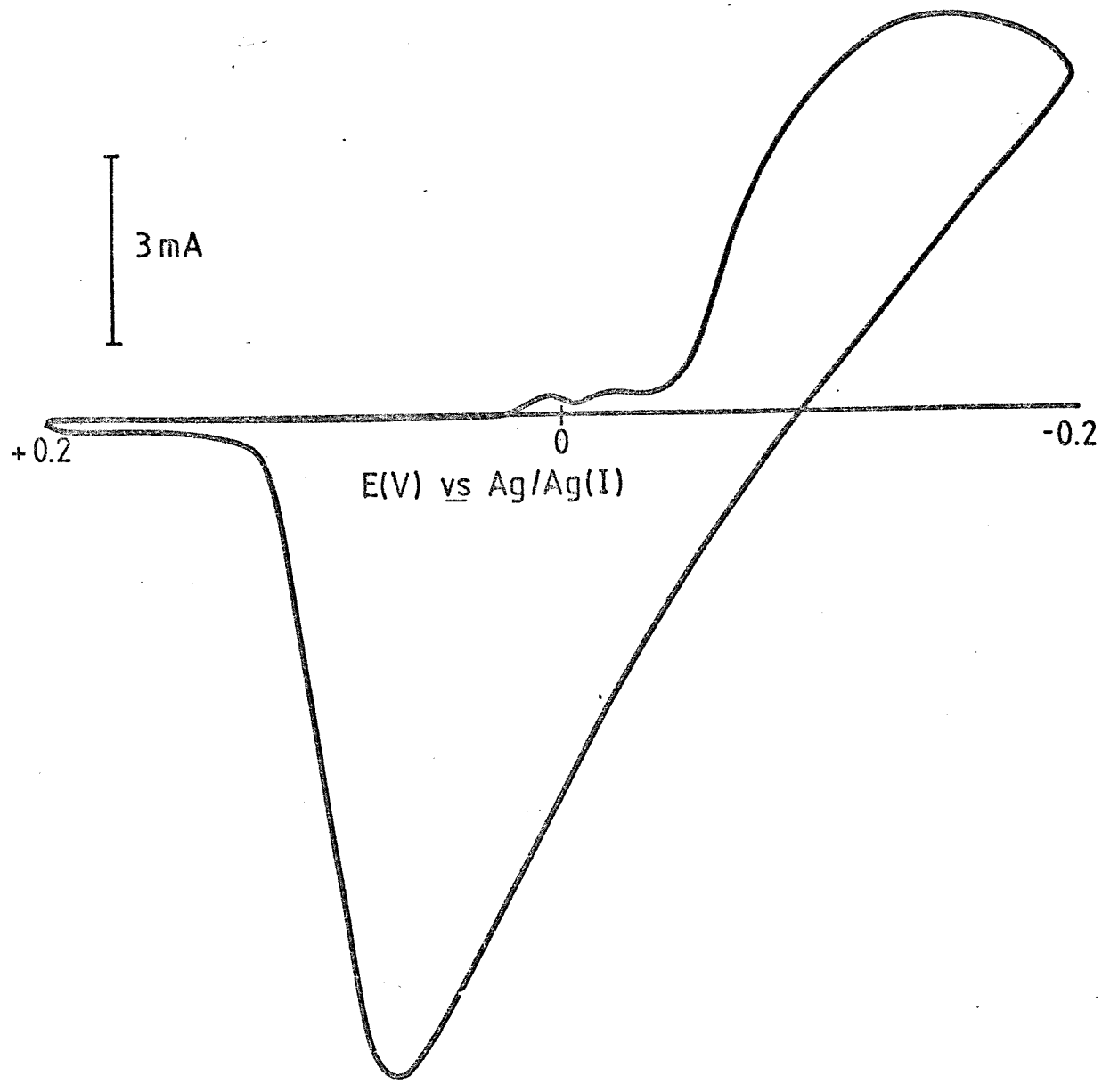

Figure 8.15 Current-potential curve for the reduction of 27.95 mM Ag(I) at platinum in LiCl-KCl eutectic at 400°C, v = 0.3 V sec^{-1}. (A= 0.043 cm^2)

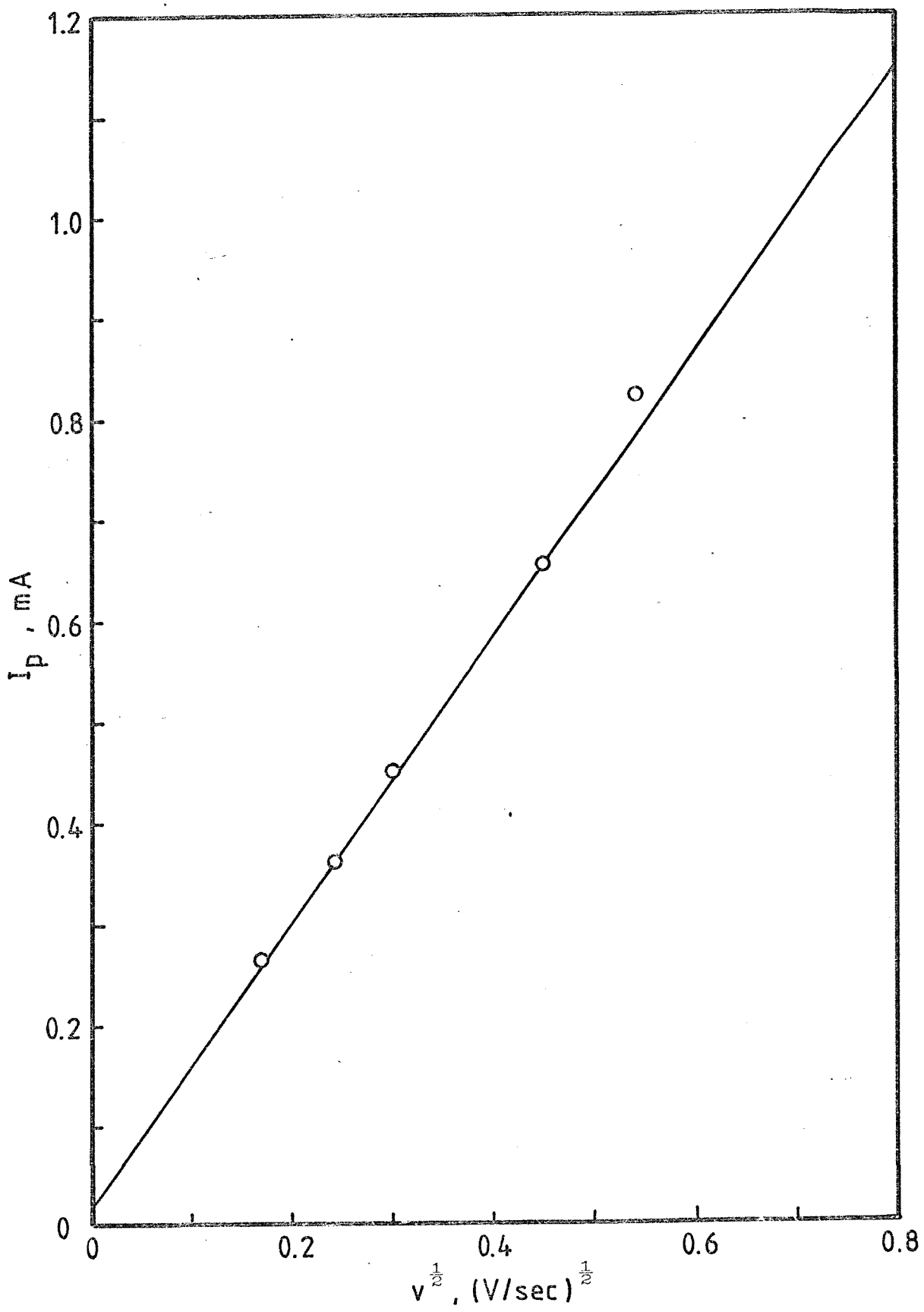

Figure 8.16 Linear relation of I_p vs $v^{\frac{1}{2}}$ for the electrodeposition of silver from 27.95 mM Ag(I) on platinum in LiCl-KCl eutectic at 400°C (A = 0.043 cm^2)

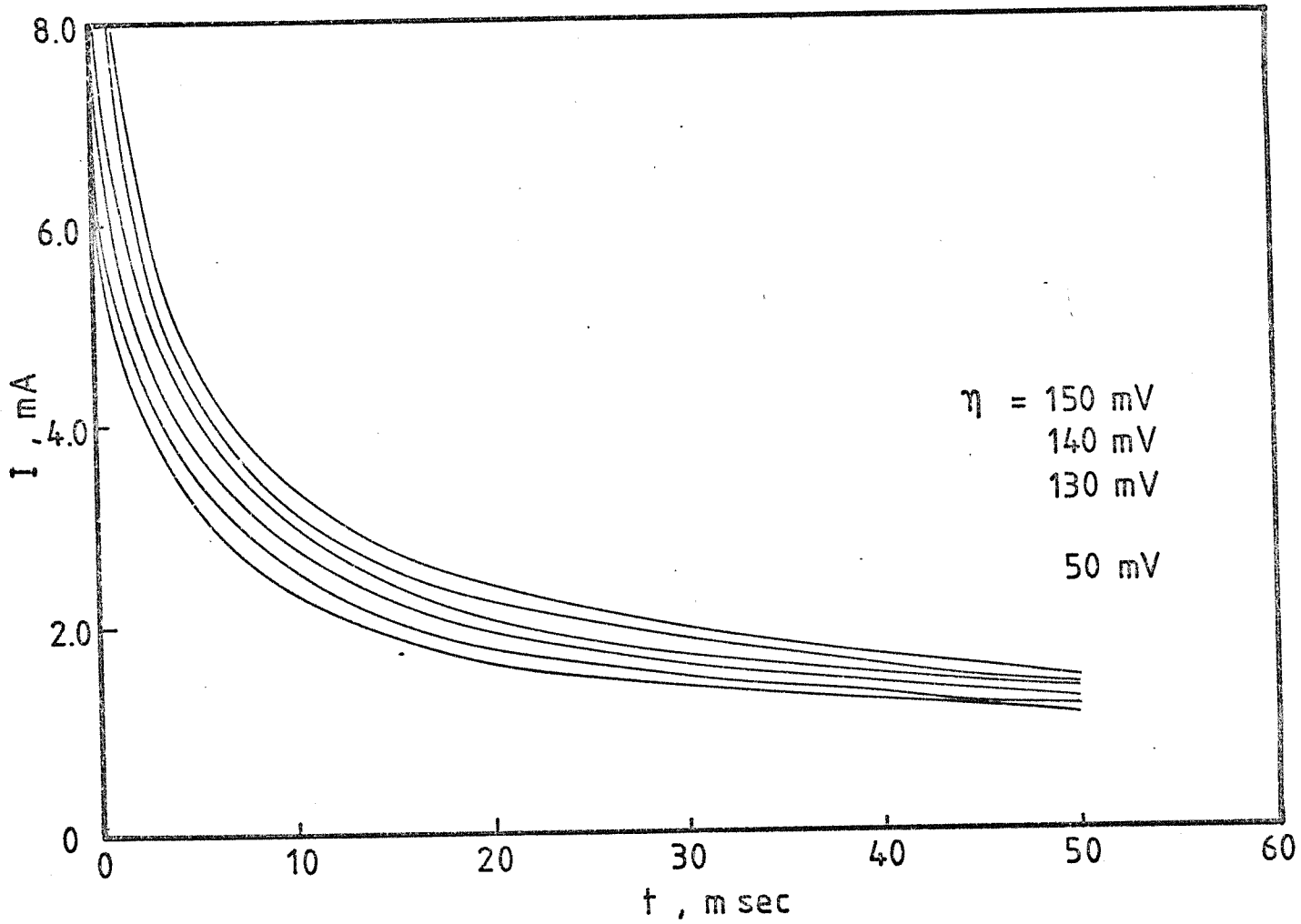

Figure 8.17 Current-time transients for the reduction of 27.95 mM Ag(I) at platinum at the over-potentials indicated. (A = 0.043 cm^2)

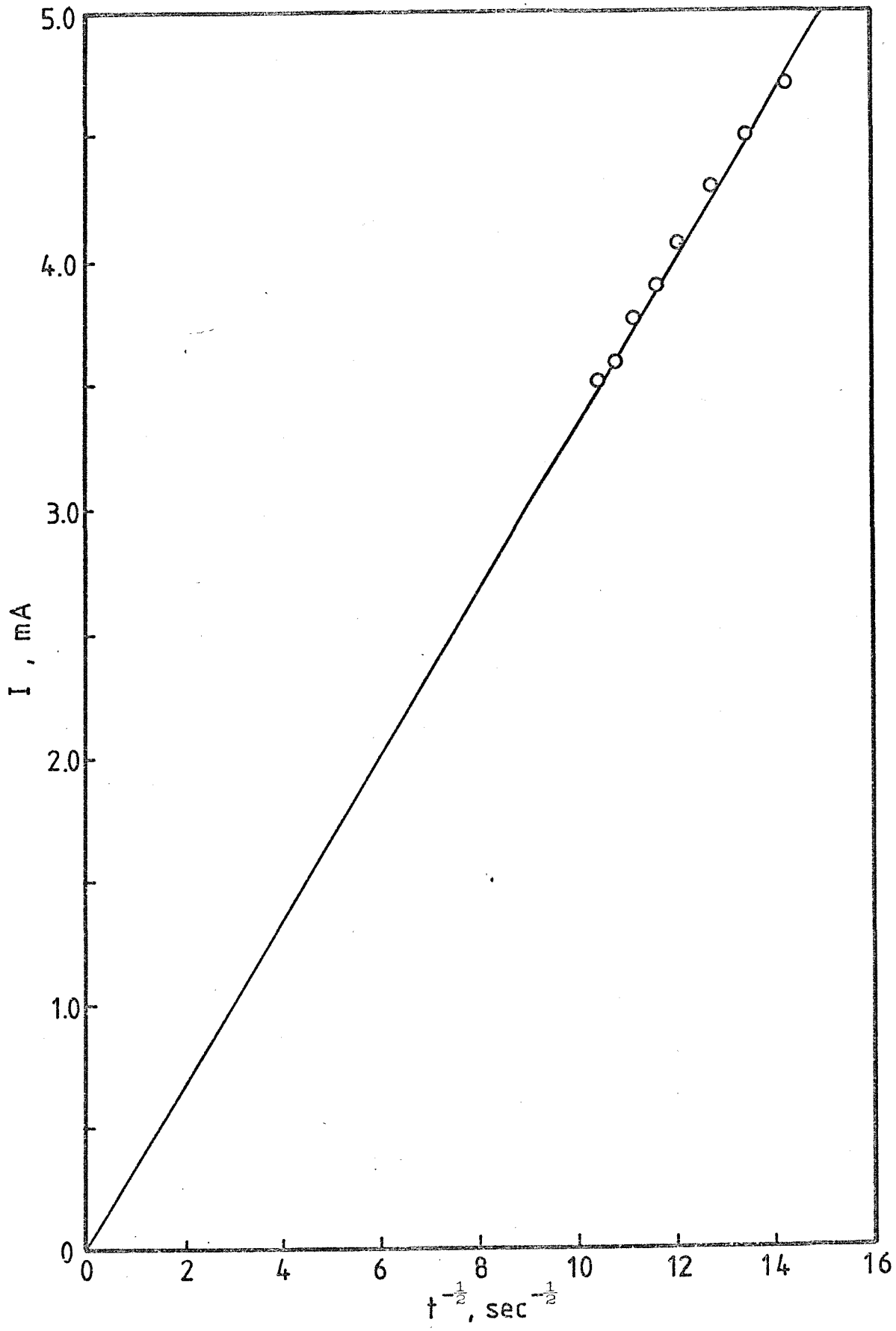

Figure 8.18 $I\text{-}t^{-\frac{1}{2}}$ relation for the reduction of 27.95 mM Ag(I) at platinum at η = 150 mV. (A = 0.043 cm^2)

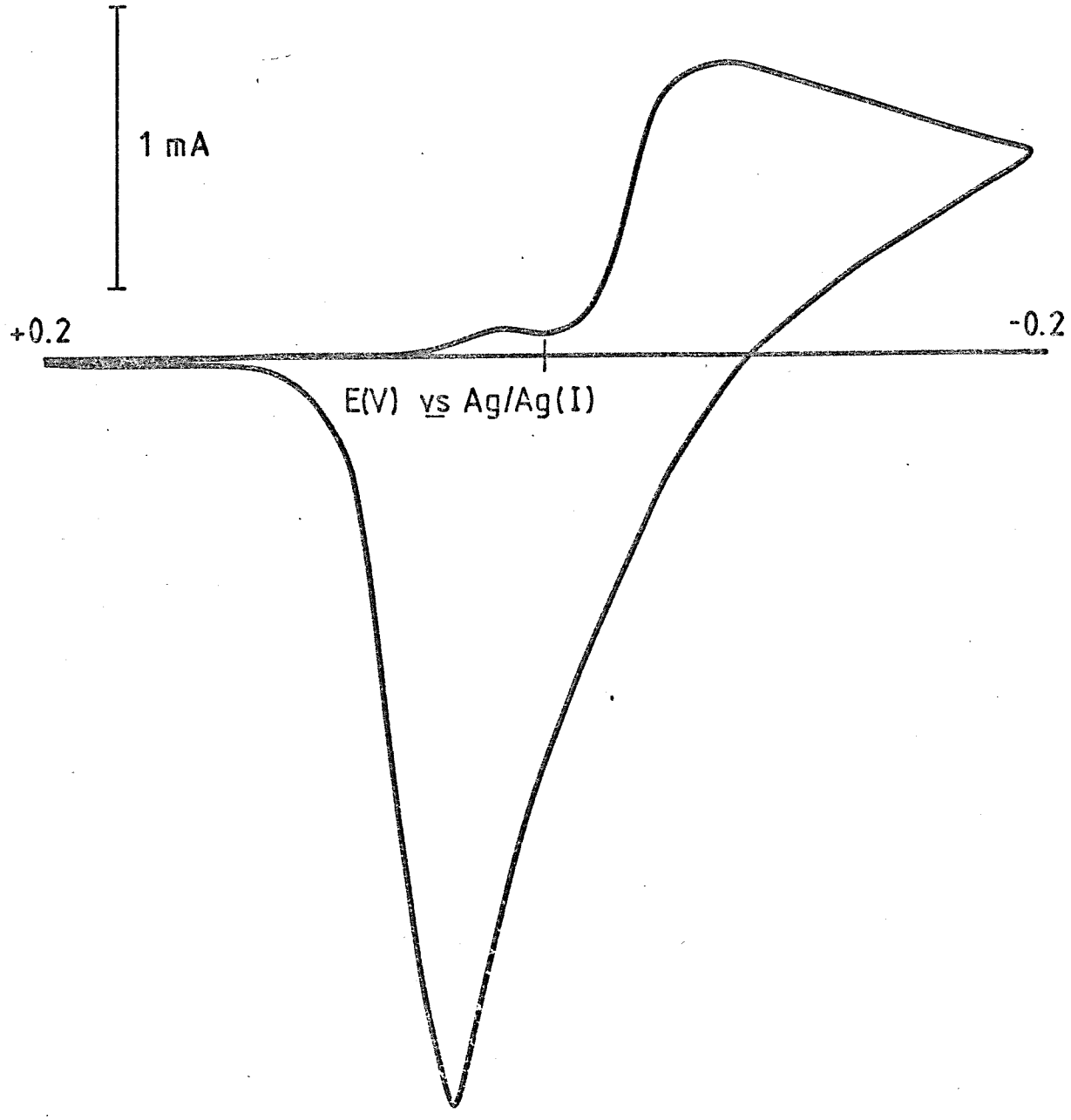

Figure 8.19 Cyclic voltammogram for the reduction of 27.95 mM Ag(I) on vitreous carbon in LiCl-KCl eutectic at 400°C, $v = 0.4$ V sec^{-1}. ($A = 0.312$ cm^2)

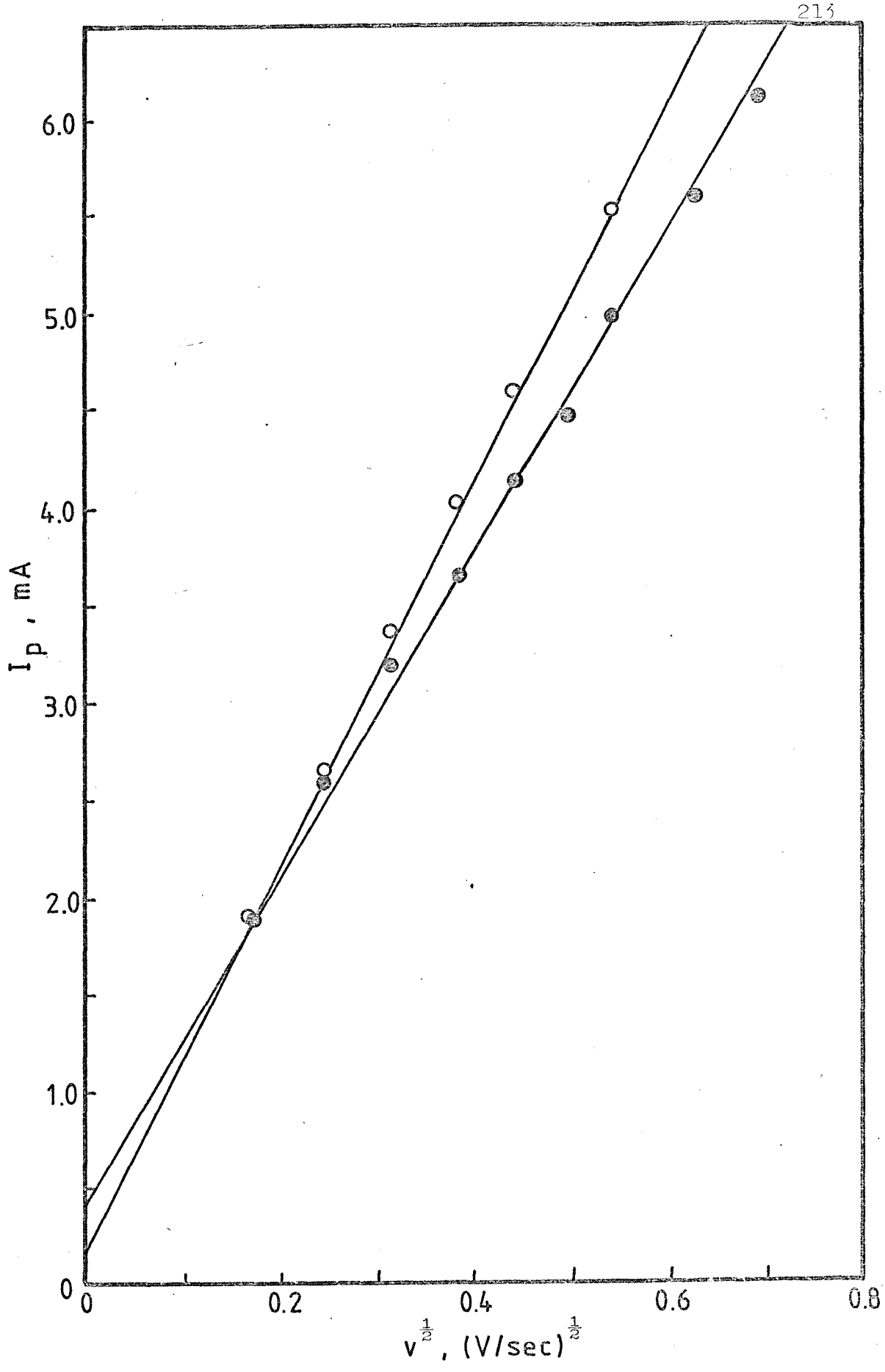

Figure 8.20 Linear plot of I_p vs $v^{\frac{1}{2}}$ for the reduction of 23.96(●) and 27.95(○) mM Ag(I) on vitreous carbon in LiCl-KCl eutectic at 400°C. (A = 0.312 cm^2)

8.3 Electrodeposition of silver onto platinum, vitreous carbon, tungsten copper and nickel in the molten LiCl-KCl eutectic at ~ 450°C

Silver metal is found to nucleate on platinum and vitreous carbon both in aqueous solutions and molten nitrates. In molten chlorides, however, there is no evidence that the formation of the new phase of silver on various electrode materials takes place by three dimensional nucleation. It is more likely that the early stages of silver deposition on platinum and vitreous carbon take place by initial formation of an epitaxial monolayer.

8.3.1 The system $AgNO_3$/Pt in the LiCl-KCl eutectic at 400°C

The I/E display for the deposition-dissolution of silver onto platinum at a concentration of silver ion of 27.95 mM is shown in Figure 8.15. A striking feature is a small predeposition peak at a positive potential with respect to reversible potential. This prepeak becomes more prominent with an increase of the scan rate and can be attributed to monolayer formation of silver which takes place before the bulk deposition. The relation between peak current and the square root of the sweep rate plot is linear but does not pass through the origin (Figure 8.16). The positive intercept is probably related to the small prewave. The slope $dI_p/dv^{\frac{1}{2}}$ leads to a diffusion coefficient of $2.2 \times 10^{-5} cm^2\ sec^{-1}$ as is shown in Table 8.1.

Over a wide range of overpotentials the potentiostatic experiment gives rise to normal falling transients. A family of transients is shown in Figure 8.17 and the corresponding regression plot of I vs $t^{-\frac{1}{2}}$ is shown in Figure 8.18. Its slope leads to a diffusion coefficient of $2.6 \times 10^{-5} cm^2\ sec^{-1}$.

8.3.2 The system $AgNO_3$/vitreous carbon in the LiCl-KCl eutectic at 400°C

The most striking characteristics of the I/E contour for the reduction of silver onto vitreous carbon (Figure 8.19) is that there are two small well defined predeposition peaks, one on the anodic side of the reversible potential and the other on the cathodic side. Both are more pronounced at high sweep rates. The first prepeak may be due to the underpotential formation of a monolayer of silver. The peak height is linearly dependent upon the square root of the sweep velocity but does not pass through the origin (Figure 8.20). The positive intercept may again be related to these prepeaks. The evaluated diffusion coefficient

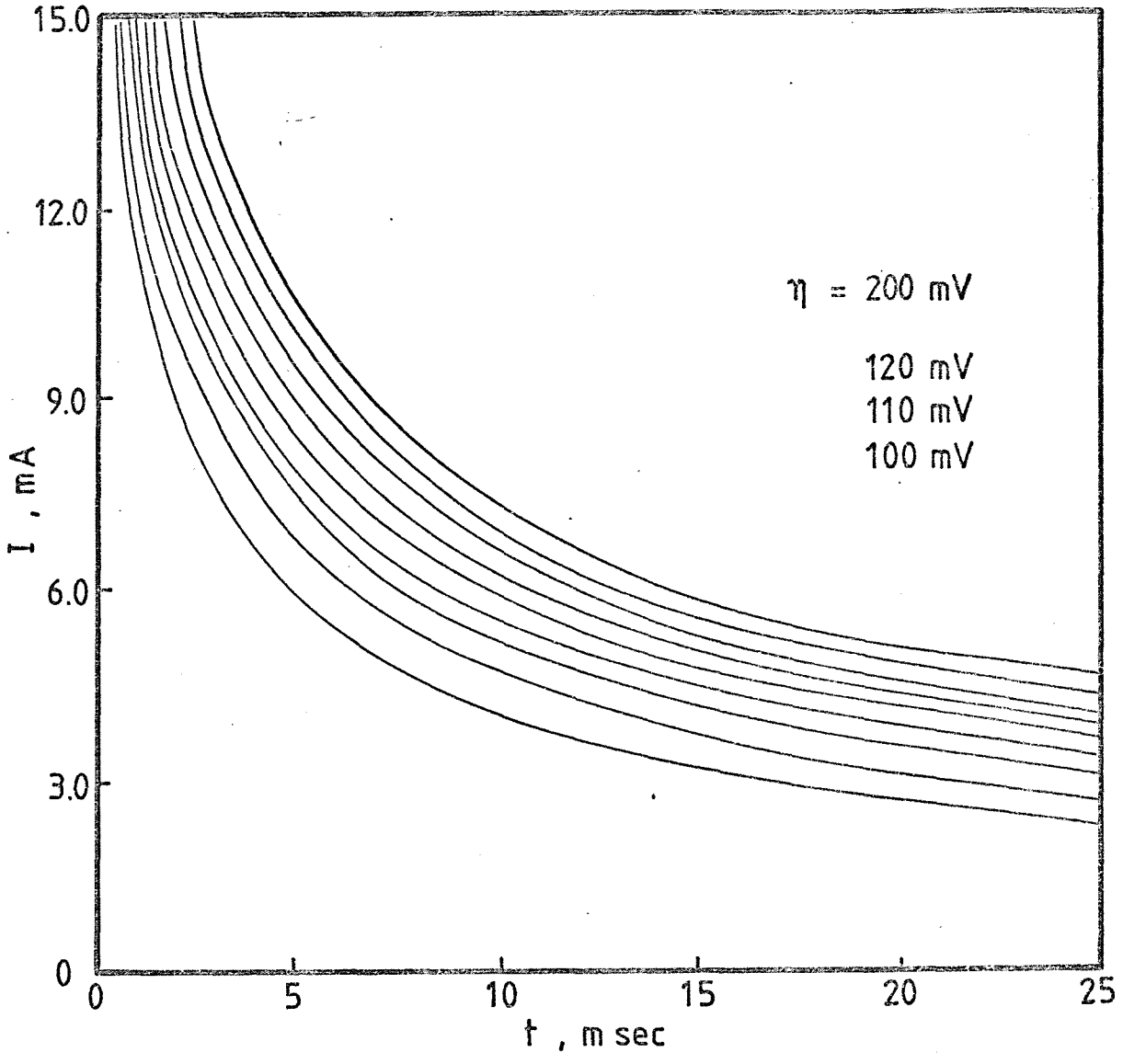

Figure 8.21 I-t transients for the reduction of 27.95 mM Ag(I) on vitreous carbon in LiCl-KCl eutectic, 400°C at the overpotentials indicated. ($A = 0.312\ cm^2$)

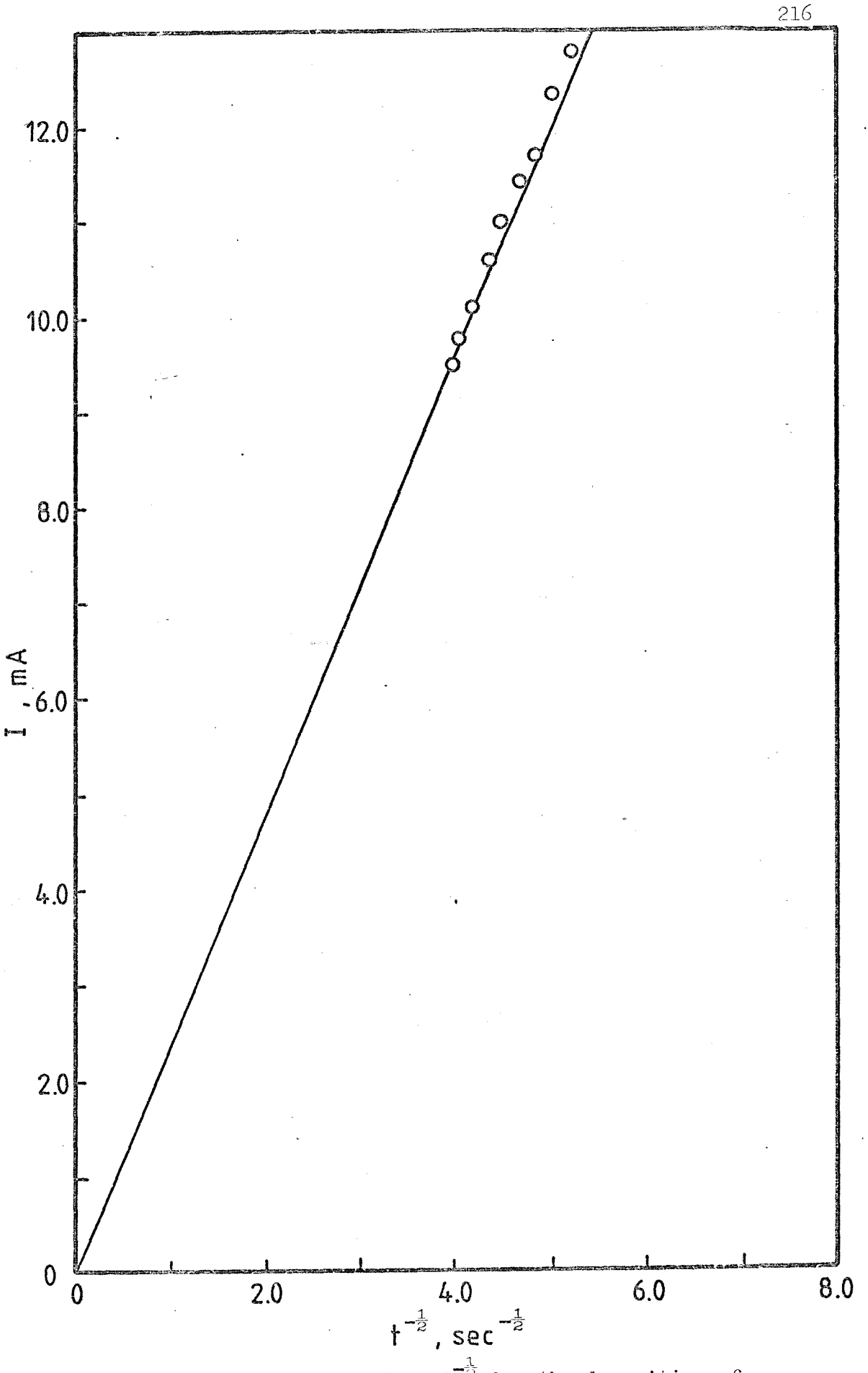

Figure 8.22 Relationship between I vs $t^{-\frac{1}{2}}$ for the deposition of 27.95 mM Ag(I) on vitreous carbon in LiCl-KCl eutectic at η = 200 mV. (A = 0.312 cm^2)

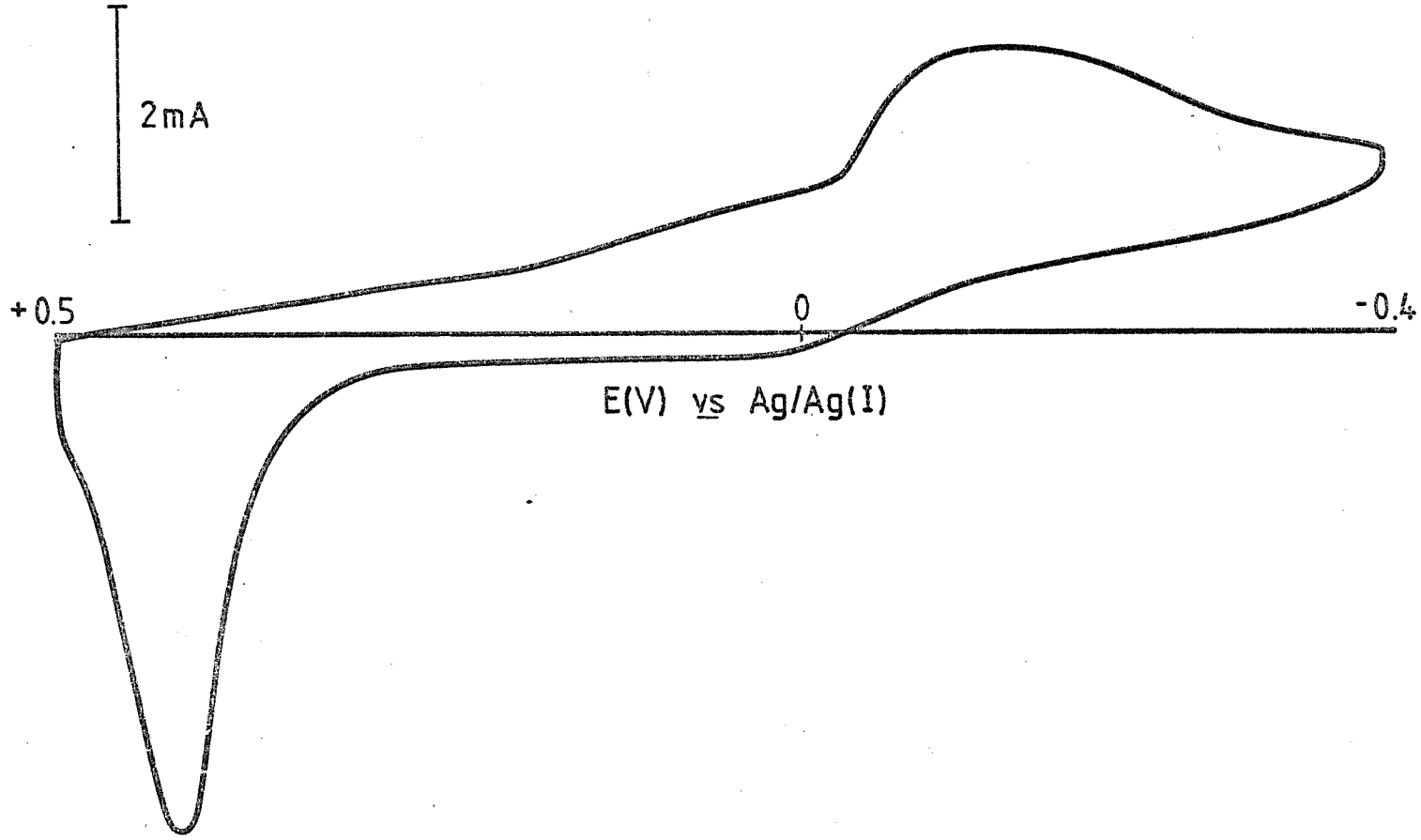

Figure 8.23 Voltammogram for the reduction of 27.95 mM Ag(I) at tungsten in LiCl-KCl eutectic at 400°C, v = 0.06 V sec^{-1}. (A = 0.13 cm^2)

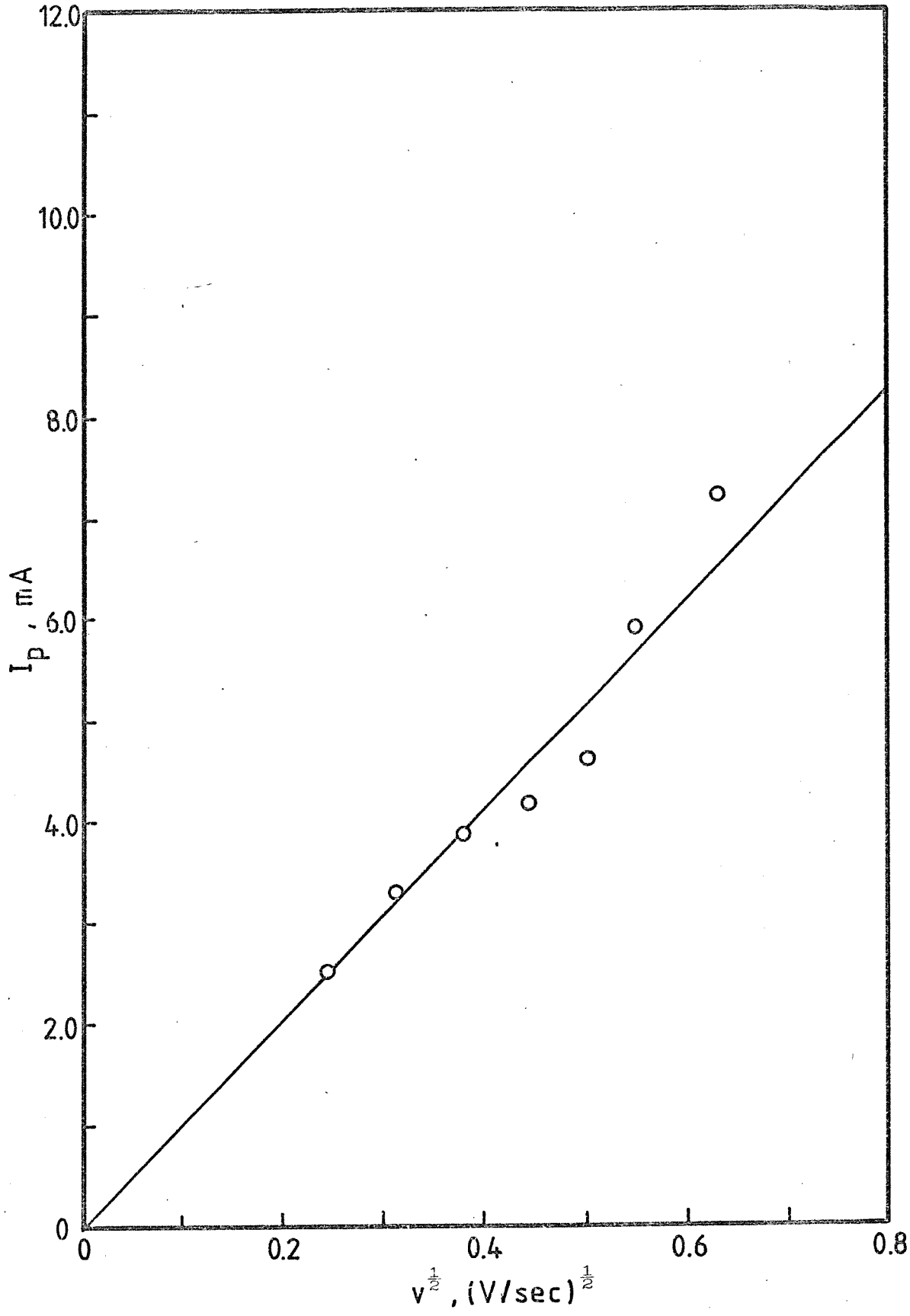

Figure 8.24 I_p vs $v^{\frac{1}{2}}$ plot for the reduction of 27.95 mM Ag(I) at tungsten in LiCl-KCl eutectic at 400°C. (A = 0.13 cm^2)

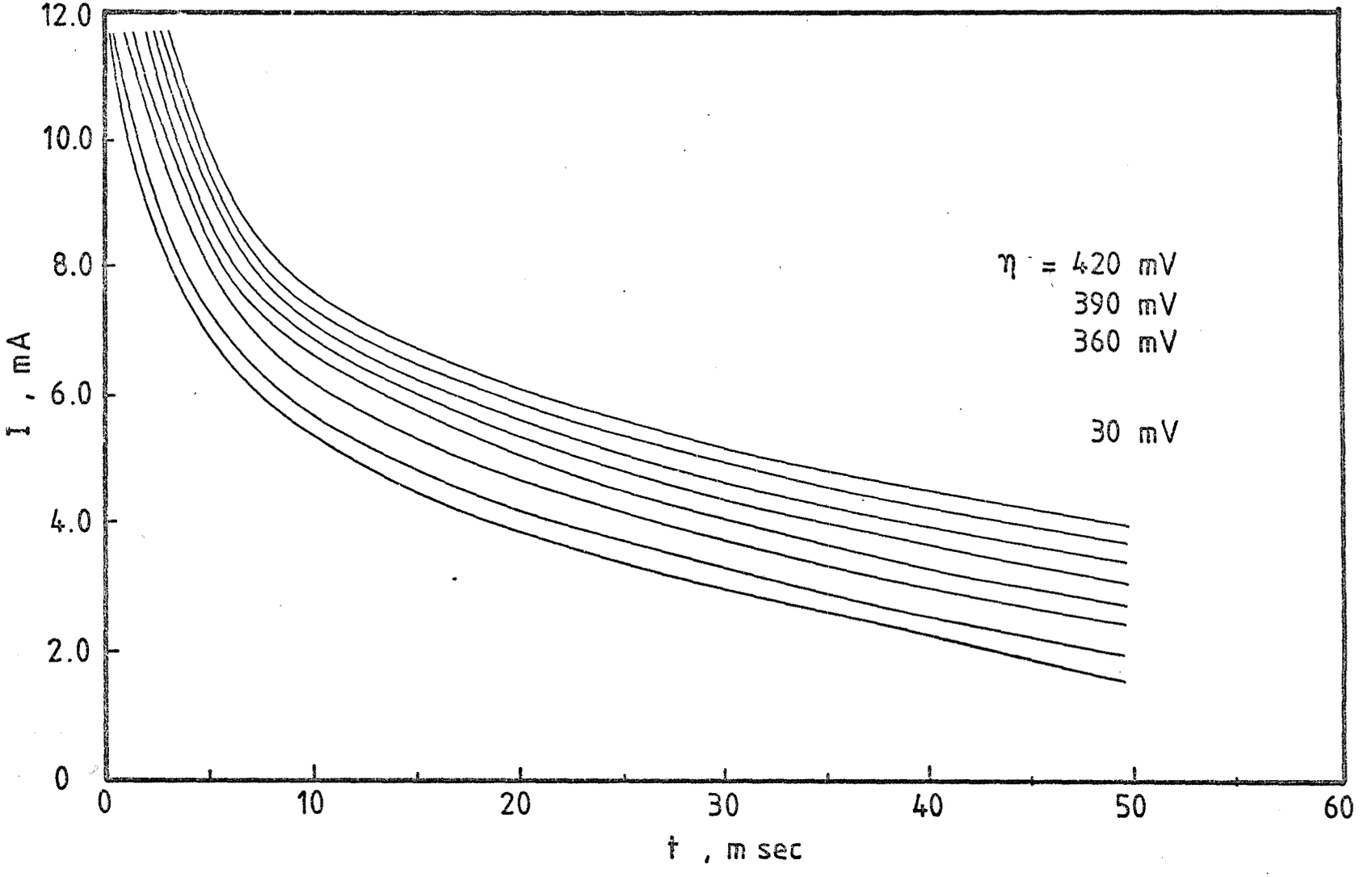

Figure 8.25 I-t transients for the reduction of 27.95 mM Ag(I) at tungsten in LiCl-KCl eutectic at 400°C at the overpotentials indicated. ($A = 0.13\ cm^2$)

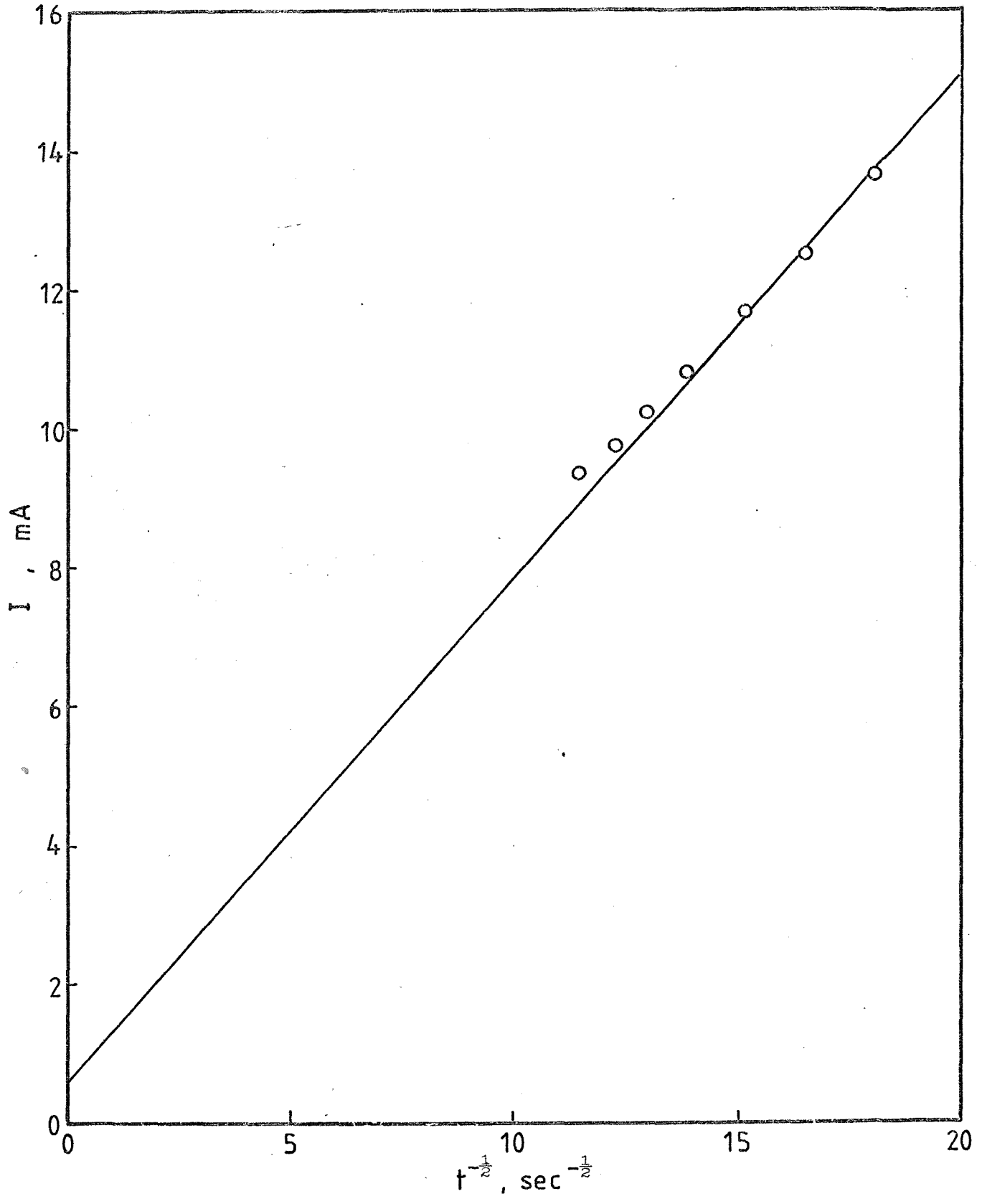

Figure 8.26 I-$t^{-\frac{1}{2}}$ relation for the reduction of 27.95 mM Ag(I) at tungsten in LiCl-KCl eutectic at 400°C at η = 360 mV. (A = 0.13 cm^2)

is $2.2 \times 10^{-5} cm^2 \ sec^{-1}$. The corresponding potential step experiment gives falling current-time curves at different applied overpotentials (Figure 8.21). A plot of I vs $t^{-\frac{1}{2}}$ is linear (Figure 8.22) and the slope $dI/dt^{\frac{1}{2}}$ leads to a diffusion coefficient of $2.5 \times 10^{-5} cm^2 \ sec^{-1}$.

8.3.3 The system $AgNO_3$/tungsten in the LiCl-KCl eutectic at 400°C

Tungsten is a useful electrode material for the study of metal deposition from molten salts although its reproducibility is not as good as for many other electrode materials. Defects in the construction of the electrode make for shorter working life in high temperature work system. The black oxide on its surface is readily removed by an appropriate pretreatments before use.

In these chloride melts the tungsten electrode was used to study the deposition of silver . It was found that the oxide film could be reduced and a clean surface was renewed in this melt. Perhaps because of this, there is no evidence of three dimensional phase formation and this situation is similar to that of silver deposition on platinum from molten alkali nitrates where no evidence of nucleation on a freely cleaned platinum electrode was observed.

A linear sweep voltammogram for the reduction of silver on tungsten is shown in Figure 8.23. A single cathodic peak is observed. The reproducibility of the results was poor and is reflected in the scatter of the points about the otherwise linear relation between I_p and $v^{\frac{1}{2}}$ shown in Figure 8.24. The slope of this line leads to a diffusion coefficient of $0.13 \times 10^{-5} cm^2 \ sec^{-1}$ which is low compared to the value obtained with a platinum electrode in the same system.

A set of normal falling current transients was observed over a range of applied overpotentials (Figure 8.25) again confirming the absence of three dimensional in this silver deposition reaction. The diffusion coefficient of silver ion evaluated from the slope $dI/dt^{\frac{1}{2}}$ (Figure 8.26) was found to be $1.7 \times 10^{-5} cm^2 \ sec^{-1}$ in better agreement with the values found above.

8.3.4 The system $AgNO_3$/Cu and Ni in the LiCl-KCl eutectic at 450°C

Copper and nickel metals were employed as 'flag' shaped electrodes for the study of the electrodeposition of silver in chloride melts. These electrodes failed to produce reliable information partly because of some technical problems in the electrode construction but mainly

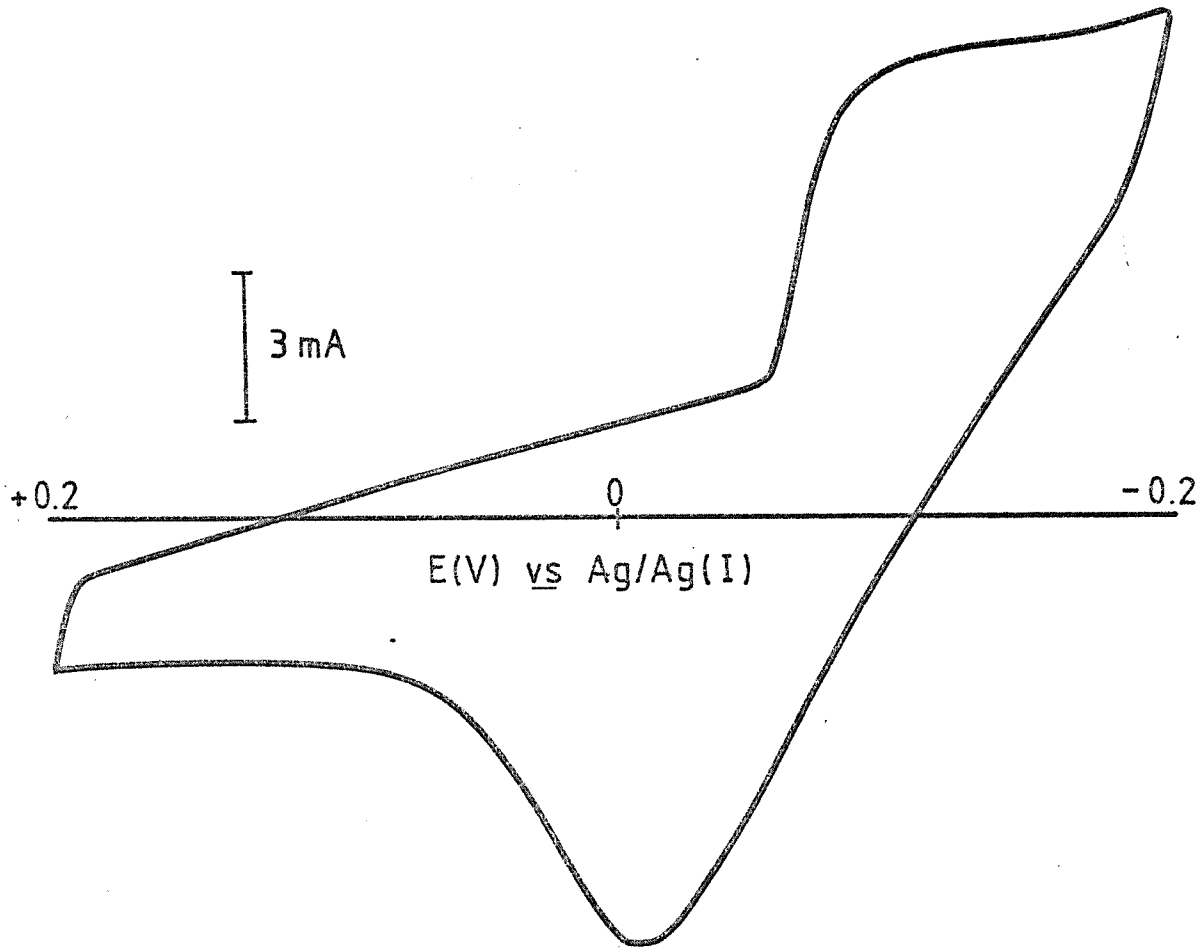

Figure 8.27 Voltammogram for the deposition of 23.96 mM Ag(I) on copper in LiCl-KCl eutectic at 400°C, v = 0.25 V sec^{-1}. (A $\sim$ 0.2 cm^2)

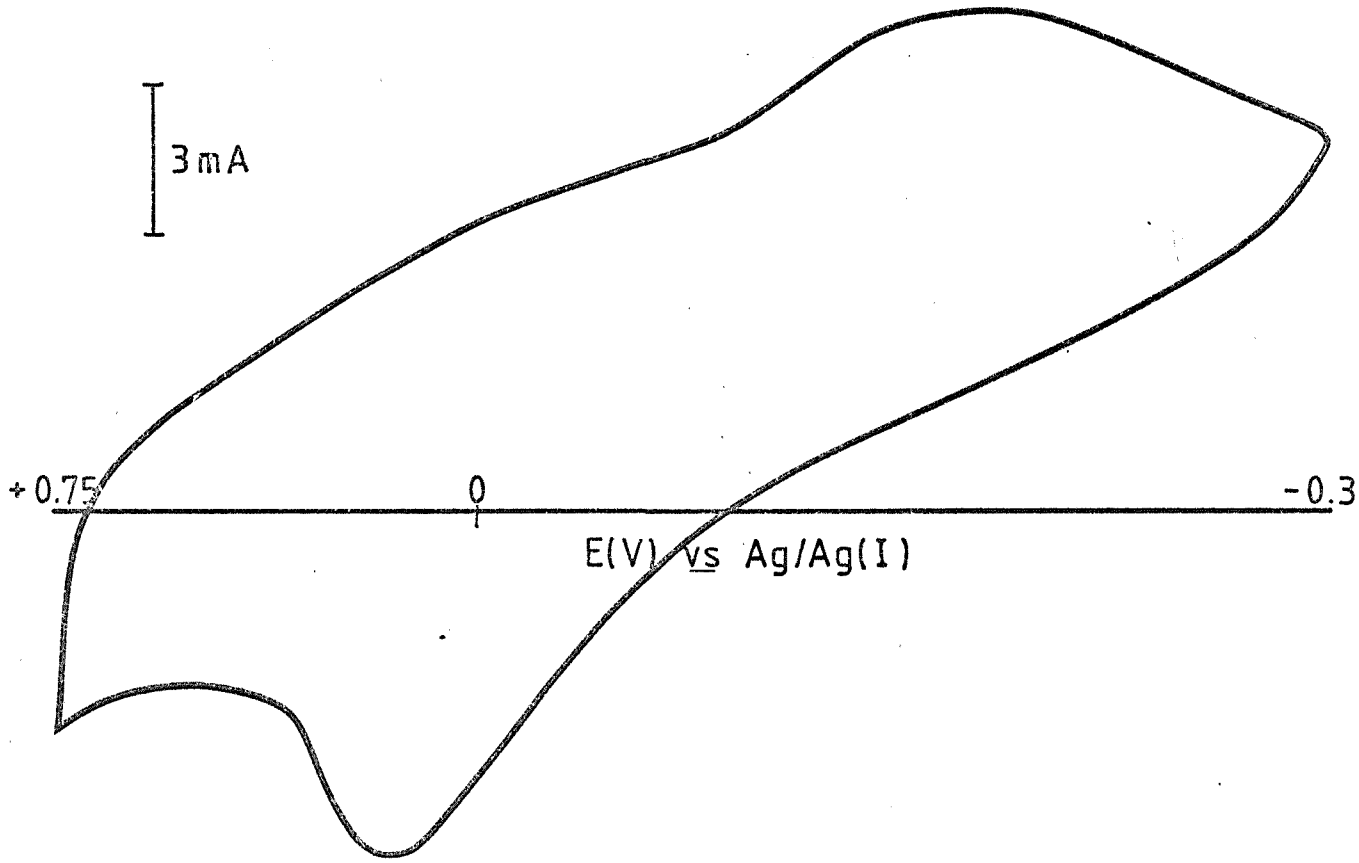

Figure 8.28 Voltammogram for the deposition of 21.06 mM Ag(I) on nickel in LiCl-KCl eutectic at 400°C, v = 0.1 V sec^{-1}. (A ~ 0.2 cm^2)

because the metallic surface can not withstand high temperature molten chlorides. Nevertheless some results from the use of these electrodes are shown in Figure 8.27 and Figure 8.28.

A search for suitable substrate on which to study the nucleation and growth of metals from molten salts therefore led back to vitreous carbon. Hundreds of such nucleation transients from a number of metal deposition systems on a number of vitreous carbon electrodes were consistently produced. It is fair to say that throughout the course of investigation, glassy carbon behaves in a simple, reproducible and reliable manner. There were no significant surface complications such as those affecting platinum although as with other electrode materials, technical problems of actually making the electrode remain. Hills and Inman[121] have developed a general microelectrode for use in molten salts. They sealed a tungsten wire into borosilicate matching glass and ground the end flat and plane with the glass. The cross sectional area was about 0.2 mm^2. Their electrode was used for voltammetric studies in LiCl-KCl eutectic up to 600°C. The application of carbon fibre microelectrode of cross sectional area of $\sim 10^{-7} cm^2$ as a nucleation site for one elemental nucleus in aqueous solutions in this laboratory seems to be well established[122], but its application to molten salts remains to be attempted.

REFERENCES

1. HILLS, G.J., SCHIFFRIN, D.J. and THOMPSON, J., Electrochim. Acta, 19, 657, 671 (1974).
2. FLEISCHMANN, M. and THIRSK, H.R., Advances in Electrochemistry and Electrochemical Engineering, Vol. 3, Edited by Delahay, P., Interscience, New York (1963); see also BINDRA, P., FLEISCHMANN, M., OLDFIELD, J.W. and SINGLETON, D., Faraday Discussion Chemical Society (London), 56, 180 (1973).
3. TOSCHEV, S. and MUTAFTSCHIEW, B., Electrochim. Acta, 9, 1203 (1964).
4. BELL, M.F. and HARRISON, J.A., J. electroanal. Chem., 41, 15 (1975).
5. KLAPKA, V., Coll. Czech. Chem. Comm., 34, 1131 (1969).
6. MEHL, W. and BOCKRIS, J.O'M., Canad. J. Chem., 37, 190 (1959).
7. TOSCHEV, S. and MARKOV, I., J. Cryst. Growth, 3, 436 (1968).
8. MARKOV, I. and KASHCHIEV, D., J. Cryst. Growth, 13/14, 131 (1972).
9. MARKOV, I., BOYNOV, A. and TOSCHEV, S., Electrochim. Acta, 18, 377 (1973).
10. KASHCHIEV, D., Thin Solid Films, 29, 193 (1975).
11. PLAMBECK, J.A., Fused Salt Systems: Encyclopedia of Electrochemistry of the Elements (Bard, A.J., ed.), Marcel Dekker, New York (1976).
12. INMAN, D., GRAVES, A.D. and SETHI, R.S., Electrochemistry (Hills, G.J., ed.), Vol.1, Chemical Society, London (1970).
13. INMAN, D., GRAVES, A.D. and NOBILE, A.A., Electrochemistry (Hills, G.J., ed.), Vol. 2, Chemical Society, London (1971).
14. INMAN, D., BOWLING, J.E., LOVERING, D.G. and WHITE, S.H., Electrochemistry (Thirsk, H.R., ed), Vol. 4, Chemical Society, London (1974).
15. GRAVES, A.D., HILLS, G.J. and INMAN, D., Advances in Electrochemistry and Electrochemical Engineering (Dalahay, P., ed.), Vol. 4, Interscience, New York (1966).
16. LAITY, R.W., Reference Electrodes: Theory and Practice (Ives, D.J.G. and Janz, G.J., eds), Academic Press, New York (1961).
17. SUNDHEIM, B.R., ed., Fused Salts, McGraw-Hill, New York (1964).
18. JAIN, R.K., GAUR, H.C., FRAZIER, E.J. and WELCH, B.J., J. Electroanal. Chem., 78, 1 (1977).
19. HILLS, G.J., INMAN, D. and YOUNG, L., Proceedings of the 8th Meeting of the International Committee of Electrochemical Thermodynamics and Kinetics, 1956, Butterworths, London (Published 1958).

20. BRAUNSTEIN, J., MAMANTOV, G. and SMITH, G.P., eds., Advances in Molten Salt Chemistry, Vol. 1-3, Plenum Press, New York (1971, 1973, 1975).
21. DELIMARSKII, Y.K. and MARKOV, B.F., Electrochemistry of Fused Salts (Translated by Peiperl, A; Wood, R.E., ed.), Sigma Press, Washington, D.C. (1961).
22. SWOFFORD, H.S. and LAITINEN, H.A., J. Electrochem. Soc., 110, 814 (1963).
23. KUST, R.N. and DUKE, F.R., J. Am. Chem. Soc., 85, 3338 (1963).
24. GUPTER, N. and SUNDHEIM, B.R., J. Electrochem. Soc., 112, 1789 (1965).
25. INMAN, D. and BRAUNSTEIN, J., Chem. Commun., 148 (1966).
26. TOPOL, L.E., OSTERYOUNG, R.A. and CHRISTIE, J.H., J. Phys. Chem., 70, 2857 (1966).
27. SWOFFORD, H.S. and McCORMICK, P.G., Anal. Chem., 37, 970 (1965).
28. HILLS, G.J. and JOHNSON, K.E., Proceedings of the 2nd International Congress on Polarography, Cambridge (1959), p. 974, Pergamon Press, London (1961).
29. ZAMBONIN, P.G. and JORDAN, J., Analyt. Letters, 1, 1 (1967).
30. ZAMBONIN, P.G. and JORDAN, J., J. Am. Chem. Soc., 89, 6365 (1967).
31. ZAMBONIN, P.G. and JORDAN, J., J. Am. Chem. Soc., 91, 2225 (1969).
32. ZAMBONIN, P.G., Anal. Chem., 41, 868 (1969).
33. ZAMBONIN, P.G., J. Electroanal. Chem., 24, App. 25 (1970).
34. ZAMBONIN, P.G., J. Electroanal. Chem., 24, 365 (1970).
35. KERRIDGE, D.H. in MTP International Review of Science, Inorganic Chemistry Series 1, Vol. 2, (Addison, C.C. and Sowerby, D.B., eds.), London, Butterworths (1972).
36. KERRIDGE, D.H., Pure Appl. Chem., 41, 355 (1975).
37. KERRIDGE, D.H. and BURKE, J.D., Electrochim. Acta, 19, 251 (1974).
38. STEINBERG, M. and NACHTRIEB, N.H., J. Am. Chem. Soc., 72, 3558 (1950).
39. INMAN, D., LOVERING, D.H. and NARAYAN, R., Trans. Faraday Soc., 63, 3017 (1967).
40. INMAN, D. and BOCKRIS, J.O'M, J. Electroanal. Chem., 3, 126 (1962).
41. MAMANTOV, G., STRONG, J.M. and CLAYTON, F.R., Anal. Chem., 40, 488 (1968).
42. BEHL, W.K. and GAUR, H.C., J. Electroanal. Chem., 32, 293 (1971).
43. NARAYAN, R. and INMAN, D., J. Polarog. Soc., 11, 27 (1965).

44. CASADIO, S., CONTE, A. and SOLVEMINI, F., Electrochim. Acta, 16, 1533 (1971).
45. BARABOSHKIN, A.N., KOSIHIN, L.T. and SALTYKOVA, N.A., Report of Academy of Science of U.S.S.R., 155, 880 (1964).
46. TOSCHEV, S., MILCHEV, A., POPOVA, K. and MARKOV, I., Report of Academy of Science of Bulgaria, 22, 1413 (1969).
47. BANSAL, N.P. and PLAMBECK, J.A., J. Electrochem. Soc., 124, 1036 (1977).
48. INMAN, D., BOCKRIS, J.O'M. and BLOMGREN, E., J. Electroanal. Chem., 2. 506 (1961).
49. LAITINEN, H.A., FERGUSON, W.S. and OSTERYOUNG, R.A., J. Electrochem. Soc., 104, 516 (1957).
50. LAITINEN, H.A. and FERGUSON, W., Anal. Chem., 29, 4 (1957).
51. LAITINEN, H.A. and GAUR, H.C., Anal. Chem. Acta, 18, 1 (1958).
52. THALMAYER, C.E., BRUCKENSTEIN, S. and GRUEN, D.M., J. Inorg. Nucl. Chem., 26, 347 (1964).
53. Van NORMAN, J., Anal. Chem., 33, 946 (1961).
54. HILLS, G.J., SCHIFFRIN, D.J. and THOMPSON, J., J. Electrochem. Soc., 120, 157 (1973).
55. INMAN, D. and LOVERING, D.G., J. Electrochem. Soc., 121, 778 (1974).
56. BEHL, W.K., J. Electrochem. Soc., 120, 1692 (1973).
57. BEHL, W.K., J. Electrochem. Soc., 118, 889 (1971).
58. LANTELME, F., HANSELIN, J.P. and CHEMLA, M., Electrochim. Acta, 22, 113 (1977).
59. REDDY, T.B., J. Electroanal. Chem., 11, 77 (1966).
60. NARYSHKIN, I.I. and YURKINSKII, V.P., Soviet Electrochem., 5, 810 (1969).
61. NARYSHKIN, I.I., YURKINSKII, V.P. and STRANGRIT, P.T., Soviet Electrochem., 5, 981 (1969).
62. NARYSHKIN, I.I., YURKINSKII, V.P. and STRANGRIT, P.T., Soviet Electrochem., 5, 1401 (1969).
63. LAITINEN, H.A., TISCHER, R.P. and ROE, D.K., J. Electrochem. Soc., 107, 546 (1960).
64. GERISCHER, H. and KRAUS, M.O., Z. Physik. Chem.(Frankfurt), 10, 264 (1957); 14, 184 (1958).
65. VIELSTICH, W. and DELAHAY, P., J. Am. Chem. Soc., 79, 1874 (1957).

66. LAITINEN, H.A. and GAUR, H.C., J. Electrochem. Soc., 104, 730 (1957).
67. HILL , D.L., HILLS, G.J., YOUNG, L. and BOCKRIS, J.O'M., J. Electroanal. Chem., 1, 79 (1960).
68. INMAN, D. and WEAVER, M.J., J. Electroanal. Chem., 51, 45 (1974).
69. VETTER, K.J. and SCHULTZE, J.W., J. Electroanal. Chem., 34, 131, 141 (1971).
70. SCHULTZE, J.W. and VETTER, K.J., Ber. Bunsenges. Phys. Chem., 75, 470 (1972).
71. WEAVER, M.J., J. Electroanal. Chem., 51, 231 (1974).
72. JANZ, G.J., ALLEN, C.B. and TOMKINS, R.P.T., J. Electrochem. Soc., 124, 51c (1977).
73. DELAHAY, P., New Instrumental Methods in Electrochemistry, Interscience, New York (1954).
74. KARAOGLANOFF, Z., Z. Elektrochem., 12, 5 (1906).
75. NICHOLSON, R.S. and SHAIN, I., Anal. Chem., 36, 706 (1964).
76. NICHOLSON, M.M., J. Am. Chem. Soc., 79, 7 (1957).
77. DEVANATHAN, M.A.V., BOCKRIS, J.O'M. and MÜLLER, K., Proc. Roy. Soc., Ser A, 274, 55 (1963).
78. GRAVES, A.D. and INMAN, D., J. Electroanal. Chem., 25, 357 (1970).
79. GIBBS, W., Collected Works, Vol. 1, Thermodynamics, Yale University Press, New Haven (1968).
80. FAHRENHEIT, D., Phil. Trans. Roy. Soc., 33, 78 (1924).
81. HIRTH, J.P. and Pound, G.M., Condensation and Evaporation, Progress in Material Science, Vol. 11, (Edited by Bruce Chalmers), Pergamon Press, London (1963).
82. VOLMER, M., Die Kinetik der Phasenbildung. Steinkopff, Dresden (1939).
83. BECKER, R. and DÖRING, W., Ann. Phys., (5)24, 719 (1935).
84. ZELDOVICH, J., J. Exp. Theor. Phys. (Russ), 12, 525 (1942).
85. FRENKEL, J., Kinetic Theory of Liquids, Oxford University Press, New York (1946).
86. TOLMAN, R.C., J. Chem. Phys., 17, 333 (1949).
87. KIRKWOOD, J.G. and BUFF, F.P., J. Chem. Phys., 17, 338 (1949).
88. REISS, H., J. Chem. Phys., 20, 1216 (1952).
89. CAHN, J.W. and HILLIARD, J.E., J. Chem. Phys., 28, 258 (1958).
90. HARD, E.W., Phys. Rev., 113, 412 (1959).
91. CAHN, J.W., J. Chem. Phys., 30, 1121 (1959).

92. LOTHE, J. and POUND, G.M., J. Chem. Phys., 36. 2080 (1962).
93. CAHN, J.W. and HILLIARD, J.E., J. Chem. Phys., 31, 688 (1959).
94. FEDER, J., RUSSELL, K.C., LOTHE, J. and POUND, C.M., Advances in Physic, 15, 111-179 (1966).
95. HIRTH, J.P. and MOAZED, K.L., Fundamental Phenomena in the Material Sciences, Vol. 3 (Edited by Borris, L.J., de Bruyn, P.L. and Duga, J.J.) Plenum Press, New York (1966).
96. COLLINS, F.C., Z. Elektrochem., 59, 404 (1955).
97. TOSCHEV, S. and MARKOV, I., Ber. Bunsenges. Phys. Chem., 73, 184 (1969).
98. KAISCHEW, R., TOSCHEV, S. and MARKOV, I., Bulg. Acad. Sci., Comm. Chem. Dept., 11, 463 (1969).
99. KALDIS, E., Crystal Growth, Vol. 1 (Edited by Goodman, C.H.L.) Plenum Press, London (1974).
100. ASTLEY, D.J., HARRISON, J.A. and THIRSK, H.R., Trans. Faraday Soc., 64, 192 (1968).
101. BOCKRIS, J.O'M. and REDDY, A.K.N., Modern Electrochemistry, Plenum Press, New York (1970).
102. DAMASKIN, B.B., The Principles of Current Methods for the Study of Electrochemical Reactions (translated by Mamantov, G.), McGraw-Hill, New York (1967).
103. WALTON, D., J. Chem. Phys., 37, 2182 (1962).
104. MILCHEV, A., STOYANOV, S. and KAISCHEV, R., Thin Solid Films, 22, 255, 267 (1974).
105. STOYANOV, S., KAISCHEW, R., International Society of Electrochemistry 28th Meeting, Electrocrystallization, Extended Abstracts, Bugaria (1977).
106. JOHNSON, K.E., Ph.D. Thesis, University of London (1959).
107. THOMPSON, J., Ph.D. Thesis, University of Southampton (1972).
108. EVERY, R.L. and GRIMSLEY, R.L., J. Electroanal. Chem., 9, 167 (1965).
109. DAMJANOVIC, A. and WARD, A.T., International Review of Science: Electrochemistry, Physical Chemistry Series Two. Vol. 6, Consultant Editor: Buckingham, A.D., Volume Editor: Bockris, J.O'M., Butterworths, London (1976).
110. ANSON, F.C. and LINGANE, J.J., J. Am. Chem. Soc., 79, 4901 (1957).
111. CABRERA, N. and MOTT, N.F., Repts. Prog. Phys., 12, 163 (1949).

112. MOTT, N.F., Trans. Faraday Soc., 43, 429 (1947).
113. VETTER, K.J. and SCHULTZE, J.W., J. Electroanal. Chem., 34, 131, 141 (1972).
114. BIXLER, J.W. and BRUCKENSTEIN, S., Anal. Chem., 37, 791 (1965).
115. TOSCHEV, S. and MUTAFTSCHIEW, B., Electrochim. Acta, 9, 1203 (1964).
116. STACKELBERG, Von M., PILGRIM, M. and TOOME, V., Z. Electrochem., 57, 342 (1953).
117. KOLTHOFF, I.M. and LINGANE, J.J., J. Polarography, Vol. 2, Interscience (1952).
118. GILMAN, S., Electroanalytical Chem., Vol. 2 (Bard, A.J., ed.), Dekker, New York (1967).
119. GUNAWARDENA, G.A., HILLS, G.J. and MONTENEGRO, I., in press.
120. SCHMIDT, E., Electrochim. Acta, 8, 23 (1963).
121. HILLS, G.J. and INMAN, D., Polarographische Berichte, Symposium on Polarographic Methods (1958).
122. SCHARIFKER, B., personal communication.